

CHAPTER 37

Densities of Amorphous and Crystalline Polymers

Vladyslav Kholodovych and William J. Welsh

Department of Pharmacology, University of Medicine & Dentistry of New Jersey (UMDNJ) – Robert Wood Johnson Medical School (RWJMS) and the UMDNJ Informatics Institute, Piscataway, NJ 08854

37.1	Definitions	611
37.2	General Trends	611
37.3	Amorphous and Crystalline Polymers	612
37.4	Density and Crystallinity	612
37.5	Experimental Determination of Density	613
37.6	Experimental Values of Density	613
	References	617

37.1 DEFINITIONS

The density ρ (or mass density) of a material is defined as its mass m per unit volume V : $\rho = m/V$. The specific volume v is the inverse of ρ : $v = 1/\rho$. The density of polymers is commonly specified in cgs units of g/cm^3 , although the SI unit is kg/m^3 ($1 \text{ g}/\text{cm}^3 = 10^3 \text{ kg}/\text{m}^3$) and the British engineering unit is slugs/ ft^3 ($1 \text{ g}/\text{cm}^3 = 1.95 \text{ slugs}/\text{ft}^3$). For some applications, it is more convenient to define a quantity called weight density D (or specific weight) as the weight w per unit volume V of the material: $D = w/V = (mg)/V = \rho g$, where g is the acceleration due to gravity. The corresponding units for D are lb/ft^3 in the British system and N/m^3 in SI.

The specific gravity (or relative density) ρ_{rel} of a material is the ratio of its density ρ to the density ρ_w of pure water at 4°C (39.2°F): $\rho_{\text{rel}} = \rho/\rho_w = D/D_w$, where D_w is the weight density of water. From this definition, it is apparent that specific gravity is a dimensionless quantity. Whereas the numerical value of density will vary from one system of units to another, the specific gravity has the same value in all systems of units. Since the density of water in the cgs system is $1 \text{ g}/\text{cm}^3$, densities in that system are numerically equal to the specific gravity: $\rho(\text{in } \text{g}/\text{cm}^3) = \rho_{\text{rel}}$.

37.2 GENERAL TRENDS

Starting from the lowest members of a homologous series, the density first increases gradually then appears to

approach an asymptotic limit. This behavior is illustrated in Fig. 37.1 by plots of ρ versus the number of repeated units n for the homologous series of alkanes $\text{H}[\text{CH}_2]_n\text{H}$ and the cycloalkanes $[\text{CH}_2]_n$ [1]. As n becomes larger, the difference in density between adjacent members of the series becomes relatively smaller since the changes in molecular structure are less marked.

Since synthetic polymers are formed mostly from light elements (carbon, hydrogen, oxygen, and nitrogen), the densities of solid polymers lie broadly in the range $0.8\text{--}1.8 \text{ g}/\text{cm}^3$. This range is considerably lower than that for inorganic materials ($2.2\text{--}4.0 \text{ g}/\text{cm}^3$) and metals ($2.7\text{--}11.5 \text{ g}/\text{cm}^3$). Polymers containing heavier elements such as fluorine, chlorine, and bromine, exhibit significantly higher densities: polytetrafluoroethylene ($2.28 \text{ g}/\text{cm}^3$), poly(vinylidene fluoride) ($1.77 \text{ g}/\text{cm}^3$), and poly(vinylidene chloride) ($1.65\text{--}1.87 \text{ g}/\text{cm}^3$). Hydrocarbon polymers with relatively open-packed structures dominate the low end of the density scale: polypropylene ($0.90 \text{ g}/\text{cm}^3$), ethylene-propylene copolymer elastomer ($0.86 \text{ g}/\text{cm}^3$), and the thermoplastic polybutylene ($0.60 \text{ g}/\text{cm}^3$) with the lowest density of all commercial polymers [2–4].

In general, the density of a polymer varies inversely with temperature but is much less sensitive to pressure. The introduction of fillers and plasticizers can alter the density and cause variations in density across a sample due to nonuniform distribution. Nevertheless, the average density is nearly invariant to small amounts of plasticizers.

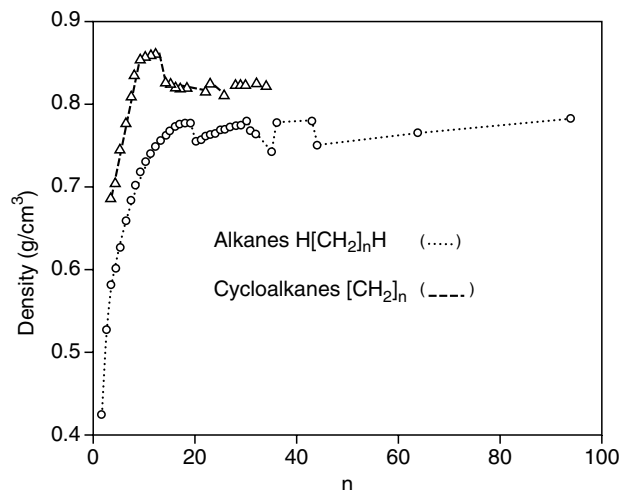


FIGURE 37.1. Density as a function of repeat unit n for the homologous series of alkanes (\circ) and cycloalkanes (Δ). Reproduced from [1].

37.3 AMORPHOUS AND CRYSTALLINE POLYMERS

Polymers can be divided into two groups morphologically: amorphous polymers and crystalline polymers. Amorphous polymers lack sufficient regularity in packing of the chains to produce the sharp x-ray diffraction pattern characteristic of highly crystalline polymers. The term crystalline polymer is actually a misnomer since no polymer is 100% crystalline, containing both crystalline domains and amorphous domains. Therefore, a more correct yet seldom used designation is “semicrystalline” polymer.

The polymer chains are packed together more efficiently and tightly in the crystalline region than in the amorphous region, consequently the density of the crystalline region ρ_c will typically be larger than that of the corresponding amorphous region ρ_a . For this reason, the density of a polymer increases with its degree of crystallinity x_c . The ratio ρ_c/ρ_a can vary considerably from polymer to polymer from the average value of 1.13 g/cm [3,5]. In typical cases, the ρ_c and ρ_a of a polymer will generally differ up to 15% [4]. Polymers with unsubstituted monomeric units, such as poly(ethylene) and nylon-6,6, show the largest difference between ρ_c and ρ_a . These chains crystallize in an *all-trans* conformation with particularly tight packing of the chains. In contrast, helix-forming polymers with large substituents, such as isotactic poly(styrene), pack less efficiently in the crystalline state thus $\rho_c - \rho_a$ is correspondingly smaller. For semicrystalline polymers, van Krevelen [5] gives the approximate relationship $\rho_{sc}/\rho_a = 1 + 0.13x_c$, where ρ_{sc} is the density of the (semi-) crystalline polymer.

The bulk density ρ of polymer solids is influenced strongly by the elemental composition and, to a certain

degree, by the packing arrangement of chains and side groups. A polymer chain must exhibit an ordered, regular structure to allow efficient packing into the crystal lattice. Consequently, a stereoregular polymer is more likely to be crystalline and possess a higher density than the corresponding stereoirregular polymer [2–4]. Polymer chains possessing bulky, protruding side groups will pack inefficiently and are rarely crystalline. Accordingly, their densities tend to be lower than average. On the other hand, polymers capable of forming strong interchain hydrogen bonds or dipole–dipole interactions induce crystallinity and typically possess above-average densities.

Amorphous polymers generally exist as hard, rigid, glassy plastics below their glass-transition temperature T_g and as soft, flexible, rubbery materials above their T_g . Comparison of the densities of the glassy state (ρ_g) and the rubbery state (ρ_r) for various amorphous polymers indicates that $\rho_g > \rho_r$ [5].

Density is often the single parameter that is most clearly related to the physical and mechanical properties of polymers. For many polymers, properties dependent on crystallinity (e.g., stiffness, tear strength, hardness, chemical resistance, softening temperature, yield point) tend to increase with increasing density. Other properties (e.g., permeability to gases and liquids, toughness, flex life) tend to decrease with increasing density [6].

37.4 DENSITY AND CRYSTALLINITY

From the preceding discussion, it is apparent that density is a convenient measure of the degree of crystallinity. Thus “low density” (0.910–0.925 g/cm³) polyethylene is about 60% crystalline, while “high density” (0.94–0.97 g/cm³) polyethylene is about 95% crystalline. These differences in density arise primarily from differences in the degree of branching. The branch points sterically preclude packing into a crystal lattice in their immediate vicinity and thus lower the degree of crystallinity x_c [2–6].

The relationship between the degree of crystallinity and the observed polymer density can be derived from two slightly different perspectives, depending on whether one assumes additivity of the crystalline and amorphous regions with respect to volume ($V = V_c + V_a$) or to mass ($M = M_c + M_a$). For the former case, one obtains the relation

$$\nu = x_m \nu_c + (1 - x_m) \nu_a, \quad (37.1)$$

where $x_m = M_c/M$ is the mass crystallinity (i.e., the mass fraction that is crystalline) and ν , ν_c , and ν_a are the bulk, crystalline, and amorphous specific volumes, respectively. Solving for x_m , Eq. (37.1) yields

$$x_m = (\nu - \nu_a)/(\nu_c - \nu_a). \quad (37.2)$$

Assuming instead additivity with respect to mass, one obtains the relation

$$\rho = x_v \rho_c + (1-x_v) \rho_a. \quad (37.3)$$

Analogous to Eq. (37.1), where $x_v = V_c/V$ is the volume crystallinity (i.e., the volume fraction that is crystalline) and ρ , ρ_c , and ρ_a are the bulk, crystalline, and amorphous densities, respectively. Solving Eq. (37.3) for x_v , one obtains

$$x_v = (\rho - \rho_a)/(\rho_c - \rho_a). \quad (37.4)$$

The mass crystallinity x_m and volume crystallinity x_v thus defined are interrelated by the equation $x_m = (v/v_c)x_v = (\rho_c/\rho)x_v$. Unfortunately, it is easy to inadvertently use x_m and x_v interchangeably even though they may differ up to a few percent. In Eq. (37.5) below taken from Tadokoro [8], his " x_c " is equivalent to the x_m in Eq. (37.1) and (37.2).

$$1/\rho = x_c/\rho_c + (1 - x_c)/\rho_a. \quad (37.5)$$

37.5 EXPERIMENTAL DETERMINATION OF DENSITY

In (semi-)crystalline polymers, the measured density of a sample provides a simple way to estimate the degree of crystallinity. For example, the density of polyethylene shows a strong linear correlation with percent crystallinity [9]. The density of the crystalline region may be calculated from the dimensions of the unit cell, while the density of the amorphous region can be estimated by extrapolations from the melt density aided with a knowledge of the polymer's coefficient of thermal expansion α_T .

For a unit cell of Z monomeric units, the density ρ_c of the crystalline region is given by

$$\rho_c(\text{in g/cm}^3) = ZM/N_A V = 1.66ZM/V(\text{\AA}^3), \quad (37.6)$$

where N_A is Avogadro's number (6.022×10^{23}), V is the volume of the unit cell, and M is the molecular weight of the monomeric unit [8]. The presence of any foreign matter (e.g., dirt, catalyst, solvent, additives, fillers) in the polymer sample will affect the measured density and likely reduce the degree of crystallinity. The presence of even a small number of voids can lead to more serious inaccuracies.

The bulk density ρ of even small samples may be readily determined using a density-gradient tube or by immersion in salt solutions of known density. The latter method is well adapted for rapid work in routine analyses. The density-gradient method is currently the standard method employed by numerous workers [10]. A density-gradient column contains a liquid whose density increases continuously from the meniscus down to the base [11]. Such liquids can consist, for

example, of mixtures of organic solvents or of salt solutions selected to wet but not swell or dissolve the polymer sample. With the appropriate mechanical apparatus, it is possible to form density gradients in which the variation of the density with column height is linear, concave, convex, etc. The polymer sample then remains suspended at a particular height of the gradient column whose density matches the sample's density. Another, presumably more accurate, technique for measuring density is with a dilatometer [11]. Other methods for measuring density are discussed elsewhere [12].

The bulk density ρ can also be determined from straightforward measurements of the polymer's mass and volume [13]. The mass of the sample is determined by weighing it on a suitable balance. If the weighing is done in air, this apparent density should be adjusted for the buoyant effect of the air on the sample to obtain the true polymer density. The density of air under normal ambient conditions is about 0.0012 g/cm^3 (0.075 lb/ft^3). The volume of the sample can be determined accurately using a procedure known as hydrostatic weighing based on Archimedes' Principle. The sample is weighed both in air and while submerged in a liquid of known density. The volume of the sample is then equal to its loss of weight in the liquid divided by the density of the liquid. All density measurements of solids are subject to error due to the presence of inhomogeneities such as surface imperfections, trapped air bubbles, presence of monomer, etc.

Finally, the appreciable variation in published density measurements from different workers is due in part to differences in the thermal, mechanical, and chemical history of the individual polymer samples, to differences in the laboratory skills and techniques of the worker, and to variations in the types and quality of methods employed to measure the density.

37.6 EXPERIMENTAL VALUES OF DENSITY

Tables 37.1 and 37.2 provide a compilation of representative values of macroscopic (bulk) density ρ for many of the more common polymers. For easy reference, the data are listed alphabetically by the name of the polymer. Table 37.1 contains polymers designated by their familiar or trade names (e.g., nylon, rubber), while Table 37.2 lists polymers designated by their chemical names using the prefix "poly." These are alphabetized by the letter following this prefix. For example, poly(ethylene) and poly(vinylacetate) are listed under "e" and "v", respectively. In many cases, the density of a given polymer is represented by a range of values (e.g., $0.87\text{--}0.93 \text{ g/cm}^3$) to reflect variations obtained from different sources of the data.

TABLE 37.1. Values of density for some polymers designated by their common or trade name.

Common or trade name	$\rho(\text{g}/\text{cm}^3)$	Reference
Acetate rayon	1.32	[6]
Acrylic	1.16	[6]
Acrylonitrile–styrene copolymer	1.075–1.10	[11a]
Acrylonitrile–styrene–butadiene copolymer (ABS)	1.04–1.07	[3]
Aniline-formaldehyde	1.22–1.25	[11a]
Ardel D-100, Arylef, U-100	1.21	[17]
Arnitel	1.17–1.27	[17]
Aramid (nomex, durette, conex, kevlar, twerlon)	1.34–1.47	[17]
Benzylcellulose	1.22	[11a]
Bisphenol-A polycarbonate (BPAPC)	1.2	[11a]
Butyl rubber	0.92	[11a]
Cellulose I	1.582–1.630	[1,14]
Cellulose II	1.583–1.62	[1,14]
Cellulose III	1.61	[14]
Cellulose IV	1.61	[1,14]
Cellulose acetate	1.28–1.32	[11a]
Cellulose acetate-butyrate	1.14–1.22	[11a]
Cellulose formate fiber	1.45	[11a]
Cellulose nitrate	1.35–1.40	[11a]
Cellulose propionate	1.18–1.24	[11a]
Cellulose triacetate	1.28–1.33	[11a,14]
Cellulose tributyrate	1.16	[14]
Chlorinated polyether	1.4	[11a]
Cotton	1.50–1.54	[1,6,11a]
Cotton, acetylated	1.43	[11a]
CXA and plexar resins (ethylene copolymers)	0.935–1.00	[17]
Durel, D-400	1.20	[17]
Ethylcellulose	1.09–1.17	[11a]
Ethylene–propylene copolymer (EPM)	0.86	[3]
Glass	3.54	[11a]
Glass and asbestos	2.5	[11a]
Hytrell	1.17–1.22	[17]
Keldax	1.67–1.83	[17]
Keltan	0.89	[17]
Kevlar	1.44	[6]
KL 1–9300/1–9310 (Bayer)	1.21–1.44	[17]
Lignocellulose	1.45	[11a]
Levasint	0.97	[17]
Levaflex	0.89–1.04	[17]
Maleic anhydride–styrene copolymer	1.286	[11a]
Melamine-formaldehyde	1.16	[11a]
Methyl polyvinyl ketone	1.12	[11a]
Methylcellulose	1.362	[11a]
Nomex	1.38	[6]
Noryl	1.06–1.2	[17]
Nylon 6	1.12–1.24	[1,3]
Nylon 66	1.13–1.15, 1.22–1.25	[1,3]
Nylon-610	1.156	[1]
Nylon-12	1.02–1.034	[1,3]
Rubber, butyl	0.92	[3]
Rubber (unvulcanized)	0.91	[1,3]
Rubber (hard) (Ebonite)	1.11–1.17	[1,11a]
Rubber, chlorinated (Neoprene) (CR), unvulcanized	1.23	[1,11a]
Rubber, chlorinated (Neoprene) (CR), vulcanized	1.32–1.42	[1]
Rubber, fluorinated silicone	1	[11a]
Rubber, silicone	0.8	[11a]
Rubber, silicone (vulcanized)	1.3–2.3	[11a]

TABLE 37.1. *Continued.*

Common or trade name	$\rho(\text{g}/\text{cm}^3)$	Reference
Rubber, styrene-butadiene (SBR), (unvulcanized)	0.93–0.94	[3,11a]
Rubber, styrene-butadiene (SBR), (vulcanized)	0.961	[11a]
Silk	1.25–1.35	[6,11a]
Santoprene	0.95–0.98	[17]
Tafmer	0.88	[17]
Toluene-sulfonamide-formaldehyde	1.21–1.35	[11a]
Urea-formaldehyde	1.16	[11a]
Urea-thiourea-formaldehyde	1.477	[11a]
Viscose Rayon	1.5	[6]
Vestopren	0.90–1.10	[17]
Wool	1.28–1.33	[6,11a]

TABLE 37.2. *Values of density for some polymers designated by their chemical name.*

Chemical name	$\rho(\text{g}/\text{cm}^3)$	Reference
Poly-		
acetaldehyde	1.07	[5]
acrolein	1.322	[11a]
acrylic acid	1.22	[11a]
acrylonitrile (PAN)	1.01–1.17, 1.20	[3,11a]
acrylonitrile-vinyl acetate	1.14	[11a]
amide-6 (PA-6)	1.12–1.24	[1,3]
amide-66 (PA-66)	1.13–1.15, 1.22–1.25	[1,3]
amide-610(PA-610)	1.156	[1]
amide-12(PA-12)	1.02–1.034	[1,3]
aryl ether ketone (PEEK)	1.2, 1.3	[16,17]
arylate	1.21	[3]
benzimidazole (PBI)	1.43	[17]
bisphenol carbonate (BPAPC)	1.2	[5]
butadiene-1,2, isotactic	0.96	[1,11a]
butadiene-1,2, syndiotactic	0.96	[1,11a]
butadiene-1,4- <i>cis</i>	1.01	[1]
butadiene-1,4- <i>trans</i>	0.93–0.97, 1.01	[1,11a]
1-butene	0.85	[5]
butene	0.91–0.92	[3]
butyl acrylate	1.08	[5]
<i>sec.</i> -butyl acrylate	1.05	[5]
butylene	0.6	[3]
<i>tert.</i> -butyl methacrylate	1.03	[5]
<i>n</i> -butyl methacrylate	1.055	[11a]
<i>sec.</i> -butyl methacrylate	1.04	[5]
<i>tert.</i> -butylstyrene	0.957	[16]
caprolactam, nylon	0.985	[16]
carbonate (PC)	1.14–1.2	[3,16]
chlorobutadiene	1.25	[11a]
chloroprene (Neoprene rubber) (CR), unvulcanized	1.23	[1,3]
chloroprene (Neoprene rubber) (CR), vulcanized	1.32–1.42	[1]
chlorotrifluoroethylene	2.03	[5]
dichlorostyrene	1.38	[11a]
2,2-dimethylpropyl acrylate	1.04	[5]
dimethylsiloxane	0.97	[16]
dodecyl methacrylate	0.93	[5]
1-ethylpropyl acrylate	1.04	[5]
etheretherketone (PEEK)	1.27	[3]

TABLE 37.2. Continued.

Chemical name	$\rho(\text{g}/\text{cm}^3)$	Reference
ethersulfone	1.4	[17]
ethyl acrylate	1.095, 1.12	[5,11a]
ethyl methacrylate	1.11, 1.12	[5,11a]
ethylbutadiene	0.891	[10c,16]
ethylene	0.870, 0.910–0.965	[1,6,10c,11a]
ethylene (amorphous)	0.85	[1,11a,14]
ethylene (crystalline)	0.99	[1,11a]
ethylene (high density:HDPE)	0.941–0.965	[1,3,6,15,17]
ethylene (linear low density: LLDPE)	0.918–0.935	[3,6,17]
ethylene (low density: LDPE)	0.910–0.925	[1,3,6,15,17]
ethylene (medium density: MDPE/IDPE)	0.926–0.940	[1,3,17]
ethylene (very low density: VLDPE)	0.900	[17]
ethylene glycol	1.0951	[11a]
ethylene glycol fumarate	1.385	[11a]
ethylene glycol isophthalate, cryst.	1.358	[11a]
ethylene glycol phthalate	1.352	[11a]
ethylene glycol waxes	1.15–1.20	[11a]
ethylene isophthalate	1.34	[5]
ethylene phthalate	1.34	[5]
ethylene terephthalate (PET)	1.33–1.42	[1,3,5,6]
formaldehyde	1.425	[11a]
- <i>n</i> -hexyl methacrylate	1.01	[11a]
imide	1.43	[3,6]
isobutene	0.917	[14]
isobutyl methacrylate	1.02–1.04	[5,11a]
isobutylene	0.87–0.93	[5,11a,16]
isoprene (1,4-)	0.900–0.913	[16]
- <i>N</i> -isopropylacrylamide	1.070–1.118	[11a]
isopropyl acrylate	1.08	[5]
isopropyl methacrylate	1.04	[5]
methacrylonitrile	1.1	[11a]
methyl acrylate	1.07–1.223	[5,11a,16]
methyl methacrylate (PMMA)	1.16–1.20	[1,5,11a,14]
- <i>p</i> -methylstyrene (PMA)	1.01	[17]
4-methyl-1-pentene	0.84	[5]
myrcene	0.895	[10c]
<i>trans</i> -octenamer (TOR)	0.91	[17]
olefin- <i>co</i> -vinyl alcohol (GL/EVAL)	0.97–1.52	[17]
oxymethylene (POM)	1.41–1.435	[1,3]
- <i>p</i> -phenylene (H resins)	1.145–1.35	[17]
phenylene oxide	1.00–1.06	[3,16]
phenylene-1,3,4-oxadiazole (POD)	1.40	[17]
polysulfide (Thiokol A)	1.6	[11a]
polysulfide (Thiokol B)	1.65	[11a]
propyl methacrylate	1.06–1.08	[5,11a]
propylene (PP)	0.85–0.92	[3,6,5,10c]
propylene, amorphous	0.87	[11a]
propylene, head-to-head	0.878	[10c]
propylene, isotactic	0.90–0.92	[1,11a]
propylene, isotactic (crystalline)	0.92–0.939	[1,11a]
propylene, syndiotactic (crystalline)	0.93	[1]
propylene oxide	1	[16]
styrene (PS)	1.04–1.09	[1,3,5,6,11a,14,17]
styrene, crystalline	1.08–1.111	[1,11a]
styrene-butadiene thermoplastic elastomer	0.93–1.10	[6]
sulfone	1.20–1.24	[3,6,17]

TABLE 37.2. Continued.

Chemical name	$\rho(\text{g}/\text{cm}^3)$	Reference
tetrafluoroethylene (PTFE)	2.28–2.344,2.17	[1], [17]
thiodiethanol	1.35	[17]
trifluorochloroethylene	2.11–2.13	[11a]
vinyl acetate (PVAC)	1.08–1.25	[1,3,5,11a]
vinyl alcohol (PVA)	1.21–1.31	[11a]
vinyl butyral	1.07–1.20	[11a]
vinylcarbazole	1.2	[11a]
vinyl chloride (PVC)	1.37–1.44	[1,3,5,11a,17]
vinyl chloride-co-methyl acrylate	1.34	[11a]
vinyl chloride, flexible	1.25–1.35	[11a]
vinyl chloride, rigid	1.35–1.55	[11a]
vinyl chloride acrylonitrile (60/40)	1.28	[11a]
vinylidene chloride (PVDC)	1.65–1.875	[3,5,6,11a]
vinylethylene	0.889	[10c,16]
vinyl formal	1.2–1.4	[11a]
- <i>p</i> -vinylphenol	1.2	[17]
- <i>p</i> -vinylphenol, brominated	1.9	[17]
vinyl pyrrolidone (PVP)	1.25	[11a]
vinyl-vinylidene chloride	1.7	[1,11a]
vinylidene fluoride (PVDF)	1.75–1.78	[1]
vinylisobutyl ether	0.91–0.92	[11a]
- <i>m</i> -xylene adipamide	1.22	[11a]

REFERENCES

1. *Physical Properties of Polymers Handbook*, Ed. James E. Mark, (AIP Press, Woodbury, New York 1996).
2. C. Hall, *Polymer Material, An Introduction for Technologists and Scientists*, second edition (Halsted Press, John Wiley & Sons, New York, 1989), p.243.
3. S. L. Rosen, *Fundamental Principles of Polymeric Materials*, second edition, (Wiley-Interscience, John Wiley & Sons, New York, 1993), pp.448.
4. H.-G. Elias, *Macromolecules*, second edition, (Plenum Press, New York, 1984), p.564.
5. D. W. van Krevelen, *Properties of Polymers: Their Correlation with Chemical Structure: Their Numerical Estimation and Prediction from Additive Group Contributions*, third edition, (Elsevier Scientific, Amsterdam, 1997), p.875.
6. F. W. Billmeyer, Jr., *Textbook of Polymer Science*, third edition (Wiley-Interscience, John Wiley & Sons, New York, 1990), p.578.
7. R. L. Miller, in *Encyclopedia of Polymer Science*, vol. 4 (John Wiley & Sons, New York, 1966), pp. 449–529.
8. H. Tadokoro, *Structure of Crystalline Polymers* (Krieger Publishing Company, Melbourne, Florida, 1990), p.486.
9. C. Tanford, *Physical Chemistry of Macromolecules* (John Wiley & Sons, New York, 1961), Chap. 2, p.710.
10. See, for example: (a) M. A. Kennedy, A. J. Peacock, and L. Mandelkern, *Macromolecules* **27**, 5297 (1994); (b) J. M. Carella, W. W. Graessley, and L. J. Fetters. *ibid.* **17**, 2775 (1984); (c) P. Hattam, S. Gauntlett, J. W. Mays *et al. ibid.* **24**, 6199 (1991).
11. (a) G. M. Brauer and E. Horowitz, in *Analytical Chemistry of Polymers*, part III, edited by G. M. Kline Interscience, (John Wiley & Sons, New York, 1962), pp. 34–45; (b) Polymer. Part B: Crystal Structure and Morphology, vol. 16, edited by R. A. Fava, in *Methods of Experimental Physics* (Editors-in Chief: L. Manor, and C. Marton) (Academic Press, New York, 1980, Chap. 10
12. (a) N. Bauer and S. Z. Lewin, "Physical Methods of Organic Chemistry", in *Technique of Organic Chemistry*, vol. 1. edited by A. Weissberger, third edition, Part I (Interscience, New York, 1959) pp. 131–190; (b) F. Schneider, *Qualitative Organic Microanalysis* (Elsevier Science & Technology Books, Amsterdam, 1964); (c) R. L. Shriner, C. Hermann, T. C. Morrill, D. Y. Curtin and R. C. Fuson. *The Systematic Identification of Organic Compounds*. 8th edition, (Wiley-Interscience, John Wiley & Sons, New York, 2003), p.723.
13. D. W. Kupke, in *McGraw-Hill Encyclopedia of Science & Technology*, edited by S. P. Parker, eighth edition (McGraw-Hill, Inc., New York, 1997), p.1510.
14. L. H. Sperling, *Introduction to Physical Polymer Science*, third edition (Wiley-Interscience, John Wiley & Sons, New York, 2001), Chaps. 4–5, p.720.
15. R. B. Seymour and C. E. Carraher, Jr., *Structure-Property Relationships in Polymers* (Kluwer Academic Publishers 1984), Chap. 12, p.246.
16. L. J. Fetters, D. J. Lohse, D. Richter *et al.*, *Macromolecules* **27**, 4639 (1994).
17. H.-G. Elias, F. Vohwinkel, *New Commercial Polymers 2*, English edition (Gordon and Breach Science publishers, New York, 1986) p.508.

CHAPTER 38

Unit Cell Information on Some Important Polymers

Edward S. Clark

Department of Materials Science and Engineering, The University of Tennessee, Knoxville, TN 37996

38.1	Polyethylene $[-(\text{CH}_2)_2-]$	619
38.2	Polypropylene $[-\text{CH}_2-\text{CH}(\text{CH}_3)-]$	620
38.3	Poly(ethylene terephthalate) $[-(\text{C}=\text{O})-(\text{C}_6\text{H}_4)-(\text{C}=\text{O})-\text{CH}_2-\text{CH}_2-]$	621
38.4	Polycaprolactam (PA6) $[-\text{NH}-(\text{CH}_2)_5-(\text{C}=\text{O})-]$	621
38.5	Poly (hexamethylene adipamide) (PA66) $[-\text{NH}-(\text{CH}_2)_6-\text{NH}-(\text{C}=\text{O})-(\text{CH}_2)_4-(\text{C}=\text{O})-]$	622
38.6	Polyoxymethylene $[-\text{CH}_2-\text{O}-]$	622
38.7	Polytetrafluoroethylene $[-(\text{CF}_2)-]$	623
38.8	Poly(p-phenylene terephthalamide) (PTTA) $[-(\text{C}=\text{O})-(\text{C}_6\text{H}_4)-(\text{C}=\text{O})-\text{NH}-(\text{C}_6\text{H}_4)-(\text{NH})-]$	624
	References	624

In this chapter, drawings are presented for the principal crystallographic forms of several important commercial polymers using CSC Chem3D Plus® (Cambridge Scientific). X ray data are presented for polymorphs where available. The crystallographic axis most nearly parallel to the continuity of the covalent bonds (fiber axis) is indicated by †. References are given for the papers used in obtaining the data. Where available, intensity data are given for the main reflections. However, it must be strongly emphasized that observed intensities are very much a function of the crystallinity and molecular orientation in the sample as well as the experimental technique used. The usual designations of *s*, *m*, *w* (strong medium and weak) are used. See Figures 38.1–38.23 and Tables 38.1–38.14. A review of unit cells of many different polymers is given in Chapter 7 of Tadokoro [1].

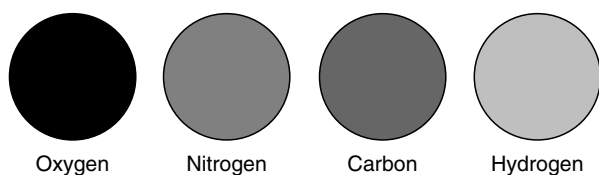


FIGURE 38.1. Key to shading of atoms.

38.1 POLYETHYLENE $[-(\text{CH}_2)_2-]$

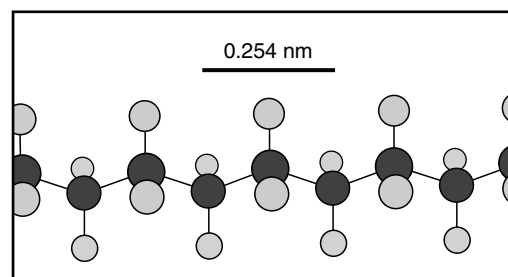


FIGURE 38.2. Polyethylene.

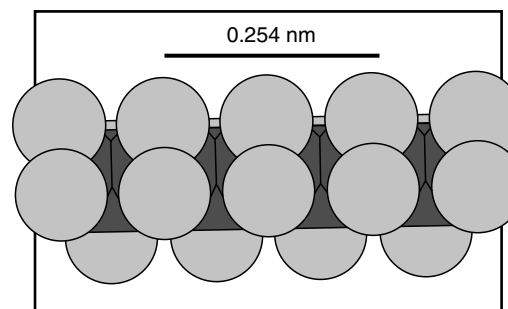


FIGURE 38.3. Polyethylene.

TABLE 38.1. Polyethylene (orthorhombic 25 °C) $[-(\text{CH}_2)_2-]$.^a

<i>hkl</i>	<i>d</i> -value (nm)	2θ (deg) (λ = 0.1542 nm)	Relative intensity
110	0.4115	21.59	vvs
200	0.3703	24.03	s
020	0.2475	36.30	m
310	0.2209	40.84	m
220	0.2058	44.01	m
011	0.2268	39.75	m
111	0.2168	41.65	m
201	0.2101	43.05	s
211	0.1934	46.98	m

^aSpace group Pnam [D_{2h}^{16}], $N = 4(\text{CH}_2)$. $a = 0.74069$ nm; $b = 0.49491$ nm; and $c = 0.25511$ nm[†]. Cell volume = 0.09352 nm³. Density = 996.2 kg/m³. (From Refs. 2 and 3.) See also Ref. 4.

TABLE 38.2. Polyethylene high pressure (>3 kbar, near melting point) $[-(\text{CH}_2)_2-]$.^a

<i>hkl</i>	<i>d</i> -value (nm)	2θ (deg) (λ = 0.1542 nm)	Relative intensity
110 (ortho)	4.227	21.02	s

^aSpace group (Hexagonal, ortho); $N = 4(\text{CH}_2)$. $a = 0.846$ nm; $b = 0.488$ nm; and $c = 0.245$ nm[†]. Cell volume = 0.101 nm³ (approx.). Density = 920 kg/m³ (approx.). (From Refs. 5 and 6.)

TABLE 38.3. Polyethylene (metastable monoclinic 25 °C) $[-(\text{CH}_2)_2-]$.^a

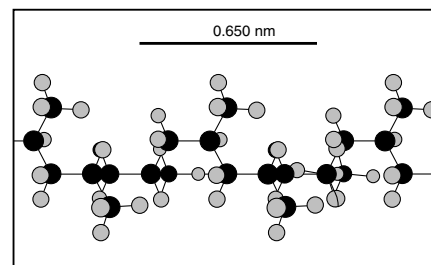
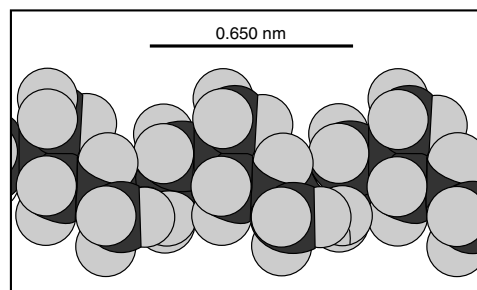
<i>hkl</i>	<i>d</i> -value (nm)	2θ (deg) (λ = 0.1542 nm)	Relative intensity
001	0.4558	19.47	s
200	0.3849	23.11	s
$\bar{2}01$	0.3523	25.28	s
201	0.2576	34.82	w
$\bar{4}01$	0.2008	45.15	m
400	0.1925	47.23	m
$11\bar{1}$	0.2216	40.72	m
111	0.2047	44.26	m
$11\bar{2}^b$	0.1739	52.62	s

^aSpace group C2/m [C_{2h}^3]; $N = 4(\text{CH}_2)$. $a = 0.809$ nm; $b = 0.253$ nm[†]; and $c = 0.479$ nm. Cell volume = 0.09329 nm³. Density = 998 kg/m³.

^bOverlap with orthorhombic phase. (From Ref. 4.)

38.2 POLYPROPYLENE $[-\text{CH}_2-\text{CH}(\text{CH}_3)-]$

Polypropylene isotactic beta form. Space group P3₁21 [D_4^3] or P3₂21 [D_6^3]. $N = 9$. $a = 1.103$ nm; $b = 1.103$ nm; $c = 0.649$ nm and $\gamma = 120^\circ$. Cell volume = 0.672 nm³. Density = 936 kg/m³. (From Ref. 14.)

**FIGURE 38.4.** Polypropylene (Alpha form).**FIGURE 38.5.** Polypropylene (Alpha form).**TABLE 38.4.** Polypropylene $[-\text{CH}_2-\text{CH}(\text{CH}_3)-]$, isotactic alpha form. Space group C2/c [C_{2h}^6] or Cc [C_s^4].^a

<i>hkl</i>	<i>d</i> -value (nm)	2θ (deg) (λ = 0.1542 nm)	Relative intensity
110	0.626	14.14	vs
040	0.524	16.92	vs
130	0.478	18.55	s
111	0.417	21.31	s
$13\bar{1},041$	0.406	21.86	s
150,060	0.351	25.35	s
200	0.328	27.18	m
220	0.313	28.51	m

^a $N = 12$. $a = 0.665$ nm; $b = 2.096$ nm; $c = 0.650$ nm[†]; and $\beta = 99.33^\circ$. Cell volume = 0.894 nm³. Density = 938 kg/m³. (From Ref. 8.)

TABLE 38.5. Polypropylene $[-\text{CH}_2-\text{CH}(\text{CH}_3)-]$, isotactic gamma form. Space group Fddd [D_{2h}^{24}].^a

<i>hkl</i>	<i>d</i> -value (nm)	2θ (deg) (λ = 0.1542 nm)	Relative intensity
111	0.6391	13.86	m
113	0.5863	15.11	w
008	0.5210	17.02	s
115	0.5110	17.35	w
117	0.4380	20.27	m
202	0.4169	21.31	s
026	0.4045	21.97	s
206	0.3628	24.53	w
0012	0.3473	25.65	m
224	0.3088	28.91	m

^a $N = 48$. $a = 0.851$ nm; $b = 0.995$ nm; and $c = 4.168$ nm[†]. Cell volume = 3.529 nm³. Density = 0.950 kg/m³. (From Refs. 15 and 16.)

TABLE 38.6. Polypropylene $[-CH_2-CH(CH_3)-]$ syndiotactic monoclinic — Form 1. Space group $P2_1 [C_{2h}^5]^a$

hkl	d -value (nm)	2θ (deg) ($\lambda = 0.1542$ nm)	Relative intensity
200	7.16	12.4	s
020	5.57	15.9	m
-211	4.70	18.9	m
220	4.39	20.2	w
121	4.26	20.8	m
002	3.75	23.7	w
400	3.58	24.9	w
-321	3.27	27.2	w

^a $N = 16$; $a = 14.31$ nm; $b = 11.15$ nm; $c = 7.5$ nm[†]; and $\gamma = 90.3^\circ$. Cell volume = 1.196 nm³. Density = 934 kg/m³. (From Ref. 12.)

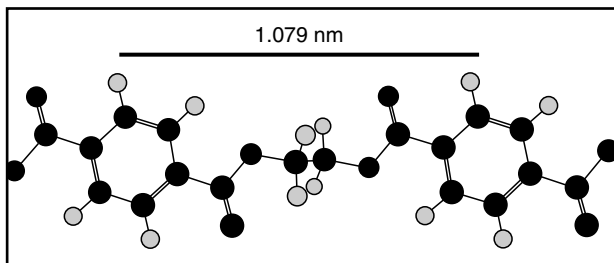
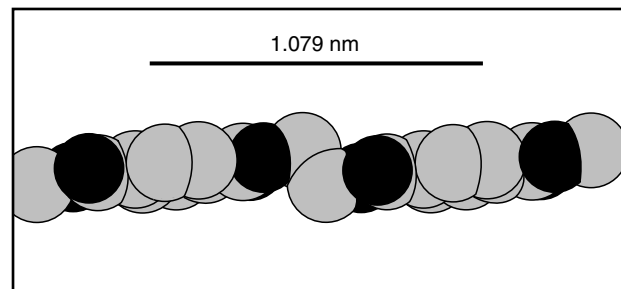
TABLE 38.7. Poly (ethylene terephthalate) $[-(C=O)-(C_6H_4)-(C=O)-CH_2-CH_2-]$; Space group $P\bar{1} [C_i^1]^a$

hkl	d -value (nm)	2θ (deg) ($\lambda = 0.1542$ nm)	Relative intensity
0 $\bar{1}$ 1	0.5417	16.36	s
010	0.5014	17.69	s
$\bar{1}$ 11	0.4092	21.72	m
1 $\bar{1}$ 0	0.3880	22.92	s
100	0.3435	25.94	vs
1 $\bar{1}$ 1	0.3164	28.20	w
101	0.2699	33.20	w

^a $N = 1$. $a = 0.4509$ nm; $b = 0.5882$ nm; $c = 1.0787$ nm[†]; $\alpha = 100.01^\circ$; $\beta = 118.36^\circ$; and $\gamma = 110.56^\circ$. Cell volume = 0.2146 nm³. Density = 1485 kg/m³. (From Refs. 8,9,10.)

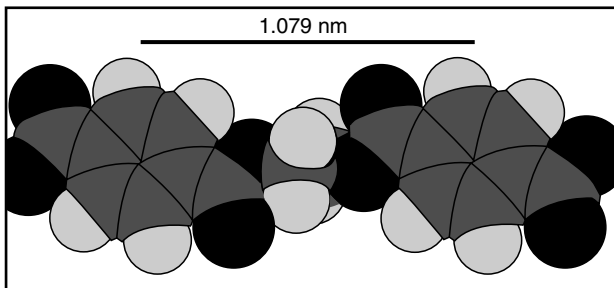
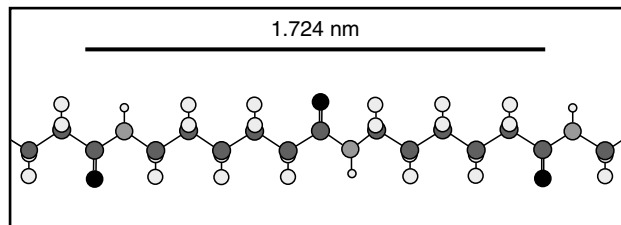
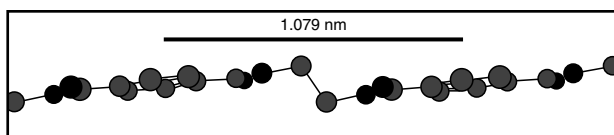
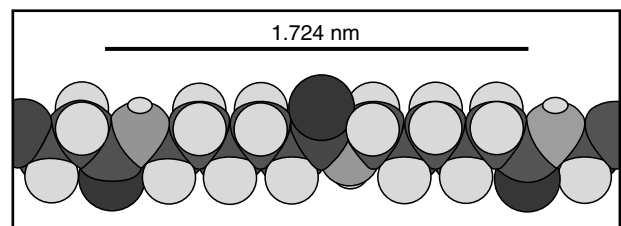
38.3 POLY (ETHYLENE TEREPHTHALATE)

$[-(C=O)-(C_6H_4)-(C=O)-CH_2-CH_2-]$


FIGURE 38.6. Poly (ethylene terephthalate).

FIGURE 38.9. Poly (ethylene terephthalate).

38.4 POLYCAPROLACTAM (PA6)

$[-NH-(CH_2)_5-(C=O)-]$


FIGURE 38.7. Poly (ethylene terephthalate).

FIGURE 38.10. Polycaprolactam.

FIGURE 38.8. Poly (ethylene terephthalate).

FIGURE 38.11. Polycaprolactam.

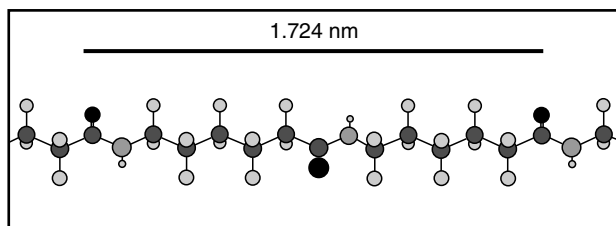


FIGURE 38.12. Polycaprolactam.

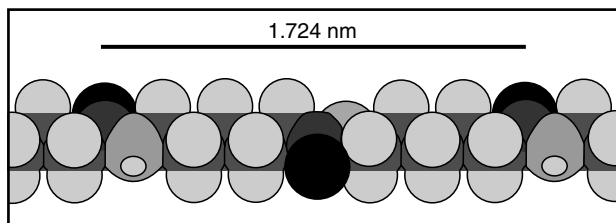


FIGURE 38.13. Polycaprolactam.

TABLE 38.8. Polycaprolactam (PA6) alpha form $[-NH-(CH_2)_5-(C=O)-]$; Space group $P2_1/m [C_{2h}^2]$.^a

<i>hkl</i>	<i>d</i> -value (nm)	2θ (deg) ($\lambda = 0.1542$ nm)	Relative intensity
200	0.4416	20.11	vs
211,210	0.4387	20.26	w
002,202	0.3646	24.42	vvs
$\bar{2}02,402$	0.2373	37.93	m
204	0.2001	45.32	w
004,404	0.1823	50.04	w
$\bar{1}71,271$	0.2186	41.30	m
$\bar{2}71,371$	0.1959	46.35	m

^a $N = 8$. $a = 0.956$ nm; $b = 1.724$ nm; $c = 0.801$ nm; and $\beta = 67.5^\circ$. Cell volume = 0.1220 nm³. Density = 1232 kg/m³. (From Refs. 16 and 17.) See also Ref. 18.

Polycaprolactam (PA6) gamma form. Space group $P2_1/a [C_{2h}^5]$. $N = 4$; $a = 0.933$ nm; $b = 1.688$ nm; $c = 0.478$ nm; and $\beta = 121^\circ$. Cell volume = 0.645 nm³. Density = 1160 kg/m³. (From Ref. 19.)

38.5 POLY (HEXAMETHYLENE ADIPAMIDE) (PA66) $[-NH-(CH_2)_6-NH-(C=O)-(CH_2)_4-(C=O)-]$

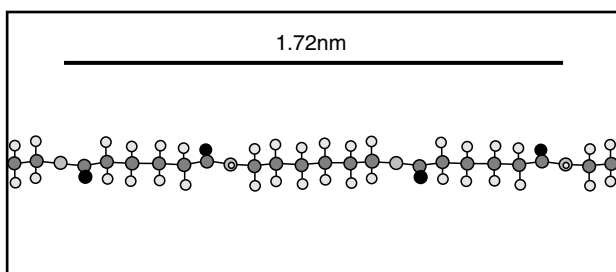


FIGURE 38.14. Poly (hexamethylene adipamide).

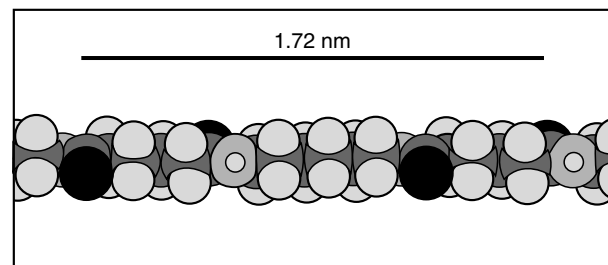


FIGURE 38.15. Poly (hexamethylene adipamide).

TABLE 38.9. Poly (hexamethylene adipamide) (PA66) alpha form $[-NH-(CH_2)_6-NH-(C=O)-(CH_2)_4-(C=O)-]$. Space group $P1[C_1]$.^a

<i>hkl</i>	<i>d</i> -value (nm)	2θ (deg) ($\lambda = 0.1542$ nm)	Relative intensity
002	0.641	13.83	w
100,010,110	0.390	22.96	vvs
015	0.335	26.65	w
$\bar{1}10,210$	0.236	38.12	s
017,127	0.233	38.69	w
117,027	0.218	41.37	w
$\bar{1}17,227$	0.194	46.71	w
020,220	0.183	49.70	s

^a $N = 1$. $a = 0.49$ nm; $b = 0.54$ nm; $c = 1.72$ nm; $\alpha = 48.5^\circ$; $\beta = 77.0^\circ$; and $\gamma = 63.5^\circ$. Cell volume = 0.303 nm³. Density = 1238 kg/m³. (From Ref. 20.)

Poly(hexamethylene adipamide) (PA 66) beta form. Space group $P1[C_1]$. $N = 2$. $a = 0.49$ nm; $b = 0.08$ nm; $c = 1.72$ nm; $\alpha = 90^\circ$; $\beta = 77.0^\circ$; and $\gamma = 67^\circ$. Cell volume = 0.602 nm³. Density = 1220 kg/m³. (From Ref. 20.)

38.6 POLYOXYMETHYLENE $[-CH_2-O-]$

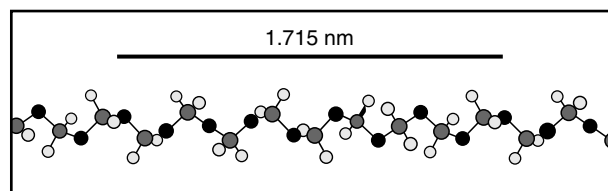


FIGURE 38.16. Polyoxymethylene.

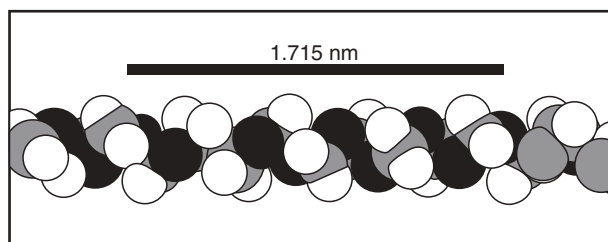


FIGURE 38.17. Polyoxymethylene.

TABLE 38.10. Polyoxymethylene [-CH₂-O-] trigonal. Space group P3₁ or P3₂ [C₃² or C₃³]; Z = 9[19]^a.

<i>hkl</i>	<i>d</i> -value (nm)	2θ (deg) (λ = 0.1542 nm)	Relative intensity
100	0.3872	22.97	vvs
105	0.2587	34.67	s
110	0.2236	40.34	s
113	0.2086	43.38	m
108	0.1895	48.00	m
115	0.1881	48.40	s
109	0.1729	52.96	m
205	0.1692	54.22	s
118	0.1558	59.29	m
208	0.1446	64.45	m

^a*a* = 0.4471 nm and *c* = 1.739 nm[†]. The repeat unit is close to 29/16 = 1.81 units/turn; 9/5 = 1.80 giving *c* = 1.739 nm which is approximate. Cell volume = 0.3011 nm³. Density = 1491 kg/m³.

^bBased on 9/5 helix (From Refs. 21–23).

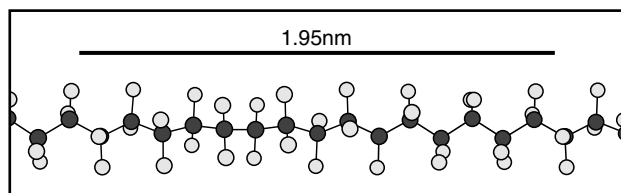
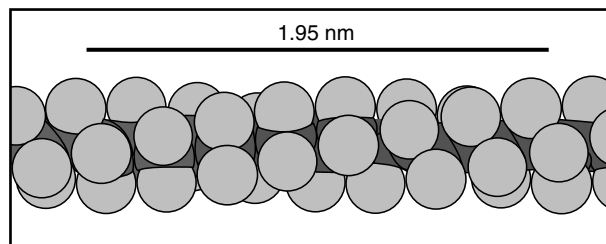
TABLE 38.11. Polyoxymethylene [-CH₂-O-] (orthorhombic). Space group P2₁2₁2₁[D₂²]^a.

<i>hkl</i>	<i>d</i> -value (nm)	2θ (deg) (λ = 0.1542 nm)	Relative intensity
020	0.3825	23.25	vs
111	0.2673	33.52	s
021	0.2606	34.41	s
201	0.1981	45.79	m
131	0.1901	47.84	m
331	0.1759	51.97	w
041	0.1685	54.46	w
132	0.1396	67.06	w
222	0.1337	70.45	w

^a*N* = 4[-CH₂-O-]. *a* = 0.477 nm; *b* = 0.765 nm; and *c* = 0.356 nm[†]. Cell volume = 1300 nm³. Density = 1540 kg/m³. (From Ref. 24.)

38.7 POLYTETRAFLUOROETHYLENE [-(CF₂)-]

Polytetrafluoroethylene [-(CF₂)-] Form I (above 30 °C). Space group (hexagonal packing of helical chains of variable twist). Hexagonal approximation *a* = 0.567 nm (35 °C) to 0.574 nm (218 °C). *c* = 0.1300 nm per CF₂ group[†]. Cell volume = 0.0362 – 0.0371 nm³ per CF₂ group. Density = 2290 – 2240 kg/m³. Diffuse pattern with sharp *hk0* reflections (hexagonal). (From Ref. 25.)

**FIGURE 38.18.** Polytetrafluoroethylene (Form IV).**FIGURE 38.19.** Polytetrafluoroethylene (Form IV).**TABLE 38.12.** Polytetrafluoroethylene [-(CF₂)-] Form II (below 19 °C). Observed *hk0* reflections^a.

<i>d</i> -value (nm)	2θ (deg) (λ = 0.1542 nm)	Relative intensity
0.4866	18.23	vvs
0.2823	31.69	vs
0.2447	36.73	s
0.2414	37.24	m
0.1850	49.26	m
0.1828	49.88	m
0.1627	56.58	m

^aSpace group (approximate) P1 [C₁¹] (Complex structure with a regular helix of 2.1598 CF₂ units per turn). Orthogonal approximation; *a* = 0.9649 nm; *b* = 0.5648; and *c* = 0.1300 nm per CF₂ group[†]. Cell volume = 0.03542 nm³ per CF₂ group. Density = 2340 kg/m³. (From Ref. 9.)

Polytetrafluoroethylene [-(CF₂)-] Form III (high pressure) Space group Pnam [D_{2h}¹⁶]. *a* = 0.75 nm; *b* = 0.56 nm; and *c* = 0.26 nm[†]. Cell volume = 0.1092 nm³. Density = 3040 kg/m³. Peaks attributed to a monoclinic phase are also observed. (From Ref. 27.)

TABLE 38.13. Polytetrafluoroethylene [-(CF₂)-] Form IV (19–30 °C)^a.

<i>hkl</i>	<i>d</i> -value (nm)	2θ (deg) (λ = 0.1542 nm)	Relative intensity
100	0.4902	18.10	vvs
110	0.2830	31.61	s
200	0.2451	36.67	s
210	0.1853	49.18	m
300	0.1634	56.30	m
220	0.1415	66.02	m
310	0.1359	69.09	m
107	0.2422	37.12	vs
108	0.2183	41.37	vs
117	0.1985	45.70	w
118	0.1847	49.34	w

^aSpace group (presumed) P3₁ or P3₂ [C₃² or C₃³]; Rotational disorder of helical chains. Z = 15(CF₂). *a* = 0.566 nm and *c* = 1.95 nm[†]. Cell volume = 0.0541 nm³. Density = 2302 kg/m³. (From Refs. 25, 26, 28 and 29.)

38.8 POLY(P-PHENYLENE TEREPHTHALAMIDE)
(PTTA) $[-(C=O)-(C_6H_4)-(C=O)-NH-(C_6H_4)-$
 $-(NH)-]$

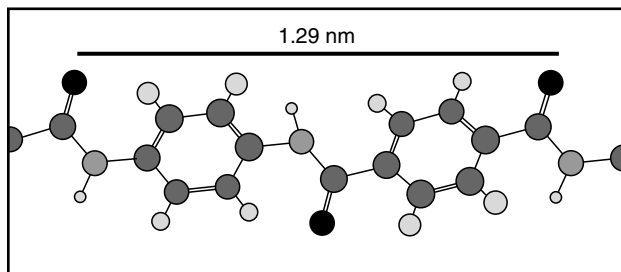


FIGURE 38.20. Poly(*p*-phenylene terephthalamide).

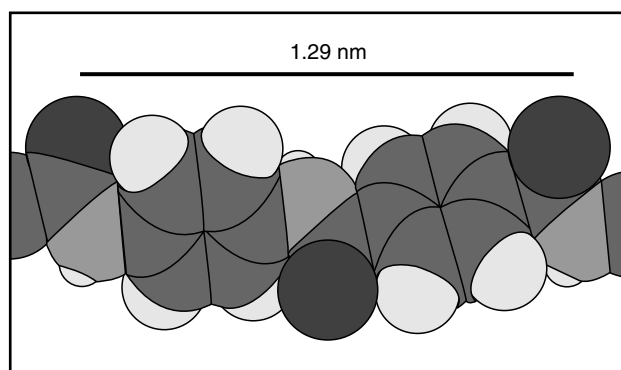


FIGURE 38.21. Poly (*p*-phenylene terephthalamide).

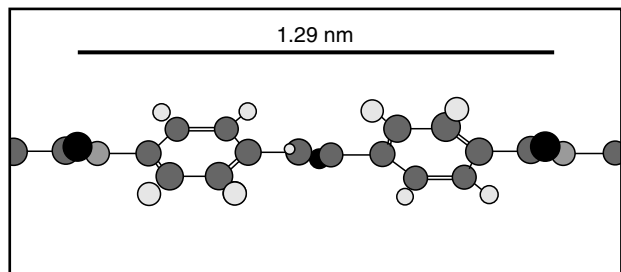


FIGURE 38.22. Poly (*p*-phenylene terephthalamide).

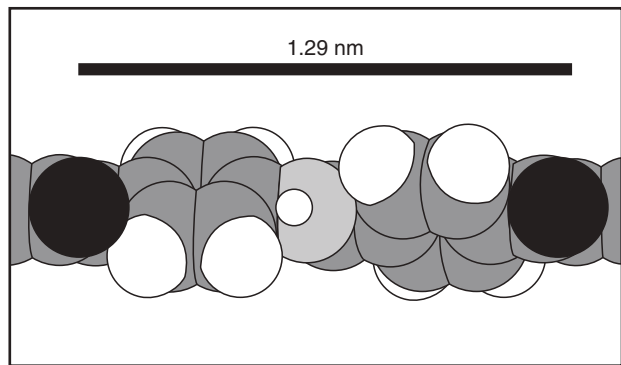


FIGURE 38.23. Poly (*p*-Phenylene terephthalamide).

TABLE 38.14. Poly (*p*-phenylene terephthalamide) (PPTA) $[-(C=O)-(C_6H_4)-(C=O)-(NH)-(C_6H_4)-(NH)-]$; Space group $P2_1/n[C_{2h}^5]$, Monoclinic (pseudo-orthorhombic)^a.

<i>hkl</i>	<i>d</i> -value (nm)	2θ (deg) (λ = 0.1542 nm)	Relative intensity
110	0.4327	20.53	vs
200	0.3935	22.60	vs
020	0.2590	34.63	vw
310	0.2340	38.46	m
220	0.2163	41.75	w
011	0.4807	18.46	vw
111	0.4102	21.66	ms
211	0.3045	29.33	s
021	0.2539	35.35	w
121	0.2417	37.20	vw
311	0.2303	39.12	vw

^a*N* = 2. *a* = 0.787 nm; *b* = 0.518 nm; and *c* = 1.29 nm[†].
 (γ = 90°) Cell volume = 0.5259 nm³. Density = 1504 kg/m³. (From Ref. 30.) (See also Ref. 31).

REFERENCES

- H. Tadokoro, in *Structure of Crystalline Polymers* (John Wiley & Sons, New York, 1979).
- W. R. Busing, *Macromolecules* **23**, 4608 (1990).
- C. W. Bunn, *Faraday Soc.* **35**, 482 (1939).
- M. Lorenzen and M. Hanfland, *Macromolecules* **36**, 6059 (2003).
- D. C. Bassett, S. Block, and J. Piermarini, *J. Appl. Phys.* **45**, 4146 (1974).
- M. Yasuniwa, R. Enoshita, and T. Takemura, *Jpn. J. Appl. Phys.* **15**, 1421 (1976).
- T. Seto, T. Hara, and K. Tanaka, *Jpn. J. Appl. Phys.* **7**, 31 (1968).
- G. Natta and P. Corradini, *Nuovo Cimento, Supplement* **15**, 40–51 (1960).
- S. V. Meille, D. R. Ferro, S. Brückner, *et al.* *Macromolecules* **27**, 2615 (1994).
- S. V. Meille, S. Brückner, and W. Porzio, *Macromolecules* **23**, 4114 (1990).
- B. Lotz, S. Graf, and J. C. Whitmann, *J. Polym. Sci.* **B24**, 2017 (1986).
- D. C. De Rosa, F. Auriemma, and P. Corradini, *Macromolecules* **29**, 7452 (1996).
- R. de P. Daubeney, C. W. Bunn, and C. J. Brown, *Proc. R. Soc. London* **226A**, 531 (1954).
- H. G. Killian, H. Halboth, and E. Jenkel, *Kolloid-Zeitschrift* **172**, 166 (1960).
- Y. Fu, W. R. Busing, Y. Jin, *et al.* *Macromolecules* **26**, 2187 (1993).
- D. R. Holmes, C. W. Bunn, and D. J. Smith, *J. Polym. Sci.* **27**, 159 (1955).
- P. Simon and Gy. Argay, *J. Polym. Sci. Polym. Phys. Ed.* **16**, 935 (1978).
- C. J. Parker and P. H. Lindenmeyer, *J. Appl. Polym. Sci.* **21**, 821 (1977).
- H. Arimoto, *J. Polym. Sci.* **A2**, 2283 (1964).
- C. W. Bunn and E. V. Garner, *Proc. R. Soc.* **A189**, 39 (1947).
- Y. Takahashi and H. Tadokoro, *J. Polym. Sci., Polym. Phys.* **17**, 537 (1979).
- G. A. Carazzolo, *J. Polym. Sci.* **A1**, 1573 (1963).
- R. Aich and P. C. Hägele, *Prog. Colloid Polym. Sci.* **71**, 86 (1985).
- G. A. Carazzolo and M. Mammì, *J. Polym. Sci.* **A1**, 965 (1963).
- E. S. Clark and L. T. Muus, *Z. Kristallogr.* **117**, 2/3 119 (1962).
- J. J. Weeks, E. S. Clark, and R. K. Eby, *Polymer* **22**, 1480 (1981).
- R. K. Eby, E. S. Clark, B. L. Farmer, *et al.* *Polymer* **31**, 2227 (1990).
- E. S. Clark, *J. Macromol. Sci. Phys.* **B1**, 795 (1967).
- M. Kimmig, G. Strobl, and B. Stühn, *Macromolecules* **27**, 2481 (1994).
- M. G. Northolt, *Eur. Polym. J.* **10**, 799 (1974).
- M. G. Northolt and H. A. Stuu, *J. Polym. Sci., Polym. Phys.*, **16**, 939 (1978).

CHAPTER 39

Crystallization Kinetics of Polymers

Rahul Patki*, Khaled Mezghani[†], and Paul J. Phillips*

*Department of Chemical and Materials Engineering, University of Cincinnati, Cincinnati, OH 45221-0012

[†]Department of Mechanical Engineering, King Fahd University of Petroleum and Minerals, Dhahran 31261, Saudi Arabia

39.1 Introduction	625
References	640

39.1 INTRODUCTION

39.1.1 Crystallization Studies and Analyses

There are several methods for studying crystallization kinetics of polymers, which fall into two general categories: bulk or volumetric analysis, and crystal growth analysis. The simplest experimental study is the bulk growth, but it is the most difficult to analyze in detail. However, it can be analyzed partially using the Avrami equation [1,2].

The Avrami equation was derived from prior work by Poisson based on expanding waves created by raindrops on a pond and results in the general equation:

$$1 - v_c(t) = \exp(-Kt^n), \quad (39.1)$$

where n is known as the Avrami index and $v_c(t)$ is the crystalline volume fraction of the polymer. In general, n and K characterize the nucleation type and the crystal growth geometry. Theoretically, the Avrami index, n , can be derived as an integer which varies between 1 and 6 (Table 39.1), but due to the crystallization complexity, n is usually a decimal number. For better interpretation of the Avrami index, one needs good information about nucleation, morphology, and the mechanism of polymer crystallization.

There are several methods available for the study of bulk crystallization, including dilatometry, differential scanning calorimetry, and x-ray diffraction. Optical microscopy is the most versatile method for the study of crystallization since the use of a trinocular permits the simultaneous measurement of bulk crystallization (using transmitted light intensity) and of crystal growth kinetics using direct observation.

Depolarized light microscopy, DLM, can be used to measure light intensity (I) as a function of time (t) and

permits Avrami type analyses. From this type of experiment the volume fraction, $v_c(t)$, is not directly available; therefore, a relationship between the light intensity, I , and $v_c(t)$ is needed. If it is assumed that complete crystallization is reached at the maximum level of the plot (I versus t) then $v_c(t)$ is related to I as follows:

$$v_c(t) = I(t) = \frac{I - I_{\min}}{I_{\max} - I_{\min}}, \quad (39.2)$$

where $I(t)$ is the relative intensity at time t , and I_{\min} and I_{\max} are the minimum and maximum intensities, respectively. Equation (39.1) can be written in a logarithmic form as:

$$1n[-1n(1 - I(t))] = 1n(K) + n1n(t). \quad (39.3)$$

The values of n and K can be determined from the plot of $1n[-1n(1 - I(t))]$ versus $1n(t)$; n is the slope, and $1n(K)$ is the intercept.

In reality, polymer crystallization is too complex to be described by a simple expression such as the Avrami equation. For example, the assumption in Avrami's expression that the volume does not change is inaccurate because the specimen tends to shrink during crystallization. In addition, secondary crystallization and crystal perfecting processes are not taken into account.

There have been many attempts to develop theories to explain the important aspects of crystallization [3,4]. The most widely accepted approach to the analysis of the linear crystal growth rates is the kinetic description due to Lauritzen and Hoffman [3]. There are alternative approaches which will not be considered here since this is not meant to be a comprehensive review chapter of theoretical approaches.

TABLE 39.1. Theoretical values of n and K for different morphologies and nucleation mechanisms.

Crystal growth shape	Nucleation mode	Avrami exponent (n)	Avrami constant (K) ^a
Rod	Heterogeneous ^b	1	NGA
	Homogeneous ^c	2	$\dot{N}GA/2$
Disc	Heterogeneous	2	πNG^2D
	Homogeneous	3	$(\pi/3)\dot{N}G^2D$
Sphere	Heterogeneous	3	$(4\pi/3)NG^3$
	Homogeneous	4	$(\pi/3)\dot{N}G^3$
Sheaf	Heterogeneous	5	—
	Homogeneous	6	—

^a A is cross-sectional area of the rod; D is thickness of the disc; G is linear growth rate; N is nucleation density; and \dot{N} is nucleation rate.

^bHeterogeneous means that the nucleation density is constant.

^cHomogeneous, also named sporadic, means that the rate of nucleation is constant.

The general expression of crystal growth as described by Lauritzen and Hoffman is:

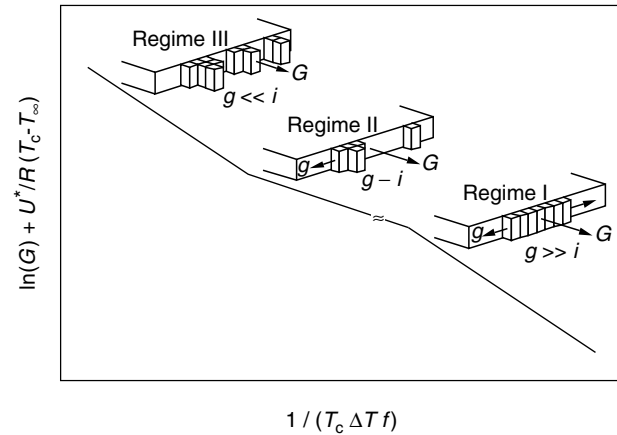
$$G = G_0 \exp\left(-\frac{U^*}{R(T_c - T_\infty)}\right) \exp\left(-\frac{K_g}{T_c \Delta T f}\right), \quad (39.4)$$

where G is the growth rate, G_0 is the growth rate constant; U^* is the activation energy for polymer diffusion; R is the gas constant; T_c is the crystallization temperature (K); $T_\infty = T_g - 30$ (K); $\Delta T =$ supercooling, $(T_m^0 - T_c)$; $f =$ correction factor, $2T_c/T_c + T_m^0$; K_g is the nucleation rate constant given by

$$K_g = \frac{j b_0 \sigma \sigma_e T_m^0}{k \Delta h_f}, \quad (39.5)$$

where b_0 is the width of the chain, σ is the lateral surface free energy, σ_e is the fold surface free energy, T_m^0 is the equilibrium melting temperature (K), $k =$ Boltzmann constant, and Δh_f is the heat of fusion. The parameter j is determined by the operating regime (see below) and is equal to 4 for regime I and III, and equal to 2 for regime II.

The Lauritzen–Hoffman theory analyzes the growth data according to competition between the rate of deposition of secondary nuclei (i) and the rate of lateral surface spreading (g), resulting in three different regimes (Fig. 39.1). Regime I occurs when $i \ll g$ and may be found at very low supercoolings; in regime II i is the order of g and occurs at moderate supercoolings; in regime III $i > g$ and is found at very high supercoolings. Regime behavior varies from polymer to polymer. For example *cis*-polyisoprene shows all regimes [5]. Until recently it was believed that polyethylene

**FIGURE 39.1.** Schematic of regime analyses.

when crystallized shows regime I and II [6,7], whereas polypropylene shows regime II and III [7–10]. Also the regimes depend on the conditions of crystallization, for example at atmospheric pressure high molecular weight polypropylene shows regime II and III; whereas the same material shows all regimes at 150 MPa [7]. An evaluation of data in terms of regime assignment for many common polymers was published by Lovinger *et al.* [11].

It has been known for many years that an increase in molecular weight results in a decrease in growth rate for unfractionated polymers [12–15]; however, definitive data is available for few commercially significant polymers. A thorough understanding of molecular weight effects requires a detailed evaluation of fractions. Few such studies are available.

The effects of molecular weight and fractionation on the growth of polymers have been analyzed and discussed in terms of the molecular reptation concept by Hoffman and Miller [16]. In their studies of different molecular weights of polyethylene, they determined the dependence of the crystal growth rate on molecular weight at constant supercooling. The concept of reptation, which was first proposed by De Gennes [17], states that the overall friction coefficient of a linear polymer chain in the melt is proportional to its length.

In the analysis of 11 polyethylene samples (M varies from 23,000 to 203,000), high molecular weight fractions exhibit lower growth rates in both regimes I and II. According to Hoffman and Miller, this observation is solely due to molecular friction being proportional to its length.

More recent studies using newer techniques for attaining high degrees of supercooling have demonstrated that all three regimes can be observed in linear polyethylene [18, 19], both an NBS standard and an unfractionated linear polymer (see Fig. 39.2).

Similarly, in the case of polypropylene, Cheng *et al.* [10] showed that the growth rate of low molecular weight isotactic polypropylene ($M_w = 15,000$) is higher than that of a high molecular fraction ($M_w = 300,000$) at the same supercooling.

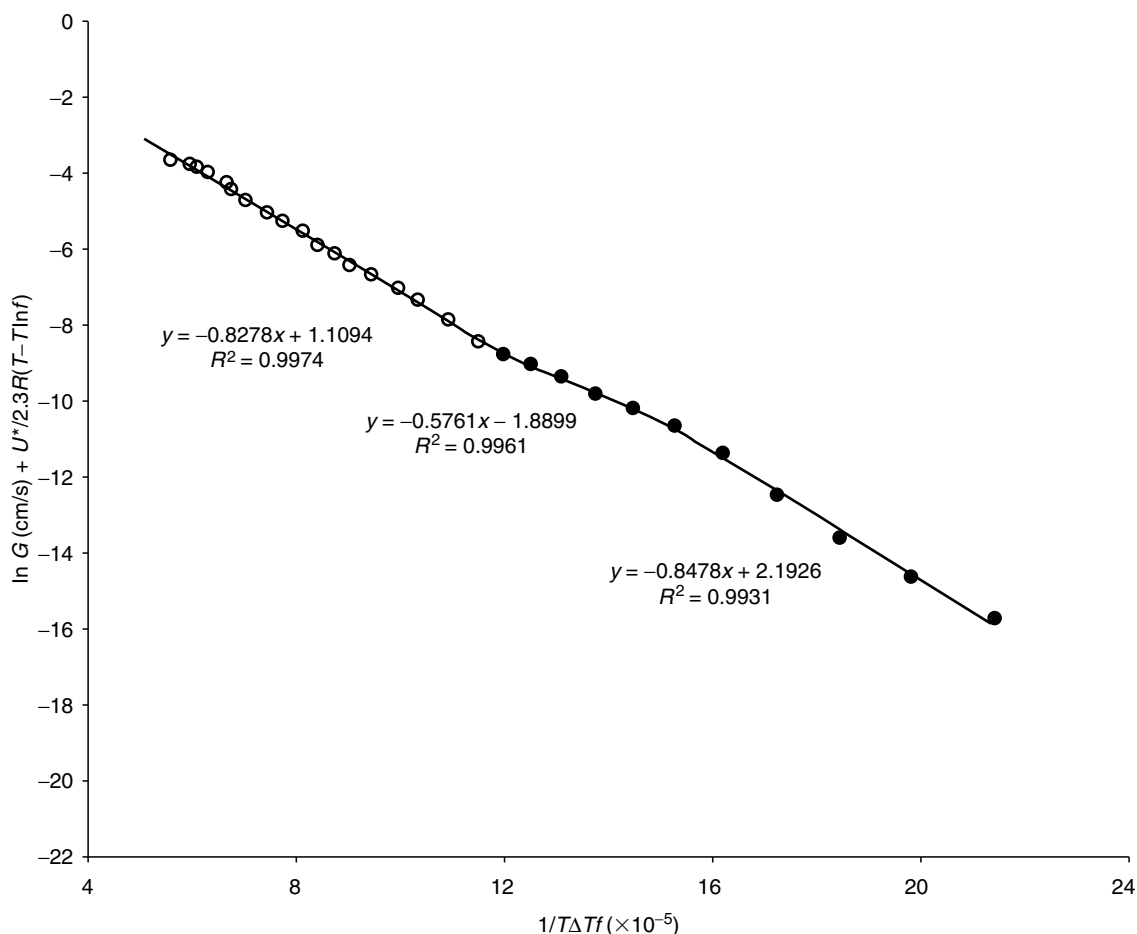


FIGURE 39.2. Secondary nucleation plot for linear polyethylene (isothermal data-filled symbols; rapid cooling data-open symbols). Reproduced from [Polymer] (2001) [19] with permission from Elsevier.

However, the reptation model is not applicable in the cases of crystallization from dilute or concentrated solutions, because in these cases considerable lateral molecular motion is possible. Nevertheless, it should be noted that regime changes have been detected in the growth of single crystals from solution [20]. Similarly, the crystallization of a polymer fraction with a large amount of noncrystallizable low molecular weight material, which is rejected at the growth front, acts like the one from concentrated solution rather than from a fully interentangled melt [21–23].

When copolymers are considered, the situation becomes very complex and depends on whether or not the comonomer units are rejected, partially or fully, from the crystal [7,24–26]. The dependences observed are controlled not only by the degree of rejection, but also by the sequence length distribution of crystallizable units. For most systems studied so far, rejection of comonomer units tends to be prevalent resulting in a decrease in growth rate. This decrease is regarded as caused primarily by the probability of formation of a critical nucleus. Systems that have been thoroughly studied so far show an inverse logarithmic dependence of growth rate on the mole fraction of impurity

units [25,26]. It is also recognized that comonomer content and molecular weight interact in the determination of the behavior of any particular system. Because of the complex, and often ill-defined, dependences found in copolymers, data are not presented in the tabulations, except for a couple of cases chosen as examples of more general principles.

The subject of the crystallization of copolymers can be quite complex, dependent on the comonomer. It should also be recognized that the effects of variations in tacticity are very similar to the effects of comonomer inclusion, since both are effectively the insertion of defects into the polymer chain. The earliest treatment [26] recognized this fact, and is applicable to any defect, whether tactic, head-to-head link or comonomer, when measured as a defect content. This approach makes the assumption that all defects are excluded from the crystal. On this basis the probability of forming a critical secondary nucleus is dependent on the distribution of the defects throughout the polymer chain. The formulation of the probabilities leads to the logarithm of the rate of linear growth of a spherulite being dependent on the defect concentration. In practice, the behavior of most copolymers

follows this prediction fairly well, the rate dropping by orders of magnitude for inclusion of a few percent defects.

Data are presented for a series of copolymers of ethylene and octene, in which the evidence suggests that defect exclusion dominates the behavior (see Fig. 39.3). Note the orders of magnitude drop in crystal growth rates with increasing defect content. An unusual observation, currently not understood fully, is that the growth rates at very high supercoolings for the linear polymer and the copolymers merge, indicating a lack of selectivity at cooling rates consistent with industrial operations [19].

For isotactic polymers and copolymers the behavior is complex and depends on the method of synthesis and the types of defects that result. For instance, isotactic polypropylene synthesized using Zeigler–Natta catalysts has a quite different defect content from the same polymer synthesized

using single site catalysts. In the ZN case the defects are primarily syndiotactic units, but in the SSC case they are predominantly head-to-head links. The latter result in methylene diads. Syndiotactic defects are excluded from the crystal in the normal manner. When ethylene is copolymerized into propylene the methylene sequence is lengthened, but ethylene can be incorporated into the crystal. So the situation becomes quite complex and it becomes necessary to carry out a thorough chemical analysis of the copolymer. This has rarely been done in the literature. The subject has been explored thoroughly by Alamo and coworkers [27–30], but without studies of linear growth rates. Some data is presented of recent work of DiMeska and Phillips [31], which does contain linear growth rate regime analyses. One of the major complications of polypropylene is that the defect content encourages the formation of the

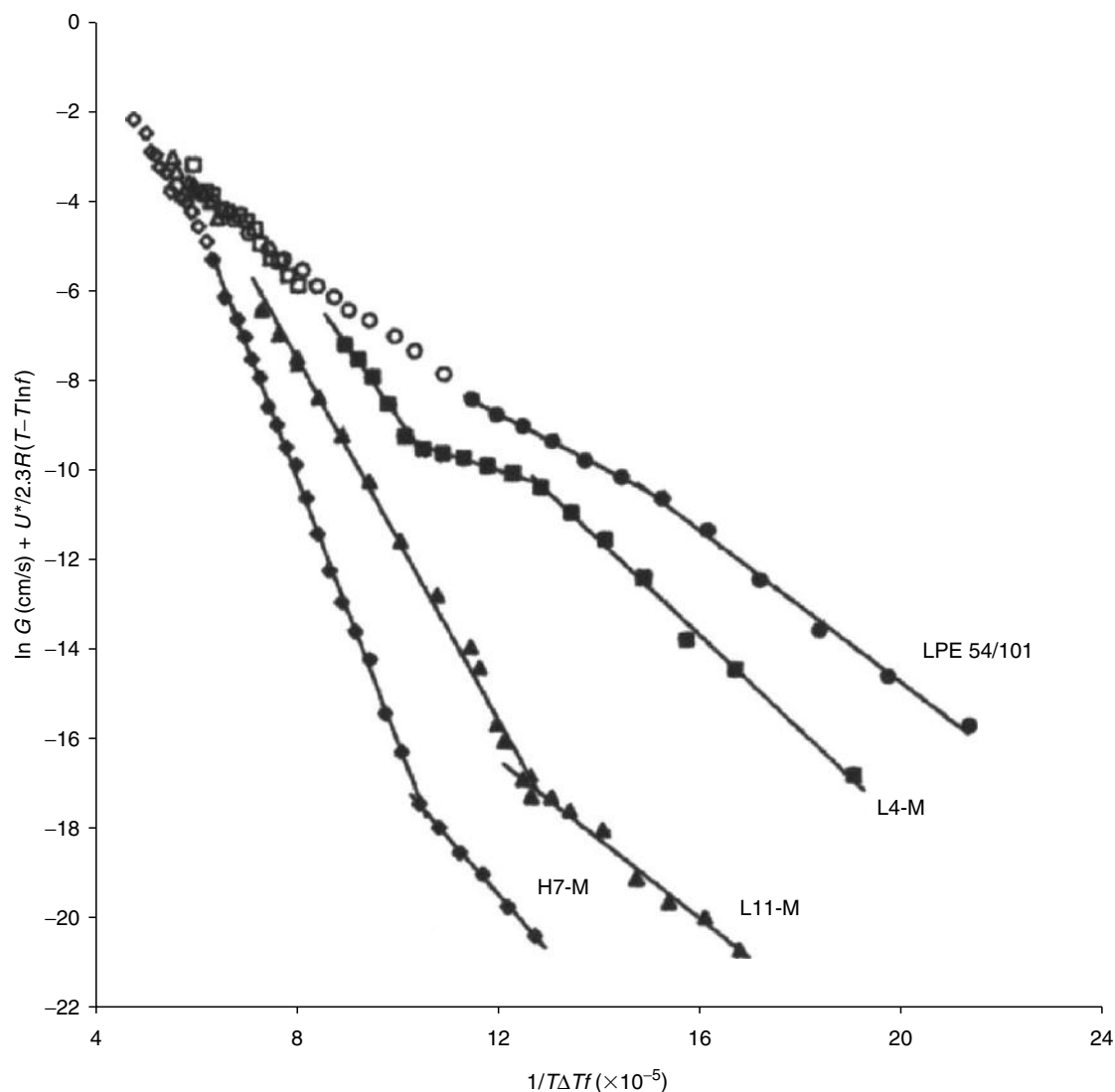


FIGURE 39.3. Secondary nucleation plot for linear polyethylene (LPE) and ethylene–octene copolymers (isothermal data-filled symbols; rapid cooling data-open symbols). For copolymers, L and H indicated low and high MW, respectively, and the number following the letters represents the number of hexyl side chains per 1,000 carbon atoms. Reproduced from [Polymer] (2001) [19] with permission from Elsevier.

γ -phase, at the expense of the commonly encountered α -phase.

For further information on current thinking and theoretical approaches to crystallization, the reader is referred to recent reviews by Phillips [32,33].

39.1.2 Case Study Using Isotactic Polypropylene

Figure 39.4 shows several chart recorded bulk crystallization traces as a function of temperatures for isotactic polypropylene (iPP, $M_w = 257,000$). Avrami's analysis takes the lower values of each plot; i.e., before impingement. The half-time is the point where half of the intensity is reached. Figure 39.5 presents Avrami's analysis for different crystallization temperatures, where it can be seen that all plots have similar slope, n , and different intercepts, k , in this case.

Examples of the change in spherulite radius with time for selected temperatures are shown in Fig. 39.6, where it can be seen that linear growth rates result. Plots of growth rate versus temperature for iPP can be seen in Fig. 39.7. When the data are analyzed using the Hoffman–Lauritzen equation, Fig. 39.8, it is seen that iPP shows the Regime II–Regime III transition, previously identified by several groups of workers [7–10]. In these analyses the values of T_m^0 and U^* were 186.1 °C and 1,500 cal/mol, respectively.

The effects of different values of the thermodynamic variables on the analyses and on the regime transition tem-

perature have been explored. Variation in T_m^0 has the greatest effect on the shape of the secondary nucleation plot, but does not significantly alter the regime transition temperature. A small change of the values of U^* and T_g simply causes the curve to move up or down without changing its shape.

The Regime II–III transition is envisioned as the point at which the rate of surface spreading becomes less than the rate of secondary nucleation. Surface spreading, for an adjacent reentry system, is essentially a reeling-in process dependent on the reptational ability of the polymer chain.

The slopes of the secondary nucleation plots can be used to estimate the fold surface free energies of the two polymers. In order for these calculations to be carried out it is necessary to have estimates of the parameters which appear within Eq. 39.5. The equilibrium melting point has to be determined in separate experimentation (see Chapter 11).

The values of $\sigma\sigma_e$ can be determined from the slope of the lines. Regime II and regime III give $\sigma\sigma_e = 562$ and $678 \text{ erg}^2/\text{cm}^4$, respectively. In order to proceed further it is necessary to estimate σ independently. One way to do this is to use the Hoffman modification of the Thomas–Stavely relation [24].

$$\sigma = 0.1\Delta h_f \sqrt{a_0 b_0}. \quad (39.6)$$

Values of σ have been calculated as $11.5 \text{ erg}/\text{cm}^2$ for iPP. Substitution of these values into the determined values of

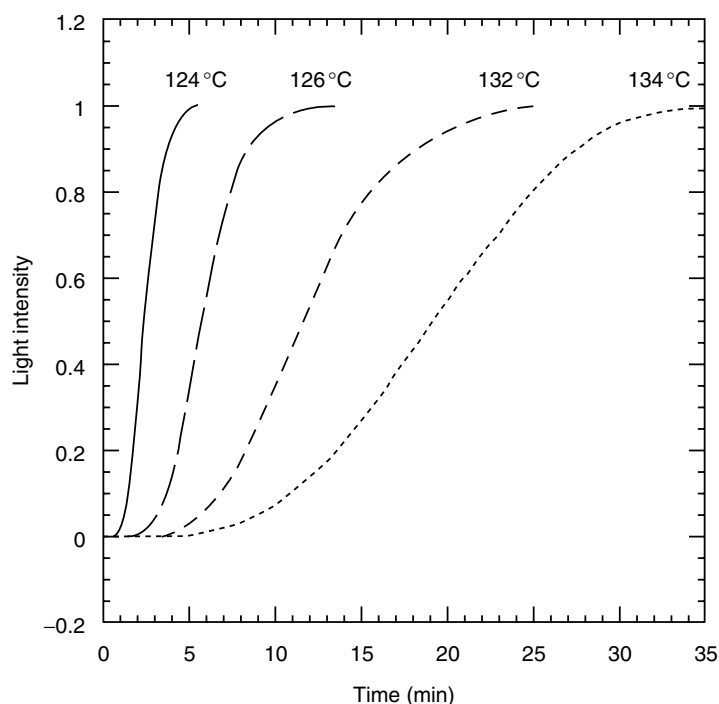


FIGURE 39.4. Isothermal bulk crystallization traces as a function of temperature.

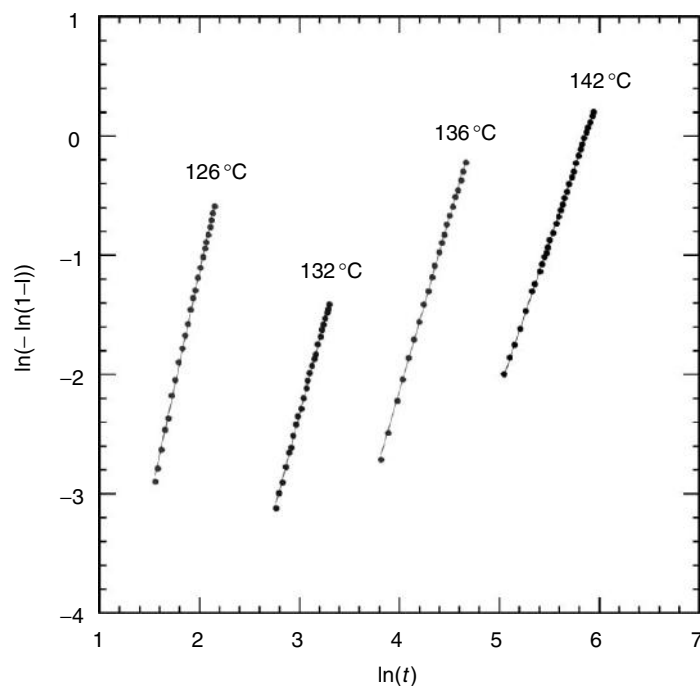


FIGURE 39.5. Avrami analyses for different crystallization temperatures.

$\sigma\sigma_e$ results in values of σ_e for regime II and regime III of 48.9 and 59.0 erg/cm², respectively.

The work done by the chain (q) to form a fold can be easily calculated from the following equation, when the fold surface energy is known.

$$q = 2a_0b_0\sigma_e \quad (39.7)$$

39.1.3 Tabulation of Data

In the tabulation, data are presented mainly for common homopolymers. When available, molecular weights are also given, but no major attempt has been made to present molecular weight dependencies. Additionally, a few illustrations of specific copolymers have been included as examples of copolymer behavior.

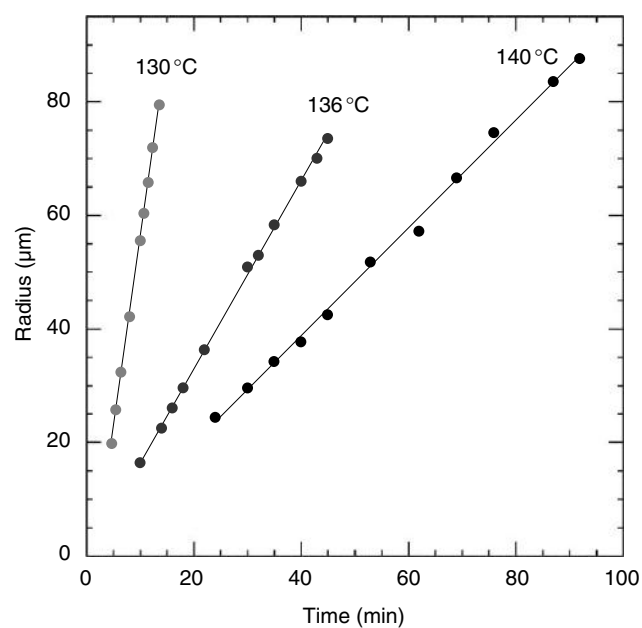


FIGURE 39.6. Spherulitic growth of iPP as a function of time for different isothermal crystallization temperatures.

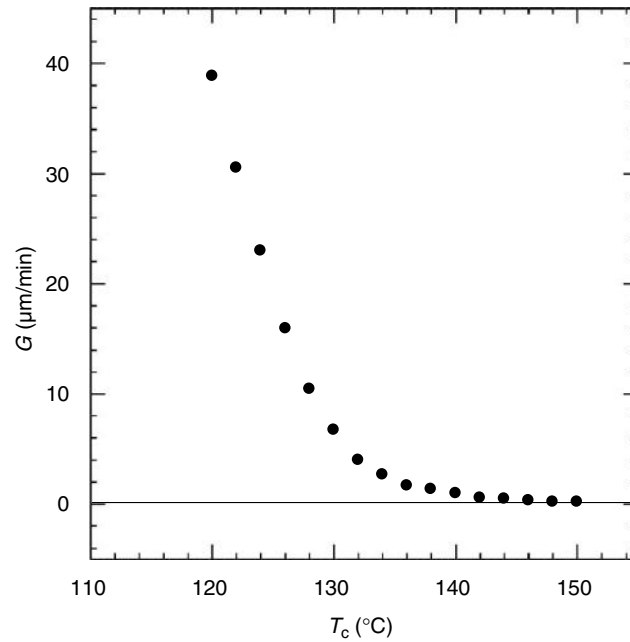


FIGURE 39.7. Growth rates of iPP versus crystallization temperature.

It should be recognized that Avrami data can vary greatly with the presence of additives, especially nucleating agents.

In Table 39.2 data are presented from bulk crystallization studies of common polymers.

In Table 39.3 data are presented from linear growth rate studies of polymers that are commonly encountered

in significant basic studies or that are of commercial significance. In addition to the values of the characteristic parameters obtained from the analyses, we have added the value of other constants such as equilibrium melting points and heats of fusion which are essential to the analyses.

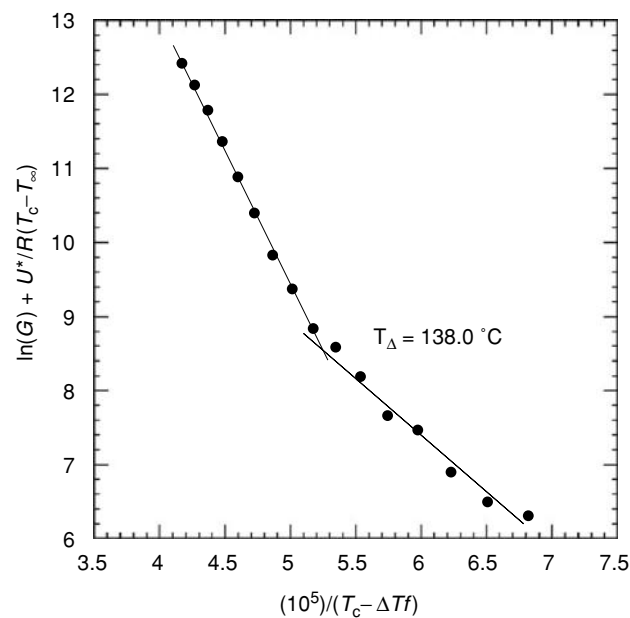


FIGURE 39.8. Secondary nucleation analyses of iPP using T_m^0 of 186.1 °C.

TABLE 39.2. Avrami coefficients.

Polymer		M_n (kg/mol)	M_w (kg/mol)	T_c (°C)	$t_{1/2}$ (s)	n	k (s ⁻ⁿ)	Remarks	Ref.	
Poly (amide)	Nylon 6	16.0	29.0	194.8	43	2.5		DSC	[34]	
				197.4	75	2.9				
				200.4	110	3.6				
				202.6	200	4.0				
				205.5	350	4.8				
	Nylon 10 12				140	10	3		DSC	[36]
					160	15	3			
					180	70	3			
					200	950	3			
	Nylon 11				165	46.2	2.21	(min ⁻ⁿ)	DSC	[37]
					167	68.4	1.97	1.34×10^{-4}		
					169	144.6	1.91	1.54×10^{-4}		
171					241.8	1.91	5.37×10^{-5}			
173					450	2.08	1.90×10^{-5}			
Nylon 12 12				164	10.3	1.6	(min ⁻ⁿ)	DSC	[38]	
				166	16.5	2.1	1.23×10^1			
				168	23.1	2.4	1.0×10^1			
				170	43.8	2.7	6.92			
				172	85.8	3.2	1.62			
Poly (butene-1)	PB-1	73	750	160	34.8	2.03	(min ⁻ⁿ)	DSC	[39]	
				164	63.6	1.67	2.12			
				168	119.4	1.68	6.2×10^{-1}			
				170	231.6	1.64	2.2×10^{-1}			
							8.0×10^{-2}			
Poly (ε-caprolactone)	PCL	43.6	48	70	60			DLM	[40]	
				80	96					
				90	456					
				95	1572					
Poly (chlorotri-fluoroethylene)	PCTFE			40	4.5	3.46		Dilatometry	[41]	
				45	17.9	3.35				
				47	45.8	2.48				
				49	97.6	2.66				
Polyethylene	HDPE			180	180	3		DSC	[42]	
				186	480	3				
				191	1500	3				
				196	4200	3				
Polyethylene	XLPE cross-link 255 avg CH ₂ units	4.5	8.7	117	0.24	3.1		DLM	[43]	
				119	0.67	2.9				
				121	4.00	3.0				
				123	20.00	2.7				
				124						

TABLE 39.2. Continued.

Polymer		M_n (kg/mol)	M_w (kg/mol)	T_c (°C)	$t_{1/2}$ (s)	n	k (s^{-n})	Remarks	Ref.	
Poly (aryl-ether-ether-ketone)	PEEK			175.2		4.7	1.6×10^{-8}	DSC	[44]	
				182.3		5.7	4.7×10^{-10}			
				188.8		5.1	1.8×10^{-7}			
Poly (ethylene-terephthalate)	PET	19	40	180		2.36	(min^{-n})	DSC	[45]	
				190		2.30	1.02×10^{-2}			
				200		2.43	7.43×10^{-3}			
				210		2.37	2.04×10^{-3}			
					190	63	1.83		DSC	[46]
					195	86	1.76			
					200	133	1.77			
210	190	1.76								
Poly (propylene-terephthalate)	PPT	36.3	78.4	185	150	2.61	1.52×10^{-6}	DSC	[47]	
				190	250	2.59	4.03×10^{-7}			
				195	500	2.61	6.51×10^{-8}			
				200	1,000	2.48	2.42×10^{-8}			
Poly (butylene-terephthalate)	PBT	36.6	77.4	180	50 75	2.47	5.61×10^{-5}	DSC	[47]	
				185	150	2.49	1.65×10^{-5}			
				190	340	2.48	2.74×10^{-6}			
				195		2.55	2.79×10^{-7}			
Poly (trimethylene-terephthalate)	PTT	43		170		2.3	(min^{-n})	DSC	[48]	
				180		2.6 3.0	7.9			
				190		2.9 3.2	3.67			
				200			0.43			
	210			9.96×10^{-3}						
			21.05	46.3	202	174	2.81	(min^{-n})	DSC	[49]
					206	279	2.72	33.7×10^{-3}		
					210	592	2.84	10.8×10^{-3}		
							1.0×10^{-3}			
Poly (isoprene)	<i>cis</i> -PIP			-38	23,400				[50]	
				-33	1,440				[51]	
				-22	9,000				[52]	
				-16	12,000					
				-11	19,800					
	-5	55,200								
	<i>trans</i> -PIP			35	768					
				40	1,260					
				45	6,780					
				51	31,800					
				57	2,91,000					
Poly (oxyethylene)	POE	9.0	9.6	40.1		1.9	0.18×10^1	DSC	[53]	
				43.4		2.0	6.8×10^{-1}			
				48.4		2.3	2.6×10^{-2}			
				49.6		2.1	8.3×10^{-4}			
			20		55	612	1.8		DSC	[54]
					56	1,200	1.9			
					57	1,476	2.0			
					58	4,884	2.1			
					59	6,900	2.5			

TABLE 39.2. Continued.

Polymer		M_n (kg/mol)	M_w (kg/mol)	T_c (°C)	$t_{1/2}$ (s)	n	k (s ⁻ⁿ)	Remarks	Ref.		
Poly (oxypropylene)	POP		300	40.3	1,650	3.0		DLM	[55]		
				42.8	2,520	3.1					
				45.5	3,540	3.3					
				47.5	8,580	3.0					
				49.7	12,600	3.1					
Poly (phenylene sulfide)	PPS			230	160	1.84		DSC	[56]		
				235	195	2.14					
				240	370	2.12					
				245	580	2.08					
Polypropylene	iPP	58.0	151	130	430	3.11	1.29×10^{-3}	DLM	[57]		
				132	650	2.61	7.59×10^{-4}				
				136	3,200	2.84	1.41×10^{-4}				
				142	13,500	2.91	1.15×10^{-5}				
					447	130	780	3.1		DLM	[58]
						133	2,220	2.9			
						134	2,820	2.9			
						137	6,600	2.9			
Polypropylene	sPP	76.2	165	60	100	2.68	1.06×10^1	DSC	[59]		
				70	118	2.68	6.66				
				80	210	3.07	8.82×10^{-1}				
				90	684	2.96	3.11×10^{-2}				
				95	1,698	2.41	1.33×10^{-2}				
				52.3	195	75	56	2.44	4.72×10^1	DSC	[59]
						80	100	2.33	1.24×10^1		
						90	439	2.40	3.43×10^{-1}		
						95	1,294	2.32	3.40×10^{-2}		
Selenium				80	32,400	2.01	1.05×10^{-2}	dynamic density	[60]		
				100	3,600	1.68	0.61×10^1				
				120	720	3.28	1.20×10^2				
				140	280	3.68	3.60×10^4				
				160	105	4.00	2.60×10^6				
Poly (oxymethylene)	POM			148	163.2	2.67	4.16×10^{-2}	DSC	[61]		
				149	316.2	2.59	9.48×10^{-2}				
				150	607.8	2.36	3.17×10^{-3}				
				151	1,141.2	2.98	1.08×10^{-4}				
Poly (tetrafluoro- ethylene)	PTFE			296	0.057	0.96	1.21×10^1	DSC	[62]		
				304	0.116	1.01	5.97				
				312	0.332	1.006	2.09				
				315	0.301	0.87	1.97				
Polystyrene	sPS	91.6	220	236	16.73	1.9	4.76×10^2	DSC	[63]		
				239	50.21	1.4	5.29×10^1				
				242	96.33	1.3	2.26×10^1				
				244	135.14	1.1	1.60×10^1				
Poly (arylene-ether- ether-phenylsulfide)		34		192	2,400	2.73	(min ⁻ⁿ) 3.05×10^{-7}	DSC	[64]		
				200	4,800	2.8	4.13×10^{-8}				
				211	30,000	2.8	9.23×10^{-9}				
				218	60,000	2.73	2.27×10^{-9}				
				226	600,000	2.73	1.69×10^{-10}				

TABLE 39.2. Continued.

Polymer		M_n (kg/mol)	M_w (kg/mol)	T_c (°C)	$t_{1/2}$ (s)	n	k (s ⁻ⁿ)	Remarks	Ref.
Poly (arylene- ether-ether- biphenylsulfide)		19.1		279	5,400	1.7	(min ⁻ⁿ) 2.75 × 10 ⁻⁵	DSC	[64]
				285	30,000	1.7	1.01 × 10 ⁻⁵		
				290	48,000	1.9	1.37 × 10 ⁻⁶		
Poly (ester-amide)				110	19.2	2.52	6.25 × 10 ⁻⁴	DSC	[65]
				120	91.8	3.06	0.8 × 10 ⁻⁶		
				130	2,124	2.71	7.4 × 10 ⁻¹⁰		
				135	3,180	2.20	1.31 × 10 ⁻⁸		
Poly (butylene adipate)	PBA	7.3		29	18	3.1	8.9 × 10 ⁻⁵	DSC	[66]
				35	42	2.6	4.2 × 10 ⁻⁵		
				40	180	3.0	1.2 × 10 ⁻⁷		
				43	486	3.1	3.3 × 10 ⁻⁹		
				45	1,156	3.1	45 × 10 ⁻¹⁰		
Poly (butylene isophthalate)	PBIP	13		70.2	1272	2.9	6.9 × 10 ⁻¹⁰	DSC	[66]
				80.2	630	2.9	5.3 × 10 ⁻⁹		
				90.2	498	2.8	1.9 × 10 ⁻⁸		
				100.2	456	3.0	7.3 × 10 ⁻⁹		
				109.7	672	3.0	2.3 × 10 ⁻⁹		
				118.7	1,068	3.1	2.8 × 10 ⁻¹⁰		
				123.7	1,590	2.9	3.6 × 10 ⁻¹⁰		
Poly (ethylene naphthalate)	PEN			180	408	2.4	(min ⁻ⁿ) 7.1 × 10 ⁻³	(DSC)	[67]
				190	270	2.9	8.6 × 10 ⁻³		
				200	174	2.7	3.8 × 10 ⁻²		
				210	186	3.2	2.0 × 10 ⁻²		
				220	204	3.1	1.6 × 10 ⁻²		
				230	384	2.3	9.2 × 10 ⁻³		
Polyimide*				240	1,507	2.39		(DSC)	[68]
				260	600	2.37			
				280	444	2.3			
				300	600	2.32			
				320	1,197				
Poly (vinylidene fluoride)	PVDF	170		147	192	2.9	(min ⁻ⁿ) 1.88 × 10 ⁻²	(DSC)	[69]
				151	720	2.9	3.12 × 10 ⁻⁴		
				153	960	3.1	1.28 × 10 ⁻⁴		
				155	1,800	2.9	1.83 × 10 ⁻⁵		
1, 2-Syndiotactic Polybutadiene	1, 2-sPB			176	97.8	3.2	(min ⁻ⁿ) 1.45 × 10 ⁻¹	(DSC)	[70]
				177	126	2.8	8.68 × 10 ⁻²		
				178	169.2	3.0	3.09 × 10 ⁻²		
				179	223.8	2.8	1.74 × 10 ⁻²		
				180	358.2	2.9	3.9 × 10 ⁻³		

*Polyimide synthesized from 3, 3', 4, 4'-benzophenonetetracarboxylic dianhydride (BTDA) and 2, 2-dimethyl-1, 3-(4-amino-phenoxy) propane (DMDA).

TABLE 39.3. Growth kinetics coefficients.

Polymer	M_n (kg/mol)	M_w kg/mol	T_g (°C)	T_m (°C)	ΔH_f (J/g)	Growth face	a_0 (Å)	b_0 (Å)	U^* (cal/mol)	Regime	T_n (°C)	G_0 (cm/s)	$K_g/10^5$ (K ²)	σ (erg/cm ²)	σ_e (erg/cm ²)	q (kcal/mol)	Ref.
Poly(amide)			30	232.0			4.78	3.70	1,430			0.65×10^1	1.74		118	6.0	[71]
	Nylon 6	24.7	-10	230	10.8 (kcal/mol)		4.78	3.70	1,840			1.05×10^5	6.70	8.0	65		[72]
	Nylon 66		45.0	272	200.8		4.76	3.70	167			1.55×10^3	1.02	8.0	40		[72]
Poly(butene-1)	Nylon 11		41.96	202.8	217.9 (J/cm ³)	(100)	5.4	4.44	1,500	II			1.66	10.6	110.6	7.61	[37]
	PB-1		-54.2	127.8					1,500			0.25×10^1	0.79				[71]
Poly(ϵ -caprolactone)		26	-60	70.3	163 (J/cm ³)	(110)	4.52	4.12	1,500				0.80	6.7	94.7	5.06	[73]
	PCL	43.6	-63	74	148 (J/cm ³)	(110)	4.50	4.10	1,500			6.03×10^1	0.91	6.1	106		[40]
Poly(chlorotrifluoroethylene)		400	52.0	224.0			6.50	5.60	4,000			6.50×10^4	1.72		53	5.6	[71]
	PCTFE		52	224	91.1 (J/cm ³)		6.50	5.60				0.17×10^5	0.17	5.2	36	3.8	[74]
PE single crystals		30	-42	114	280 (J/cm ³)	(110)	4.15	4.55	1,500	I			2.11	13.7	93.4	5.1	[3]
	PE		-42.2	144.6	280 (J/cm ³)		4.55	4.15	1,500	I		4.40×10^9	2.16	14.1	90.4	5.0	[71]
Polyethylene			-20	141	280 (J/cm ³)	(110)	4.45	4.11		II	127	2.24×10^3 16.00×10^5	1.15 1.24	14.1 12.2	97.8 49	2.6	[74]
	HDPE	13.0	-40.0	144.5	288.7				1,500	I II	125.3	1.45×10^{13} 1.91×10^7		11.8 11.8	105.6 111.8		[32] [75]
HDPE-NBS standard, fractionated		66.4		144.7		(110)			5,736	I II III		1.4×10^{10} 1.02×10^3 1.65×10^7	1.98 0.94 1.85	11.8	88.3 122.0		[18]
	HDPE, un-fractionated	53.9	101.3	-83	142.7				1,500	I II III	125.6 120.8						[19]
Poly(3-hydroxybutyrate)	4 branches/ 1,000 CH ₂	16.1	-40.0	143.7	256.3				1,500	I II		3.63×10^{11} 8.91×10^7		11.8 11.8	88.3 122.0		[25]
	22 branches/ 1,000 CH ₂	15.2	-40.0	139.2	212.5				1,500	I II	124.1 123.1	6.45×10^{15} 8.51×10^6		11.8 11.8	86.0 79.0		[25]
PHB	133	358	2	197	146	(100)			2,450	II III	130		4.99 2.47	38			[76]
	14.1	38.6	143.0	395.0		(200) & (110)			3,980		165.0			12.1	25.1		[77] [78] [79]

Polymer	M_n (kg/mol)	M_w kg/mol	T_g (°C)	T_m (°C)	ΔH_f (J/g)	Growth face	a_0 (Å)	b_0 (Å)	U^* (cal/mol)	Regime	T_{it} (°C)	G_0 (cm/s)	$K_g/10^5$ (K ²)	σ (erg/cm ²)	σ_e (erg/cm ²)	q (kcal/mol)	Ref.
Poly(aryl-ether- ether-ketone)	60.2	79.5	150.6	404.0	130			4.68	4,140				18.20	38.0	101		[80]
	30.9	39.2	148.6	401.2	130			4.68	4,560				12.60	38.0	65		[80]
	14.5	18.0	145.3	395.0	130			4.68	4,560				9.8	38.0	45		[80]
Poly(ethylene-naphthalate 2, 6 dicarboxylate)			144.0	395.0	130	(110)		4.68	2,000					38.0	49.0		[78]
	48			300	190		6.51	5.66							60		[81]
Poly(ethylene-terephthalate)	19.0	37.0	70	280	140	(100)	4.56	5.53	2,000					10.2	190	13.1	[82]
			80	343	135	(010)		5.07	2,000					36	93		[78]
	21.0		80	278	1.8 (J/cm ³)	(100)	4.56	5.53	3,050	II III	165		12.8	10.5 10.5	255 301		[83]
Poly(trimethylene-terephthalate)	19-39		67	300					1,544				9.42				[12]
	43		45	252	28.8 (kJ/mol)	(010)	4.637	5.71	2,500	I II III	215 195		7.3 3.5 8.4	84.9 19.2	81.3 98.8	6.5 6.2 7.5	[48]
	262	351	-72	35.5					1,500	I II III			2.63 1.50 2.80	14.0 14.0 14.0	21.6 24.6 22.9		[84]
Poly(isoprene)	344	543	-72	35.5					1,500	II III			1.28 2.46	14.0 14.0	21.0 20.1		[84]
	512	897	-72	35.5					1,500	III			2.47	14.0	20.3		[84]
						(100)		6.23						9.16	23.9	2.13	[85]
Poly(oxyethylene)						(120)		4.19							50.3	3.45	[85]
	170	390	-62.2	87.0			5.87	3.95	1,500	II		1.10×10^3	2.17		109	7.3	[71]
	165		-59	74	3,040 (cal/mol)									285 (cal/mol)	1,175 (cal/mol)	27.2	[86]
Poly(oxyethylene)	12.0	9.97		66.2	230 (J/cm ³)	(100)		4.6						3.4	65		[87]
			-67.2	75.2			4.67	4.65	1,500			1.15×10^5	0.81		37	2.3	[71]
	307	325	-67.2	69.0	231 (J/cm ³)		4.67	4.65	2,000	I II	53.0	15.00×10^5	1.18 0.60	10 10	64.33 65.59		[88]
Poly(oxyethylene)			-60.2	186.0			4.53	3.86	1,500			1.28×10^1	1.27		61	3.0	[71]
				211	221 (J/cm ³)			4.46						14.3	150		[89]
Poly(oxypropylene)			-73.2	75.0			4.67	5.20	1,320			0.296×10^1	0.785		43	3	[71]
Poly(pivalolactone)			-3	269	183 (J/cm ³)	(120)	7.8	5.7	1,500	II III	203	1.50×10^2 4.30×10^8	4.32 8.59	30 30	58.1 58.4		[90]
	34	51	92	315	80	(020)	4.33	5.61	1,400	II III	208	5.43 3.86×10^4	8.84 18.35	16.9 16.9	125 130	8.9	[26]

TABLE 39.3. Continued.

Polymer	M_n (kg/mol)	M_w kg/mol	T_g (°C)	T_m (°C)	ΔH_f (J/g)	Growth face	a_0 (Å)	b_0 (Å)	U^* (cal/mol)	Regime	T_{it} (°C)	G_0 (cm/s)	$K_g/10^5$ (K ²)	σ (erg/cm ²)	σ_e (erg/cm ²)	q (kcal/mol)	Ref.
iPP		350	-12	186.1	209	(110) (040)	5.49 6.56	6.26 5.24	1,500	II III	138	3.40×10^{-1} 3.98×10^3		11.5	62.3		[91]
		257	-12	186.1	165	(110)	5.49	6.26	1,500	II III	138.0	3.45×10^{-1} 3.03×10^4	1.365 3.659	11.5 11.5	48.1 59.0		[92]
		300	-3.4	185.0	8.3	(110)	5.49	6.26	1,500	II III	137		1.250 2.554	11.5 11.5	51.3 52.3	5.07 5.19	[93]
Polypropylene		25.5	-6.0	170.0	8.3	(110)	5.49	6.26	1,500	I II III	133 122		2.996 1.607 3.196	11.5 11.5 11.5	63.5 68.2 67.7	6.28 6.74 6.69	[93]
	sPP	76.2	-6.1	168.7	177	(010) (200)	7.25 5.60	5.60 7.25	1,500	III	110	9.07×10^4	5.69	11.28 11.28	124.5 96.2	14.6 11.2	[59]
			90.5	242.0	91.1		12.8	5.5	1,560	II			1.20	7.64	34.8	7.1	[3]
Polystyrene					9.1	(110)	12.8	5.5				1.31×10^1		5.3	28.8		[95]
	sPS	91.6	100	278.8	57.5	(040)	4.41	7.2	1,500	II III	239		1.58 3.67	3.24 3.24	48.15 56.5	4.11 4.87	[63]
Poly(tetramethyl- <i>p</i> -silyphenylene)-siloxane		56	-24.0	153.8	20.8		6.43	6.41	990			2.16×10^{-1}	1.14		34	4.0	[71]
	or TMPS	286	-24.0	152	20.8			6.41	1,230			1.03×10^{-1}		3.5	36.3		[13-15]
Selenium			26.8	219.2			4.36	3.78	2,180			0.458×10^1	2.53		190	9.0	[71]
Poly(tetrafluoroethylene)			184.6	331	47.4				1,500				0.154				[62]
Poly(arylene-ether-ether-sulfide)		34	100	292					1,500	II III	205						[64]
	Poly(ester-amide)		21	170					2,800	II III							[65]
Poly(vinylidene fluoride)	170			178	201			4.83						9.7	38		[69]
1,2-Syndiotactic polybutadiene			18	208					1,500	II					48		[70]
Ethylene-octene copolymers (random, metallocene)	L-04 ^a	27.3		139.3					1,500	I II III	119.5 113.5						[19]
	H-07 ^a	43.6		134.1					1,500	II III	115.1						
	L-11 ^a	21.2	43.7	134.9					1,500	II III	114.2						

TABLE 39.3. Continued.

Polymer	M_n (kg/mol)	M_w kg/mol	T_g (°C)	T_m^c (°C)	ΔH_f (J/g)	Growth face	a_0 (Å)	b_0 (Å)	U^* (cal/mol)	Regime	T_{11} (°C)	G_0 (cm/s)	$K_g/10^5$ (K ²)	σ (erg/cm ²)	σ_e (erg/cm ²)	q (kcal/mol)	Ref.	
Propylene-ethylene copolymers (random, fractionated, Ziegler-Natta)				172.6	209	(110)				I II III	119.6 114.6		2.808 1.883 4.115	11.5	59.6 79.9 87.3	5.89 7.90 8.62	[31]	
		120.6	252.2		150	(001)			1,500	I II III	121.6 116.6		2.478 1.702 3.758	8.2	62.5 85.8 94.8	6.16 8.47 9.36		
				165.7	209	(110)					I II III	112.7 101.7		3.024 2.113 4.211	11.5	64.8 90.6 90.2	6.40 8.95 8.93	
		145.1	287.1		150	(001)			1,500	I II III	112.7 103.7		2.96 2.091 4.138	8.2	75.1 106.1 105	7.40 10.46 10.36		
				159.5	209	(110)					I II III	106.5 101.5		2.621 1.595 3.935	11.5	57 69.3 85.6	5.63 6.85 8.45	
		36.14	86.19		157.6	150	(001)			1,500	I II III	107.6 100.6		2.406 1.474 3.683	8.2	62.1 76.1 95.1	6.13 7.49 9.38	
				149.3	209	(110)					II III	74.3		2.353 4.205	11.5	104.8 93.6	10.36 9.26	
		31.85	74.94		147.8	150	(001)			1,500	II III	76.8		2.081 3.79	8.2	109.9 100.1	10.84 9.28	

^aL and H represent low and high MW, respectively. The numbers following the letters represent the number of hexyl side chains per 1,000 carbon atoms.

^bThe numbers represent mole percent ethylene in the copolymers.

REFERENCES

1. M. J. Avrami, *Chem. Phys.* **7**, 1103 (1939).
2. M. J. Avrami, *Chem. Phys.* **8**, 212 (1940).
3. J. I. Lauritzen Jr. and J. D. Hoffman, *J. Appl. Phys.* **44**, 4340 (1973).
4. D. M. Sadler and G. H. Gilmer, *Polymer* **25**, 1446 (1984).
5. P. J. Phillips and N. Vatansver, *Macromolecules* **20**, 2138 (1987).
6. J. J. Point and M. Dosière, *Polymer* **30**, 2292 (1989).
7. P. J. Phillips, in *Crystallization of Polymers*, edited by M. Dosière (Kluwer, The Netherlands, 1993).
8. E. J. Clark and J. D. Hoffman, *Macromolecules* **17**, 878 (1984).
9. B. Monnasse and J. M. Handin, *Colloid Polym. Sci.* **263**, 822 (1985).
10. S. Z. D. Cheng, J. J. Janimak, and A. Zhang, *Macromolecules* **23**, 298 (1990).
11. A. Lovinger, D. D. Davis, and F. J. Padden, *Polymer* **26**, 1595 (1985).
12. F. Van Antwerpen and D.W. Van Krevelen, *J. Polym. Sci., Polym. Phys. Ed.* **10**, 2423 (1972).
13. J. H. Magill, *J. Polym. Sci.* **A27**, 1184 (1969).
14. J. H. Magill, *J. Polym. Sci.* **A25**, 89 (1967).
15. J. H. Magill, *J. Appl. Phys.* **35**, 3249 (1964).
16. J. D. Hoffman and R. L. Miller, *Macromolecules* **21**, 3038 (1988).
17. P. G. De Gennes, *J. Chem. Phys.* **55**, 672 (1971).
18. J. P. Armistead and J. D. Hoffman, *Macromolecules* **35**, 3895 (2002).
19. J. Wagner and P. J. Phillips, *Polymer* **42**, 8999 (2001).
20. A. Toda, in *Crystallization of Polymers*, edited by M. Dosière (Kluwer, The Netherlands, 1993) p. 141.
21. H. D. Keith and F. J. Padden, *J. Appl. Phys.* **34**, 2409 (1963).
22. H. D. Keith and F. J. Padden, *J. Appl. Phys.* **35**, 1270 (1964).
23. H. D. Keith and F. J. Padden, *J. Appl. Phys.* **35**, 1286 (1964).
24. J. D. Hoffman, *Faraday Discuss. Chem. Soc.* **68**, 378 (1979).
25. W. S. Lambert and P. J. Phillips, *Macromolecules* **27**, 3537 (1994).
26. E. H. Andrews, P. J. Owen, and A. Singh, *Proc. R. Soc. Lond.* **A324**, 79 (1971).
27. R. G. Alamo, D. L. Vanderhart, *et al.*, *Macromolecules* **33**, 6094 (2000).
28. M. R. Nyden, D. L. Vanderhart, and R. G. Alamo, *Comput. Theor. Polym. Sci.* **11**, 175 (2001).
29. I. L. Hosier, R. G. Alamo *et al.*, *Macromolecules* **36**, 5623 (2003).
30. I. L. Hosier, R. G. Alamo, and J. S. Lin, *Polymer* **45**, 3441 (2004).
31. A. Dimeska, Ph.D. Dissertation, The University of Tennessee, Knoxville, 2004.
32. P. J. Phillips, *Rep. Prog. Phys.* **53**, 549 (1990).
33. P. J. Phillips, in *Handbook of Crystal Growth*, edited by D.T.J. Hurle, vol. 2 (Amsterdam, Elsevier Science, 1994), p. 1168.
34. B. G. Risch, G. L. Wilkes, and J. M. Warakowski, *Polymer* **34**, 2330 (1993).
35. J. H. Magill, *Polymer* **3**, 655 (1962).
36. Y. Li, X. Zhu, and D. Yan, *Polym. Eng. Sci.* **40**, 1989 (2000).
37. S. Liu, Y. Yu *et al.*, *J. Appl. Polym. Sci.* **70**, 2371 (1998).
38. M. Liu, Q. Zhao *et al.*, *Polymer* **44**, 2537 (2003).
39. R. D. Icenogle, *J. Polym. Sci. (Polym. Phys. Ed.)* **23**, 1369 (1985).
40. L. Goulet and R. E. Prud'homme, *J. Polym. Sci. Part B, Polym. Phys.* **28**, 2329 (1990).
41. F. Rybnikar, *Collect. Czech. Chem. Commun.* **27**, 2307 (1962).
42. D. M. Hoffman and B. M. McKinley, *Polym. Eng. Sci.* **25**, 567 (1985).
43. P. J. Phillips and W. S. Lambert, *Macromolecules* **23**, 2075 (1990).
44. P. Cebe, *Am. Chem. Soc., Polym.* **27**, 449 (1986).
45. S. P. Kim and S. C. Kim, *Polym. Eng. Sci.* **31**, 110 (1991).
46. K. Ravindranath and J. P. Jog, *J. Appl. Polym. Sci.* **49**, 1395 (1993).
47. B. J. Chisholm and J. G. Zimmer, *J. Appl. Polym. Sci.* **76**, 1296 (2000).
48. P. D. Hong, W. T. Chung, and C. F. Hsu, *Polymer* **43**, 3335 (2002).
49. J. M. Huang and F. C. Chang, *J. Polym. Sci. B: Polym. Phys.* **38**, 934 (2000).
50. L. A. Wood and N. Bekkdahl, *J. Res. Natl. Bur. Std.* **36**, 487 (1946).
51. L. Mandelkem, F. A. Quinn, and D. E. Roberts, Jr., *J. Am. Chem. Soc.* **78**, 926 (1956).
52. W. Cooper and G. Vaughan, *Polymer* **4**, 329 (1963).
53. S. Z. D. Cheng and B. Wunderlich, *J. Polym. Sci. B: Polym. Phys.* **24**, 595 (1986).
54. Yu K. Godovsky, G. L. Slonimsky, *et al.*, *J. Polym. Sci., C* **38**, 1 (1972).
55. Yu K. Godovsky and G. L. Slonimsky, *J. Polym. Sci. B: Polym. Phys.* **12**, 1053 (1974).
56. J. M. Kenny and A. Maffezzoli, *Polym. Eng. Sci.* **31**, 607 (1991).
57. R. A. Campbell, Ph.D. Dissertation, The University of Tennessee, Knoxville, 1991.
58. Yu K. Godovsky and G. L. Slonimsky, *J. Polym. Sci.: Polym. Phys. Ed.* **12**, 1053 (1974).
59. P. Supaphol and J. E. Spruiell, *J. Appl. Polym. Sci.* **75**, 44 (2000).
60. R. G. Crystal, *J. Polym. Sci. A-2* **8**, 2153 (1970).
61. W. Xu and P. He, *J. Appl. Polym. Sci.* **80**, 304 (2001).
62. X. Q. Wang *et al.*, *J. Appl. Polym. Sci.* **83**, 990 (2002).
63. Q. Chen *et al.*, *J. Appl. Polym. Sci.* **83**, 2528 (2002).
64. S. Srinivas *et al.*, *Polym. Eng. Sci.* **37**, 497 (1997).
65. E. Botines *et al.*, *J. Polym. Sci. B: Polym. Phys.* **41**, 903 (2003).
66. M. C. Righetti *et al.*, *Macromol. Chem. Phys.* **199**, 2063 (1998).
67. Y. S. Hu *et al.*, *J. Appl. Polym. Sci.* **86**, 98 (2002).
68. S. Z. D. Cheng *et al.*, *Polym. Int.* **29**, 201 (1992).
69. Y. S. Yadav, P. C. Jain, and V. S. Nanda, *Thermochim. Acta* **80**, 231 (1984).
70. F. Bertini, M. Canetti, and G. Ricci, *J. Appl. Polym. Sci.* **92**, 1680 (2004).
71. J. D. Hoffman, G. T. Davis, and J. I. Lauritzen, Jr., in *Treatise on Solid State Chemistry*, edited by N. B. Hannay (1976), p. 497.
72. J. H. Magill, *Polymer* **367** (1965).
73. P. J. Phillips, G. J. Rensch, and K. D. Taylor, *J. Polym. Sci.: Polym. Phys.* **25**, 1725 (1987).
74. J. D. Hoffman and J. J. Weeks, *J. Chem. Phys.* **37**, 1723 (1962).
75. J. D. Hoffman, L. J. Frolen, G. S. Ross *et al.*, *J. Res. Natl. Bur. Std.* **79A**, 671 (1975).
76. P. J. Barham, A. Keller, E. L. Otun *et al.*, *J. Mater. Sci.* **19**, 2781 (1984).
77. F. J. Iy and P. J. Phillips, *Polym. Eng. Sci.* **30**, 860 (1990).
78. D. J. Blundell and B. N. Osborn, *Polymer* **24**, 953 (1983).
79. Y. Lee and R. S. Porter, *Polym. Eng. Sci.* **26**, 633 (1986).
80. Y. Deslandes, F.-N. Sabir, and J. Roovers, *Polymer* **32**, 1267 (1991).
81. S. Buchner, D. Wiswe, and H. G. Zachmann, *Polymer* **30**, 480 (1989).
82. L. H. Palys and P. J. Phillips, *J. Polym. Sci.: Polym. Phys.* **18**, 829 (1980).
83. P. J. Phillips and H. T. Tseng, *Macromolecules* **22**, 1649 (1989).
84. P. J. Phillips and N. Vatansver, *Macromolecules* **20**, 2138 (1987).
85. B. C. Edwards, *J. Polym. Sci.: Polym. Phys. Ed.* **13**, 1387 (1975).
86. E. G. Lovering, *J. Polym. Sci.* **C30**, 329 (1970).
87. A. J. Kovacs and A. Gonthier, *Kolloid-Z. Polym.* **250**, 530 (1972).
88. Ni Ding and E. J. Amis, *Macromolecules* **24**, 3906 (1991).
89. D. R. Carter and E. Baer, *J. Appl. Phys.* **37**, 4060 (1966).
90. D. B. Roitman, H. Marand, and R. L. Miller, *J. Phys. Chem.* **93**, 6919 (1989).
91. E. J. Clark and J. D. Hoffman, *Macromolecules* **17**, 878 (1984).
92. K. Mezghani and P. J. Phillips, *Polymer* **36**, 2407 (1995).
93. S. Z. D. Cheng, J. J. Janimak, and A. Zhang, *Macromolecules* **23**, 298 (1990).
94. P. Supaphol and J. E. Spruiell, *Polymer* **41**, 1205 (2000).
95. B. C. Edwards and P. J. Phillips, *Polymer* **15**, 351 (1974).

CHAPTER 40

Block Copolymer Melts

V. Castelletto and I. W. Hamley

Department of Chemistry, University of Reading, Reading RG6 6AD, UK

Glossary	649
References	649

The interest in the phase behaviour of block copolymer melts stems from microphase separation of polymers that leads to nanoscale ordered morphologies. This subject has been reviewed extensively [1–4]. The identification of the structure of bicontinuous phases has only recently been confirmed, and this together with major advances in the theoretical understanding of block copolymers, means that the most up-to-date reviews should be consulted [1,3]. The dynamics of block copolymer melts, in particular rheological behaviour and studies of chain diffusion via light scattering and NMR techniques have also been the focus of several reviews [1,5,6].

The phase behaviour of block copolymer melts is, to a first approximation, represented in a morphology diagram in terms of χN and f [1]. Here f is the volume fraction of one block and χ is the Flory-Huggins interaction parameter, which is inversely proportional to temperature, that reflects the interaction energy between different segments. The configurational entropy contribution to the Gibbs energy is proportional to N , the degree of polymerization. Figure 40.1 presents a morphology diagram computed using self-consistent field theory [7,8]. It has been shown to describe qualitatively (at least in terms of the relative sequence of phases and overall topology of the phase diagram) the behaviour of real systems [1,9], and so is used as a roadmap here. When the product χN exceeds a critical value, $(\chi N)_{\text{ODT}}$ (ODT: order–disorder transition) the block copolymer microphase separates into a periodically ordered structure, with a lengthscale ~ 5 –500 nm. The structure that is formed depends on the copolymer architecture and composition [1]. For diblock copolymers, a lamellar (lam) phase is observed for symmetric diblocks ($f = 0.5$), whereas more asymmetric diblocks form hexagonal-packed cylinder (hex) or body centred cubic (BCC) spherical structures. A complex bicontinuous cubic gyroid (gyr) (spacegroup $Ia\bar{3}d$) phase has also been identified [10,11] for block copolymers between the

lam and hex phases near the ODT, and a hexagonal-perforated layer (HPL) phase has been found to be metastable in this region [12–14]. Table 40.1 provides a compilation of the morphology of two component (A–B or A–B–A) block copolymers of various chemistries, and Table 40.2 lists studies on A–B–C triblocks.

The main techniques for investigating block copolymer microstructures are transmission electron microscopy (TEM) and small-angle x-ray or neutron scattering. TEM provides direct visual images of the structure, albeit over a small area of the sample. Usually samples are stained using the vapours from a solution of a heavy metal acid (OsO_4 or RuO_4) to increase the contrast for electrons between domains [15]. Small-angle scattering probes the structure over the whole sample volume, giving a diffraction pattern. The positions of the reflections in the diffraction pattern can be indexed to identify the symmetry of the phase [1,2]. The preparation method can have a dramatic influence on the apparent morphology, for example whether solvent casting or melt processing is performed. Numerous cases of mistaken identification of “equilibrium phases” have appeared in the literature, when the phase was simply an artifact. For instance, Lipic et al. [16] obtained different morphologies by varying the preparation conditions for a polyolefin diblock examined by them. In other cases, phases such as HPL have been observed [12] which although reproducible, have turned out to be only long-lived metastable phases, ultimately transforming to the equilibrium gyroid phase [13,14]. The ODT in block copolymers can be located via a number of methods—from discontinuities in the dynamic shear modulus [17–19] or small-angle scattering peak shape [20,21] or from calorimetry measurements [22].

To establish relationships between different block copolymer phase diagrams and also to facilitate comparison with theory, it is necessary to specify parameters in addition to χN and f . First, asymmetry of the conformation

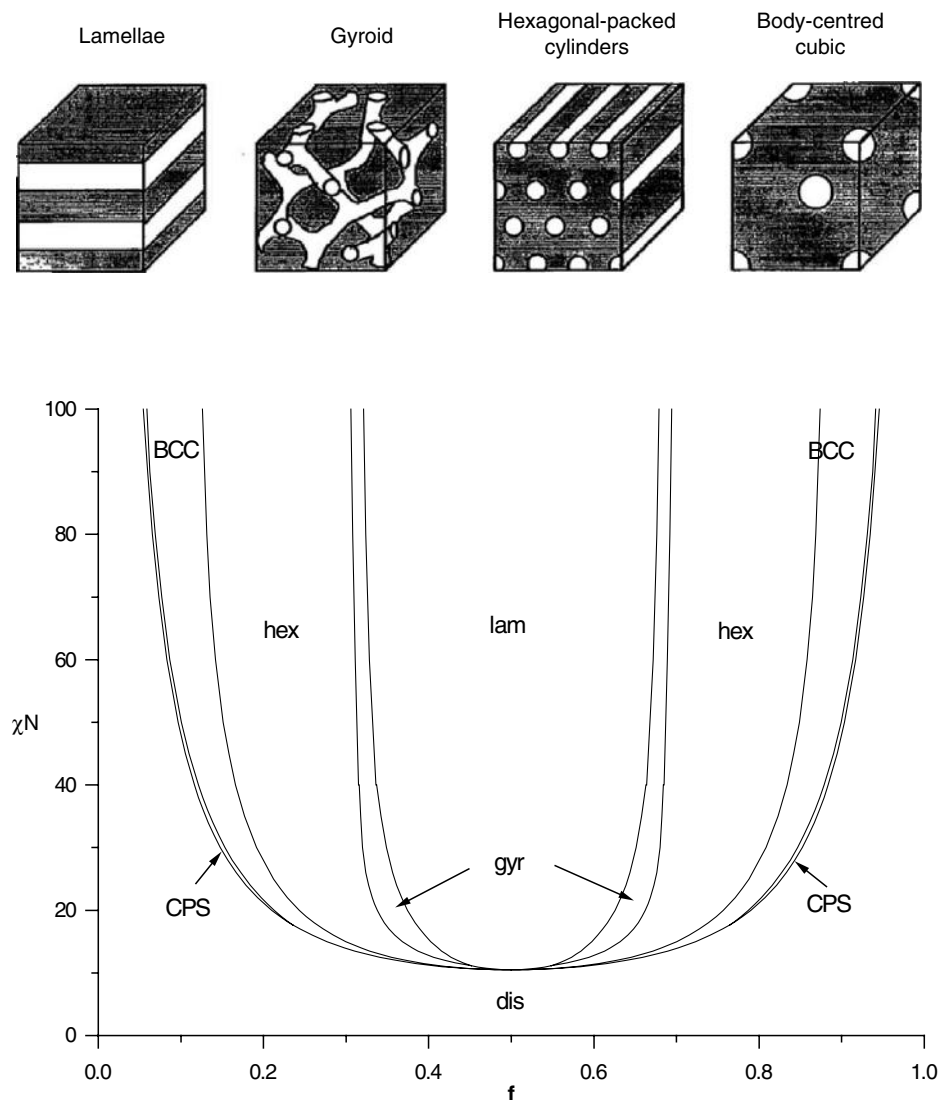


FIGURE 40.1. Phase diagram for a conformationally symmetric diblock copolymer, calculated using self-consistent mean field theory [7,8,199], along with illustrations of the equilibrium morphologies. In the phase diagram, regions of stability of disordered (dis), lamellar (lam), gyroid (gyr), hexagonal (hex), body-centred cubic (BCC) and close-packed sphere (CPS) phases are indicated.

of the copolymer breaks the symmetry of the phase diagram about $f = 0.5$. For A–B diblocks, conformational asymmetry is quantified using the “asymmetry parameter” $\varepsilon = (b_A^2/v_A)/(b_B^2/v_B)$ [23,24], where b_j is the segment length for block J and v_j is the segment volume. Composition fluctuations also modify the phase diagram, and this has been accounted for theoretically via the Ginzburg parameter $\bar{N} = Nb^6\rho^2$, where ρ is the number density of chains [25,26]. The extent of segregation of block copolymers depends on the magnitude of χN . For small χN , close to the order–disorder transition (up to $\chi N = 12$ for symmetric diblocks for which $\chi N_{\text{ODT}} = 10.495$), the composition profile (density of either component) is approximately sinusoidal. This is

termed the weak segregation limit. At much larger values of χN ($\chi N > \sim 100$), the components are strongly segregated and each domain is almost pure, with a narrow interphase between them. This is the strong segregation limit.

The first theories for block copolymers were introduced for the strong segregation limit (SSL) and the essential physical principles underlying phase behaviour in the SSL were established in the early 1970s [1]. Most notably, Helfand and coworkers [27–29] developed the self-consistent field (SCF) theory, this permitting the calculation of free energies, composition profiles and chain conformations. In the SCF theory, the external mean fields acting on a polymer chain are calculated self-consistently with the composition

TABLE 40.1. Studies on the morphology of A-B and A-B-A block copolymers.

System	Microstructure	Architecture	Comments	References
PB-PDMS	Cylinders	A-B		[47]
	Spheres	A-B		[47]
PE-PEE	Spheres	A-B		[48]
	Lamellae	A-B		[48-51]
	Cylinders	A-B		[48,49]
	HML	A-B		[49,50]
	HPL	A-B		[48-50]
	Bicontinuous $la\bar{3}d$ (gyroid)	A-B		[48,49]
PE-PEP	Lamellae	A-B		[50-52]
	Cylinders	A-B		[49]
	Spheres	A-B		[49]
	HML	A-B		[50]
	HPL	A-B		[50]
PE-PVCH	Lamellae	A-B		[50,53]
PEE-PVCH	Lamellae	A-B		[53]
	HML	A-B		[50]
PEO-PtBMA	Lamellae	A-B		[54]
PE-PtBMA	Cylinders	A-B		[55]
PEP-PEE	Lamellae	A-B		[12,17,41,42,49-51,56-58]
		A-B-A		[57]
	Cylinders	A-B		[12,49,50,59-61]
	Spheres	A-B		[49,60,62]
	HML	A-B		[12,49,50]
	HPL	A-B		[12,49,50]
	Bicontinuous $la\bar{3}d$ (gyroid)	A-B		[49]
PEP-PVCH	Lamellae	A-B		[53]
PMTD-PxNB	Lamellae	A-B	x contains Sn or Pb or Zn	[63,64]
			x contains Pd or Pt	[65]
	Cylinders	A-B	x contains Pd or Pt	[65]
	Spheres	A-B	x contains Pd or Pt	[65]
			x contains Zn	[64]
PNB-PA	Lamellae	A-B		[66]
PxNB-PA		A-B	x contains Sn	[63,67]
	Cylinders	A-B		[66]
		A-B	x contains Sn	[67]
	Spheres	A-B	x contains Sn	[67]
PNORPHOS-PMTD	Lamellae	A-B	Complexed with Ag or Au	[68]
	Cylinders	A-B	Complexed with Ag or Au	[68]
	Spheres	A-B	Complexed with Ag or Au	[68]
PS-PB	Lamellae	A-B		[69-73]
		A-B-A		[74-78]
		$(A-B-)_n-$	$n \geq 3$	[74]
	PL	A-B		[73]
	Cylinders	A-B		[69,70,79]
		A-B-A		[74,77,78,80-83]
	Spheres	$(A-B-)_n-$	$n \geq 3$	[74]
		A-B		[84,85]
		A-B-A		[74]
PS-PnBMA	Lamellae	A-B		[86]
	Cylinders	A-B		[87,88]
	Spheres	A-B		[87]
PS-PChEMA	Cylinders	A-B	Tetragonal packing	[88]
		A-B-A	Tetragonal packing	[88]
PS-PDMS	Lamellae	A-B		[89]
	Cylinders	A-B		[89]
	Spheres	A-B		[72]

TABLE 40.1. Continued.

System	Microstructure	Architecture	Comments	References
PS-PEB	Lamellae	A-B		[90]
	Cylinders	A-B		[90]
	Spheres	A-B		[72]
PS-PEP	Lamellae	A-B		[91,92]
	Cylinders	A-B		[91]
	Spheres	A-B		[91,93]
PS-PI	Lamellae	A-B		[10,11,49,69,70,94-114]
		A-B-A		[110,112,115]
		(A-B-) _n -	$n \geq 3$	[116,117]
		(A-B-) _n -	$n \geq 2$	[118,119]
		Miktoarm star (A) _n B	$n = 2$	[120]
	PL	A-B		[11,49,94,114]
	Bicontinuous $la\bar{3}d$ (gyroid)	A-B		[10,11,49,94,111,114]
		(A-B-) _n -	$n \geq 3$	[121]
		A-B-A		[122]
	Bicontinuous $Pn\bar{3}m$ (OBDD)	A-B		[73,98,102,103,111,123]
	Cylinders	(A-B-) _n -	$n \geq 3$	[121,124-127]
		A-B		[11,49,69,70,94,98,102,109-111,113,123,128,129]
		A-B-A		[110,126,130,131]
		(A-B-) _n -	$n \geq 3$	[117,125-127]
		Miktoarm star A(B) _n	$n = 2$	[132]
Spheres	Miktoarm star (A) _n B	$n = 2$	[120]	
	A-B		[11,94,102,106,109-111,113,123,128,129,133]	
	A-B-A		[110,126,130,131]	
	(A-B-) _n -	$n \geq 3$	[116,117,126,127]	
	A-B/star		[134]	
PI-PS	Cylinders	Miktoarm star (A) _n B	$n = 2,3$	[120]
	Bicontinuous cubic	Miktoarm star (A) _n B	$n = 2$	[120]
	Lamellae	Miktoarm star (A) _n B	$n = 3,5$	[120,135]
PEO-PEE	Lamellae	Miktoarm star (A) _n (B) _n	$n = 8$	[136]
		A-B		[114]
		A-B		[114]
PS-PMMA	Lamellae	A-B		[137,138]
		A-B		[105,106,139-142]
		A-B		[106,143,144]
PS-P2VP	Lamellae	A-B		[145]
		A-B		[145]
		A-B		[145]
PS-P4VP	Lamellae	A-B		[146,147]
		A-B		[146,147]
		A-B		[149]
PEP-PDMS	Lamellae	A-B		[14]
		A-B		[14,114,148]
		A-B		[149]
PI-PDMS	Lamellae	A-B		[148]
		A-B		[148]
		A-B		[148]
PEO-PI	Spheres	A-B		[150]
		A-B		[150]
		A-B		[150]
P2VP-PCMA	Lamellae	A-B		[142]
PS-P2MP	Lamellae	Miktoarm star A(B) _n	$n = 3$	[151]
		A-B		[151]
	Spheres	Miktoarm star A(B) _n	$n = 2$	[151]

TABLE 40.1. Continued.

System	Microstructure	Architecture	Comments	References
	Cylinders	A-B		[151]
		Miktoarm star A(B) ₂		[151]
	Double gyroid	Miktoarm star A(B) ₃		[151]
PIB-PPVL	Lamellae	A-B		[152]
	Spheres	A-B		[152]
PS-PnPMA	Lamellae	A-B		[153]
	Cylinders	A-B		[153]
	Spheres	A-B		[153]
PI-PLA	Lamellae	A-B		[154]
PEP-PLA	Lamellae	A-B		[155]
	Cylinders	A-B		[155]
	Spheres	A-B		[155]
	Bicontinuous $la\bar{3}d$ (gyroid)	A-B		[155]

TABLE 40.2. Studies on the morphology of A-B-C block copolymers.

System	Microstructure	Architecture	References
PI-PS-P2VP	Lamellae	A-B-C	[156-159]
	Cylinders	A-B-C	[156,158,159]
	Spheres	A-B-C	[156,159]
	Ordered tricontinuous double diamond (OTDD)		
	Other	A-B-C	[156-158]
PS-PB-P4VP	Lamellae	A-B-C	[160,161]
	Other	A-B-C	[160]
PS-PEB-PMMA	Lamellae	A-B-C	[162]
	Cylinders	A-B-C	[162]
	Other	A-B-C	[162]
PS-PI-P2VP	Lamellae	A-B-C	[163]
	Cylinders	A-B-C	[163]
		miktoarm star A-B-C	[164]
PS-PEB-PMMA	Others	A-B-C	[163]
	lc	A-B-C	[162,165,166]
	hel	A-B-C	[165,167]
	s(o)c	A-B-C	[165,167]
	c(a)c	A-B-C	[165,167]
	u-c(i)c	A-B-C	[165,167]
	s(o)s	A-B-C	[168]
	Knitting pattern	A-B-C	[169]
PS-PEB-PMMA (upon hydrogenation of the central PEB block)	Knitting pattern		[166,170]
PS-PB-PMMA	ll	A-B-C	[171,172]
	hel	A-B-C	[167,171-173]
	s(o)c	A-B-C	[167,171-173]
	c(a)c	A-B-C	[167,171-173]
	u-c(i)c	A-B-C	[167,171-173]
	ml	A-B-C	[172]
	c(i)c	A-B-C	[172]
	s(o)s	A-B-C	[168,172]
	lc	A-B-C	[165,172]
	ls	A-B-C	[165,172,174,175]
	dl	A-B-C	[172]

TABLE 40.2. Continued.

System	Microstructure	Architecture	References
PS-PB-P2VP	Lamellae	A-B-C	[176,177]
	Cylinders	A-B-C	[176,177]
	Bicontinuous double Gyroid	A-B-C	[177,178]
PB-PS-P2VP	Lamellae	A-B-C	[177]
PS-PI-PMMA	Ic	A-B-C	[179]
	II	A-B-C	[180]
PS-PI-PMMA	Cylinders	A-B-C	[181]
	Cylinders	miktoarm star A-B-C	[182]
PS-PI-PB	Cylinders	miktoarm star A-B-C	[132]
PS-PDMS-PtBMA	Tricontinuous microdomain structure	Star A-B-C	[183]
PEP-PEB-PS	Spheres	A-B-C	[184]
	Cylinders	A-B-C	[184]
	Continuous morphology	A-B-C	[184]
PI-PB-PS	Spheres	A-B-C	[184,185]
	Cylinders	A-B-C	[184,185]
PB-PS-PI	Lamellae	A-B-C	[186]
	Cylinders	A-B-C	[186]
PS-PB-PI	Lamellae	A-B-C	[186]
PCE-PEE-PE	Tricontinuous (10, 3)c network (orthorhombic symmetry)	A-B-C	[187]
PI-PS-PEO	Tricontinuous (10, 3)c network (orthorhombic symmetry)	A-B-C	[188,189]
	Lamellae	A-B-C	[188,190]
	c(i)c	A-B-C	[190]
	Pentacontinuous Gyroid $Ia\bar{3}d$	A-B-C	[190,191]
PS-PI-PDMS	Cylinders	miktoarm star A-B-C	[192]
PS-zw-PI	Lamellae	A-B-C	[193]
PPVL-PIB-PPVL	Lamellae	A-B-A	[152]
	Spheres	A-B-A	[152]
PI-PS-PI	Spheres	super-H star A_3BA_3	[194]
	Cylinders	super-H star A_3BA_3	[194]
PLA-PI-PLA	Lamellae	A-B-A	[195]
	Spheres	A-B-A	[195]
	Cylinders	A-B-A	[195]
PI-PPMDSS-PI	Tricontinuous Gyroid $Ia\bar{3}d$	A-B-A	[196]
PPMDSS-PI-PPMDSS	Spheres	A-B-A	[196]

profile. The theory of Leibler [30] describes block copolymers in the weak segregation limit. It employs a Landau-Ginzburg approach to analyse the free energy, which is expanded with reference to the average composition profile. The free energy coefficients are computed within the random phase approximation. Weak segregation limit theory can be extended to allow for thermal composition fluctuations. This changes the mean field prediction of a second-order phase transition for a symmetric diblock copolymer to a first-order transition. Fredrickson and Helfand [25] studied this effect for block copolymers and showed that composition fluctuations, incorporated via the renormalization method of Brazovskii, lead to a “finite size effect”, where the phase diagram depends on the degree of polymerization, \bar{N} . A powerful new method to solve the self-consistent field equations for block copolymers has been applied by Matsen

and coworkers to analyse the ordering of many types of block copolymer in bulk and in thin films [7–9,31]. The strong and weak segregation limits are spanned, as well as the intermediate regime where the other methods do not apply. This implementation of SCF theory predicts phase diagrams, and other quantities such as domain spacings, in good agreement with experiment and represents an impressive state-of-the-art for modelling the ordering of soft materials. Accurate liquid state theories have also been used to model block copolymer melts [32,33], although they are hard to implement and consequently the method is often regrettably overlooked [1]. Recently, a method has been developed to directly simulate field theories for polymers without introducing approximations such as mean field approaches, perturbation expansions, etc. [34]. This technique holds much promise for examining the thermodynamics of

block copolymers in the limit of low molecular weight where approximate methods such as mean field theory or renormalization techniques break down.

The phase behaviour of A–B–C triblocks is much richer [3] than two-component diblocks or triblocks, as expected because multiple interaction parameters (χ_{AB} , χ_{AC} and χ_{BC}) result from the presence of a distinct third block. Summaries of work on A–B–C triblock morphologies have appeared [1,35] and Table 40.2 contains a listing of relevant studies.

Figure 40.2 illustrates representative morphologies that have been observed. Because of the large number of possible morphologies, theorists are presently working to predict the phase behaviour of these copolymers using methods that do not require *a priori* knowledge of the space group symmetries of trial structures [36,37]. Some systems, such as the *poly* (styrene–butadiene–methacrylate) (PS–PB–PMMA) triblock copolymers, exhibit a particularly rich complexity in phase behaviour (Figure 40.3), forming multiple ordered

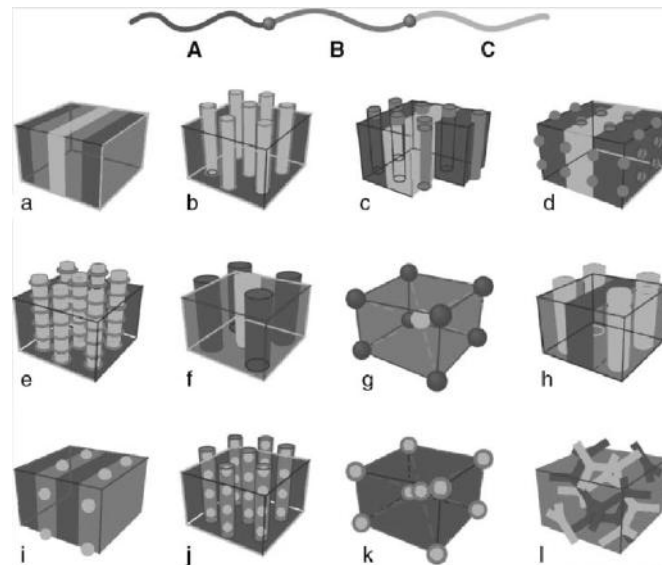


FIGURE 40.2. Schematic of several morphologies observed for ABC triblock copolymer melts [3].

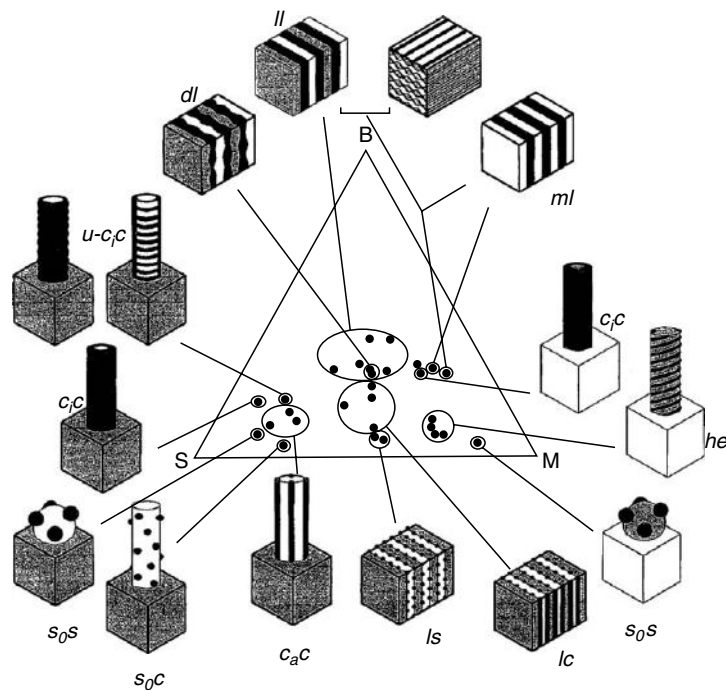


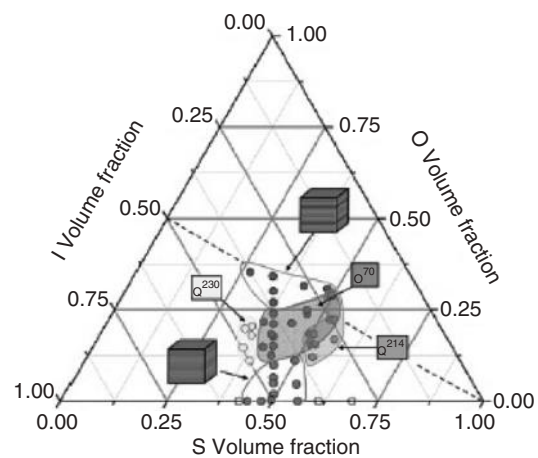
FIGURE 40.3. Morphology diagram for PS–PB–PMMA triblocks [197].

phases as listed in Table 2. Other systems form several network phases, as shown in Fig. 40.4 and listed in Table 2 for the *poly*(isoprene–styrene–ethylene oxide) (PI–PS–PEO) triblock copolymer. However, the list of phases in Table 2 is not exhaustive—many more are still to be discovered. Elucidating which are in equilibrium will be a particular challenge for these systems which often have high molecular weight and contain strongly incompatible blocks.

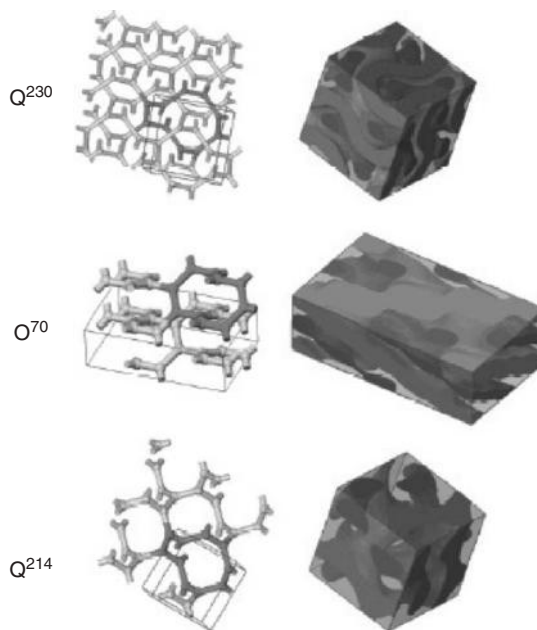
During processing block copolymers are subjected to flow. For example thermoplastic elastomers formed by *poly*(styrene–butadiene–styrene) (PS–PB–PS) triblock copolymers, are moulded by extrusion. This leads to alignment

of microphase-separated structures. This was investigated in the early 1970s by Keller and coworkers [2,38] who obtained transmission electron micrographs from highly oriented specimens of Kraton PS–PB–PS copolymers following extrusion.

Work on the effect of flow on block copolymer melts has been reviewed [1,5,39,40]. Due to the convenience and well defined nature of the shear geometry most model studies have exploited this type of flow. The application of shear leads to orientation of block copolymer microstructures at sufficiently high shear rates and/or strain amplitudes (in the case of oscillatory shear). Depending on shear conditions



(a)



(b)

FIGURE 40.4. (a) Phase diagram for a PI–PS–PEO triblock showing regions of network phases, illustrated in part (b) (structures are identified by space group number) [189,198].

and temperature, different orientations of a morphology with respect to the shear plane can be accessed. This has been particularly well studied for the lamellar phase where so-called “parallel” (lamellar normal along shear gradient direction) and “perpendicular” (lamellar normal along the neutral direction) orientations have been observed [41]. Distinct orientation states of hex and cubic phases have also been investigated, details being provided elsewhere [40]. The ability to generate distinct macroscopic orientation states of block copolymers by shear is important in future applications of block copolymers where alignment will be important (reinforced composites, optoelectronic materials and separation media). Shear also influences thermodynamics, since the order–disorder transition shifts upwards on increasing shear rate because the ordered phase is stabilized under shear [42,43].

The phase behaviour of rod–coil block copolymers is already known to be much richer than that of coil–coil block copolymers, because the rod block can orient into liquid crystal structures [1]. The rod block may be analogous to a biomacromolecule, for example *poly*(benzyl glutamates) [44,45] and *poly*(peptides) [46] forming helical rod-like blocks have been incorporated in block copolymers. Possible applications of these materials arising from their biocompatibility are evident.

GLOSSARY

Compound names abbreviations used in Table 40.1 and Table 40.2

PLA	: <i>poly</i> (lactide)
PA	: <i>poly</i> (acetylene)
PB	: <i>poly</i> (butadiene)
PnBMA	: <i>poly</i> (<i>n</i> -butylmethacrylate)
PtBMA	: <i>poly</i> (<i>tert</i> -butylmethacrylate)
PChEMA	: <i>poly</i> (2-(3-cholesteryl-oxycarbonyloxy)ethylmethacrylate)
PE	: <i>poly</i> (ethylene)
PEB	: <i>poly</i> (ethylenebutene)
PEE	: <i>poly</i> (ethylethylene)
PEP	: <i>poly</i> (ethylenepropylene)
PEO	: <i>poly</i> (ethyleneoxide)
PI	: <i>poly</i> (isoprene)
PIB	: <i>poly</i> (isobutylene)
PMMA	: <i>poly</i> (methylmethacrylate)
PCMA	: <i>poly</i> (cyclohexylmethacrylate)
PCE	: <i>poly</i> (cyclohexylethylene)
PMDT	: <i>poly</i> (methyltetracyclododecene)
PNB	: <i>poly</i> (norbornene)
PxNB	: organometallic derivative of <i>poly</i> (norbornene)
PNORPHOS	: <i>poly</i> (2- <i>exo</i> -3- <i>endo</i> -bis(diphenylphosphophino)bicyclo[2,2,1] heptene)
PS	: <i>poly</i> (styrene)

PVCH	: <i>poly</i> (vinylcyclohexane)
P2VP	: <i>poly</i> (2-vinylpyridine)
P4VP	: <i>poly</i> (4-vinylpyridine)
PDMS	: <i>poly</i> (dimethylsiloxane)
P2MP	: <i>poly</i> (2-methyl-1,3-pentadiene)
zw	: zwitterionic group
PPVL	: <i>poly</i> (pivalolactone)
PnPMA	: <i>poly</i> (<i>n</i> -pentyl methacrylate)
PPMDSS	: <i>Poly</i> (pentamethyldisilylstyrene)

Phase morphology abbreviations used in Table 40.1 and Table 40.2

HML	: Hexagonal modulated layers
HPL	: Hexagonal perforated layers
PL	: Perforated layers
s(o)s	: spheres on spheres, according to the nomenclature shown in Fig. 40.3.

hel, c(a)c, uc(i)c, u-c(i)c, c(i)c and s(o)c are cylindrical phases named according to the nomenclature shown in Fig. 40.3.

lc, ls, ll, dl and ml are lamellar phases named according to the nomenclature shown in Fig. 40.3.

REFERENCES

- Hamley, I. W. *The Physics of Block Copolymers*; Oxford University Press:Oxford, 1998.
- Folkes, M. J.; Keller, A. In *The Physics of Glassy Polymers*; Haward, R. N., Ed.; Applied Science:London, 1973; pp 548–603.
- Bates, F. S.; Fredrickson, G. H. *Phys. Today* 1999, 52 (February issue), 32.
- Bates, F. S.; Fredrickson, G. H. *Ann. Rev. Phys. Chem.* 1990, 41, 525–557.
- Fredrickson, G. H.; Bates, F. S. *Annu. Rev. Mater. Sci.* 1996, 26, 501–550.
- Colby, R. H. *Curr. Opin. Colloid Interface Sci.* 1996, 1, 454–465.
- Matsen, M. W.; Schick, M. *Phys. Rev. Lett.* 1994, 72, 2660–2663.
- Matsen, M. W.; Bates, F. S. *Macromolecules* 1996, 29, 1091–1098.
- Matsen, M. W. *J. Phys. Condens. Matter* 2001, 14, R21–R47.
- Hajduk, D. A.; Harper, P. E.; Gruner, S. M.; Honeker, C. C. Kim, G.; Thomas, E. L.; Fetters, L. J. *Macromolecules* 1994, 27, 4063–4075.
- Förster, S.; Khandpur, A. K.; Zhao, J.; Bates, F. S.; Hamley, I. W.; Ryan, A. J.; Bras, W. *Macromolecules* 1994, 27, 6922–6935.
- Hamley, I. W.; Koppi, K. A.; Rosedale, J. H.; Bates, F. S.; Almdal, K.; Mortensen, K. *Macromolecules* 1993, 26, 5959–5970.
- Hajduk, D. A.; Takenouchi, H.; Hillmyer, M. A.; Bates, F. S.; Vigild, M. E.; Almdal, K. *Macromolecules* 1997, 30, 3788–3795.
- Vigild, M. E.; Almdal, K.; Mortensen, K.; Hamley, I. W.; Fairclough, J. P. A.; Ryan, A. J. *Macromolecules* 1998, 31, 5702–5716.
- Kato, K. *J. Electron Microsc. (Jpn.)* 1965, 14, 220.
- Lipic, P. M.; Bates, F. S.; Matsen, M. W. *J. Polym. Sci. B:Polym. Phys.* 2001, 37, 2229–2238.
- Bates, F. S.; Rosedale, J. H.; Fredrickson, G. H. *J. Chem. Phys.* 1990, 92, 6255–6270.
- Rosedale, J. H.; Bates, F. S. *Macromolecules* 1990, 23, 2329–2338.
- Han, C. D.; Baek, D. M.; Kim, J. K.; Ogawa, T.; Sakamoto, N.; Hashimoto, T. *Macromolecules* 1995, 28, 5043–5062.
- Mai, S. M.; Fairclough, J. P. A.; Hamley, I. W.; Denny, R. C.; Liao, B.; Booth, C.; Ryan, A. J. *Macromolecules* 1996, 29, 6212–6221.
- Sakamoto, N.; Hashimoto, T. *Macromolecules* 1995, 28, 6825–6834.
- Voronov, V. P.; Buleiko, V. M.; Podneks, V. E.; Hamley, I. W.; Fairclough, J. P. A.; Ryan, A. J.; Mai, S.-M.; Liao, B.-X.; Booth, C. *Macromolecules* 1997, 30, 6674–6676.

23. Helfand, E.; Sapse, A. M. *J. Chem. Phys.* 1975, *62*, 1327–1331.
24. Bates, F. S.; Fredrickson, G. H. *Macromolecules* 1994, *27*, 1065–1067.
25. Fredrickson, G. H.; Helfand, E. *J. Chem. Phys.* 1987, *87*, 697–705.
26. Fredrickson, G. H.; Binder, K. *J. Chem. Phys.* 1989, *91*, 7265–7275.
27. Helfand, E. *Macromolecules* 1975, *8*, 552–556.
28. Helfand, E.; Wasserman, Z. R. *Macromolecules* 1976, *9*, 879–888.
29. Helfand, E.; Wasserman, Z. R. In *Developments in Block Copolymers I*; Goodman, I., Ed.; Applied Science: London, 1982; pp 99–125.
30. Leibler, L. *Macromolecules* 1980, *13*, 1602–1617.
31. Matsen, M. W.; Schick, M. *Curr. Opin. Colloid Interface Sci.* 1996, *1*, 329–336.
32. David, E. F.; Schweizer, K. S. *J. Chem. Phys.* 1994, *100*, 7767–7783.
33. David, E. F.; Schweizer, K. S. *J. Chem. Phys.* 1994, *100*, 7784–7795.
34. Ganesan, V.; Fredrickson, G. H. *Europhys. Lett.* 2001, *55*, 814–820.
35. Ryan, A. J.; Hamley, I. W. In *The Physics of Glassy Polymers*; Haward, R. N.; Young, R. J., Eds.; Chapman and Hall: London, 1997.
36. Drolet, F.; Fredrickson, G. H. *Phys. Rev. Lett.* 1999, *83*, 4317–4320.
37. Bohbot-Raviv, Y.; Wang, Z.-G. *Phys. Rev. Lett.* 2000, *85*, 3428–3431.
38. Keller, A.; Pedemonte, E.; Willmouth, F. M. *Nature* 1970, *225*, 538.
39. Honeker, C. C.; Thomas, E. L. *Chem. Mater.* 1996, *8*, 1702–1714.
40. Hamley, I. W. *J. Phys. Condens. Matter*, 2001, *13*, R643–R671.
41. Koppi, K. A.; Tirrell, M.; Bates, F. S.; Almdal, K.; Colby, R. H. *J. Phys. France II*, 1992, *2*, 1941–1959.
42. Koppi, K. A.; Tirrell, M.; Bates, F. S. *Phys. Rev. Lett.* 1993, *70*, 1449–1452.
43. Almdal, K.; Mortensen, K.; Koppi, K. A.; Tirrell, M.; Bates, F. S. *J. Phys. France II*, 1996, *6*, 617–637.
44. Nakajima, A.; Hayashi, T.; Kugo, K.; Shinoda, K. *Macromolecules* 1979, *12*, 840–843.
45. Nakajima, A.; Kugo, K.; Hayashi, T. *Macromolecules* 1979, *12*, 844–848.
46. Cornelissen, J. J. L. M.; Fischer, M.; Sommerdijk, N. A. J. M.; Nolte, R. J. M. *Science* 1998, *280*, 1427–1430.
47. Li, W.; Huang, J. *J. Polym. Sci.: Part B: Polym. Phys.* 1992, *30*, 727–732.
48. Zhao, J.; Majumdar, B.; Schulz, M. F.; Bates, F. S.; Almdal, K.; Mortensen, K.; Hajduk, D. A.; Gruner, S. M. *Macromolecules* 1996, *29*, 1204–1215.
49. Bates, F. S.; Schulz, M. F.; Khanpur, A. K.; Forster, S.; Rosedale, J. H.; Almdal, K.; Mortensen, K. *Faraday Discuss.* 1994, *98*, 7–18.
50. Hamley, I. W.; Gehlsen, M. D.; Khandpur, A. K.; Koppi, K. A.; Rosedale, J. H.; Schulz, M. F.; Bates, F. S.; Almdal, K.; Mortensen, K. *J. Phys. France II*, 1994, *4*, 2161–2186.
51. Rosedale, J. H.; Bates, F. S.; Almdal, K.; Mortensen, K.; Wignall, G. D. *Macromolecules* 1995, *28*, 1429–1443.
52. Kofinas, P.; Cohen, R. E. *Macromolecules* 1994, *27*, 3002–3008.
53. Gehlsen, M. D.; Bates, F. S. *Macromolecules* 1994, *27*, 3611–3618.
54. Unger, R.; Beyer, D.; Donth, E. *Polymer* 1991, *32*, 3305–3312.
55. Schipper, F. J. M.; Floudas, G.; Pispas, S.; Hadjichristidis, N.; Pakula, T. *Macromolecules* 2002, *35*, 8860–8868.
56. Almdal, K.; Rosedale, J. H.; Bates, F. S.; Wignall, G. D.; Fredrickson, G. H. *Phys. Rev. Lett.* 1990, *65*, 1112–1115.
57. Gehlsen, M. D.; Almdal, K.; Bates, F. S. *Macromolecules* 1992, *25*, 939–943.
58. Almdal, K.; Rosedale, J. H.; Bates, F. S. *Macromolecules* 1990, *23*, 4336–4338.
59. Almdal, K.; Bates, F. S.; Mortensen, K. *J. Chem. Phys.* 1992, *96*, 9122–9132.
60. Koppi, K. A.; Tirrell, M.; Bates, F. S.; Almdal, K.; Mortensen, K. *J. Rheol.* 1994, *38*, 999–1027.
61. Karim, A.; Singh, N.; Sikka, M.; Bates, F. S.; Dozier, W. D.; Felcher, G. P. *J. Chem. Phys.* 1994, *100*, 1620–1629.
62. Almdal, K.; Koppi, K.; Bates, F. S. *Macromolecules* 1993, *26*, 4058–4060.
63. Cummins, C. C.; Beachy, M. D.; Schrock, R. R.; Vale, M. G.; Sankaran, V.; Cohen, R. E. *Chem. Mater.* 1991, *3*, 1153–1163.
64. Sankaran, V.; Yue, J.; Cohen, R. E.; Schrock, R. R.; Silbey, R. J. *Chem. Mater.* 1993, *5*, 1133–1142.
65. Chan, Y. N. C.; Craig, G. S. W.; Schrock, R. R.; Cohen, R. E. *Chem. Mater.* 1992, *4*, 885–894.
66. Saunders, R. S.; Cohen, R. E.; Schrock, R. R. *Macromolecules* 1991, *24*, 5599–5605.
67. Sankaran, V.; Cohen, R. E.; Cummins, C. C.; Schrock, R. R. *Macromolecules* 1991, *24*, 6664–6669.
68. Chan, Y. N. C.; Schrock, R. R.; Cohen, R. E. *Chem. Mater.* 1992, *4*, 24–27.
69. Winey, K. I.; Thomas, E. L.; Fetters, E. L. *Macromolecules* 1992, *25*, 2645–2650.
70. Winey, K. I.; Thomas, E. L.; Fetters, L. J. *Macromolecules* 1992, *25*, 422–428.
71. Disko, M. M.; Liang, K. S.; Behal, S. K.; Roe, R. J.; Jeon, K. J. *Macromolecules* 1993, *26*, 2983–2986.
72. Cohen, R. E.; Cheng, P.-L.; Douzinas, K.; Kofinas, P.; Berney, C. V. *Macromolecules* 1990, *23*, 324–327.
73. Thomas, E. L.; Anderson, D. M.; Henke, C. S. *Nature* 1988, *334*, 598.
74. Aggarwal, S. L. *Polymer* 1976, *17*, 938–956.
75. Morrison, F. A.; Mays, J. W.; Muthukumar, M.; Nakatani, A. I.; Han, C. C. *Macromolecules* 1993, *26*, 5271–5273.
76. Yamaoka, I.; Kimura, M. *Polymer* 1993, *34*, 4339.
77. Sakurai, S.; Momii, T.; Taie, K.; Shibayama, M.; Nomura, S.; Hashimoto, T. *Macromolecules* 1993, *26*, 485–491.
78. Han, C. D.; Baek, D. M.; Kim, J.; Kimishima, K.; Hashimoto, T. *Macromolecules* 1992, *25*, 3052–3067.
79. Smith, D. R.; Meier, D. J. *Polymer* 1992, *33*, 3777–3782.
80. Scott, D. B.; Waddon, A. J.; Lin, Y. G.; Karasz, F. E.; Winter, H. H. *Macromolecules* 1992, *25*, 4175–4181.
81. Spontak, R. J.; Williams, M. C.; Agard, D. A. *Polymer* 1988, *29*, 387–395.
82. Albalak, R. J.; Thomas, E. L. *J. Polym. Sci. Part B: Polym. Phys.* 1994, *32*, 341–350.
83. Pakula, T.; Saijo, K.; Kawai, H.; Hashimoto, T. *Macromolecules* 1985, *18*, 1294–1302.
84. Bates, F. S.; Berney, C. V.; Cohen, R. E. *Macromolecules* 1983, *16*, 1101–1108.
85. Bates, F. S.; Cohen, R. E.; Berney, C. V. *Macromolecules* 1982, *15*, 589–592.
86. Russell, T. P.; Karis, T. E.; Gallot, Y. *Nature* 1994, *368*, 729.
87. Cohen, R. E.; Bates, F. S. *J. Polym. Sci.: Part B: Polym. Phys.* 1980, *18*, 2143–2148.
88. Fischer, H. *Polymer* 1994, *35*, 3786–3788.
89. Chu, J. H.; Rangarajan, P.; Adams, J. L.; Register, R. A. *Polymer* 1995, *36*, 1569–1575.
90. Hajduk, D. A.; Gruner, S. M.; Rangarajan, P.; Register, R. A.; Fetters, L. J.; Honeker, C.; Albalak, R. J.; Thomas, E. L. *Macromolecules* 1994, *27*, 490–501.
91. Hashimoto, T.; Kawamura, T.; Harada, M.; Tanaka, H. *Macromolecules* 1994, *27*, 3063–3072.
92. Sakurai, S.; Okamoto, S.; Kawamura, T.; Hashimoto, T. *J. Appl. Cryst.* 1991, *24*, 679–684.
93. Okamoto, S.; Saijo, K.; Hashimoto, T. *Macromolecules* 1994, *27*, 3753–3758.
94. Khandpur, A. K.; Förster, S.; Bates, F. S.; Hamley, I. W.; Ryan, A. J.; Bras, W.; Almdal, K.; Mortensen, K. *Macromolecules* 1995, *28*, 8796–8806.
95. Winey, K. I.; Thomas, E. L.; Fetters, L. J. *J. Chem. Phys.* 1991, *95*, 9367–9375.
96. Winey, K. I.; Patel, S. S.; Larson, R. G.; Watanabe, H. *Macromolecules* 1993, *26*, 2542–2549.
97. Winey, K. I.; Patel, S. S.; Larson, R. G.; Watanabe, H. *Macromolecules* 1993, *26*, 4373–4375.
98. Winey, K. I.; Gobran, D. A.; Xu, Z. D.; Fetters, L. J.; Thomas, E. L. *Macromolecules* 1994, *27*, 2392–2397.
99. Hashimoto, T.; Shibayama, M.; Kawai, H. *Macromolecules* 1980, *13*, 1237–1247.
100. Hasegawa, H.; Hashimoto, T.; Kawai, H.; Lodge, T. P.; Amis, E. J.; Glinka, C. J.; Han, C. C. *Macromolecules* 1985, *18*, 67–78.
101. Hashimoto, T.; Hideaki, T.; Hasegawa, H. *Macromolecules* 1990, *23*, 4378–4386.
102. Mori, K.; Hasegawa, H.; Hashimoto, T. *Polymer* 1990, *31*, 2368–2376.
103. Hashimoto, T.; Yamasaki, K.; Koizumi, S.; Hasegawa, H. *Macromolecules* 1993, *26*, 2895–2904.
104. Hashimoto, T.; Koizumi, S.; Hasegawa, H. *Macromolecules* 1994, *27*, 1562–1570.
105. Ishizu, K.; Yamada, Y.; Fukutomi, T. *Polymer* 1990, *31*, 2047–2052.
106. Ishizu, K.; Omote, A.; Fukutomi, T. *Polymer* 1990, *31*, 2135–2140.

107. Spontak, R. J.; Smith, S. D.; Ashraf, A. *Macromolecules* 1993, 26, 956–962.
108. Spontak, R. J.; Smith, S. D.; Ashraf, A. *Polymer* 1993, 34, 2233–2236.
109. Richards, R. W.; Thomason, J. L. *Polymer* 1981, 22, 581–589.
110. Richards, R. W.; Thomason, J. L. *Macromolecules* 1983, 16, 982–992.
111. Thomas, E. L.; Lescanec, R. L. *Phil. Trans. R. Soc. London* 1994, 348, 149–166.
112. Hadziioannou, G.; Skoulios, A. *Macromolecules* 1982, 15, 267–271.
113. Koizumi, S.; Hasegawa, H.; Hashimoto, T. *Macromolecules* 1994, 27, 4371–4381.
114. Hajduk, D. A.; Ho, R.-M.; Hillmyer, M. A.; Bates, F. S.; Almdal, K. *J. Chem. Phys. B* 1998, 102, 1356–1363.
115. Widmaier, J. M.; Meyer, G. C. *J. Polym. Sci. Part B: Polym. Phys.* 1980, 18, 2217–2225.
116. Herman, D. S.; Kinning, D. J.; Thomas, E. L. *Macromolecules* 1987, 20, 2940–2942.
117. Matsushita, Y.; Taskasu, T.; Yagi, K. *Polymer* 1994, 35, 2862–2866.
118. Spontak, R. J.; Smith, S. D.; Ashraf, A. *Macromolecules* 1993, 26, 5118–5124.
119. Matsushita, Y.; Mogi, Y.; Mukai, H.; Watanabe, J.; Noda, I. *Polymer* 1994, 35, 246–249.
120. Tselikas, Y.; Iatrou, H.; Hadjichristidis, N.; Liang, K. S.; Mohanty, K.; Lohse, D. J. *J. Chem. Phys.* 1996, 105, 2456–2462.
121. Hajduk, D. A.; Harper, P. E.; Gruner, S. M.; Honeker, C. C.; Thomas, E. L.; Fetters, L. J. *Macromolecules* 1995, 28, 2570–2573.
122. Avgeropoulos, A.; Dair, B. J.; Hadjichristidis, N.; Thomas, E. L. *Macromolecules* 1997, 30, 5634–5642.
123. Hasegawa, H.; Tanaka, H.; Yamasaki, K.; Hashimoto, T. *Macromolecules* 1987, 20, 1651–1662.
124. Thomas, E. L.; Alward, D. B.; Kinning, D. J.; Martin, D. C.; Handlin, D. L.; Fetters, L. J. *Macromolecules* 1986, 19, 2197–2202.
125. Herman, D. S.; Kinning, D. J.; Thomas, E. L.; Fetters, L. J. *Macromolecules* 1987, 20, 2940–2942.
126. Alward, D. B.; Kinning, D. J.; Thomnas, E. L.; Fetters, L. J. *Macromolecules* 1986, 19, 215–224.
127. Kinning, D. J.; Thomas, E. L.; Alward, D. B.; Fetters, L. J.; Handlin, D. L. *Macromolecules* 1986, 19, 1288–1290.
128. Sakurai, S.; Kawada, H.; Hashimoto, T.; Fetters, L. J. *Macromolecules* 1993, 26, 5796–5802.
129. Sakurai, S.; Kawada, H.; Hashimoto, T.; Fetters, L. J. *Proc. Jpn. Acad.* 1993, 69, 13.
130. Morrison, F. A.; Winter, H. H.; Gronski, W.; Barnes, J. D. *Macromolecules* 1990, 23, 4200–4205.
131. Winter, H. H.; Scott, D. B.; Gronski, W.; Okamoto, S.; Hashimoto, T. *Macromolecules* 1993, 26, 7236–7244.
132. Floudas, G.; Hadjichristidis, N.; Iatrou, H.; Pakula, T. *Macromolecules* 1996, 29, 3139–3146.
133. Hashimoto, T.; Fujimura, M.; Kawai, H. *Macromolecules* 1980, 13, 1660–1669.
134. Floudas, G.; Pispas, S.; Hadjichristidis, N.; Pakula, T.; Erukhimovich, I. *Macromolecules* 1996, 29, 4142–4154.
135. Yang, L.; Hong, S.; Gido, S. P.; Velis, G.; Hadjichristidis, N. *Macromolecules* 2001, 34, 9069–9073.
136. Beyer, F. L.; Gido, S. P.; Poulos, Y.; Avgeropoulos, A.; Hadjichristidis, N. *Macromolecules* 1997, 30.
137. Löwenhaupt, B.; Hellmann, G. P. *Polymer* 1991, 32, 1065–1076.
138. Akiyama, M.; Jamieson, A. M. *Polymer* 1992, 33, 3582–3592.
139. Schulz, M. F.; Bates, F. S.; Almdal, K.; Mortensen, K. *Phys. Rev. Lett.* 1994, 73, 86–89.
140. Matsushita, Y.; Mori, K.; Saguchi, R.; Nakao, Y.; Noda, I.; Nagasawa, M. *Macromolecules* 1990, 23, 4313–4316.
141. Matsushita, Y.; Mori, K.; Saguchi, R.; Noda, I.; Nagasawa, M.; Chang, T.; Glinka, C. J.; Han, C. C. *Macromolecules* 1990, 23, 4317–4321.
142. Jiang, S.; Gopfert, A.; Abetz, V. *Macromol. Rapid Commun.* 2003, 24, 932–937.
143. Saito, R.; Kawachi, N.; Ishizu, K. *Polymer* 1994, 35, 866–871.
144. Saito, R.; Kotsubo, H.; Ishizu, K. *Polymer* 1994, 35, 1747–1753.
145. Schulz, M. F.; Khandpur, A. K.; Bates, F. S.; Almdal, K.; Mortensen, K.; Hajduk, D. A.; Gruner, S. *Macromolecules* 1996, 29, 2857–2867.
146. Ishizu, K.; Inagaki, K.; Bessho, K. *Makromol. Chem.* 1984, 185, 1169.
147. Saito, R.; Kotsubo, H.; Ishizu, K. *Polymer* 1994, 35, 1580–1585.
148. Almdal, K.; Mortensen, K.; Ryan, A. J.; Bates, F. S. *Macromolecules* 1996, 29, 5940–5947.
149. Papadakis, C. M.; Almdal, K.; Mortensen, K.; Vigild, M. E.; Stepanek, M. *J. Chem. Phys.* 1999, 111, 4319–4326.
150. Floudas, G.; Vazaiou, B.; Schipper, F.; Ulrich, R.; Wiesner, U.; Iatrou, H.; Hadjichristidis, N. *Macromolecules* 2001, 34, 2947–2957.
151. Mavroudis, A.; Avgeropoulos, A.; Hadjichristidis, N.; Thomas, E. L.; Lohse, D. J. *Chem. Mater.* 2003, 15, 1976–1983.
152. Known, Y.; Faust, R.; Chen, C. X.; Thomas, E. L. *Macromolecules* 2002, 35, 3348–3357.
153. Ryu, C. Y.; Lee, D. H.; Jeong, U.; Yun, S.-H.; Park, S.; Kwon, K.; Sohn, B.-H.; Chang, T.; Kim, J. K. *Macromolecules* 2004, 37, 3717–3724.
154. Schmidt, S. G.; Hillmyer, M. A. *Macromolecules* 1999, 32, 4794–4801.
155. Schmidt, C. S.; Hillmyer, M. A. *J. Polym. Sci. Part B: Polym. Phys.* 2002, 40, 2364–2376.
156. Mogi, Y.; Kotsuji, H.; Kaneko, Y.; Mori, K.; Matsushita, Y.; Noda, I. *Macromolecules* 1992, 25, 5408–5411.
157. Mogi, Y.; Mori, K.; Matsushita, Y.; Noda, I. *Macromolecules* 1992, 25, 5412–5415.
158. Matsushita, Y.; Tamura, M.; Noda, I. *Macromolecules* 1994, 27, 3680–3682.
159. Mogi, Y.; Nomura, M.; Kotsuji, H.; Ohnishi, K.; Matsushita, Y.; Noda, I. *Macromolecules* 1994, 27, 6755–6760.
160. Arai, K.; Kotaka, T.; Kitano, Y.; Yoshimura, K. *Macromolecules* 1980, 13, 1670–1678.
161. Liang, L.; Ying, S. *J. Polym. Sci. Part B: Polym. Phys.* 1993, 31, 1075–1081.
162. Auschra, C.; Stadler, R. *Macromolecules* 1993, 26, 2171–2174.
163. Gido, S. P.; Schwark, D. W.; Thomas, E. L.; Gonçalves, M. C. *Macromolecules* 1993, 26, 2636–2640.
164. Zioga, A.; Sioula, S.; Hadjichristidis, N. *Macromol. Symp.* 2000, 157, 239–249.
165. Stadler, R.; Auschra, C.; Beckmann, J.; Krappe, U.; Voigt-Martin, I.; Leibler, L. *Macromolecules* 1995, 28, 3080–3097.
166. Breiner, U.; Krappe, U.; Thomas, E. L.; Stabler, R. *Macromolecules* 1998, 31, 135–141.
167. Breiner, U.; Krappe, U.; Abetz, V.; Stadler, R. *Macromol. Chem. Phys.* 1997, 198, 1051–1083.
168. Breiner, U.; Krappe, U.; Jakob, T.; Abetz, V.; Stadler, R. *Polym. Bull.* 1998, 40, 219.
169. Ott, H.; Abetz, R.; Altstadt, V. *Macromolecules* 2001, 34, 2121–2128.
170. Breiner, U.; Krappe, U.; Stadler, R. *Macromol. Rapid Commun.* 1996, 17, 567–575.
171. Brinkmann, S.; Stadler, R.; Thomas, E. L. *Macromolecules* 1998, 31, 6566–6572.
172. Brinkmann, S. Doctoral Thesis, Mainz, 1998.
173. Krappe, U.; Stadler, R.; Voigt-Martin, I. *Macromolecules* 1995, 28, 4558–4561.
174. Beckmann, J.; Auschra, C.; Stadler, R. *Macromol. Rapid Commun.* 1994, 15, 67.
175. Stocker, W.; Beckmann, J.; Stadler, R.; Rabe, J. *Macromolecules* 1996, 29, 7502–7507.
176. Huckstadt, H.; Gopfert, A.; Abetz, V. *Macromol. Chem. Phys.* 2000, 201, 296–307.
177. Huckstadt, H.; Gopfert, A.; Abetz, V. *Polymer* 2000, 41, 9089–9094.
178. Huckstadt, H.; Goldacker, T.; Gopfert, A.; Abetz, V. *Macromolecules* 2000, 33, 3757–3761.
179. Stangler, S.; Abetz, V. *Rheol. Acta* 2003, 42, 569–577.
180. Schmalz, H.; Muller, A. J.; Abetz, V. *Macromol. Chem. Phys.* 2003, 204, 111–124.
181. Jung, K.; Abetz, R.; Stadler, R. *Macromolecules* 1996, 29, 1076–1078.
182. Sioula, S.; Hadjichristidis, N.; Thomas, E. L. *Macromolecules* 1998, 31, 5272–5277.
183. Okamoto, S.; Hasegawa, H.; Hashimoto, T.; Fujimoto, T.; Zhang, H.; Kazama, T.; Takano, A.; Isono, Y. *Polymer* 1997, 38, 5275–5281.
184. Neumann, C.; Loveday, D. R.; Abetz, V.; Stadler, R. *Macromolecules* 1998, 31, 2493–2500.
185. Neumann, C.; Abetz, V.; Stadler, R. *Colloid Polym. Sci.* 1998, 276, 19.

186. Avgeropoulos, A.; Paraskeva, S.; Hadjichristidis, N.; Thomas, E. L. *Macromolecules* 2002, *35*, 4030–4035.
187. Cochran, E.; Bates, F. S. *Phys. Rev. Lett.* 2004, *93*, 8702.
188. Bailey, T. S.; Hardy, C. M.; Eps III, T. H.; Bates, F. S. *Macromolecules* 2002, *35*, 7007–7017.
189. Eps III, T. H.; Cochran, E.; Bailey, T. S.; Waletzko, S.; Hardy, C. M.; Bates, F. S. *Macromolecules* 2004, *37*, 8325–8341.
190. Bailey, T. S.; Pham, H. D.; Bates, F. S. *Macromolecules* 2001, *34*, 6994–7008.
191. Shefelbine, T. A.; Vigild, M. E.; Matsen, M. W.; Hajduk, D. A.; Hillmyer, M. A. *J. Am. Chem. Soc.* 1999, *121*, 8457–8465.
192. Yamauchi, K.; Takahashi, K.; Hasegawa, H.; Iatrou, H.; Hadjichristidis, N.; Kaneko, T.; Nishikawa, Y.; Jinnai, H.; Matsui, T.; Nishioka, H.; Shimizu, M.; Furukawa, H. *Macromolecules* 2003, *36*, 6962–6966.
193. Pispas, S.; Floudas, G.; Hadjichristidis, N. *Macromolecules* 1999, *32*, 9074–9077.
194. Floudas, G.; Hadjichristidis, N.; Iatrou, H.; Avgeropoulos, A.; Pakula, T. *Macromolecules* 1998, *31*, 6943–6950.
195. Frick, E. M.; Zalusky, A. S.; Hillmyer, M. A. *Biomacromolecules* 2003, *4*, 216–223.
196. Avgeropoulos, A.; Chan, V. Z.-H.; Lee, V. Y.; Ngo, D.; Miller, R. D.; Hadjichristidis, N.; Thomas, E. L. *Chem. Mater.* 1998, *10*, 2109–2115.
197. Abetz, V.; Goldacker, T. *Macromol. Rapid Commun.* 2000, *21*, 16–34.
198. Eps III, T. H.; Cochran, E.; Hardy, C. M.; Bailey, T. S.; Waletzko, R. S.; Bates, F. S. *Macromolecules* 2004, *37*, 7085–7088.
199. Cochran, E. W.; Garcia-Cervera, C. J.; Fredrickson, G. H. *Macromolecules* 2006, *39*, 2449–2451; erratum 4864.

CHAPTER 41

Polymer Liquid Crystals and Their Blends

Witold Brostow

LAPOM, Department of Materials Science and Engineering and Department of Physics, University of North Texas,
P.O. Box 305310, Denton, TX 76203-5310 <http://www.unt.edu/LAPOM/>; brostow@unt.edu

41.1	Introduction	653
41.2	Molecular Structures	655
41.3	Hierarchical Structures, LC Phases and Thermophysical Properties	657
41.4	Mechanical properties	659
41.5	Tribological Properties	661
41.6	Blending and Rheological Properties	662
41.7	Electrical and Magnetic Properties	664
41.8	Optical Properties	665
41.9	Theory and Computer Simulations	666
	Acknowledgments	669
	References	669

41.1 INTRODUCTION

41.1.1 Liquid crystals, plastic crystals and condiscrystals

We already know much about flexible polymers, particularly because massively produced engineering polymers (EPs) are typically flexible. More complicated, and therefore more challenging, are systems involving polymer liquid crystals (PLCs)—which are copolymers containing simultaneously relatively rigid and flexible sequences. PLCs have much better properties than EPs, and also than fiber-reinforced composites and other classes of polymer-based materials; see Section 41.1.4. However, the use of these other classes of polymers is by no means in jeopardy, and will continue to grow, since PLCs are expensive. There is a way out: blend PLCs with EPs in such proportions that the good properties of PLCs “show up,” while at the same time there is in each case enough of an EP to keep the costs at bay. This can be done, but it is not exactly easy; so often polymers—PLCs including—“do not like each other”; their miscibility or at least compatibility is a problem. In this chapter we shall define what PLCs are, what molecular and phase structures they have, what properties do they have, and what are current and potential applications. The

problem of blending is clearly related to extending the application range.

To begin with, and contrary to a still widely held belief, the words “liquid-crystalline” and “mesomorphic” are *not* synonymous. The term *mesomorphic phases* was introduced by Friedel in 1922 [1]; it is now often abbreviated to *mesophases*. He defined them as phases with microscopic structures between solids and ordinary isotropic liquids. Not much happened in this area until 1955 when Kast [2] tried to characterize such phases in terms of lateral, longitudinal, and steric disorder. The next step occurred in 1984 when Wunderlich and Grebowicz [3] defined condiscrystals for the first time. Following them [3,4] we now distinguish three kinds of mesophases: liquid crystals, plastic crystals, and condiscrystals.

To see the distinctions between these three kinds of phases, we need to define first positional, orientational, and conformational ordering; this can be done easily using an example. When methane melts, various relative positions of its quasi-spherical molecules become possible—since *positional disordering* occurs. When we move to the next homolog in the *n*-alkane series, ethane, its melting is accompanied also by positional disordering; intermolecular distances become less uniform. However, melting of ethane involves at the same time *orientational disordering* since

two molecules can now be perpendicular to each other, or parallel as they largely were before, or anything in between. A longer paraffin hydrocarbon molecule such as *n*-decane also undergoes positional and orientational disordering, but *conformational disordering* dominates here: the segments acquire freedom to execute rotations about single bonds. Wunderlich and Grebowicz [3] provide an instructive example: the camphor molecule contains 10 carbon atoms, as does *n*-decane. However, the former is nearly spherical and rigid, hence there are no orientational or conformational effects on melting. Therefore, the entropy of fusion of camphor is much lower than that of *n*-decane.

With the information on the three types of disordering processes, we can now define three kinds of mesophases:

- liquid crystals exhibit positional disordering;
- plastic crystals show orientational disordering; and
- condensation crystals exhibit conformational disordering.

All three kinds of mesophases show some degree of long-range order—similarly as “decent” crystals. Similarly to isotropic liquids, however, these three kinds of phases exhibit also some degree of mobility other than segment vibrations known in ordinary crystals.

41.1.2 Monomer liquid crystals (MLCs) and polymer liquid crystals (PLCs)

Before going any further, let us adopt the terminology introduced by Samulski [5]. We have already used above the abbreviation PLCs. Samulski contrasted PLCs to MLCs, and defined the latter as low molecular mass LCs—irrespective of the fact whether they *can or cannot* polymerize. His terminology is unequivocal and succinct. People unfamiliar with it use long and not necessarily well-defined terms, such as “liquid-crystalline substances with low molecular weights”—when they presumably mean MLCs. Other names such as liquid crystalline polymers (LCPs) for PLCs or LMMLCs for MLCs are also in use. The abbreviation SRPs for self-reinforcing polymers and the name *in situ*—composites [6] are used as well. Moreover, PLCs are sometimes also called *molecular composites*.

PLC phases which appear in certain temperature intervals are called *thermotropic*; this chapter is devoted to them almost exclusively. There are also materials called *lyotropic* in which LC properties are induced by the presence of a solvent. Basic properties of such PLCs have been reviewed by Hall and Tiddy and by Northolt and Sikkema [7]. Hsiao, Shaw, and Samulski [8] have shown that liquid crystallinity can also be brought about by pressure elevation; by analogy, such materials have been called *barotropic* [9].

It is important to note that both MLCs and PLCs can adopt the same *phase structures*—such as nematic or smectic B. The phase structures of LC systems will be discussed in Section 41.3.1.

Let us also note that there exist oligomers intermediate between MLCs and PLCs, as studied by Abe and coworkers [10] as well as by Henderson and Imrie [11]. They are trimers or tetramers from the point of view of liquid crystallinity with flexible spacers in-between, and serve as models for longitudinal PLCs (see Section 41.2.1),

41.1.3 A brief history of MLCs and PLCs

Contrary to another widely held opinion, LCs have not been first synthesized by humans. *Silkworms* have been at it for quite a while. Li and Yu [12] in 1989 have found that the middle gland of silk fibroin is liquid crystalline—nematic to be more accurate. More results on this subject were reported for instance by Kerkam and coworkers [13].

The discovery of liquid crystals by humans is due to the Austrian botanist Friedrich Reinitzer [14]; what he observed in 1888 were cholesteric MLCs (see Section 41.3.1). Some people did not believe Reinitzer that such strange structures are possible. However, a German scientist named Otto Lehmann asked Reinitzer for some samples, conducted similar experiments, and reported virtually identical results a year later [15]. Given the popular disbelief, Lehmann’s results were not exactly trivial. Lehmann also coined the name “liquid crystals”—over objections of Reinitzer, who said the name is wrong and constitutes a contradiction. As you can easily imagine, there were centennial celebrations in Austria in 1988 and in Germany in 1989.

Some people believe that “serious” research on liquid crystals started only fairly recently. In fact, there is one city in the world where such work has been going on continuously for more than a century: Halle on the Saale. In 1900 or so Vorländer started at the University of Halle-Wittenberg a research group working on LCs; already in 1908 he published a book about them [16].

In 1923 Vorländer, having worked on MLCs for more than 20 years, realized that PLCs must exist as well. He asked [17]: “What happens to the molecules when one makes them longer and longer? Will the liquid-crystalline state disappear? From my experience, there is no limit to that state from chain elongation...” (my translation—W.B.). Even more importantly, Vorländer obtained from Hermann Fischer some polymers prepared by Emil Fischer, father of Hermann. It turned out that these polymers—synthesized in the XIXth century—were liquid crystalline [17]. Thus, not only studies of MLCs but also studies of PLCs started more than a century ago—although Emil Fischer did not quite realize this at the time. The Vorländer school founded so long ago is alive and well, continued later by Horst Sackmann, Dietrich Demus, Frank Kuschel, today also by Alfred Saupe, Gerhard Pelzl, Wolfgang Weissflog, Jürgen Lindau, and others, now at the Martin Luther University of Halle-Wittenberg as well as at the Max Planck Institute for Polymer Research in Halle.

41.1.4 PLCs Among Other Classes of Polymeric Materials

For many centuries the market place—and consequently large parts of science and technology—were dominated by proprietors of *raw materials*. However, in the last quarter of the XXth century this situation has changed. As pointed out in [18], a new generation of *end-users* says: “I need this and this, I don’t care whether it has been invented yet.” Therefore, instead of the traditional question: “What applications can be found for the material I am now working with?”, with an increasing frequency one asks: “What options do I have? What kinds of materials are or might be available?”. Preparing for a meeting on polymeric materials back in December 1990, I was surprised to find that nobody before applied the last question to them. Therefore, I prepared an answer. The answer has been modified by later developments and now we need to distinguish at least the following classes of polymer-based materials:

Flexible polymers—polyethylene (PE) and other EPs (see the first sentence of this Chapter) belong here, along with for instance polysiloxanes, poly(vinyl ether) and polyphosphazenes. Their properties are typically well known, processing conditions optimized, and many are available in large quantities and at low cost per unit weight. Their mechanical strength is for certain applications insufficient—which is the reason why other classes of polymeric materials are of interest.

Semiflexible polymers—including regular AB type copolymers in which A is rigid while B flexible. Cellulose derivatives belong here, as well as poly(*p*-hydroxybenzoic acid) (PHB), and for instance poly(*p*-phenylene terephthalamide). They are of course stronger than flexible polymers, but their processing is more difficult.

Rigid polymers—which include polyphenyl, α -helical peptides, and poly(*p*-phenylenebenzobis thiazole) (PPT). Problem with processing are here somewhat similar to those with the preceding class, but more acute. These materials typically require “exotic” and highly corrosive solvents.

Heterogeneous composites (HCs)—we have coined this name in 1988 [19] to distinguish them from molecular composites (see the last item) and from PLCs and PLC blends. HCs consist of a flexible matrix with a heterogeneous reinforcement such as glass fibers, carbon fibers, or glass spheres. The reinforcement can be polymeric (polymer fibers) or else ceramic or even metal. In the last two cases we have *hybrids* that is materials which include inorganic as well as organic constituents. We know from textbooks of materials science and engineering (see for instance Chapter 10 in [18]) that the components in fiber composites perform different functions: rigid fibers carry load while a matrix distributes load. However, given the disparity in the nature of fibers and the matrix, sufficient adhesion between these two types of constituents is often a problem. Cases of fiber pullout and delamination are well known. Problems of

creep, fracture initiation, and failure in fiber composites have been discussed by Piggott [20] and by Jansson and Sundström [21]. A thorough review of fiber-reinforced HCs has been provided by Pisanova and Zhandarov [22].

Polymer based nanohybrids—as in HCs, the matrix is polymeric. In contrast to HCs, however, the size of the minority component units (often powders) is on the scale of nanometers [23,24].

Molecular composites (MCs)—which are *polymer liquid crystals* and *PLC blends*. As in HCs, there is a rigid reinforcement. However, the reinforcement is at the molecular level—what applies to pure PLCs as well as to PLC-containing blends. Now, against the background just provided, and before going into details, let us compare PLCs with the most widely used type of polymers, that is EPs. Such comparisons have been made before [9,25,26,27]; one can summarize them by saying that PLCs

- show clear superiority over EPs with regard to *chemical stability*;
- show on the average *lower flammability* than EPs;
- have better *overall mechanical properties* than other classes listed above;
- have quite low *thermal expansivity*—sometimes even zero or negative;
- can be used at *higher temperatures* than EPs;
- thermotropic PLCs are often *easily processable* with conventional processing equipment for thermoplastics—this in contrast to rigid polymers and HCs;
- have high *stability* under *ultraviolet* (uv) and *visible light*;
- are *easily oriented* in shearing, electric and magnetic fields;
- exhibit *high stability under vacuum*.

41.2 MOLECULAR STRUCTURES

41.2.1 Classification of PLCs

The sequences in PLC chains which cause the LC character can be of different shapes: elongated (represented in the following by rectangles), approximately spherical (which will be represented by discs), or stars. The LC sequences can be placed in the main chain, or in side chains, or in both. To survey existing and possible structures, a comprehensive classification of PLCs based on their molecular structures was developed [25] and subsequently amplified [9,27]; a recent version is shown in Table 41.1.

Before the classification in [25] was proposed, one talked about main-chain and side-chain PLCs. It is clear from looking at classes such as α , β , γ , and ζ that the name “main-chain” is far from sufficient, since it includes

TABLE 41.1. Classification of PLCs on the basis of molecular structures [9,25,27].

Class	Structure	Name	
		English	German
α		longitudinal	longitudinal
β		orthogonal	orthogonal
γ		star (cross)	Stern (Kreuz)
ζS		soft disc	biegsamer Diskus
ζR		rigid disc	steifer Diskus
ζM		multiple disc	Multidiskus
εO		one-comb	Einzelkamm
εP		polisode-comb	Palisadenkamm
εD		double comb	Doppelkamm
φ		disc comb	Kammdiskus
κ		inverse comb	invertierter Kamm
$\theta 1$		parallel	parallel
$\theta 2$		biparallel	biparallel
$\lambda 1$		mixed	gemischt
$\lambda 2$			
$\lambda 3$			
$\psi 1$		double	doppelt
$\psi 2$			
σ		network	Netzwerk
ω		conic	kegelförmig

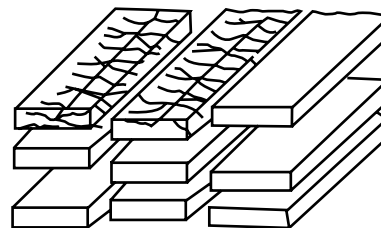
classes with vastly different structures; the same is true for “side-chain PLCs.” Incidentally, since the original classification was published in *Kunststoffe*, German names for the classes were coined at the same time as the English ones, and both series of names are listed in the Table. A couple of names (cross, network) were already in existence earlier, but most names were created while building up the classification. Examples of specific PLCs belonging to each class are given in [9,25] and [27]; we do not have enough space in this Chapter for examples.

41.2.2 Molecular Structure–Property Connection

As mentioned above, the initial objective of the classification was just to survey the structures. However, already while constructing the present Table 41.1, a much better reason was found: properties of PLCs depend strongly on the molecular structures of the chains. In other words, PLC materials such that each material consists of chains from a different class have different properties. Two years after the original classification [25], Ebert and coworkers [28] reached a similar conclusion: “in most liquid-crystalline systems it is predominantly the molecular shape which determines which kind of liquid-crystalline phase is formed.” Needless to say, the phase structure formed has important consequences for the properties. Similarly, Gasparoux and his colleagues [29] say that “... the riches of chemistry of polymer liquid crystals make possible, via molecular engineering, to impart structural and functional properties to a polymeric mesomorphic material aimed at new applications” (my translation—W.B.). Thus, for instance mesogenic groups can be introduced at external surfaces of dendrimers [30] leading to PLC formation. Hydrogen-bonded supramolecular complexes also can lead to PLC materials [31].

The molecular structure—macroscopic property connection is a vast subject; we shall provide an example. Consider simple or one-row combs, subclass εO . Transition from a LC state such as nematic into isotropic liquid, accomplished by a temperature increase, results in lowering the viscosity [32]—as usual and as expected. However, for longitudinal polymers, class α , similar isotropization results in a viscosity *increase*: the rigid LC sequences were aligned in the LC state, but in the isotropic state all directions are equiprobable, and the flow is more difficult.

Since molecular structures affect also packing of LC chains in the solid phases, let us provide at least one example of this. In the subclass ζR we have single discs in the main chain but with rigid spacers; see again Table 41.1. Wendorff, Ringsdorf, and collaborators who have obtained and studied such PLCs [33,34] have proposed a *sanidic* (from the Greek for board-like) structure for their packing which is shown in Fig. 41.1. Disks can form columnar structures [27]. Self-assembly of disks into structures such as columnar has been reported [35].

**FIGURE 41.1.** Sanidic packing of GR subclass PLCs; after [33,34].

41.3 HIERARCHICAL STRUCTURES, LC PHASES AND THERMOPHYSICAL PROPERTIES

41.3.1 Kinds of LC Phases

As noted before, MLCs and PLCs share essentially the same kinds of phases; these are: nematic, cholesteric, and a variety of smectic phases. These three names have been proposed by Friedel [1] in 1922 who imagined that such phases should exist—long before his concepts were confirmed by diffractometric experiments. In all these phases the entire molecules (in MLCs) or the LC sequences in the chains (in PLCs) are oriented approximately—but not quite—perpendicularly to a preferred axis in space called *director*. The degree of alignment is characterized by the order parameter (also called the anisotropy factor) defined in 1946 by Hermans [36] as

$$s = (3\langle \cos^2 \theta \rangle - 1)/2, \quad (41.1)$$

where θ is the angle between the molecular axis and the director, and the braces $\langle \rangle$ denote an average for the material (or a layer). We see from Eq. (41.1) that in a completely isotropic system $s = 0$ while a system perfectly aligned along the director would have $s = 1$.

The simplest among LC phases are *nematic*, in which the orientation along the director is the only kind of long-range order present; see Fig. 41.2(a).

A *cholesteric* phase is formed by a pile of nematic phases with the director changing from one layer to another; see Fig. 41.2(b).

Smectic phases have also layers, but each layer has at least one more element of long-range order in addition to the director. There are several such phases, distinguished by capital Latin letters. Thus, in each smectic A phase the centers of molecules (in MLCs) or of LC sequences (in PLCs) lie on equidistant planes perpendicular to the director. In smectic B phases there are also such planes, but there is additionally a two-dimensional hexagonal lattice within each plane. There is no hexagonal structure in smectic C phases, while the director is tilted with respect to the plane normal (otherwise we would have another smectic A phase); an example is shown in Fig. 41.2(c). For a more detailed discussion of LC phases see for instance Chapter 6 in [18]. Phase transitions in MLCs are listed in books by Demus,

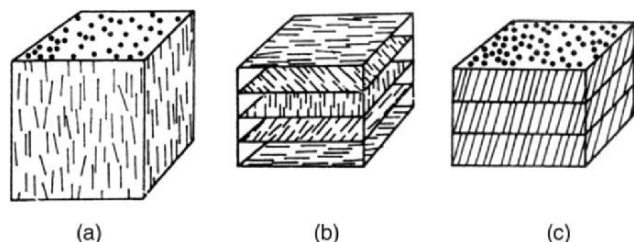


FIGURE 41.2. An example of a nematic (a), cholesteric (b) and smectic C (c) phase.

Demus, and Zschke [37,38]. *Textures* in LC phases which are sometimes colorful or even spectacular in polarized light are illustrated in a book by Demus and Richter [39].

41.3.2 Hierarchical Structures

It cannot be stressed enough that in PLCs the flexible and the LC sequences form separate phases. Since these two types of sequences are typically connected by primary chemical bonds, then each predominantly flexible phase contains a certain number of LC sequences; such a phase is called a *LC-poor phase* or simply a flexible matrix. Each predominantly liquid crystalline phase, called a *LC-rich phase* or an *island* [19] contains necessarily a certain number of flexible sequences. Thus, even a pure PLC—not a blend—typically contains at least two phases. This fact was discussed already in 1980 by Menczel and Wunderlich [40] who using differential scanning calorimetry (DSC) observed two glass transition temperatures, one for the flexible and one for the LC-rich phase; their subsequent more extensive studies confirmed this conclusion [41].

PLCs form hierarchical structures, and a hierarchical model of PLC morphology was proposed by Sawyer and Jaffe [42] and further refined by Sawyer and her colleagues [43,44]. They point out the differences between synthetic materials and biological systems, and conclude [45] that “... an increased understanding of biology will not increase our understanding of the origin of hierarchical morphologies. ...” They refer to the fact that biological structures also are hierarchical. Not only their argument makes sense, but I believe that the inverse might work: since synthetic systems are simpler, an increased understanding of hierarchies in synthetic materials will help the biologists to deal with their systems.

Since the islands constitute the primary mechanical reinforcement regions, we need to know more about them. Using a combination of scanning electron microscopy (SEM) and wide-angle x-ray diffractometry (WAXD) we have found that the islands have a hierarchical structure [45]; see Fig. 41.3. The islands in the scanning electron micrograph have the sizes between 1.0 and 1.4 μm . In turn, an individual crystallite has the average linear dimension of 12 nm—that is two orders of magnitude less—as found by WAXD.

As seen in Fig. 41.3, hierarchical arrangements occur within individual molecules as well as in phases built by the molecules. Using the concept of *homeomorphism*, we have formulated five rules governing ascension and descension in the hierarchies as well as characterizing structures at a given hierarchical level [45]. Two sets, X and Y , are homeomorphic if f is a one-to-one mapping of X onto Y (therefore: $f^c: Y \rightarrow X$) and both f and f^c are continuous. Our approach is based on the fact that each PLC molecule contains at least two kinds of building blocks which are *not* homeomorphic with respect to each other. Starting from this observation, the following rules for hierarchical structures have been formulated [45]:

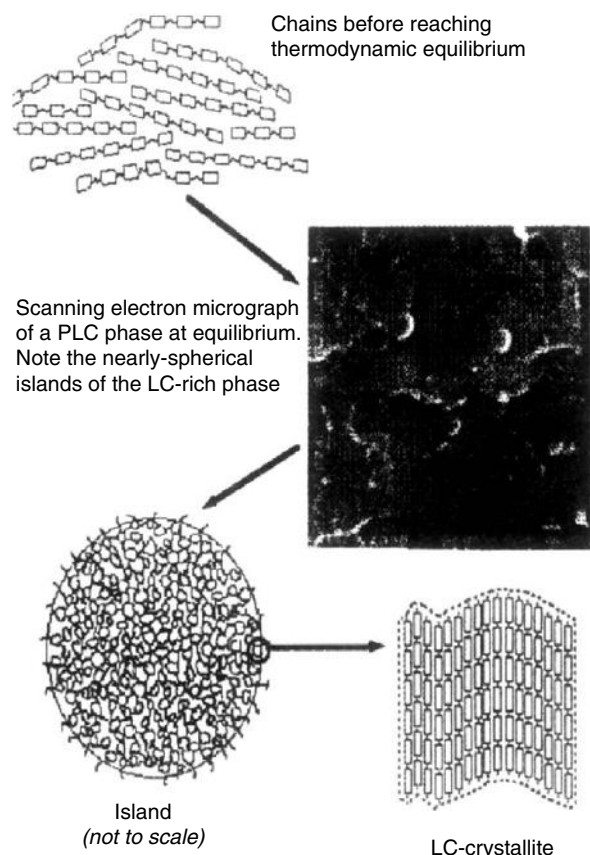


FIGURE 41.3. A hierarchical structure of LC-rich islands in a LC-poor matrix; after [45].

Rule 1. The complexity of hierarchical structures goes symbiotically with the number of building block types which are *not* homeomorphic with respect to one another.

Rule 2. Each level of hierarchy is defined by the constituting (nonhomeomorphic) types of entities, and by relations between the types. In materials the relations include (but are not limited to) connectedness by primary chemical bonds, hydrogen bridges, dispersion interactions, and interactions between phases such as adhesion forces.

Rule 3. Ascension in the hierarchy consists in defining relations such that the entities at the h level are divided into subsets, an entity at the $h + 1$ level corresponds to each subset, while each subset can consist of elements of one or more homeomorphic types. As a corollary, descent involves a relation between each h level entity and a subset of entities at the $h - 1$ level.

Rule 4. The structure of a *smaller* entity (such as the size and shape of a single molecule) determines the size, shape and structure of a *larger* entity (such as a LC phase). Since macroscopic properties are determined through *ascension* in the hierarchy, they are dependent on entities and their interactions at lower levels.

Rule 5. Assembling entities in a specified way can achieve properties which a system of unassembled entities does not have.

Let us provide at least one example of application of these rules. Sawyer and her colleagues [42–44] have defined the hierarchical fibrillar structure of LC materials after processing. Macrofibrils, fibrils, and microfibrils they consider constitute the key entities at three different levels—as defined in Rule 3.

A comment on Rule 2 also seems needed, since even some researchers working on LC materials believe that LC phase formation requires structures involving primary chemical bonds—while that Rule involves a more general concept of relations. Kato and Fréchet [46] and also Bazuin and her collaborators [47,48] have found that hydrogen bonds or ionic interactions are sufficient for the formation of LC phases. Somewhat similarly, Zhao and Lei [49] have obtained ionomers which form simple one-row combs, that is class ϵ O PLCs. Recall also the already mentioned work by Felekis and coworkers [31]. In other words, covalent bonds do *not* constitute a necessary condition for the formation of LC phases in polymers.

41.3.3 Phase Diagrams

The existence of a number of LC phases defined in Section 41.3.1 and of hierarchical structures of LC materials just discussed above has a number of consequences, including the following: phase diagrams of LC-containing systems are quite complicated.

Even if we do not have blends but only pure LC materials, multiphasicity appears a rule rather than an exception. Thus, the phase diagram of copolymers with the formula PET/ x PHB was determined [50]; PET is poly(ethylene terephthalate), PHB is *p*-hydroxybenzoic acid; x is the mole fraction of the LC component (here PHB) in the copolymers and constitutes the horizontal variable. The diagram contains 12 phase regions. Long-living nonequilibrium phases—typical in LC systems—are *included*, and thus each region contains up to four phases, such as: PET crystals, PHB-rich islands, isotropic PET-rich glass, and PHB-rich glass.

A new phase called *quasiliquid* (q1) was defined in the course of work on phase diagrams [50,51]. It originates from the amorphous state which existed below the glass transition temperature T_g , but q1 appears between T_g and the melting transition T_m . The q1 phase has the following characteristic features:

q1 is uncrosslinked and yet it does *not* exhibit the ordinary liquid mobility. The presence of another (liquid-crystalline) component below its glass transition and/or of crystallites prevents this phase from flowing like a liquid does. The hindrance to the flow is caused by the LC sequences, which in this respect act somewhat similarly to the junctions in polymer networks. This situation

is in contrast to nonLC polymers between T_g and T_m , in which the formerly amorphous phase flows around the crystalline regions, and the liquid viscosity depends on the temperature only. The viscosity of q1 depends also on the *concentration* of LC sequences. Pertinent here are the deuteron nuclear magnetic resonance (2H-NMR) results of Zachmann and collaborators [52]: they have found in PET/xPHB copolymers that the PHB sequences decrease considerably the mobility of PET sequences.

A liquid upon heating can only undergo vaporization or, if it is an isotropic polymer melt, no further phase transition at all. By contrast, q1 has to undergo at least two more transitions: melting and isotropization at the *clearing point*. If more than one LC phase is formed, then there will be even more transitions; for instance, PET/xPHB forms a smectic E and a smectic B phase.

The cold crystallization occurs in the q1 phase.

q1 shows an analogy with the leathery state in the elastomers. Both types of systems are immediately above their glass transition regions, and both exhibit *retarded* responses to application of external forces.

So far we have discussed pure PLCs, where the only variable was the concentration of the LC sequences in the copolymers. One can easily imagine that blends have even more complicated phase diagrams, as found for blends of PET/0.6PHB with EPs, for instance with polycarbonate [51]. An important reason for the study of phase diagrams is using them as a basis of processing optimization. In other words, in contrast to the usual establishment of processing parameters by trial and error, the knowledge of a phase diagram makes possible *intelligent processing*.

41.3.4 Isobaric Thermal Expansivity

Let us first define the quantity we are going to discuss:

$$\alpha = V^{-1}(\partial V/\partial T)_P, \quad (41.2)$$

which is called *isobaric expansivity*. The names “thermal expansivity” and particularly often “coefficient of thermal expansion” (abbreviated to CTE) are also in use. However, over a century ago Lord Kelvin [53] said that the use of the word “coefficient” when talking about viscosity, elasticity, compressibility, conductivity, and the like is “illogical,” “vicious,” and also “a mystery of circumlocution.” I admit to having used the phrase “coefficient of thermal expansion” myself, but after reading Lord Kelvin’s admonition I am not going to do it again. Incidentally, members of the Commission for Symbols, Units, and Nomenclature of the International Union of Pure and Applied Physics (IUPAC) have not read Lord Kelvin either, since they recommend [54] the name “cubic expansion coefficient”; the fact that this is a quantity pertaining to constant pressure is not included in their name either. However, there is

something rational in their name, because *linear isobaric expansivity* exists also:

$$\alpha_L = L^{-1}(\partial L/\partial T)_P, \quad (41.3)$$

where L is the specimen length. If a material is isotropic, then the two quantities in question can be related by simple algebra [55]

$$\alpha = (1 + \alpha_L)^3 - 1. \quad (41.4)$$

If a material is anisotropic, that is oriented during melt flow as PLCs are, we have the linear expansivity parallel to the flow α_{\parallel} and linear expansivity α_{\perp} perpendicular to the flow. The respective relation then is [56]

$$\alpha = (1 + \alpha_{\parallel})(1 + \alpha_{\perp})^2 - 1. \quad (41.5)$$

Clearly Eq. (41.5) reduces to Eq. (41.4) for the isotropic case as it should.

There is in this Handbook a whole Chapter 7 by Robert Orwoll on equation-of-state P–V–T properties of polymers. Briefly, confining our attention to what is pertinent for PLCs, there are basically two experimental procedures for α determination. One can measure α_L in a thermomechanical analysis (TMA) apparatus and then calculate α from Eqs. (41.4) or (41.5) [57,58]. Or, one can use an apparatus which produces full P–V–T data, that is specific volume v as a function of temperature T , $v(T)$, plus $\alpha(T)$ plus also isothermal compressibility $\kappa_T(T)$, where

$$\kappa_T = V^{-1}(\partial V/\partial P)_T. \quad (41.6)$$

Such an apparatus for polymer solids and melts called Gnomix has been developed decades ago [59] and it is being used with good results for polymers [60,61] and not only [62].

Industry needs more and more materials with low isobaric expansivity. PLC sequences are typically relatively rigid, and it is well known that rigid constituents exhibit low expansivity. A simple comparison of two numbers provides a good picture of the situation. The expansivity of polyethylene $\alpha(\text{PE}, 140^\circ\text{C}) = 7.20 \times 10^{-4}\text{K}^{-1}$. At the same temperature we have $\alpha(\text{PET}/0.6\text{PHB}, 140^\circ\text{C}) = 1.97 \times 10^{-4}\text{K}^{-1}$. Clearly, low isobaric expansivity constitutes another reason why PLCs are going to be used more and more.

Finally, let us note that the specific volume is an important parameter characterizing the glass transition and can be connected to other quantities pertaining to that transition. A scaling relationship along these lines has been proposed by Tölle [63] and developed further by Casalini and Roland [64,65].

41.4 MECHANICAL PROPERTIES

41.4.1 Areas of Application of PLCs

As briefly noted in Section 41.1.4, PLCs provide mechanical strength without the problems of easy separation of the reinforcement from the flexible matrix (fiber pullout)

characteristic for HCs. Thermotropic PLCs do not exhibit the difficulties in processing inherent to rigid polymers, HCs, and MCs.

Given the advantages of PLCs listed at the end of the Section 41.1.4, the number of applications of these materials is already considerable, and will increase along with further progress in synthesis, characterization, mechanical testing, phase diagram determination, and intelligent processing. Areas of application of PLCs have been reviewed by Jansson [66]. Following him, let us make a brief list of typical applications:

- connectors, surface-mount components, relay bobbins, capacitor housings, potentiometers, and switches in electronic and electrical industries;
- strength members, couplers, and connectors for fiber optics;
- fuel system components and electrical systems for automotive industry;
- motor components, lamp housings, conveyor belt components, and gears for industrial plants;
- tower packings, pump housings, pump shafts, and valves for chemical industry;
- compact disc components, microwav equipment, and turntables for domestic use; and
- other applications including medical components, watch components, safety equipment, chemical analysis equipment, and leisure goods.

Jansson [66] discusses also PLC rods, oriented sheets, films, and fibers. PLC fibers can be obtained by several procedures including melt spinning and dry-jet wet spinning. He also covers in some detail reasons for the applications of PLC fibers in ballistic vests, protective gloves and clothing, tarpaulins, conveyor belts, inflatable boats, sails, ropes, cables (for oil rig mooring), filament-wound pressure vessels, sails, sewing threads, radial tires, space and aircraft applications, boats, canoes and kayaks, military helmets, sporting goods, as cement reinforcements, in building materials and pipes, and in friction uses, and/or as asbestos replacements in brake linings, clutch, facings, and gasket packing.

Even with the space limitations we have, we need to mention also applications of PLCs in *coatings*, in particular as binders for higher solid bake coatings. This subject was also reviewed by Jansson [66].

41.4.1 Strengthening of PLC Materials

As we have seen in Section 41.3.1, LC sequences or molecules are oriented approximately parallel to the director. This is related to packing and caused by thermodynamic reasons (the usual tendency to lower the Gibbs function). Then we have a second stage of improved orien-

tation—caused by processing procedures such as extrusion or injection molding. However, we can improve the orientation still further by cold working operations. Given the natural orientation from the start, the effects here are more significant than in cold working of metals.

We shall provide an example of the effects of cold drawing as reported in [19]: specimens of PET/0.3PHB (note a relatively low concentration of the LC constituent) were drawn at 25 °C up to the elongation of 300% and then the tensile properties determined (for a discussion of tensile testing see Section 3 in Chapter 24). The elastic modulus as a function of elongation is shown in Fig. 41.4. It is clear that drawing has resulted in a fourfold increase of the modulus. The tensile strength changes similarly; see Fig. 41.5.

Instead of cold working, we have also the option of varying the concentration of LC sequences during synthesis. In Fig. 41.6 we show the modulus as a function of x in PET/ x PHB copolymers [19] in the direction parallel to flow. First

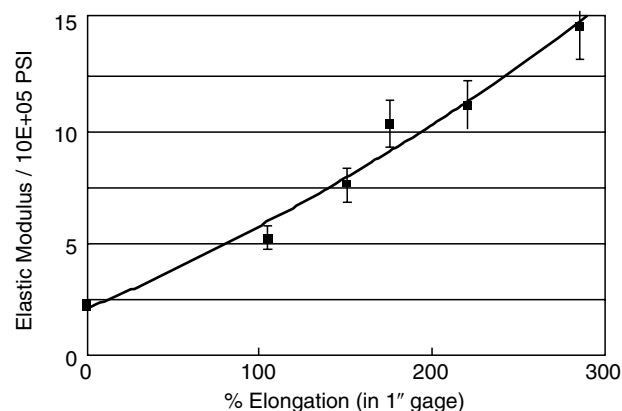


FIGURE 41.4. Elastic modulus changes at 25 °C resulting from cold drawing specimens of PET/0.3PHB. Filled squares represent each an average from five determinations; after [46].

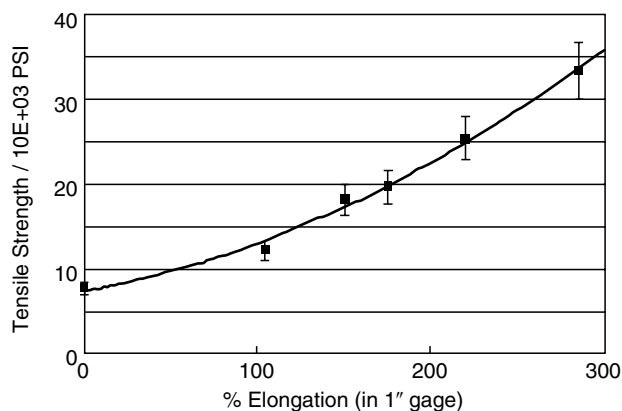


FIGURE 41.5. Tensile strength changes at 25 °C resulting from cold drawing specimens of PET/0.3PHB. Filled squares represent each an average from five determinations; after [50].

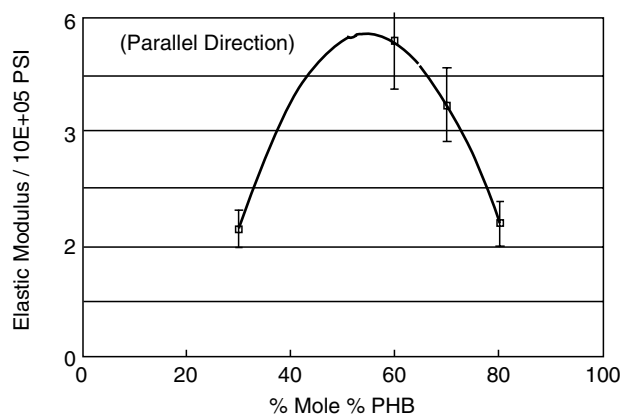


FIGURE 41.6. Elastic modulus at 25 °C of PET/xPHB copolymers as a function of x in the direction parallel to the flow during processing; after [50].

an increase in the concentration of the LC sequences x enhances the modulus. However, after reaching a maximum the modulus begins to decrease; we explain this by the fact that an increase in x also increases the brittleness of the material. The tensile strength behaves in a similar way; see Fig. 41.7. However, the story is different in the directions perpendicular (transverse) to the flow. Here increasing x leads to decreases in both modulus and the tensile strength; see, respectively, Figs. 41.8 and 41.9.

It should be kept in mind that the behavior just described pertains to longitudinal polymers, class α . We have noted in Section 41.2.2 connections between belonging of a PLC to a specific class and the properties. To acquire a better picture, consider now briefly networks, class σ . K pfer and Finkelmann [67] have developed a two-step procedure for creating such networks, subsequently amplified by K pfer, Nishikawa, and Finkelmann [68]. They first align mechanically a weakly crosslinked σ PLC; then a second crosslinking reaction of remaining free reactive groups freezes that alignment, creating materials which these authors call liquid

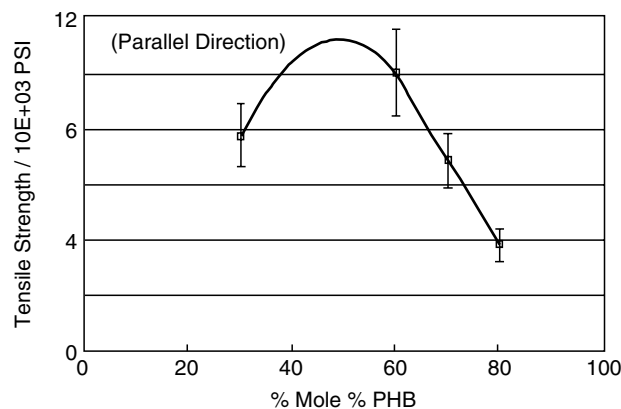


FIGURE 41.7. Tensile strength at 25 °C of PET/xPHB copolymers as a function of x in the direction parallel to the flow during processing; after [50].

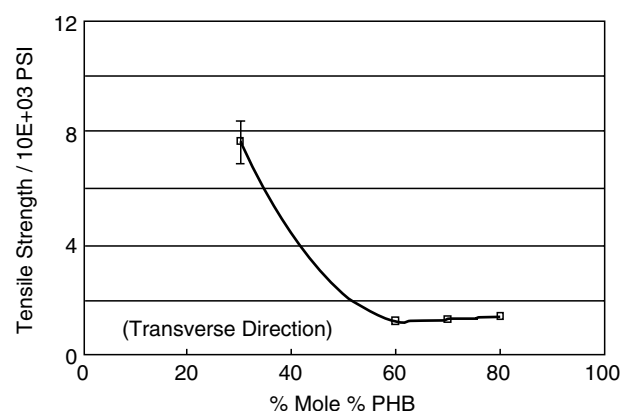


FIGURE 41.8. Elastic modulus at 25 °C of PET/xPHB copolymers as a function of x in the direction transverse to the flow during processing; after [50].

single crystal elastomers (LSCEs). This second stage can be performed at different temperatures, resulting in different degrees of the alignment. As expected, the alignment is higher if the second stage is performed in a LC state, and lower if it is performed above the isotropization (clearing) temperature. On the other hand Ambrogio and her colleagues [69] say that liquid crystal elastomers (LCEs) are lightly crosslinked, apparently stopping at the first stage of the procedure of Finkelmann and coworkers.

41.5 TRIBOLOGICAL PROPERTIES

41.5.1 Basic Concepts

Tribology is considered by some as a part of Mechanics, and by others as a discipline within Materials Science and Engineering (MSE) at the same level as Mechanics. Our own work seems to support the latter point of view. Tribological characterization of materials deals with *friction*,

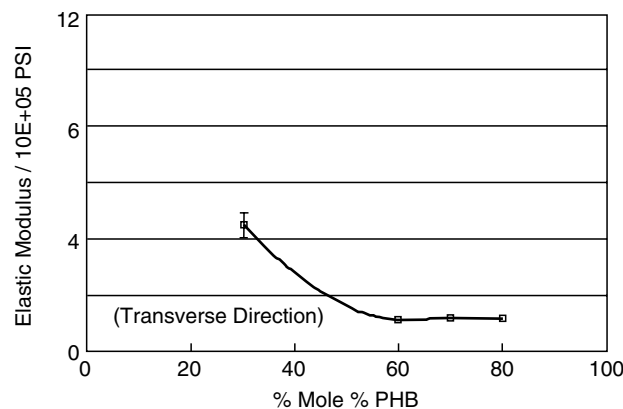


FIGURE 41.9. Tensile strength at 25 °C of PET/xPHB copolymers as a function of x in the direction transverse to the flow during processing; after [50].

wear, scratch resistance and design of interactive surfaces in relative motion [70,71]. Tribology is very well developed for metals [70] but it is quite difficult for polymers. For metals external lubricants work nicely, lowering friction and wear. Application of external lubricants to polymers in most cases results in lubricant absorption and polymer swelling. However, there is some recent progress in polymer tribology and one review of this subject [71].

Before we talk about tribological properties of PLCs, let us define some basic concepts [70, 71]. *Friction* can be defined as the tangential force of resistance to a relative motion of two contacting surfaces. In a stationary specimen we have *the static friction*, namely the force required to create motion divided by the force pressing mating surfaces together. This quantity is often called the static coefficient of friction. In Section 41.3.4 we have quoted Lord Kelvin [53]; the word “coefficient” conveys no information. For a specimen in motion we have *the dynamic friction* (also called *kinematic friction*), that is the force required to sustain motion at a specified surface velocity divided by the force pressing mating surfaces together. Similarly here, the term dynamic coefficient of friction is still used.

A *scratch test* method involves scratching the surface of samples and measuring the depth of the groove while the scratch is being made. This can be done under either a constant load, or a progressively increasing load, or else under a stepwise increasing load. The instantaneous depth values are called the *penetration depths* and we represent them by the symbol R_p [72]. Since polymers are viscoelastic materials, they should recover or heal after the scratch, with the bottom of the groove going up and settling at a final level called the *residual depth* R_h . Multiple scratching along the same groove is possible and serves to determine the sliding wear [73].

41.5.2 Friction and Scratch Resistance

In Section 41.7.2 we shall talk more about the fact that different force fields can produce effects on the PLC orientation. Already mentioned before PET/0.6PHB was subjected to magnetic fields and its tribological properties determined [74]. In Fig. 41.10 we display static and dynamic friction for three types of samples: unoriented, oriented along the field, and perpendicularly to the field. We know from Fig. 41.3 that the LC-rich regions form islands in a LC-poor matrix. Imposition of a magnetic field results in growth of the islands [74]. Apparently the feathery or fibrous surfaces of the islands cause higher friction. The effect is larger for the orientation along the field, smaller perpendicularly to the field, but the island growth results in both cases in higher friction than for unoriented samples. The island resistance to movement also causes *higher* dynamic than static friction, while for most polymer surfaces the reverse is true.

Since higher friction is desirable in rare cases only, one can ask what is the advantage of imposing magnetic fields on PLCs. An answer can be seen in Fig. 41.11: penetration

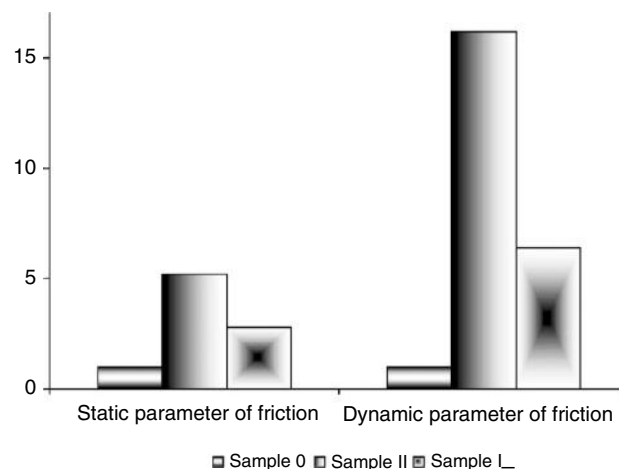


FIGURE 41.10. Static and dynamic friction at 25 °C of PET/0.6PHB as a function of orientation imposed by a magnetic field; after [74].

depth of different samples, here also unoriented one, oriented along the magnetic field, and perpendicularly to the field. We see that the field-imposed orientation and island growth enhance the scratch resistance. The depth values are lower for oriented samples. It is easy to understand why the effect is larger along the orientation direction.

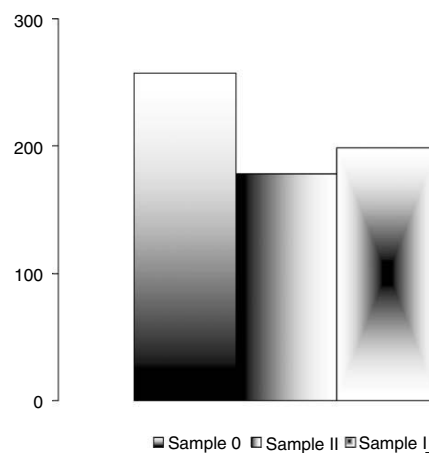


FIGURE 41.11. Penetration depth in scratching at 25 °C of PET/0.6PHB as a function of orientation imposed by a magnetic field; after [74].

41.6 BLENDING AND RHEOLOGICAL PROPERTIES

41.6.1 Rheology of Pure PLCs and of EP + PLC Blends

We discuss blending and rheology “in one breath”—that is in one section—because PLCs are often used as rheology modifiers for EPs.

To see what the presence of a PLC can do to the viscosity of an EP, consider two examples. In Fig. 41.12 we show

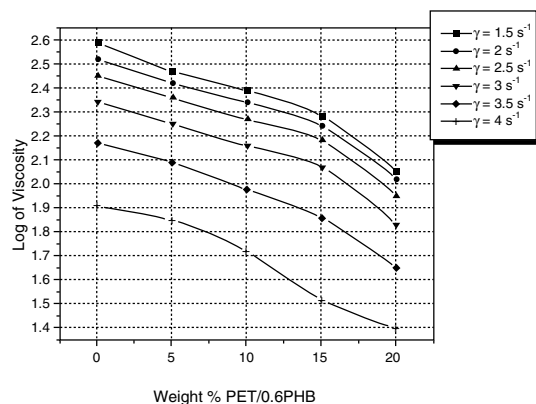


FIGURE 41.12. Logarithmic viscosity $\log h$ of polycarbonate + PET/0.6PHB blends at 290 °C as a function of the wt% of the PLC; shear rates defined in an insert; after [76].

logarithmic viscosity, $\log \eta$, of bisphenol-A polycarbonate (PCarb) to which up to 20 wt% of PET/0.6PHB is being added [76]; curves for several shear rates are shown. We see that the effects of addition of the PLC are smaller up to 10 or 15%, and then more pronounced at higher PLC concentrations. However, this is not a general phenomenon. Analogous curves where the same PLC is added to polypropylene (PP) are different [76]; see Fig. 41.13. Already the addition of only 5% of PET/0.6PHB to PP causes a pronounced $\log \eta$ lowering, while further addition of the PLC has little effect. The differences between these two kinds of behavior can be explained in terms of miscibilities of the respective pairs: PET/0.6PHB exhibits more affinity to PCarb than to PP [51].

The common feature of Figs. 41.12 and 41.13 is the fact that the presence of LC sequences in a flexible matrix lowers viscosity to a certain degree—much or little. However, even this assumption is not universally valid. Jackson and Kuhfuss [77] determined viscosity of PET/ x PHB copolymers as a function of x at 275 °C. They found that,

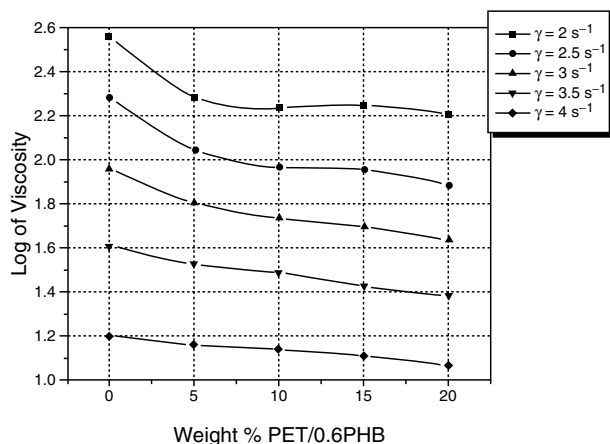


FIGURE 41.13. Logarithmic viscosity $\log h$ of polypropylene + PET/0.6PHB blends at 230 °C as a function of the wt% of the PLC; shear rates defined in an insert; after [76].

starting from pure PET ($x = 0$), $\log \eta$ first increases, goes through a maximum, falls, goes through a minimum, and then for $x > 0.7$ increases rapidly. One has to agree with Roetting and Hinrichsen [78] that PLC rheology “is a rather complex subject.” The findings of Jackson and Kuhfuss reflect a combination of effects of molecular structure (see Section 41.2), hierarchical structures (Section 41.3.2) and results of varying composition.

In spite of the complexity of the situation, there have been attempts to create theories of rheological behavior of PLCs. Wissbrun [79] represents a PLC material as a space-filling system of domains. At rest, the minimum energy arrangement is achieved when the directors in the planes of contact are parallel. Under shear, the domains slide over each other. The model predicts shear sensitiveness, a phenomenon observed experimentally: the curves of viscosity as a function of the shear rate are horizontal for low shear rates and then go down. In fact, for instance the results for PCarb + PET/0.6PHB blends—if we employ such coordinates rather than those in Fig. 41.12—exhibit shear sensitiveness [76].

It is instructive to compare rheological behavior of isotropic molten polymer phases to the simplest LC phases, that is nematic ones. In an isotropic phase molecular orientations are completely random; the flow process can only introduce some order. In a nematic PLC a certain degree of order (as measured by the parameter s , see Section 41.3.1) already exists. Therefore, a flow process can *either enhance or reduce* the existing order. This problem has been analyzed by Marrucci and Maffettone [80]. If instead of the order parameter we consider viscosity, then—as defined for MLCs already in 1946 by Miesowicz [81]—one has to distinguish three viscosities dependent on the direction: parallel to the flow direction; parallel to the gradient of viscosity; and perpendicular to both directions just named.

A very important feature of PLCs has been already mentioned in Section 41.1.4: thermotropic PLCs are often processable with conventional processing equipment for thermoplastics—in fact, given the orientation of LC sequences, more easily than thermoplastics. It is this ease of orientation which is the reason for one more name for PLCs, already mentioned above, namely self-reinforcing plastics.

Readers who want to know more about PLC rheology will find extensive literature on it. Fortunately, there is a whole book on this subject [82].

41.6.2 Properties of Blends

Here is another vast subject with which we can deal only briefly, but reviews are available [27]. Instructive here is to know a rule formulated already in 1960 by Arnold and Sackmann [83,84] for MLC + MLC pairs: complete miscibility always involves isomorphism. That is, if a nematic phase is miscible with a second LC phase, that second phase is also nematic. However, isomorphism is a necessary but not a sufficient condition. Several decades after the original

work, Sackmann [85] reviewed investigations pertaining to this rule—which all confirmed it.

As for EP + PLC blends, the main reason for using them was defined in the beginning of this Chapter; sometimes fillers (and/or other additives) are used as well. Needless to say, blends are more complicated than pure PLCs. For instance, cold crystallization of a constituent depends on the relative proportions and chemical nature of other constituents present [50,51]. Given the problems with polymer + polymer miscibility, the trial-and-error procedures (“We shall mix a PLC with an EP, and hopefully get good properties . . .”) are *even less* usable here than for EP + EP blends.

While in a previous section we have shown elastic modulus and tensile strength of *copolymers, blends* exhibit typically similar behavior: an increase in the concentration of the LC component enhances the mechanical properties along the orientation direction first, but a further increase worsens these properties because of higher brittleness. The elongation at break depends strongly on the brittleness, and decreases already at PLC concentrations of only a few percent. For other mechanical properties, Figs. 41.7–41.10 qualitatively *represent blends as well*; there is little point in providing numerical values for any specific blends. The existence of the maxima is advantageous for keeping the costs reasonable. The location of a maximum depends on the particular EP + PLC pair. At very low concentrations such as 5% there is not enough of the LC component to form the reinforcing islands (or fibrils if strongly elongated), hence the reinforcing effect is absent. However, similarly as in the viscosity curves shown in Figs. 41.12 and 41.13, sometimes less than 20 wt% PLC might be sufficient for a considerable improvement of mechanical properties [50]. There is thus a clear parallelism between rheological and mechanical behavior.

One more similarity between pure PLC copolymers and PLC-containing blends shows in results of cold working. In Figs. 41.4 and 41.5 we have seen the effects of drawing on a PLC. Similar effects are observed when subjecting to drawing EP + PLC blends.

Experimental results show that the reinforcement depends primarily on the EP + PLC miscibility, PLC concentration, and sizes and shapes of the islands. A method of miscibility improvement was developed by Schlee, Kossmehl, and Hinrichsen [86–88] who synthesized poly(*p*-phenylene terephthalates) with pentoxy groups as flexible side chains. Needless to say, such side chains mix well with EPs.

As for the islands, there is a problem of their optimization for the best mechanical properties. Too many too small islands do not do the job, because the lines of force apparently go around the islands. For a given LC sequence concentration, too large islands leave between them too large purely flexible unprotected regions. Since it is difficult to create experimentally islands of arbitrary size and shape, the problem of optimization can be solved best by computer simulations; see Section 41.8.

41.7 ELECTRICAL AND MAGNETIC PROPERTIES

41.7.1 Effects of Electric Fields

Before focusing on PLCs, let us quote the basic definitions [89]. The relative dielectric permittivity ϵ is the ratio of the capacities of a parallel plate condenser measured with and without (in vacuum) the dielectric material placed between the plates. If ϵ is independent of the field strength, it is called *dielectric constant*. Polymers are typically dielectric, so that—in contrast to electric conductors—there is a certain reversal of the relative positions of the electric charges after the removal of the field. If no permanent dipoles are present in the material, then the following Maxwell relation is valid:

$$\epsilon = n^2, \quad (41.7)$$

where n is the refractive index. Thus, there is a connection to optical properties to be discussed in the next section. Clear deviations from Eq. (41.7) might be caused by semiconductor behavior, but more frequently by the presence of permanent dipoles in the material.

Anisotropy of structure is reflected also in the dielectric constant. Similarly as for isobaric expansivity discussed in Section 41.3.4, one distinguishes here the parameter in the along-the-flow (parallel to the director) direction ϵ_{\parallel} from the perpendicular quantity ϵ_{\perp} . The anisotropy of the dielectric constant is usually expressed as

$$\Delta\epsilon = \epsilon_{\parallel} - \epsilon_{\perp} \quad (41.8)$$

and is typically larger in smectic than in nematic phases. For MLCs both positive and negative values of $\Delta\epsilon$ are known [90].

When an electric field is imposed upon a material, charged particles move in various ways: Electrons move with respect to the nuclei, creating induced dipole moments and electronic polarization; atoms and groups of atoms move similarly, causing atomic polarization; free ions if present move over long distances, usually to surfaces, what leads to interfacial polarization; permanent dipole moments align along the field, thus increasing in LC materials the order parameter s . In *dielectric relaxation spectroscopy* (DRS) sinusoidal electric fields are imposed upon the sample. This resembles sinusoidal mechanical fields discussed in Chapter 24.

Since various motions mentioned occur on various time scales, it is worthwhile to cover a wide range of frequencies. An important advantage of DRS over other spectroscopic techniques is the capability to explore a range of timescales from as slow as 10^4 s to as fast as 10^{-11} s. Therefore, this single technique allows to study a broad spectrum of motions as a function of temperature, pressure, or composition. Decomposition of DRS spectra into constituents corresponding to various processes is needed. A procedure for doing this which handles also the temperature dependencies of relaxational processes has been devised by Schlosser and his colleagues [91].

DRS results for PLCs have been reviewed by Moscicki [92]. We shall name here two findings. First, in simple one-row combs (see again Table 41.1) there are different rates of reorientation of different polar groups in side chains. This phenomenon was observed even in MLCs [93], but is apparently stronger in PLCs. Second, also in analogy to MLCs, in PLCs we observe *slow* relaxational processes along the director, and noticeably faster perpendicularly to it.

Table 41.1 shows us also a way to vary the numbers of both permanent and induced dipoles. This gives us the capability to *manipulate* dielectric properties of PLC materials over quite wide ranges.

41.7.2 Effects of Magnetic Fields and NMR Spectroscopy

It cannot be stressed enough that electric, magnetic, and mechanical (shear fields) produce in fact *similar effects of enhancing orientation*, thus increasing the order parameter s , and also affecting mechanical and other properties in ways already discussed above. There exist even favorite methods of achieving orientation for certain classes of materials. Thus, magnetic fields are typically used to orient polyacrylates, while polysiloxanes are routinely oriented by imposition of ac electric fields.

Since effects of magnetic field imposition are already known to us, we shall now discuss a method of studying the chain dynamics in PLCs at the molecular level involving such fields: nuclear magnetic resonance (NMR) spectroscopy.

A good review of NMR spectroscopy of PLCs has been written by Lauprêtre [94]. Therefore, in this Chapter we shall describe only a specific aspect of the problem. Because PLC chains typically contain both flexible and LC sequences, *orientational ordering of flexible sequences between LC sequences* is of interest. Similar behavior appears in PLC + EP blends, and also in solutions of LCs in low-molecular-mass flexible molecules. Photinos, Samulski, and Toriumi (PST) developed a theory of orientational ordering [95–97]. They regard flexible molecules as sets of rigid submolecular segments that can take different relative positions according to conformations, and formulate the potential of mean torque of the entire molecules in a modularly additive fashion. Samulski and his colleagues considered various choices of submolecular units in neat nematic LCs as well as in flexible alkane solute + nematic systems, and compared predictions of their theory with NMR data. The results indicate that in carbonlike chains a relatively simple choice of subunits (slightly biaxial atom-blocks) and a segment-wise additive potential provide an explicit and accurate representation of anisotropy of molecular shapes present simultaneously with molecular flexibility. The main reason for the success of the PST approach is fairly clear: the alignment of LC sequences is determined by the *CORDS* (or blocks) and not by the bonds. This is why previous treatments in terms of independent bonds did not

provide satisfactory results. Moreover, a chain of $N + 1$ segments contains N bonds, $N + 1$ blocks and $N + 1$ cords, so the alternative representations are of the same complexity. When switching from the bond to the chord representation, the number of parameters in the interaction potential necessary to obtain meaningful results does not increase either. Terms beyond second neighbors are too small to be visible in NMR spectra studied by PST.

While in this section we do not deal with thermophysical properties, they are connected to those now under discussion as well. Roth and Krücke [98] have shown that the glass transition temperatures of comb PLCs can be evaluated from the line shape of the wide line NMR signals.

41.8 OPTICAL PROPERTIES

41.8.1 Nonlinear Optical (NLO) Effects

We have already noted in Section 41.6.1 the connection between electrical and optical properties. The effects of light propagation through a material can be described in terms of the polarization

$$P = P_0 + \chi_1 \cdot \mathbf{E} + \chi_2 \cdot \mathbf{E} \cdot \mathbf{E} + \chi_3 \cdot \mathbf{E} \cdot \mathbf{E} \cdot \mathbf{E} + \dots, \quad (41.9)$$

where P_0 is the spontaneous polarization of the material, \mathbf{E} is the tensor of field strength of the electrical component of the optical field, while each c_i is the optical susceptibility of the i th order of the material. In linear optical materials the propagation of light is characterized by the independence of refraction on light intensity and also for instance on the absence of any changes in frequency of the light.

The establishment of presence of nonlinear optical (NLO) effects requires very strong optical fields, typically created by laser pulses. We talk about second-order NLO materials if the term with χ_2 in Eq. (41.9) dominates, third if the χ_3 -containing term is dominant, etc. The third-order optical materials are also called Kerr media. Returning once again to Table 41.1 with its variety of possible structures, we note that the NLO character of certain—even numerous—constituting units of a PLC is not enough for the whole material to exhibit NLO properties. If centers of symmetry are present, the induced dipoles largely cancel out, and χ_2 properties of the polymer are negligible.

One can base polymer design for NLO applications on the expression for the dipole moment μ in the effective electric field \mathbf{F} while \mathbf{E} is now a perturbing (such as oscillating) electric field:

$$\mu(\mathbf{F}, \mathbf{E}) = \mu_0(\mathbf{F}) + \alpha_0(\mathbf{F})\mathbf{E} + \beta_0(\mathbf{F})\mathbf{E} \cdot \mathbf{E}/2! + \gamma_0(\mathbf{F})\mathbf{E} \cdot \mathbf{E} \cdot \mathbf{E}/3! + \dots \quad (41.10)$$

Here μ_0 is the intrinsic dipole moment, α_0 is the linear polarizability, β_0 the hyperpolarizability, γ_0 the second hyperpolarizability, etc. Equation (41.10) is a molecular level analog of Eq. (41.9) for the macroscopic polarization. Thus, we are for instance interested in the second harmonic

generation (SHG), that is in doubling the frequency of the incident laser light. Equation (41.10) tells us that we need a second-order NLO material (= a χ_2 material) the dipole moment of which has a substantial hyperpolarizability contribution.

Marder and coworkers [99] have stressed the fact—almost universally disregarded or not even noticed before—that α_0 , β_0 , γ_0 , etc. are derivatives with respect to \mathbf{F} of their next order polarization or polarizability; thus, β_0 is the derivative of α_0 , and so on. Before them, some groups were for instance trying to optimize γ_0 in an NLO material by optimizing β_0 —not knowing that the β_0 optimization will automatically result in $\gamma_0 = 0$. The work of Marder and his colleagues has useful consequences. Certain chemical changes can affect the electron density similarly as applying an electric field to the molecule. Such changes include putting donor and acceptor groups on the polyene chain (alternating single and double carbon-carbon bonds), incorporating groups that gain aromaticity on polarization, or placing the molecule in a solvent that will stabilize charge separation.

41.8.2 PLCs for NLO Applications

Discussing optical applications of polymers, it is worth noting first of all that research objectives here go in two diametrically opposite directions. In some cases one wants to minimize the interactions with the light. This is the case with polymer optical fibers, and with all attempts to reduce the noise for optical recording and information storage on optical discs. In other cases the main objective is to maximize the polymer + light interactions, as in photonic devices when one wants to augment the light-intensity dependent change of the refractive index. Polymeric materials for optical applications have significant advantages in comparison with inorganic materials: low weights of optical components, good mechanical properties, and the ease of manufacturing parts even with complex geometries.

We have already mentioned before SHG materials; doubling of the light frequency enables a laser to encode four times as much information on a compact disc. NLO effects have significant technological implications for optical signal processing, generation of variable-frequency laser light, tunable filters, and optical data storage. The g_0 parameter is important for functions such as optical switching: a light beam alters the path of a second beam by changing the refractive index.

Optical data storage is an alternative to magnetic storage. There are several variations here: ROMs or read-only memories, DRAWs (= direct read after write) for writing once but reading many times, and erasable memories. The last technique can be realized by using comb PLCs. Such a PLC in its LC state (say one of the smectic states) is frozen below its glass transition temperature T_g , and then locally distorted by the heat absorbed from a laser pulse. Such a distortion is readable, since it scatters light. Aging of the material in the glassy state (see the section on aging in Chapter 24 on

mechanical properties) can be assumed slow enough for the time period during which the information is needed. That information can be erased by simply heating the material above T_g , but below its isotropization (clearing) temperature.

MLCs also have their place in optical applications, mainly as so-called polymer-dispersed LCs (PDLCs). A PDLC constitutes a microemulsion of an MLC in a film of a conventional (nonPLC) polymer. In the “switched off” state the MLC and the polymer have different refractive indices, dispersed MLC droplets (not unlike to the islands in PLCs) scatter light quite effectively, and the film is opaque. Then an external electric field is applied, for instance across a capacitor-like metal coating on both sides of the film. The director in all MLC droplets becomes the same. One can choose the MLC + polymer pair so that the refractive index along the director is the same as that of the host polymer. In that case the film in the electric field becomes transparent. Switching the field off and on, one has a light valve with a fairly large area.

Let us mention a few more capabilities created in this growing field. Laser-induced reorientation of the optical axis is possible in PLC combs; optically induced *trans-cis* isomerization occurs. Erasable holograms can be created in PLC materials—as discussed by Eich and Wendorff [100] and pursued since by many. The rubbing of a polymer leads to an anisotropic surface morphology, since the LC molecules become aligned [101]. Scanning force microscopy can be used to create in a controlled way areas with a similar anisotropy and with a desired refractive index patterns.

A combination of approaches serves well achieving specific objectives. We have discussed above the fact that hydrogen bonds can also serve to create liquid crystallinity. Thus, cholesteric liquid crystal phases can be made by hydrogen bonding [102a,b]. Among interesting properties is the capability described by Shibaev e.a. [102b] of changing color of cholesteric PLC films by addition of certain aminoacids. In self-organized helical structures light is reflected when the wavelength matches the pitch (twice the periodicity). Cholesteric LCs are not only colored filters, but also reflectors and polarizers. Mitov and Dessaud [102c] show how MLCs converted into PLCs by curing provide reflectance exceeding 50 %.

Before going into the last section on theory and computer simulations, let us stop and ponder what various properties of PLCs briefly described above signify. It becomes clear that PLCs have current and potential applications in electrical, electronic, chemical, aircraft, aerospace, automobile, petroleum as well as other industries.

41.9 THEORY AND COMPUTER SIMULATIONS

41.9.1 Theory

One can distinguish at least four major theories of LC systems. Already in 1949 Onsager [103] formulated a dens-

ity expansion of the Helmholtz function A of anisometric particles—what made possible a prediction of the nematic-to-isotropic (N–I) transition. Flory [104] developed in 1956 a lattice model which after a period of inactivity led to significant further developments characterized below. Between 1958 and 1960 Maier and Saupe [105–107] created a theory in terms of a potential of mean torque experienced by LC or solute molecules in nematic phases. Their work became a “standard” in the sense of asking the question: is any new theory, first of all, able to reproduce the results of Maier and Saupe? Finally, Landau developed a molecular field theory [108] adapted by de Gennes [109] to LC systems, and is based on expanding the Helmholtz function A (or the Gibbs function G) as a power series of the order parameter s .

The framework of the Flory theory [104,105–117] can be summarized as follows. A chain segment has the length equal to its diameter, what makes possible placement at a given lattice site of either a segment or a solvent molecule. The objective is the formulation of the partition function Z . One makes the standard approximation

$$Z = Z_{\text{comb}}Z_{\text{orient}} \quad (4.11)$$

where Z_{comb} is the combinatorial (steric) contribution while Z_{orient} arises from the various orientations of the rigid sequences as well as the anisotropic interactions between their segments. Evaluation of Z_{comb} requires taking into account various possible orientations of LC sequences with respect to the director. Flory developed an ingenious method of representing such orientations on a lattice—shown in Fig. 41.14. Without going into details (which are provided for instance in [112]) let us note that for every sequence (there are four of them in the Figure) there is a parameter y which is equal to unity if that sequence is parallel to the director, and increases along with the deviation of the direction of the sequence from the LC director.

In earlier version of the theory, only fully rigid chains were treated. However, Matheson and Flory [113] extended the theory to the cases when $\theta < 1$, where θ is the average

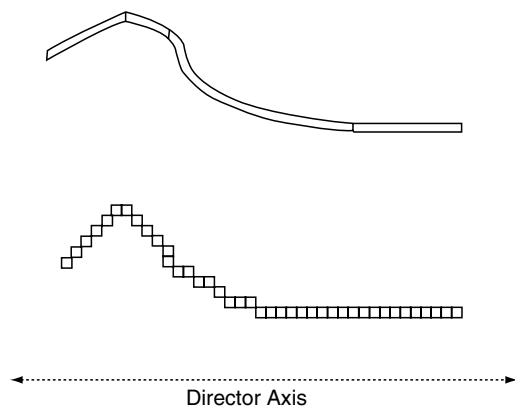


FIGURE 41.14. A four-sequence part of a chain (top) and its lattice representation (bottom). The third sequence from the left is flexible; the remaining ones are liquid-crystalline; after [115].

concentration of LC segments in PLC chains. A subsequent amplification [115] of the Matheson–Flory model includes the orientational distribution function of Flory and Ronca [112]. The amplified theory predicts a drastic change in the slope of s vs. η when going from $\theta = 0.1$ to 0.2 , indicating a large increase in the chain alignment; here η is the average length of rigid sequences. Moreover, the liquid-crystalline-to-isotropic transition temperature T_{LC-i} as a function of η shows a minimum for all θ values [115].

The quality of any theory can best be evaluated by comparing its predictions with the experiment. Ternary systems of the type PLC + flexible polymer + solvent were treated as well [116]. Ternary miscibility gaps were predicted; it turned out that the tie lines usually are not parallel to the PLC + flexible polymer basis of the Gibbs triangle, and the critical point is not at the top of the gap. Experimental data for such a system exist, namely PET/0.27PHB + poly(bisphenol-A-carbonate) + CHCl_3 [117]. As can be seen in Fig. 41.15, the predicted miscibility gap is in good agreement with the gap determined by extinction cloud point measurements [116].

One more result obtained following the Flory approach was that the concentration of hard rods q is much more important for the LC phase formation than the system temperature [115]. To pursue this issue further, the Maier–Saupe theory of MLCs was extended to PLCs taking particularly into account the system temperature [118–122]. This approach makes possible inclusion of external deformations via the system volume and also via the end-to-end distance vectors of the chains. The affine deformation developed by Flory [123] and well explained by Mark [124] was incorporated in to the model—applicable strictly to the longitudinal PLCs. Among other things, it turns out that the behavior of rigid (= LC) sequences is largely governed by orienting interactions while for the flexible sequences short-range interactions (dependent mainly on chemical structures) are

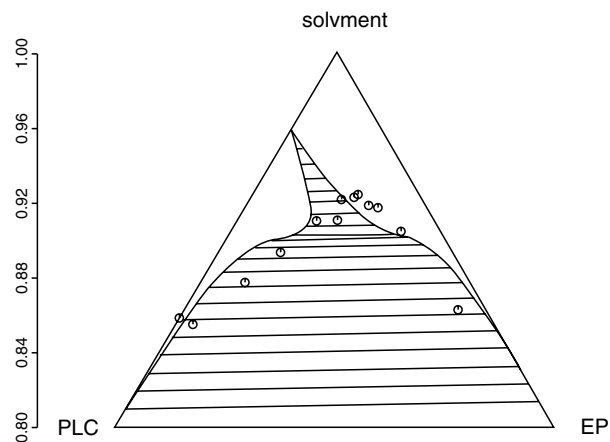


FIGURE 41.15. Comparison of experimental (circle points from [117]) and predicted (continuous lines) phase diagram. Lines calculated for the degrees of polymerization $r_{\text{PLC}} = 600$ and $r_{\text{EP}} = 1,200$ and for the temperature $T = 295\text{K}$; after [116].

the most important. The results include evaluation of orientation vs. deformation and stress vs. strain relations [122].

41.9.2 Advantages of Computer Simulations of Polymers

Getting answers from experiments is often difficult, time consuming, and the results hardly unequivocal. So-called hidden variables which exist in nature do not manifest themselves in simulations. Moreover, changing only one parameter at a time is easy in simulations, but not in real materials. One example should suffice here: to lower the density in an experiment one increases the temperature of the material. However, then the energetics changes too, heating has pumped more energy into the material. There is hardly a procedure for the separation of the two effects.

Starting with a theory, one has an advantage, particularly in multicomponent systems such as PLC + EP + solvent: it is easy to define the concentration of a flexible polymer (EP) and the average concentration q of LC sequences in PLC chains. The average concentration of flexible sequences in PLC molecules is of course $1 - \theta$, and other model parameters such as in the Flory theory can be defined as well. Somewhat similarly, it is easy in molecular dynamics (MD) simulations to set up certain chains with $\theta > 0$ and other chains with $\theta = 0$.

41.9.3 Molecular Dynamics Simulations of PLCs

We shall briefly summarize MD simulations of systems of PLC chains. First, the chains systems have to be constructed. There are various ways of generating them, and the mechanical behavior is little if at all influenced by the generation procedure. It is influenced, however, by the vacancies, or the amount of free volume v^f , as predicted by the chain relaxation capability (CRC) theory [125]. The problem is to create a realistic bulk polymer system. A procedure originally developed by Mom [126] has been modified to achieve a more realistic representation of polymeric chains [127–129].

The interaction potentials used take into account the relative rigidity of the LC sequences, possibility of *trans*-to-*gauche* conversions in flexible sequences (accomplished by using a double-well potential), and make possible bond scission (a Morse-like potential for large extensions). The simulations are typically performed at a constant temperature, multiplying the particle velocities in every time step by a factor related to the actual kinetic energy and to a reference energy [130]. The Newton differential equations of motion are transformed into difference equations employing a finite time step. The positions after a successive time step are computed using a so-called leap-frog algorithm [130]. Since the forces acting on a given particle depend on its neighbors, a list of nearest neighbors is renewed after every time step.

Fully flexible chains are of course simulated for comparison, so as to see the effects of liquid crystallinity. In our simulations we subject the materials to a tensile force (applied to top and bottom in two-dimensional specimens). As expected, under application of that force, chain conformation changes (from *gauche* to *trans*) are observed. Bond scission followed by crack propagation are observed as well. See Fig. 41.16, and note that the cracks do not propagate straight along the lines of application of the force, since the LC reinforcing units are “doing their job” [131]. In each case (that is for a given θ and LC sequence configuration) a stress level is observed at which the fraction of broken bonds increases dramatically—clearly when CRC was exceeded. Thus, simulations provide a direct confirmation of the CRC approach—discussed more in detail in this Handbook in Chapter 24 on mechanical properties of polymers.

In tensile experiments one determined always the engineering stress but determination of the true stress is much more difficult. A simulation method has been developed which allows calculation of the true stress based on cutting the specimen into sections [129,132,133]. There are significant differences between the two kinds of stresses; see Fig. 41.17.

Other issues concerning PLCs are also such that simulations provide answers to questions to which experiments cannot. For instance, what is the skin-core effect on properties? In processing of real materials always a skin which is

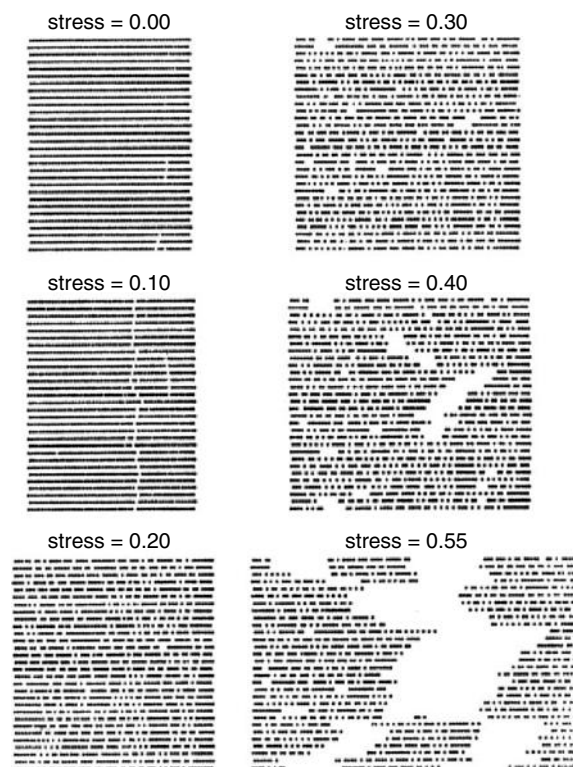


FIGURE 41.16. MD simulations of a random PLC with $\theta = 0.5$ under tensile deformations applied vertically with various stress levels (stress in reduced units); after [131].

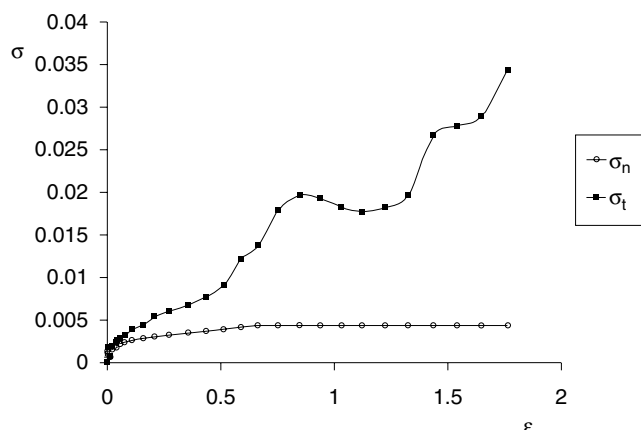


FIGURE 41.17. Engineering or nominal stress (index n) and true stress (index t) as a function of engineering strain e for a PLC simulated by molecular dynamics; after [132].

more oriented appears—but it is in simulations that we can create materials with arbitrary thickness of the skin, thickness of the core, and also create layers with intermediate properties. Another question is the crack propagation in PLCs. Do cracks propagate preferentially through the LC-rich islands since the islands are rigid and thus brittle, or rather through the LC-poor matrix since the matrix is mechanically weak? The answer is: cracks propagate near the island surfaces on the matrix side [127].

ACKNOWLEDGMENTS

I have learned what LCs are and which of their features are important from the late Professors Paul J. Flory, Stanford, and Horst Sackmann, Halle. This Chapter has been influenced by discussions with many colleagues and collaborators, including Antonio M. Cunha, Henryk Galina, Michael Hess, Georg Hinrichsen, Hans R. Kricheldorf, Betty L. López, Robert Maksimov, Gerhard Pelzl, Monika Plass, Edward T. Samulski, Alfred Saupe, Jukka V. Seppälä, Valery P. Shibaev, Ricardo Simoes, Jürgen Springer, Tomasz Sterzynski, Franciska Sundholm, and Janusz Walaśek. Our own research referred to herein was supported by the NATO, Brussels; National Science Foundation, Washington, DC; and the Robert A. Welch Foundation (Grant B-1203), Houston.

REFERENCES

- M.G. Friedel, *Ann. Phys.* **18**, 273 (1922).
- W. Kast, *Angew. Chem.* **67**, 592 (1955).
- B. Wunderlich and J. Grebowicz, *Adv. Polym. Sci.* **60/61**, 1 (1984).
- B. Wunderlich, M. Möller, J. Grebowicz, and H. Baur, *Adv. Polym. Sci.* **87**, 1 (1988).
- E.T. Samulski, *Faraday Discuss.* **79**, 7 (1985).
- G. Kiss, *Polym. Eng. Sci.* **27**, 410 (1987).
- P.J. Hall and G.J.T. Tiddy, in *Liquid Crystalline Polymers: From Structures to Applications*, edited by A.A. Collyer (Elsevier, New York 1992), Chapter 5; M.G. Northolt and D.J. Sikkema, in *Liquid Crystalline Polymers: From Structures to Applications*, edited by A.A. Collyer (Elsevier, New York 1992), Chapter 6.
- B.S. Hsiao, M.T. Shaw, and E.T. Samulski, *Macromolecules* **21**, 543 (1988).
- W. Brostow, *Polymer* **31**, 979 (1990).
- A. Abe, T. Hiejima, T. Takeda, and C. Nakufuku, *Polymer* **44**, 3117 (2003).
- P.A. Henderson and C.T. Imrie, *Macromolecules* **38**, 3307 (2005).
- G. Li and T. Yu, *Makromol. Chem. Rapid Commun.* **10**, 387 (1989).
- K. Kerkam, C. Viney, D. Kaplan, and S. Lombardi, *Nature* **349**, 596 (1991).
- F. Reinitzer, *Monatsh. Chem.* **9**, 421 (1888).
- O. Lehmann, *Z. Phys. Chem.* **4**, 462 (1889).
- D. Vorländer, *Kristallinisch-flüssige Substanzen*, (Enke-Verlag, Stuttgart 1908).
- D. Vorländer, *Z. Phys. Chem.* **105**, 211 (1923).
- W. Brostow, *Science of Materials* (Wiley, New York 1979; Robert E. Krieger Publ. Co., Malabar, FL 1985); W. Brostow, *Introducción a la ciencia de los materiales* (Editorial Limusa, México, D.F. 1981); W. Brostow, *Einstieg in die moderne Werkstoffwissenschaft* (Carl Hanser Verlag, München 1985; Deutscher Verlag für Grundstoffindustrie, Leipzig 1985); updated Ukrainian edition to be published by Lvivska Politechnika.
- W. Brostow, T.S. Dziemianowicz, J. Romanski, and W. Werber, *Polym. Eng. Sci.* **28**, 785 (1988).
- M.R. Piggott, in *Failure of Plastics*, edited by W. Brostow and R.D. Corneliussen (Hanser, Munich 1986), Chapter 23.
- J.-F. Jansson and H. Sundström, in *Failure of Plastics*, edited by W. Brostow and R.D. Corneliussen (Hanser, Munich 1986), Chapter 24.
- E. Pisanova and S. Zhandarov, in *Performance of Plastics*, edited by W. Brostow (Hanser, Munich 2000), Chapter 19.
- W. Brostow, V.M. Castaño, A. Huanosta, M. de Icaza, M.E. Nicho, and J.M. Saniger, *Mater. Res. Innovat.* **3**, 85 (1999).
- V.M. Castaño and R. Rodriguez, in *Performance of Plastics*, edited by W. Brostow (Hanser, Munich 2000), Chapter 24.
- W. Brostow, *Kunststoffe* **78**, 411 (1988).
- W. Witt, *Kunststoffe* **78**, 795 (1988).
- M. Hess, in *Performance of Plastics*, edited by W. Brostow (Hanser, Munich 2000), Chapter 21.
- M. Ebert, R. Kleppinger, M. Soliman, M. Wolf, J.H. Wendorff, G. Latterman, and G. Staufner, *Liq. Cryst.* **7**, 553 (1990).
- H. Gasparoux, F. Hardoin, C. Destrade, and H.T. Nguyen, *New J. Chem.* **16**, 295 (1992).
- J.M. Fréchet and A. Tomalia, *Dendrimers and Other Dendritic Polymers* (Wiley, New York 2002).
- T. Felekis, L. Tziveleka, D. Tsiourvas, and C.M. Paleos, *Macromolecules* **38**, 1705 (2005).
- R. Zentel and J. Wu, *Makromol. Chem.* **187**, 1727 (1986).
- O. Hermann-Schönherr, J.H. Wendorff, H. Ringsdorf, and P. Tschirner, *Makromol. Chem. Rapid Commun.* **7**, 791 (1986).
- H. Ringsdorf, P. Tschirner, O. Hermann-Schönherr, and J.H. Wendorff, *Makromol. Chem.* **188**, 1431 (1987).
- L. Cui, J. Miao, L. Zhu, I. Sics and B.H. Siao, *Macromolecules* **38**, 3386 (2005).
- P.H. Hermans, *Contributions to the Physics of Cellulosic Fibres* (Elsevier, Amsterdam 1946), p. 133.
- D. Demus, H. Demus, and H. Zschke, *Flüssige Kristalle in Tabellen*, 2nd ed. (Deutscher Verlag für Grundstoffindustrie, Leipzig 1974).
- D. Demus, and H. Zschke, *Flüssige Kristalle in Tabellen II*, 2nd ed. (Deutscher Verlag für Grundstoffindustrie, Leipzig 1984).
- D. Demus and L. Richter, *Textures of Liquid Crystals* (Verlag Chemie, Weinheim 1978).
- J. Menczel and B. Wunderlich, *J. Polym. Sci. Phys.* **18**, 1433 (1980).
- W. Meeris, J. Menczel, U. Gaur, and B. Wunderlich, *J. Polym. Sci. Phys.* **20**, 719 (1982).
- L.C. Sawyer and M. Jaffe, *J. Mater. Sci.* **21**, 1897 (1986).
- L.C. Sawyer, R.T. Chen, M.G. Jamieson, I.H. Musselman, and P.E. Russell, *J. Mater. Sci. Lett.* **11**, 69 (1992).
- L.C. Sawyer and M. Jaffe, *Mater. Res. Soc. Symp.* **255**, 75 (1992).
- W. Brostow and M. Hess, *Mater. Res. Soc. Symp.* **255**, 57 (1992).
- T. Kato and J.M.J. Fréchet, *Macromolecules* **22**, 3819 (1989).

47. C.G. Bazuin and F.A. Brandys, *Chem. Mater.* **4**, 970 (1992).
48. C.G. Bazuin, F.A. Brandys, T.G. Eve, and M. Plante, *Macromol. Symp.* **84**, 183 (1994).
49. Y. Zhao and H. Lei, *Macromolecules* **27**, 4525 (1994).
50. W. Brostow, M. Hess, and B.L. López, *Macromolecules* **27**, 2262 (1994).
51. W. Brostow, M. Hess, B.L. López, and T. Sterzynski, *Polymer* **37**, 1551 (1996).
52. S. Buchner, D. Chen, R. Gehrke, and H.G. Zachmann, *Mol. Cryst. Liq. Cryst.* **155**, 357 (1988).
53. Lord Kelvin, *Math. Phys. Papers* **3**, 437 (1890).
54. IUPAC Commission for Symbols, Units and Nomenclature, *Physica A* **93**, 1 (1978).
55. W. Brostow, J.V. Duffy, G.F. Lee, and K. Madejczyk, *Macromolecules* **24**, 479 (1991).
56. W. Brostow, N.A. D'Souza, M. Hess, and E.G. Jacobs, *Polymer* **39**, 4081 (1998).
57. K.P. Menard, *Dynamic Mechanical Analysis—An Introduction* (CRC Press, Boca Raton 1999).
58. K.P. Menard, in *Performance of Plastics*, edited by W. Brostow (Hanser, Munich 2000), Chapter 8.
59. P. Zoller, P. Bolli, V. Pahud, and H. Ackermann, *Rev. Sci. Instrum.* **47**, 948 (1976).
60. W. Brostow, V.M. Castaño, G. Martinez-Barrera, and D. Pietkiewicz, *Physica B* **344**, 206 (2004).
61. G. Broza, V.M. Castaño, G. Martinez-Barrera, K.P. Menard, and C. Simoes, *Physica B* **357**, 500 (2005).
62. W. Brostow, V.M. Castaño, G. Martinez-Barrera, and J.-M. Saiter, *Physica B* **334**, 436 (2003).
63. A. Tölle, *Rep. Prog. Phys.* **64**, 1473 (2001).
64. R. Casalini and C.M. Roland, *Phys. Rev. E* **69**, 62501 (2004).
65. R. Casalini and C.M. Roland, *Colloid Polym. Sci.* **283**, 107 (2004).
66. J.-F. Jansson, in *Liquid Crystalline Polymers: From Structures to Applications*, edited by A.A. Collyer (Elsevier, New York 1992), Chapter 9.
67. J. Küpfer and H. Finkelmann, *Makromol. Chem. Rapid Commun.* **12**, 717 (1991).
68. J. Küpfer, E. Nishikawa, and H. Finkelmann, *Polym. Adv. Technol.* **5**, 110 (1994).
69. V. Ambrogio, M. Giamberini, P. Cernuti, P. Pucci, N. Menna, R. Mascolo, and C. Carfagna, *Polymer* **46**, 2105 (2005).
70. E. Rabinowicz, *Friction and Wear of Materials*, 2nd ed. (Wiley, New York 1995).
71. W. Brostow, J.-L. Deborde, M. Jaklewicz, and P. Olszynski, *J. Mater. Ed.* **24**, 119 (2003).
72. W. Brostow, B. Bujard, P.E. Cassidy, H.E. Hagg, and P.E. Montemartini, *Mater. Res. Innovat.* **6**, 7 (2002).
73. W. Brostow, G. Damarla, J. Howe, and D. Pietkiewicz, e-Polymers no. 025 (2004); <http://www.e-polymers.org/>
74. W. Brostow and M. Jaklewicz, *J. Mater. Res.* **19**, 1038 (2004).
75. W. Brostow, editor, *Mechanical and Thermophysical Properties of Polymer Liquid Crystals* (Chapman & Hall, London 1998).
76. W. Brostow, T. Sterzynski, and S. Triouleyre, *Polymer* **37**, 1561 (1996).
77. W.J. Jackson, Jr. and H.F. Kuhfuss, *J. Polym. Sci. Phys.* **14**, 2043 (1976).
78. O. Roetting and G. Hinrichsen, *Adv. Polym. Technol.* **13**, 57 (1994).
79. K.R. Wissbrun, *Faraday Discuss.* **79**, 161 (1985).
80. G. Marrucci and P.L. Maffettone, *Macromolecules* **22**, 4076 (1989).
81. M. Miesowicz, *Nature* **158**, 27 (1946).
82. D. Acierno and A.A. Collyer, editors, *Polymer Liquid Crystals Vol. 2—Rheology* (Chapman & Hall, London, 1996).
83. H. Arnold and H. Sackmann, *Z. Phys. Chem.* **213**, 137 (1960).
84. H. Arnold and H. Sackmann, *Z. Phys. Chem.* **213**, 145 (1960).
85. H. Sackmann, *Prog. Colloid Polym. Sci.* **69**, 73 (1984).
86. T. Schlee, G. Kossmehl, and G. Hinrichsen, *Makromol. Chem.* **191**, 1075 (1990).
87. T. Schlee, G. Hinrichsen, and G. Kossmehl, *Colloid Polym. Sci.* **270**, 207 (1992).
88. T. Schlee, O. Roetting, D. Bettge, G. Hinrichsen, and G. Kossmehl, *Makromol. Chem.* **194**, 791 (1993).
89. D.W. van Krevelen, *Properties of Polymers*, 3rd ed. (Elsevier, Amsterdam 1990).
90. D. Demus, *Z. Chemie* **15**, 1 (1975).
91. E. Schlosser, A. Schönhals, H.-E. Carius, and H. Goering, *Macromolecules* **26**, 6027 (1993).
92. J.K. Moscicki, in *Liquid Crystalline Polymers: From Structures to Applications*, edited by A.A. Collyer (Elsevier, New York 1992), Chapter 4.
93. V.P. Shibaev and N.A. Platé, *Polym. Sci. USSR A* **19**, 1065 (1978).
94. F. Lauprêtre, in *Liquid Crystalline Polymers: From Structures to Applications*, edited by A.A. Collyer (Elsevier, New York 1992), Chapter 3.
95. D.J. Photinos, E.T. Samulski, and H. Toriumi, *J. Phys. Chem.* **94**, 4688, 4694 (1990).
96. D.J. Photinos, E.T. Samulski, and H. Toriumi, *J. Chem. Phys.* **94**, 2758 (1991).
97. D.J. Photinos, E.T. Samulski, and H. Toriumi, *Mol. Cryst. Liq. Cryst.* **204**, 61 (1991).
98. H. Roth and B. Krücke, *Makromol. Chem.* **187**, 2655 (1986).
99. S.R. Marder, C.B. Gorman, F. Meyers, J.W. Perry, G. Bourhill, J.-L. Brédas, and B.M. Pierce, *Science* **265**, 632 (1994).
100. M. Eich and J. H. Wendorff, *Makromol. Chem. Rapid Commun.* **8**, 467 (1987).
101. M. Rüetschi, P. Grütter, J. Fünfschilling, and H.-J. Güntherodt, *Science* **265**, 512 (1994).
102. a) A.V. Medvedev, E.B. Barnatov, A.S. Medvedev, V.P. Shibaev, S.A. Ivanov, M. Kozlovsky, and J. Stumpe, *Macromolecules* **38**, 2223 (2005); b) P.V. Shibaev, D. Chiappetta, R.L. Sanford, P. Palffy-Muhoray, M. Moreira, W. Cao, and M.W. Green, *Macromolecules* **39**, 3986 (2006); c) M. Mitov and N. Dessaud, *Nature Materials* **5**, 361 (2006).
103. L. Onsager, *Ann. NY Acad. Sci.* **51**, 627 (1949).
104. P.J. Flory, *Proc. R. Soc. A* **234**, 60, 73 (1956).
105. W. Maier and A. Saupe, *Z. Naturforsch. A* **13**, 564 (1958).
106. W. Maier and A. Saupe, *Z. Naturforsch. A* **14**, 1909 (1959).
107. W. Maier and A. Saupe, *Z. Naturforsch. A* **15**, 282 (1960).
108. L.D. Landau, *Collected Papers*, edited by D. ter Haar (Gordon & Breach, New York 1965), p. 193.
109. P.G. de Gennes, *The Physics of Liquid Crystals* (Oxford University Press, Oxford 1979).
110. P.J. Flory and A. Abe, *Macromolecules* **11**, 1119 (1978).
111. A. Abe and P.J. Flory, *Macromolecules* **11**, 1122 (1978).
112. P.J. Flory and G. Ronca, *Mol. Cryst. Liq. Cryst.* **54**, 289, 311 (1979).
113. R.R. Matheson, Jr. and P.J. Flory, *Macromolecules* **14**, 954 (1981).
114. R.R. Matheson, Jr., *Macromolecules* **19**, 1286 (1986).
115. D.A. Jonah, W. Brostow, and M. Hess, *Macromolecules* **26**, 76 (1993).
116. S. Blonski, W. Brostow, D.A. Jonah, and M. Hess, *Macromolecules* **26**, 84 (1993).
117. F. Schubert, K. Friedrich, M. Hess, and R. Kosfeld, *Mol. Cryst. Liq. Cryst.* **155**, 477 (1988).
118. W. Brostow and J. Walasek, *J. Chem. Phys.* **105**, 4367 (1996).
119. W. Brostow, K. Hibner, and J. Walasek, *J. Chem. Phys.* **108**, 6484 (1998).
120. W. Brostow and J. Walasek, *J. Chem. Phys.* **114**, 2466 (2001).
121. W. Brostow and J. Walasek, *J. Chem. Phys.* **115**, 8692 (2001).
122. W. Brostow and J. Walasek, *J. Chem. Phys.* **121**, 3272 (2004).
123. P.J. Flory, *Selected Works*, Vol. III. (Stanford University Press, Stanford, CA 1985).
124. J.E. Mark and B. Erman, *Rubberlike Elasticity—A Molecular Primer* (Wiley, New York 1988).
125. W. Brostow, in *Performance of Plastics*, edited by W. Brostow (Hanser, Munich 2000), Chapter 5.
126. V. Mom, *J. Comput. Chem.* **2**, 446 (1981).
127. W. Brostow, M. Donahue III, C.E. Karashin, and R. Simoes, *Mater. Res. Innovat.* **4**, 75 (2001).
128. W. Brostow, A.M. Cunha, and R. Simoes, *Mater. Res. Innovat.* **7**, 19 (2003).
129. R. Simoes, A.M. Cunha, and W. Brostow, *Polymer* **45**, 7767 (2004).
130. W.F. van Gunsteren, in *Mathematical Frontiers in Computational Chemical Physics*, edited by D.G. Truhlar (Springer, New York 1988).
131. S. Blonski and W. Brostow, *J. Chem. Phys.* **95**, 2890 (1991).
132. R. Simoes, A.M. Cunha, and W. Brostow, *Model. & Simul. Mater. Sci. & Eng.* **14**, 157 (2006).
133. R. Simoes, A.M. Cunha, and W. Brostow, *Comput. Mater. Sci.* **36**, 319 (2006).

CHAPTER 42

The Emergence of a New Macromolecular Architecture: “The Dendritic State”

Donald A. Tomalia

*Dendritic Nanotechnologies, Inc., 2625 Denison Drive, Mount Pleasant, MI 48858;
Central Michigan University, Mount Pleasant, MI 48859*

42.1	Introduction	671
42.2	Historical	672
42.3	The Dendritic State	676
42.4	Dendritic Structures as Intermediary Architectures between Thermoplastics and Thermosets	687
42.5	Conclusions	690
	Acknowledgments	691
	References	691

42.1 INTRODUCTION

The seminal “macromolecular hypothesis” proposed by H. Staudinger nearly 85 years ago both inspired and initiated one of the most significant technology revolutions experienced during the 20th century, namely; *the polymer(plastics) revolution* [1]. In an abstract way, Staudinger’s concept, which involved chemically linking (n) multiples of monomeric building blocks into a myriad of macromolecular complexity [2], may be viewed as an elegant continuation of J. Dalton’s hypothesis (i.e., “New System of Chemical Philosophy (1808)”) for chemically connecting (n') multiples of atomic modules (Fig. 42.1).

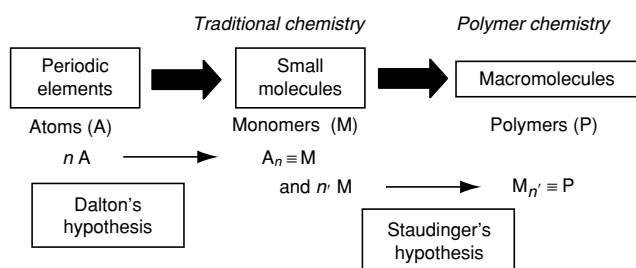


FIGURE 42.1. Historical overview of major technology revolutions “traditional chemistry” and “polymer chemistry” and associated pioneers.

This earlier concept produced the endless array of small molecules that are now recognized as our 200 year old “traditional chemistry” science. Although the intrinsic features of atoms or monomers as well as the rules for defining the values of (n') and (n) are most assuredly different, the enormous role that each of these technologies has played, both in the improvement of the “human condition” and enhancement of the world economy, is indisputable. These benefits were largely derived from unique and extraordinary “new properties” that emerged in each of these areas, as the technologies advanced to higher levels of complexity. A pervasive pattern that has become obvious in each of these scientific fields is the significant role that “*architecture*” plays in the determination of these new properties. More specifically, the importance of new macromolecular architectures has been amply recognized by a preponderance of Nobel awards associated with the discovery of such architectural features and their consequential unique properties (Fig. 42.2).

History has shown that each time a major new architecture has been discovered it has been accompanied by the emergence of a plethora of new properties, concepts, applications, products, and activities, all of which have led to enhanced new commercial markets, quality of life, and prosperity. Since the mid 1930s, four major macromolecular architectures have evolved leading to well-known classes of

Nobel laureates		Commercial applications	Emerging properties and applications
<div style="display: flex; justify-content: space-between;"> <div style="width: 45%;"> <p>Heeger, MacDiarmid & Shirakawa (Conductive polymers) (2000)</p> <p>Merrifield (Controlled sequencing) (1984)</p> <p>Natta & Ziegler (Tacticity) (1963)</p> <p>Staudinger (Macromolecular hypothesis) (Linear-architecture) (1953)</p> </div> <div style="width: 45%;"> <p>Flory (Gellation) (Cross-linked architecture) (1974)</p> </div> </div>	<p>Metalocene-based poly(olefins)</p> <ul style="list-style-type: none"> • Dow (Insite) • DSM • Dupont <p>Viscosity modifiers</p> <ul style="list-style-type: none"> • Exxon mobil • Phillips petroleum 	<p>Synthetic Control of macromolecular structure <i>Size, shape and functionality</i></p> <ul style="list-style-type: none"> • Artificial proteins • MRI contrast agents • Nanodrugs • Nano containers (Drug delivery, quantum dots) • Photon harvesting 	
Architectural classes	I. Linear	III. Branched	IV. Dendritic

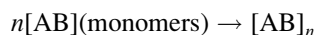
FIGURE 42.2. Nobel recognition, commercial applications/emerging properties for the four major macromolecular architectures.

thermoplastic or thermoset polymers, beginning with: (I) linear, (II) cross-linked, (III) branched and now (IV) dendritic topologies, as illustrated in Fig. 42.3.

42.2 HISTORICAL

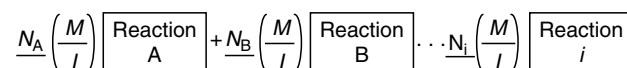
42.2.1 Overview

Over the past 85 years, Staudinger's macromolecular synthesis strategy has evolved based on the catenation of reactive small molecular modules (monomers). Broadly speaking, these catenations involve the use of reactive (AB-type monomers) that may be engaged to produce large molecules with polydispersed masses. Such multiple bond formation may be driven by (a) chain growth, (b) ring opening, (c) step-growth condensation or (d) enzyme catalyzed processes. Staudinger first introduced this paradigm in the 1920s [1,3–6] by demonstrating that reactive monomers could be used to produce a statistical distribution of one-dimensional (linear) molecules with very high molecular weights (i.e., $> 10^6$ Da). As many as 10,000 or more covalent bonds may be formed in a single chain reaction of monomers. Although these macro/megamolecules may possess nanoscale dimensions, structure control of critical macromolecular design parameters, such as size, molecular shape, spatial positioning of atoms, or covalent connectivity—other than those affording linear or cross-linked topologies—is difficult. However, recently progress has been made using “living polymerization” techniques that afford better control over molecular weight and certain structural elements as described by Matyjaszewski and others [7,8].



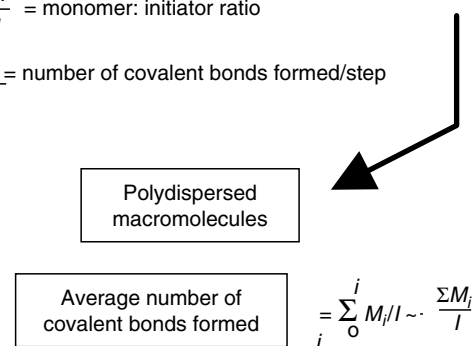
Traditional polymerizations usually involve AB-type monomers based on substituted ethylenes or strained small ring compounds using chain reactions that may be initiated by free radical, anionic or cationic initiators [9]. Alternatively, AB-type monomers may be used in polycondensation reactions [9].

Multiple covalent bonds are formed to produce each macromolecule, generally giving statistical, polydispersed structures. In the case of controlled vinyl polymerizations, the average length of the macromolecule is determined by monomer to initiator ratios. If one visualizes these polymerizations as extraordinarily long sequences of individual reaction steps, the average number of covalent bonds formed/chain may be described as shown in Scheme 42.1.



Where: $\frac{M}{I}$ = monomer: initiator ratio

N = number of covalent bonds formed/step



SCHEME 42.1.

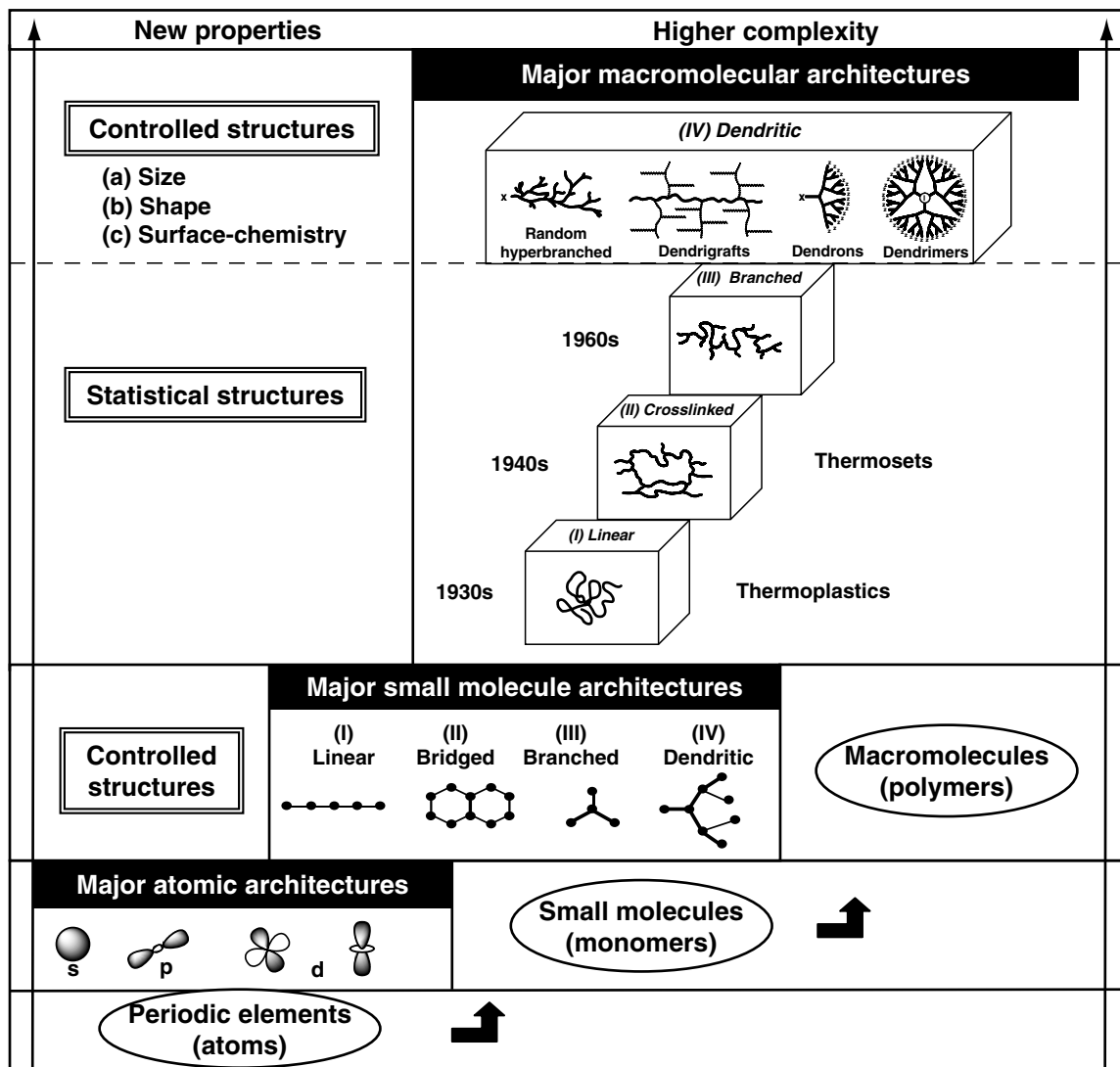


FIGURE 42.3. A comparison of major architecture for the elements (atoms), small molecules, and macromolecules (polymers) as a function of new properties and complexity.

The first traditional polymerization strategies generally produced linear architectures, however, it was soon found that branched topologies may be formed either by chain-transfer processes, or intentionally introduced by grafting techniques. In any case, the linear and branched architectural classes have traditionally defined the broad area of *thermoplastics*. Of equal importance is the major architectural class that is formed by the introduction of covalent (bridging) bonds between linear or branched polymeric topologies. These cross-linked (bridged) topologies were studied by Flory in the early 1940s and constitute the second major area of traditional polymer chemistry—namely, *thermosets*. These two broad areas of polymer science—thermoplastics and thermosets—account for billions of dollars of commerce and constitute a vast array of familiar macromolecular compositions and applications as shown in Fig. 42.4.

Historically, even 50 years after Staudinger's introduction of the "macromolecular hypothesis," the entire field of polymer science was viewed to consist of only the two major architectural classes: (i) "linear topologies" as found in *thermoplastics* and (ii) "cross-linked architectures" as found in *thermosets*. The major focus of polymer science during the time frame spanning the period of the 1920s to the 1970s was on the unique architecturally driven properties manifested by either linear or cross-linked topologies. Based on the new properties exhibited by these topologies, many natural polymers critical to the World War II effort were replaced with synthetic polymers for which the combination of availability and properties were of utmost strategic importance [2]. During the 1960s and 1970s, pioneering investigation into long chain branching (LCB) involving polyolefins and other related branched systems began to emerge [10,11]. More recently, intense commercial

42.3 THE DENDRITIC STATE

42.3.1 Historical

The origins of the present three-dimensional, dendritic branching concepts can be traced back to the initial introduction of infinite network theory by Flory [17–20] and Stockmayer [21–23]. In 1943, Flory introduced the term *network cell*, which he defined as the most fundamental unit in a molecular network structure [24]. To paraphrase the original definition, *it is the recurring branch juncture in a network system as well as the excluded volume associated with this branch juncture*. Graessley [25,26] took the notion one step further by describing ensembles of these network cells as micronetworks. Extending the concept of Flory's statistical treatment of Gaussian-coil networks, analogous species that are part of an open, branched/dendritic organization are known as *branch cells* and *dendritic assemblies*.

Statistical modeling by Gordon *et al.* [27,28], Dusek [29], Burchard [30] and others reduced such branched species to graph theory designed to mimic the morphological branching of trees. These dendritic models were combined with "cascade theory" [31,32] mathematics to give a reasonable statistical treatment for network-forming events at that time.

The growth of branched and dendritic macromolecules in the sol phase of a traditional cross-linking process may be thought of as geometric aggregations of various branch cells

or dendritic/network assemblies as described above. Beginning as molecular species, they advance through the dimensional complexity hierarchy to oligomeric, macromolecular, megamolecular, and ultimately to infinite network macro-scale systems. The intermediacy of dendritic architecture in this continuum will be discussed later. Traditional network-forming systems (e.g., epoxy resins, urethanes, polyesters) progress through this growth process in a statistical, random fashion. The resulting infinite networks may be visualized as a collection of unequally segmented, Gaussian chains between *f*-functional branch junctures, cross-links (loops), and dangling terminal groups.

More recently, nontraditional polymerization strategies have evolved to produce a fourth new major polymer architectural class, now referred to as *dendritic polymers*. This new architectural polymer class consists of four major subsets, namely: (a) *random hyperbranched*, (b) *dendrigrfts*, (c) *dendrons*, and (d) *dendrimers*. Dendrimers, the most extensively studied subset, were discovered by the Tomalia group while at The Dow Chemical Company laboratories (1979). They represent the first example of synthetic, macromolecular dendritic architecture [33,34]. First use of the term "dendrimer" appeared in preprints for the 1st SPSJ International Polymer Conference held in Kyoto, Japan (1984). The following year, a full article (*Polymer Journal*, Vol. 17, No. 1, pp. 117–132 (1985)) (see article abstract, Fig. 42.7) described the first preparation of a complete family of

Polymer Journal, Vol. 17, No. 1, pp 117--132 (1985)

A New Class of Polymers: Starburst-Dendritic Macromolecules

D. A. TOMALIA,* H. BAKER, J. DEWALD, M. HALL,
G. KALLOS, S. MARTIN, J. ROECK,
J. RYDER, and P. SMITH

Functional Polymers/Process and *The Analytical Laboratory,
Dow Chemical U.S.A., Midland, Michigan 48640, U.S.A.

(Received August 20, 1984)

ABSTRACT: This paper describes the first synthesis of a new class of topological macromolecules which we refer to as "starburst polymers." The fundamental building blocks to this new polymer class are referred to as "dendrimers." These dendrimers differ from classical monomers/oligomers by their extraordinary symmetry, high branching and maximized (telechelic) terminal functionality density. The dendrimers possess "reactive end groups" which allow (a) controlled molecular weight building (monodispersity), (b) controlled branching (topology), and (c) versatility in design and modification of the terminal end groups. Dendrimer synthesis is accomplished by a variety of strategies involving "time sequenced propagation" techniques. The resulting dendrimers grow in a geometrically progressive fashion as shown: Chemically bridging these dendrimers leads to the new class of macromolecules—"starburst polymers" (e.g., (A)_n, (B)_n, or (C)_n).

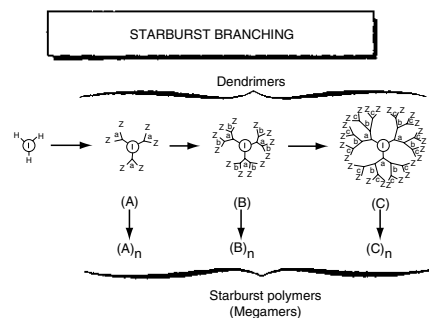


FIGURE 42.7. Abstract of the first full article describing the synthesis of a complete family of Tomalia-type PAMAM dendrimers.

Tomalia-type poly(amidoamine) (PAMAM) dendrimers and their use as precise, fundamental building blocks to form poly(dendrimers) or so-called “starburst polymers.” These poly(dendrimers) are now referred to as *megamers* [35,36] and are described in more detail later. Other pioneers in the “dendritic polymer” field include Vogtle, Newkome, Frechet, and others. These historical contributions have been reviewed recently [33].

This article will overview the “dendritic architectural state,” its unique architecturally driven properties, its role relative to traditional polymer science as well as describe the many enabling features that dendrimers are expected to offer to the emerging nanotechnology revolution.

42.3.2 A Fourth Major New Architectural Polymer Class

Dendritic topology has now been recognized as a fourth major class of macromolecular architecture [33,37–39]. The signature for such a distinction is the unique repertoire of new properties manifested by this class of polymers [40–45]. Numerous synthetic strategies have been reported for the preparation of these materials, and have led to a

broad range of dendritic structures. Presently, this architectural class consists of four dendritic subclasses; namely, (IVa) *random hyperbranched polymers*, (IVb) *dendrigrraft polymers* and (IVc) *dendrons/dendrimers* (Fig. 42.8). The order of this subset, from a to c, reflects the relative degree of structural control present in each of these dendritic architectures.

All dendritic polymers are open covalent assemblies of branch cells. They may be organized as very symmetrical, monodispersed arrays, as is the case for dendrimers, or as irregular polydispersed assemblies that typically define random hyperbranched polymers. As such, the respective subclasses and the level of structure control are defined by the propagation methodology used to produce these assemblies, as well as by the branch-cell (BC) construction parameters. The BC parameters are determined by the composition of the BC monomers, as well as the nature of the “excluded volume” defined by the BC. The excluded volume of the BC is determined by the length of the arms, the symmetry, rigidity/flexibility, as well as the branching and rotation angles involved within each of the branch-cell domains. As shown in Fig. 42.8 these dendritic arrays of branch cells usually manifest covalent connectivity relative to some molecular reference marker (I) or core. As such,

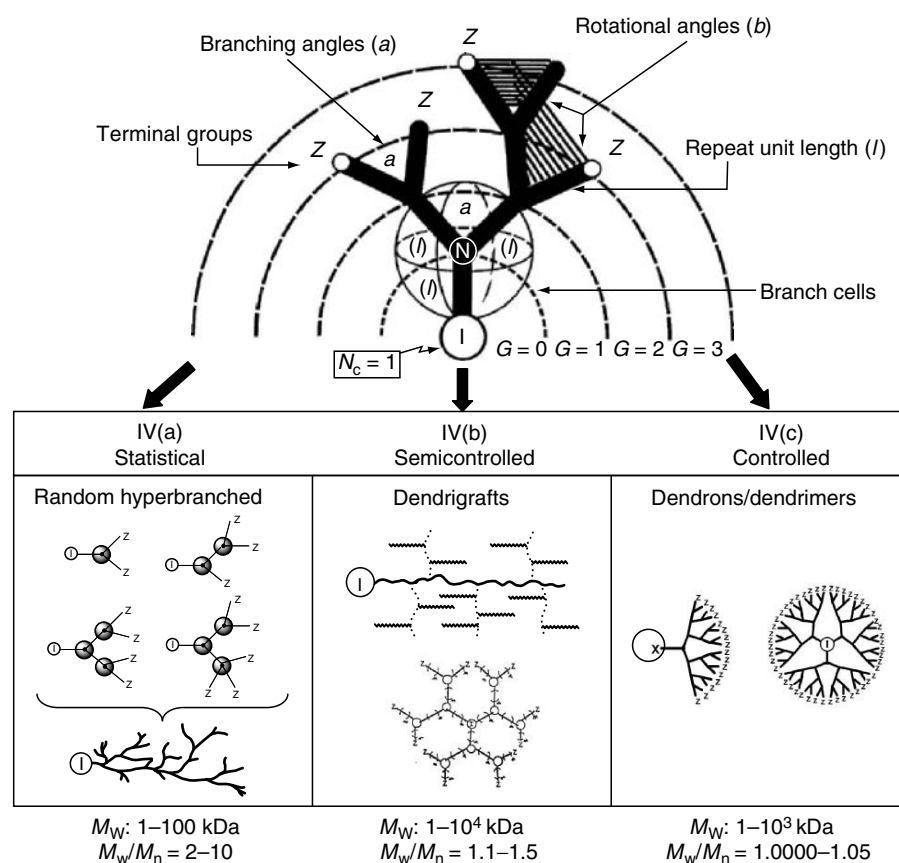


FIGURE 42.8. Branch cell structural parameters (a) branching angles, (b) rotation angles, (l) repeat unit lengths, (Z) terminal groups, and dendritic subclasses derived from branches (IVa) random hyperbranched, (IVb) dendrigrrafts, and (IVc) dendrons/dendrimers.

these branch-cell arrays may be very nonideal and polydispersed (e.g., $M_w/M_n \cong 2-10$), as observed for random hyperbranched polymers (IVa), or very ideally organized into highly controlled core-shell type structures as noted for dendrons/dendrimers (IVc): $M_w/M_n \cong 1.01-1.0001$ and less. Dendrigraft (arborescent) polymers reside between these two extremes of structure control, frequently manifesting rather narrow polydispersities of $M_w/M_n \cong 1.1-1.5$, depending on their mode of preparation.

42.3.3 Dendritic Polymer Subclasses

Random Hyperbranched Polymers

Flory first hypothesized dendritic polymer concepts [18,20], which are now recognized to apply to statistical, or random hyperbranched polymers. However, the first experimental confirmation of dendritic topologies did not produce random hyperbranched polymers but rather the more precise, structure-controlled, dendrimer architecture [33,34,46,47]. This work was initiated nearly a decade before the first examples of random hyperbranched polymers were confirmed independently by Gunatillake *et al.* [48] and by Kim and Webster [49,50] in 1988. At that time, Kim and Webster coined the popular term “hyperbranched polymers” that has been widely used to describe this subclass of dendritic macromolecules. Hyperbranched polymers are typically prepared by polymerization of AB_x monomers. When x is 2 or more, polymerization of such monomers gives highly branched polymers (Figs. 42.3 and 42.8), as long as A reacts only with B from another molecule. Reactions between A and B from the same molecule result in termination of polymerization by cyclization. This approach produces hyperbranched polymers with a degree of polymerization n , possessing one unreacted A functional group and $[(x-1)_n + 1]$ unreacted B terminal groups. In a similar fashion, copolymerization of A_2 and B_3 or other such polyvalent monomers can give hyperbranched polymers [51,52], if the polymerization is maintained below the gel point by manipulating monomer stoichiometry or limiting polymer conversion. Random hyperbranched polymers are generally produced by the one-pot polymerization of AB_x -type monomers or macromonomers involving polycondensation, ring opening, or polyaddition reactions. Hence, the products usually have broad, statistical molecular-weight distributions, much as is observed for traditional polymers. Over the past decade, literally dozens of new AB_2 -type monomers have been reported leading to an enormously diverse array of hyperbranched structures. Some general types include poly(phenylenes) obtained by the Suzuki coupling [49,50]; poly(phenylacetylenes) prepared by the Heck reaction [53]; polycarbosilanes, polycarbosiloxanes [54], and poly(siloxysilanes) by hydrosilylation [55]; poly(ether ketones) by nucleophilic aromatic substitution [56]; and polyesters [57]

or polyethers [58] by polycondensations or by ring-opening polymerization [59].

New advances beyond the traditional AB_2 Flory-type, branch-cell monomers have been reported by Fréchet and coworkers [60,61]. They have introduced the concept of latent AB_2 monomers, referred to as self-condensing vinyl polymerizations (SCVP). These monomers, which possess both initiation and propagation properties, may follow two modes of polymerization; namely, polymerization of the double bond (i.e., chain growth) and condensation of the initiating group with the double bond (i.e., step growth). Recent progress involving the derivative process of self-condensing, ring-opening polymerizations (SCROP) has been reviewed by Sunder *et al.* [62] In addition, the use of enhanced processing techniques, such as pseudochain growth by slow monomer addition [63], allow somewhat better control of hyperbranched structures [62].

Dendrigraft Polymers

Dendrigraft polymers are the most recently discovered and currently the least understood subset of dendritic polymers. The first examples were reported in 1991 independently by Tomalia *et al.* [64] and Gauthier and Möller [65]. Whereas, traditional monomers are generally employed in constructing dendrimers, reactive oligomers or polymers are used in protect-deprotect or activation schemes to produce dendrigrafts. Consequently, dendrigraft polymers are generally larger structures than dendrimers, grow much faster, and amplify surface groups more dramatically as a function of generational development. Both hydrophilic (e.g., poly(oxazolines) and poly(ethyleneimines)) and hydrophobic dendrigrafts (e.g., polystyrenes) were reported in these early works. These first methodologies involved the iterative grafting of oligomeric reagents derived from living polymerization processes in various iterative *graft-on-graft* strategies. By analogy to dendrimers, each iterative grafting step is referred to as a generation. An important feature of this approach is that branch densities, as well as the size of the grafted branches can be varied independently for each generation. Furthermore, by initiating these iterative grafting steps from a point-like core versus a linear core it is possible to produce spheroidal and cylindrical dendrigrafts, respectively. Depending on the graft densities and molecular weights of the grafted branches, ultrahigh molecular-weight dendrigrafts (e.g., $M_w > 104$ kDa) can be obtained at very low generation levels (e.g., $G = 3$). Dramatic molecular-weight enhancements vis-à-vis other dendrimer propagation methodologies are possible using dendrigraft techniques [66]. Further elaboration of these dendrigraft principles allowed the synthesis of a variety of core-shell-type dendrigrafts, in which elemental composition as well as the hydrophobic or hydrophilic character of the core were controlled independently [65].

In general, the above methodologies have involved convergent-type grafting principles, wherein preformed, reactive oligomers are grafted onto successive branched precursors to produce semicontrolled structures. Compared to dendrimers, dendrigraft structures are less controlled since grafting may occur along the entire length of each generational branch, and the exact branching densities are somewhat arbitrary and difficult to control. More recently, both Gnanou [67,68] and Hedrick [69,70] have developed approaches to dendrigrafts that mimic dendrimer topologies by confining the graft sites to the branch termini for each generation. These methods involve so-called *graft* from techniques, and allow better control of branching topologies and densities as a function of generation. Topologies produced by these methods are reminiscent of the dendrimer architecture. Since the branch-cell arms are derived from oligomeric segments, they are referred to as polymeric dendrimers [10,69,70]. These more flexible and extended structures exhibit unique and different properties as compared to the more compact traditional dendrimers. Fréchet, Hawker, and coworkers [71] have utilized the techniques of living polymerization and a staged polymerization process—in which latent polymerization sites are incorporated within growing chains—to produce dendrigrafts of mixed composition and narrow polydispersity.

Another exciting development has been the emerging role that dendritic architecture is playing in the production of commodity polymers. A recent report by Guan *et al.* [12] has shown that ethylene polymerizes to *dendrigraft*-poly ethylene at low pressures in contrast to high-pressure conditions, which produce only branched topologies. This occurs when using late-transition metal or Brookhart catalysts. Furthermore, these authors also state that small amounts of *dendrigraft*-poly(ethylene) architecture may be expected from analogous early-transition-metal metallocene catalysts.

Dendrons and Dendrimers

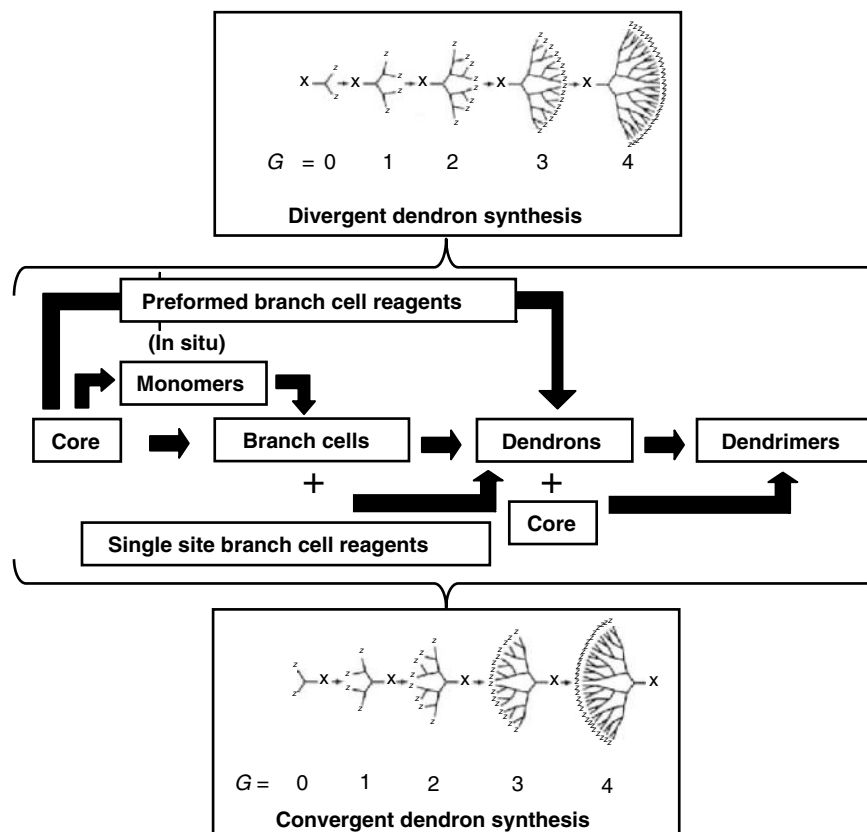
Dendrons and dendrimers are the most intensely investigated subset of dendritic polymers. In the past decade, over 6,000 literature references have appeared dealing with this unique class of structure-controlled polymers. The word dendrimer is derived from the Greek words *dendri-* (tree branch-like) and *meros* (part of), and was coined by Tomalia *et al.* about 20 years ago in the first full paper on poly(amidoamine) (PAMAM) dendrimers [47,72]. Since this early disclosure, over 100 dendrimer compositions (families) and 1,000 dendrimer surface modifications have been reported. The two most widely studied dendrimer families are the Fréchet-type polyether compositions and the Tomalia-type PAMAM dendrimers. PAMAM dendrimers constitute the first dendrimer family to be commercialized, and represent the most extensively characterized and best-understood series at this time [46].

In view of the vast amount of literature in this field, the remaining overview will focus on PAMAM dendrimers. Its scope will be limited to a discussion of their critical properties and unique quantized nanomodule features that make these materials very suitable for nanoscale synthesis and manipulations.

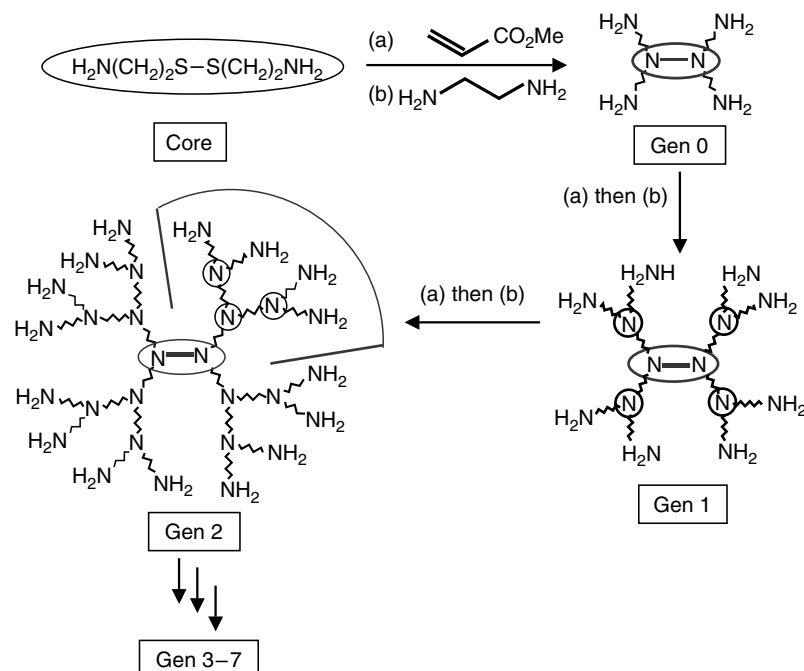
Dendrimer Synthesis: Divergent and Convergent Methods

In contrast to traditional polymers, dendrimers are unique core-shell structures possessing three basic architectural components: a core (I), an interior of shells (generations) consisting of repeating branch-cell units (II), and terminal functional groups (the outer shell or periphery) (III). In general, dendrimer synthesis involves divergent or convergent hierarchical assembly strategies that require the construction components shown in Scheme 42.3. Within each of these major approaches there may be variations in methodology for branch-cell construction or dendron construction. Many of these issues, together with experimental laboratory procedures, have been reviewed elsewhere [73–75].

PAMAM dendrimers are synthesized by the divergent approach. This methodology involves in situ branch-cell construction in stepwise, iterative stages around a desired core to produce mathematically defined core-shell structures. Typically, ethylenediamine [core multiplicity (N_c) = 4], ammonia ($N_c = 3$), or cystamine ($N_c = 4$) may be used as cores and allowed to undergo reiterative, two-step reaction sequences. These sequences consist of: (a) an exhaustive alkylation of primary amines (Michael addition) with methyl acrylate and (b) amidation of amplified ester groups with a large excess of ethylenediamine to produce primary amine terminal groups (Scheme 42.4). This first reaction sequence on the exposed core creates $G = 0$ (i.e., the core branch cell), wherein the number of arms (i.e., dendrons) anchored to the core is determined by N_c . Iteration of the alkylation-amidation sequence produces an amplification of terminal groups from 1 to 2 with the in situ creation of a branch cell at the anchoring site of the dendron that constitutes $G = 1$. Repeating these iterative sequences (Scheme 42.4) produces additional shells (generations) of branch cells that amplify mass and terminal groups according to the mathematical expressions described in the box (Fig. 42.9). It is apparent that both the core multiplicity (N_c) and branch-cell multiplicity (N_b) determine the precise number of terminal groups (Z) and mass amplification as a function of generation (G). One may view those generation sequences as quantized polymerization events. The assembly of reactive monomers [34,76], branch cells [42,46,77] or dendrons [46,78,79] around atomic or molecular cores, to produce dendrimers according to divergent or convergent dendritic branching principles, has been well demonstrated. Such systematic filling of molecular space around cores with branch cells as a function of generational growth stages (branch-cell shells)—to



SCHEME 42.3. Hierarchical assemble scheme illustrating the options for constructing dendrimers by either divergent or convergent synthetic strategies.



SCHEME 42.4. Divergent synthesis of [cystamine] *dendri*-PAMAM dendrimers utilizing the iterative sequence: (a) alkylation with methyl acrylate, followed by (b) amidation with excess ethylenediamine to produce generations 3–7.

Number of surface groups	$Z = N_c N_b^G$	Surface group amplification per generation
Number of branch cells	$BC = N_c \left[\frac{N_b^G - 1}{N_b - 1} \right] =$	Number of covalent bonds per generation
Molecular weights	$M_W = M_c + N_c \left[M_{RU} \left(\frac{N_b^G - 1}{N_b - 1} \right) + M_t N_b^G \right]$	

FIGURE 42.9. Mathematical expressions for calculating the theoretical number of surface groups (Z), branch cells (BC) and molecular weights (MW) as a function of generation, N_c = core multiplicities and N_b = branch cell multiplicity.

give discrete, quantized bundles of nanoscale mass—has been shown to be mathematically predictable [14,80,81]. Predicted molecular weights have been confirmed by mass spectrometry [82–85] and other analytical methods [42,78,86,87]. Predicted numbers of branch cells, terminal groups (Z), and molecular weights as a function of generation for a cystamine-core ($N_c = 4$) PAMAM dendrimer are shown in Fig. 42.10. It should be noted that the molecular weights approximately double as one progresses from one generation to the next. The surface groups (Z) and branch cells (BC) amplify mathematically according to a power function, thus producing discrete, monodispersed structures with precise molecular weights and a nanoscale diameter enhancement as described in Fig. 42.10. These predicted values are routinely verified by mass spectrometry for the earlier generations (i.e., $G = 4$ – 5); however, with divergent dendrimers, minor mass defects are often observed for higher generations as congestion-induced *de Gennes dense packing* begins to take effect [42,88].

Dendrimer Features of Interest to Nanoscientists

Dendrimers may be thought of as unique nanoscale devices [16,89]. Each architectural component manifests a specific function while at the same time defining properties for these nanostructures as they are grown generation by generation. For example, the *core* may be thought of as the molecular information center from which *size, shape, directionality, and multiplicity* are expressed *via* the covalent connectivity to the outer shells. Within the *interior*, one finds the *branch-cell amplification region*, which defines the type and amount of interior void space that may be enclosed by the terminal groups as the dendrimer is grown. Branch-cell multiplicity (N_b) determines the density and degree of amplification as an exponential function of generation (G). The interior composition and amount of solvent filled void space determines the extent and nature of guest–host (endoreceptor) properties that are possible with a particular dendrimer family and generation. Finally, the surface consists of reactive or passive terminal groups that may perform several functions. With appropriate function, they serve as a *template polymerization region* as each generation

is amplified and covalently attached to the precursor generation. Secondly, the surface groups may function as passive or reactive gates controlling control entry or departure of guest molecules from the dendrimer interior. These three architectural components essentially determine the physico-chemical properties, as well as the overall sizes, shapes, and flexibility of dendrimers. It is important to note that dendrimer diameters increase linearly as a function of shells or generations added; whereas, the terminal functional groups increase exponentially as a function of generation. This dilemma enhances “tethered congestion” of the anchored dendrons, as a function of generation, due to the steric crowding of the end groups. As a consequence, lower generations are generally open, floppy structures; whereas, higher generations become robust, less deformable spheroids, ellipsoids or cylinders depending on the shape and directionality of the core (Fig. 42.11).

Dendrimer Shape Changes

As illustrated in Fig. 42.12, dendrimers undergo “congestion induced” molecular shape changes from flat, floppy conformations to robust spheroids as first predicted by Goddard *et al.* [76]. Shape change transitions were subsequently confirmed by extensive photophysical measurements, pioneered by Turro *et al.* [90–93] and solvatochromic measurements by Hawker, Wooley, and Fréchet [94]. Depending upon the accumulative core and branch-cell multiplicities of the dendrimer family under consideration, these transitions were found to occur between $G = 3$ and $G = 5$. Ammonia core, PAMAM dendrimers ($N_c = 3, N_b = 2$) exhibited a molecular morphogenesis break at $G = 4.5$; whereas, the ethylenediamine (EDA) PAMAM dendrimer family ($N_c = 4, N_b = 2$) manifested a shape change break around $G = 3$ – 4 [76] and the Fréchet-type convergent dendrons ($N_b = 2$) around $G = 4$ [94]. It is readily apparent that increasing the core multiplicity to $N_c = 4$ accelerates congestion and forces a shape change at least one generation earlier. Beyond these generational transitions, one can visualize these dendrimeric shapes as nearly spheroidal or slightly ellipsoidal *core–shell type architecture*.

Gen	No. of NH ₂ surface groups	Molecular formula	MW	Hydrodynamic diameter (nm)
0	4	C ₂₄ H ₅₂ N ₁₀ O ₄ S ₂	609	1.5
1	8	C ₆₄ H ₁₃₂ N ₂₆ O ₁₂ S ₂	1,522	2.2
2	16	C ₁₄₄ H ₂₉₂ N ₅₈ O ₂₈ S ₂	3,348	2.9
3	32	C ₃₀₄ H ₆₁₂ N ₁₂₂ O ₆₀ S ₂	7,001	3.6
4	64	C ₆₂₄ H ₁₂₅₂ N ₂₅₀ O ₁₂₄ S ₂	14,307	4.5
5	128	C ₁₂₆₄ H ₂₅₃₂ N ₅₀₆ O ₂₅₂ S ₂	28,918	5.4
6	256	C ₂₅₄₄ H ₅₀₉₂ N ₁₀₁₈ O ₅₀₈ S ₂	58,140	6.7
7	512	C ₅₁₀₄ H ₁₀₂₁₂ N ₂₀₄₂ O ₁₀₂₀ S ₂	116,585	8.1

Z = monomer-shell-saturation level, N_c = core (cystamine) multiplicity, N_b = branch-cell (BC) multiplicity, G = generation.

FIGURE 42.10. Approximate hydrodynamic diameters (Gen = 0–7) based on gel electrophoretic comparison with the corresponding [ethylenediamine core]-PAMAM dendrimers.

De Gennes Dense Packing

As a consequence of the excluded volume associated with the core, interior, and surface branch cells, steric congestion is expected to occur due to tethered connectivity to the core. Furthermore, the number of dendrimer surface groups, Z, amplifies with each subsequent generation (G). This occurs according to geometric *branching laws*, which are related to core multiplicity, (N_c) and branch-cell multiplicity (N_b). These values are defined by the following equation:

$$Z = N_c N_b^G.$$

Since the radii of the dendrimers increase in a linear manner as a function of G, whereas, the surface cells amplify according to $N_c N_b^G$, it is implicit from this equation that generational reiteration of branch cells ultimately will lead to a so-called “dense-packed state.”

As early as 1983, de Gennes and Hervet [95] proposed a simple equation derived from fundamental principles, to predict the dense-packed generation, for Tomalia-type PAMAM dendrimers. It was predicted that at this generation ideal branching can no longer occur since available surface space becomes too limited for the mathematically predicted

number of surface cells to occupy. This produces a “closed geometric structure.” The surface is “crowded” with exterior groups, which although potentially chemically reactive, are sterically prohibited from participating in ideal dendrimer growth.

This “critical packing state” does not preclude further dendrimer growth beyond this point in the genealogical history of the dendrimer preparation. On the contrary, although continuation of dendrimer step-growth beyond the dense-packed state cannot yield structurally ideal, next generation dendrimer, it can nevertheless occur, as indicated by further increases in the molecular weight of the resulting products. Predictions by de Gennes [95] suggested that the Tomalia-type PAMAM dendrimer series should reach a critical packing state at generations 9–10. Experimentally, we observed a moderate molecular weight deviation from predicted ideal values beginning at generation 4–7. This digression became very significant at generation 7–8 as dendrimer growth was continued to generations 12 [96]. The products thus obtained are of “imperfect” structure because of the inability of all surface groups to undergo further reaction. Presumably a fraction of these surface groups remain trapped under the surface of the newly formed dendrimer

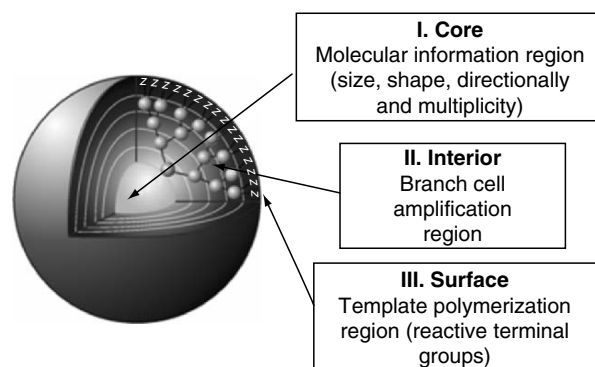


FIGURE 42.11. Three-dimensional projection of dendrimer core-shell architecture for G = 4.5 poly(amidoamine) (PAMAM) dendrimer with principal architectural components (I) core, (II) interior and (III) surface.

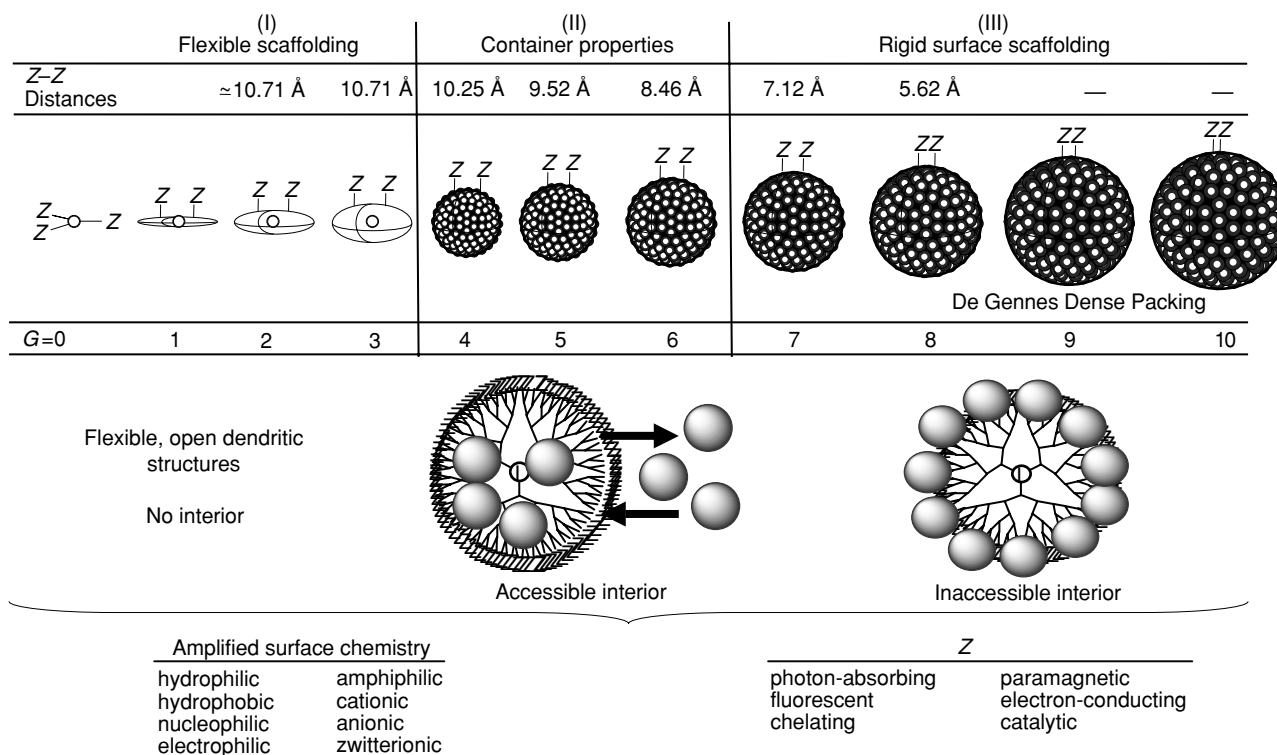


FIGURE 42.12. Periodic properties of PAMAM dendrimers as a function of generation. Various chemophysical dendrimer surfaces amplified according to $Z = N_c N_b^G$, where N_c = core multiplicity, N_b = branch-cell multiplicity and G = generation. (Reproduced from [88] with permission of J. Wiley & Sons.)

shell, yielding a unique architecture possessing two types of terminal groups. This new surface group population will consist of both those that are accessible to subsequent reiteration reagents and those that will be sterically screened. The total number of these groups will not, however, correspond to the predictions of the mathematical branching law, but will fall between that value, which was mathematically predicted for the next generations (i.e., $G + 1$), and that expected for the precursor generation (G). Thus, a mass defective dendrimer “generation” is formed.

Dendrimer surface congestion can be appraised mathematically as a function of generation, from the following simple relationship:

$$A_z = \frac{A_D}{N_z} \alpha \frac{r^2}{N_c N_b^G}$$

where A_z is the surface area per terminal group Z , A_D the dendrimer surface area, and N_z the number of surface groups Z per generation. This relationship predicts that at higher generations G , the surface area per Z group becomes increasingly smaller and experimentally approaches the cross-sectional area or van der Waals dimension of the surface groups Z . The generation G thus reached is referred to as the “de Gennes” dense-packed generation. Ideal dendritic growth without branch defects is possible only for those

generations preceding this dense-packed state. This critical dendrimer property gives rise to self-limiting dendrimer dimensions, which are a function of the branch-cell segment length (l), the core multiplicity N_c , the branch-cell juncture multiplicity N_b , and the steric dimensions of the terminal group Z . Whereas, the dendrimer radius r in the above expression is dependent on the branch-cell segment lengths l , large l values delay this congestion. On the other hand, larger N_c , N_b values and larger Z dimensions dramatically hasten it.

Additional physical evidence supporting the anticipated development of congestion as a function of generation is shown in the composite comparison in Fig. 42.13. Plots of intrinsic viscosity $[\eta]$, density z , surface area per Z group (A_z), and refractive index n as a function of generation clearly show maxima or minima at generations = 3–5, paralleling computer-assisted molecular-simulation predictions [76] as well as extensive photochemical probe experiments reported by Turro *et al.* [90–93].

The intrinsic viscosities $[\eta]$ is expected to increase in a very classical fashion as a function of molar mass (generation) but should decline beyond a certain generation because of a change from an extended to a globular shape [42]. In effect, once this critical generation is reached, the dendrimer begins to act more like an Einstein spheroid. The intrinsic viscosity is a physical property that is expressed in dL/g—the ratio of a volume to a mass. As the generation

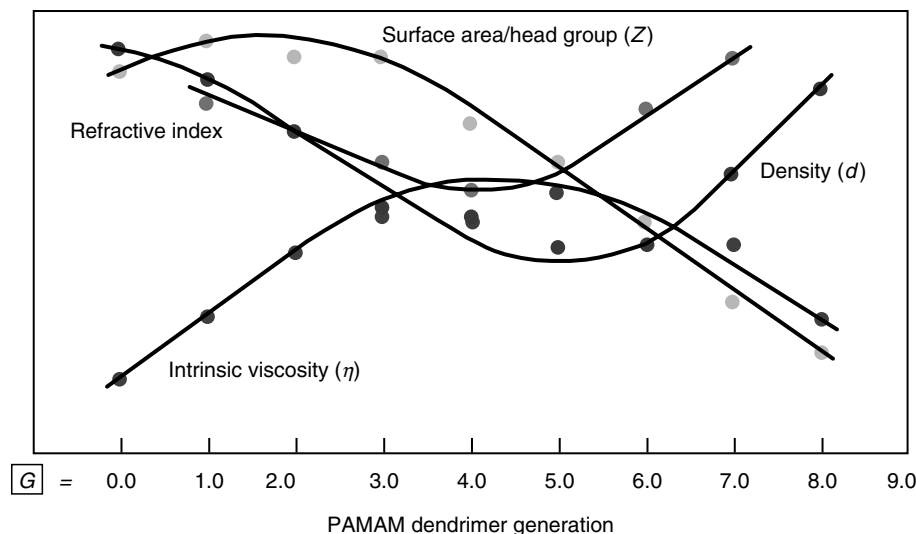


FIGURE 42.13. Comparison of surface area/head group (Z), refractive index, density (d) and intrinsic viscosity (η) as a function of generation: $G = 1-9$. (Reproduced from [88] with permission of J. Wiley & Sons.)

number increases and transition to a spherical shape takes place, the volume of the spherical dendrimer roughly increases in cubic fashion while its mass increases exponentially, hence the value of $[\eta]$ must decrease once a certain generation is reached. This prediction has now been confirmed experimentally [97].

The dendrimer density z (atomic mass units per unit volume) clearly minimizes between generations 4 and 5, then begins to increase as a function of generation due to the increasingly larger, exponential accumulation of surface groups. Since refractive indices are directly related to density parameters, their values minimize and parallel the above density relationship.

Clearly, this de Gennes dense packed congestion would be expected to contribute to (a) sterically inhibited reaction rates and (b) sterically induced stoichiometry [42]. Each of these effects was observed experimentally at higher generations. The latter would be expected to induce dendrimer mass defects at higher generations which we have used as a diagnostic signature for appraising the “de Gennes dense packing” effect. These issues have been reviewed extensively elsewhere [36,46].

42.3.4 New Properties Driven by the Dendritic State

Throughout much of the early growth and evolution of polymer science, the quest for new properties was focused primarily on the two traditional architectures that defined thermoplastic (linear) and thermoset (cross-linked polymers). Within each of these areas, there was intense activity to evaluate and optimize certain critical parameters. These parameters included various macromolecular chemical compositions, copolymer compositions, molecular weight effects, molecular weight distributions, and cross-link

densities, just to mention a few. Relatively little attention was given to the influence of architecture until the 1970s and 1980s. During that time, the first stirring of interest began concerning the influence of long chain branching on polymer properties [10]. Significant activity ensued thereafter, as it became apparent that single site metallocene/Brookhart catalysts were producing unique poly(olefin) families with completely new, commercially valuable properties [12,13]. It is now recognized that both branched and dendritic architecture, in addition to molecular weight control, are key parameters influencing these new properties. These successful commercial developments, together with the rapid evolution of many new synthetic strategies to branched and dendritic architectures, have intensified the interest that macromolecular architecture may offer for the discovery of new properties.

Comparison of Traditional Linear Polymer and Dendritic Polymer Properties

The affect of architecture on small molecular properties has been recognized since the historical Berzelius (1832) discovery that defined the following premise: *substances of identical compositions but different architectures—“skeletal isomers”—will differ in one or more properties* [98]. These effects are very apparent when comparing the fuel combustion benefits of certain isomeric octanes or the dramatic property differences observed in the three architectural isomers of carbon; namely: graphite, diamond, and buckminsterfullerene (Fig. 42.3).

Similar patterns of property differentiation are clearly recognized at the macromolecular level. For example, dramatic changes in physical and chemical properties are observed by simply converting a linear topology of common

composition to a cross-linked architecture. In traditional macromolecular science, these issues were considered apparent and obvious. However, as novel architectures emerged, new architecture–property relationships have not been so clearly articulated and exploited. Prompted by the synthetic accessibility of many new polymeric architectures based on common compositional monomers (i.e., branch-cell monomers), this perspective was more clearly defined as early as 1994 in experiments by Fréchet and coworkers aimed at determining the influence of shape on the reactivity and physical properties of a series of comparable macromolecules including a dendrimer, a random hyperbranched polymer, and a linear aromatic polyesters all obtained from analogous building blocks [99]. This work clearly demonstrated the very significant shape-related changes in chemical reactivity as well as solubility that exist for polymers possessing the same average molecular weight and composition but differ only in their architecture and polydispersity. Following this report Tomalia introduced in 1996 the concept of “macromolecular (architectural) isomerism.” Simply stated—“macromolecular substances derived in the same proportions from the same monomer compositions, but in different architectural (configurations) will be expected to manifest different chemo/physical properties” [100,101]. This hypothesis proposed a unique strategy for obtaining new polymeric properties by simply converting cost-effective traditional monomers into new macromolecular topologies (architectures). In 1997 Hawker *et al.* [102] provided the ultimate validation of this concept by preparing exact, size monodisperse, linear, and dendritic polyethers analogs with the same composition. Their study revealed significant physical property differences between the two “architectural isomers” confirming the earlier work of Fréchet and coworkers [99]. Most notable were substantially smaller

hydrodynamic volumes (i.e., 40% smaller), as well as amorphous character (i.e., significantly more solvent soluble) for the dendritic isomers compared to the linear analog.

Parallel studies on Tomalia type PAMAM dendrimers, the Fréchet type poly(ether)dendrons, and other dendrimer families have generated an extensive list of unique properties driven by the “dendritic state.” Figure 42.14 compares several significant physical property differences between the linear and dendritic topologies related to conformations, crystallinity, solubilities, intrinsic viscosities, entanglement, diffusion/mobility, and electronic conductivity.

In contrast to linear polymers, that obey the Mark–Houwink–Sakurada equation, the intrinsic viscosities of dendrimers do not increase continuously with molecular weight, but reach a maximum at a certain dendrimer generation. These maxima were predicted by Tomalia *et al.* for poly(amidoamine) dendrimers [42] and later measured for poly(arylethers) [97], as well as for poly(propyleneimine) dendrimers [103], thus indicating they were not composition dependent. This property is presumably due to the fact that the dendrimer structure becomes spherical at a specific generation level due to tethered congestion, hence its volume grows by a first approximation as n^3 , whereas, mass grows as 2^n (where n = generation number). Since the intrinsic viscosity $[\eta]$ is expressed in volume per mass, the quotient of the foregoing volumes and mass functions is indeed expected to display a maximum. A study of the melt viscosity of convergently grown Fréchet-type polyether dendrimers [61] also demonstrated this unique behavior, quite unlike that of comparable linear polymers. It is clear that the lack of entanglement of globular dendrimers—another attribute of the dendritic state—is largely responsible for the most unusual dendritic melt viscosity behavior [61,104,105].

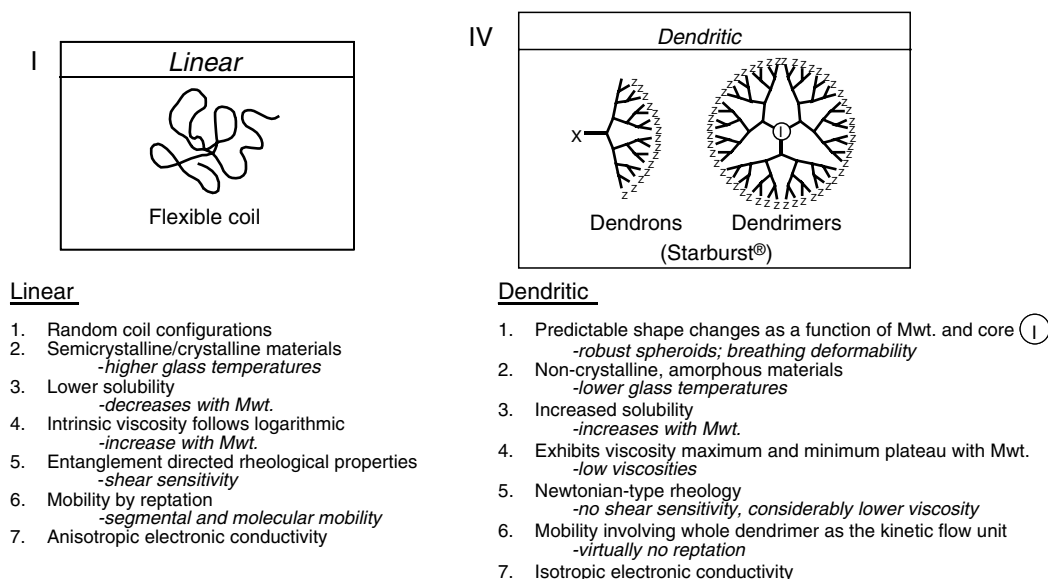


FIGURE 42.14. Comparison of properties for (I) linear and (IV) dendritic architecture. (Reproduced from [88] with permission of J. Wiley & Sons.)

Fréchet [43,106] was the first to compare viscosity parameters for (A) linear topologies, as well as (B) random hyperbranched polymers and (C) dendrimers. More recently, we reported such parameters for (D) dendrigraft polymers [105] as shown in Fig. 42.15. It is clear that all three dendritic topologies behave differently than the linear architecture. There is, however, a continuum of behavior; wherein, random hyperbranched polymers behave most nearly like the linear systems. Dendrigrafts exhibit intermediary behavior; whereas, dendrimers show a completely different relationship as a function of molecular weight.

Important physical property subtleties were noted within the dendrimer subset. For example, dendrimers possessing asymmetrical branch cells (i.e., Denkewalter type) exhibit a constant density versus generation relationship (Fig. 42.20). This is in sharp contrast to symmetrical branch-cell dendrimers (Tomalia-type PAMAM) that exhibit a minimum in density between $G = 4$ and $G = 7$ (NH_3 core) [42,76]. This is a transition pattern that is consistent with the observed development of “container properties” described in Fig. 42.16.

Finally, other unique features offered by the “dendritic state,” that appear to have no equivalency in the linear topologies, and are found almost exclusively in the dendron/dendrimer subset include the following; (a) *nearly complete monodispersity*, (b) *the ability to control unimolecular nanoscale container/scaffolding properties*, (c) *exponential amplification of terminal functional groups*, and (d) *persistent nanoscale dimensions/shape* as a function of molecular weight (generation). These features are captured to some degree with dendrigraft polymers, but are either absent or present to a minor extent in random hyperbranched polymers.

Monodispersity

The monodispersed nature of dendrimers has been verified extensively by mass spectroscopy, size exclusion chromatography, gel electrophoresis, and electron microscopy (TEM). As is always the case, the level of monodispersity is

determined by the skill of the synthetic chemist, as well as the isolation/purification methods utilized.

In general, convergent methods produce the most nearly isomolecular dendrimers. This is because the convergent growth process allows purification at each step of the synthesis and therefore no cumulative effects of failed couplings are found. Appropriately purified convergent dendrimers are probably the most precise synthetic macromolecules that exist today.

As discussed earlier, mass spectroscopy has shown that PAMAM dendrimers produced by the “divergent method” are very monodisperse and have masses consistent with predicted values for the earlier generations (i.e., $G = 0-5$). Even at higher generations, as one enters the de Gennes dense packed region, the molecular weight distributions remain very narrow (i.e., 1.05) and consistent in spite of the fact that experimental masses deviate substantially from predicted theoretical values. Presumably, de Gennes dense packing produces a very regular and dependable effect that is manifested in the narrow molecular weight distribution.

Unimolecular Nanoscale Container/ Scaffolding Properties

Unimolecular container/scaffolding behavior appears to be a periodic property that is specific to each dendrimer family or series. These properties will be determined by the size, shape, and multiplicity of the construction components that are used for the core, interior, and surface of the dendrimer. Higher multiplicity components and those that contribute to “tethered congestion” will hasten the development of “container properties” or rigid surface scaffolding as a function of generation. Within the PAMAM dendrimer family, these periodic properties are generally manifested in three phases as shown in Fig. 42.12.

The earlier generations (i.e., $G = 0-3$) exhibit no well-defined interior characteristics; whereas, interior development related to geometric closure is observed for the intermediate generations (i.e., $G = 4-7$). Accessibility and departure from the interior is determined by the “size and

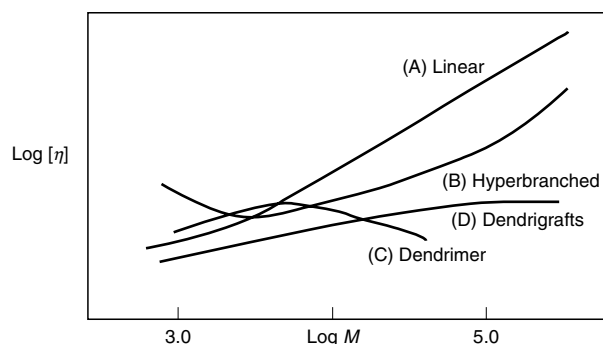


FIGURE 42.15. Comparison of intrinsic viscosities ($\log [\eta]$) versus molecular weight ($\log M$) for (A) linear, (B) random hyperbranched, (C) dendrimers, and (D) dendrigraft topologies. (Reproduced from [88] with permission of J. Wiley & Sons.)

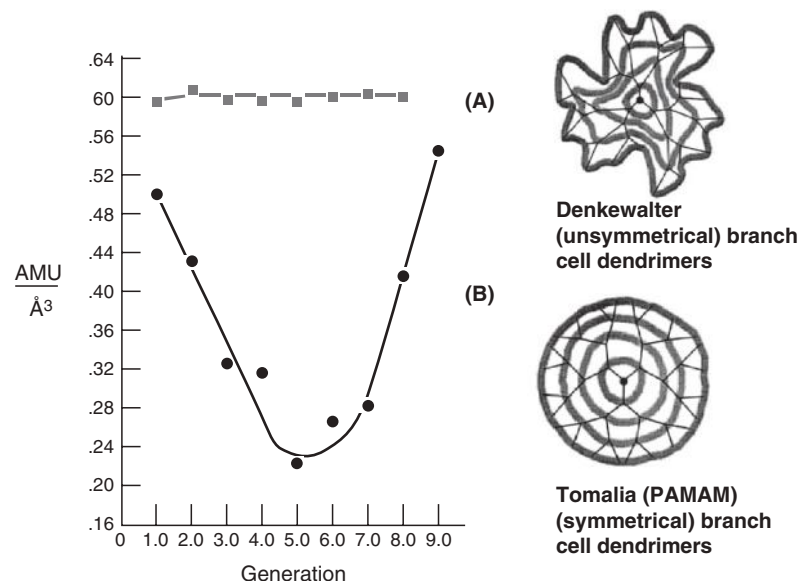


FIGURE 42.16. Comparison of densities as a function of generation for (A) assymetrical branch cell in Denkewalter-type dendrimers, (B) symmetrical branch cell in Tomalia-type dendrimers ([densities calculated from experimental hydrodynamic diameters and theoretical, D.A. Tomalia, M. Hall, D.M. Hedstrand, *J. Am. Chem. Soc.*, **109**, 1601 (1987)]. (Reproduced from [88] with permission of J. Wiley & Sons.)

gating properties” of the surface groups. At higher generations (i.e., $G \Rightarrow 7$) where de Gennes dense packing is severe, rigid scaffolding properties are observed, allowing relatively little access to the interior except for very small guest molecules. The site-isolation and encapsulation properties of dendrimers have been reviewed recently by Hecht and Fréchet [41].

Amplification of Terminal Surface Groups

Dendrimers within a generational series can be expected to present their terminal groups in at least three different modes, namely: *flexible*, *semiflexible*, or *rigid functionalized scaffolding*. Based on mathematically defined dendritic branching rules (i.e., $Z = N_c N_b^G$) the various surface presentations are expected to become more congested and rigid as a function of generation level. It is implicit that this surface amplification can be designed to control gating properties associated with unimolecular container development. Furthermore, dendrimers may be viewed as versatile, nanosized objects that can be surface functionalized with a vast array of features (Fig. 42.17). The ability to control and engineer these parameters provides an endless list of possibilities for utilizing dendrimers as modules for the design of nanodevices [81,107]. Recent publications have begun to focus on this area [41,108–113].

Persistent Nanoscale Shapes and Dimensions

In view of the extraordinary structure control and nanoscale dimensions observed for dendrimers, it is not surprising

to find extensive interest in their use as globular protein mimics. Based on their systematic, dimensional length scaling properties (Fig. 20.18) and electrophoretic/hydrodynamic behavior [86], they are sometimes referred to as *artificial proteins*. These fundamental properties have in fact led to their commercial use as globular protein replacements for gene therapy [114] and immunodiagnostics [115–118]. Substantial effort has been focused recently on the use of dendrimers for “site isolation” mimicry of proteins [41], enzyme-like catalysis [119], as well as other biomimetic applications [79,120].

42.4 DENDRITIC STRUCTURES AS INTERMEDIARY ARCHITECTURES BETWEEN THERMOPLASTICS AND THERMOSETS

The first two major domains defined in polymer science were associated with certain distinguishing properties and architecture. One domain included linear, random coil thermoplastic polymers such as poly(styrenes) or poly(acrylates). These architectures were characterized as one-dimensional chains possessing two terminal groups per molecule, specific molecular weight distributions, reasonable solvent solubility, melt flow characteristics, chain entanglements consisting of inter- and intramolecular knots and loops, mobility *via* snakelike reptation, and they exhibited expanded, large molecular volumes when immersed in “good solvents.” The second domain of “thermoset polymers” included cross-linked architectures such as vulcanized rubber, epoxies, and melamine resins all of which

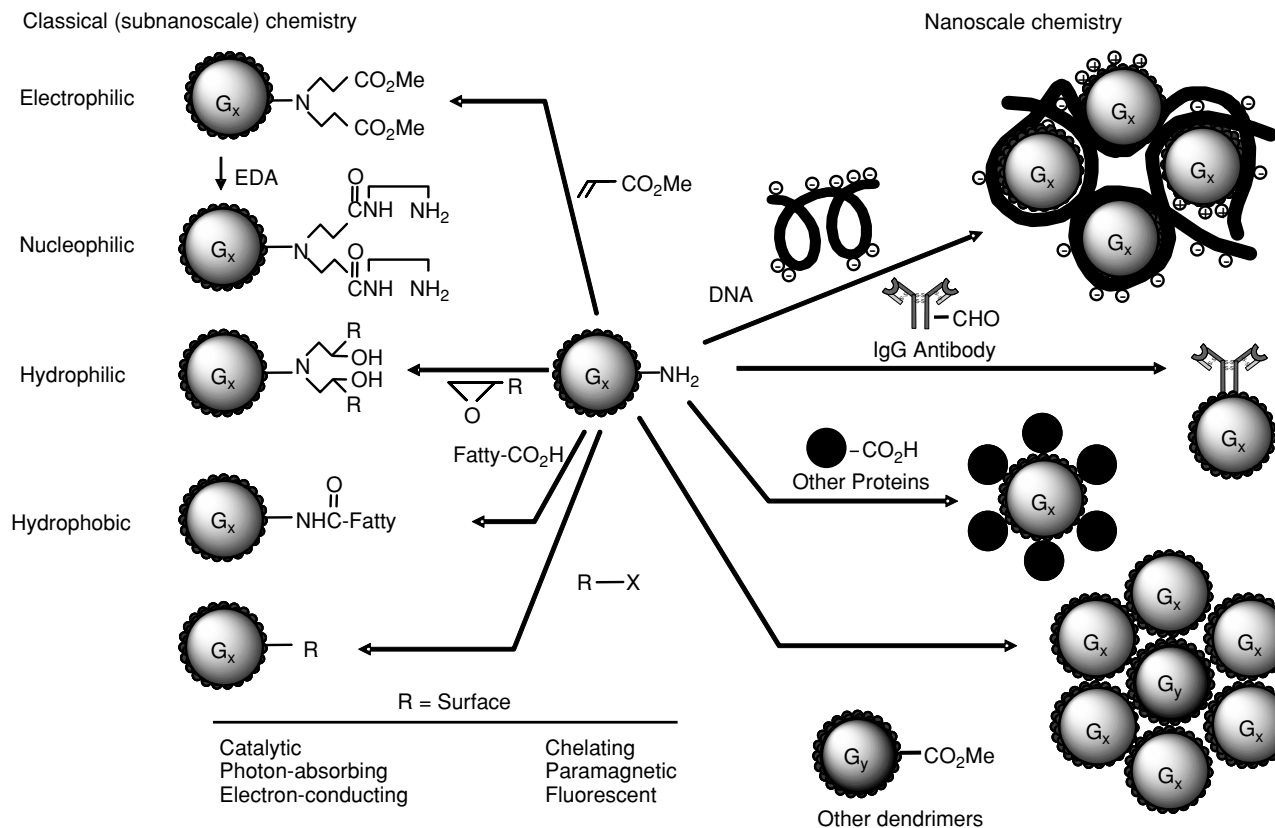


FIGURE 42.17. Options for modifying amine terminated dendrimers utilizing classical subnanoscale and nanoscale reagents. (Reproduced from [129] with permission of Aldrichimica Acta.)

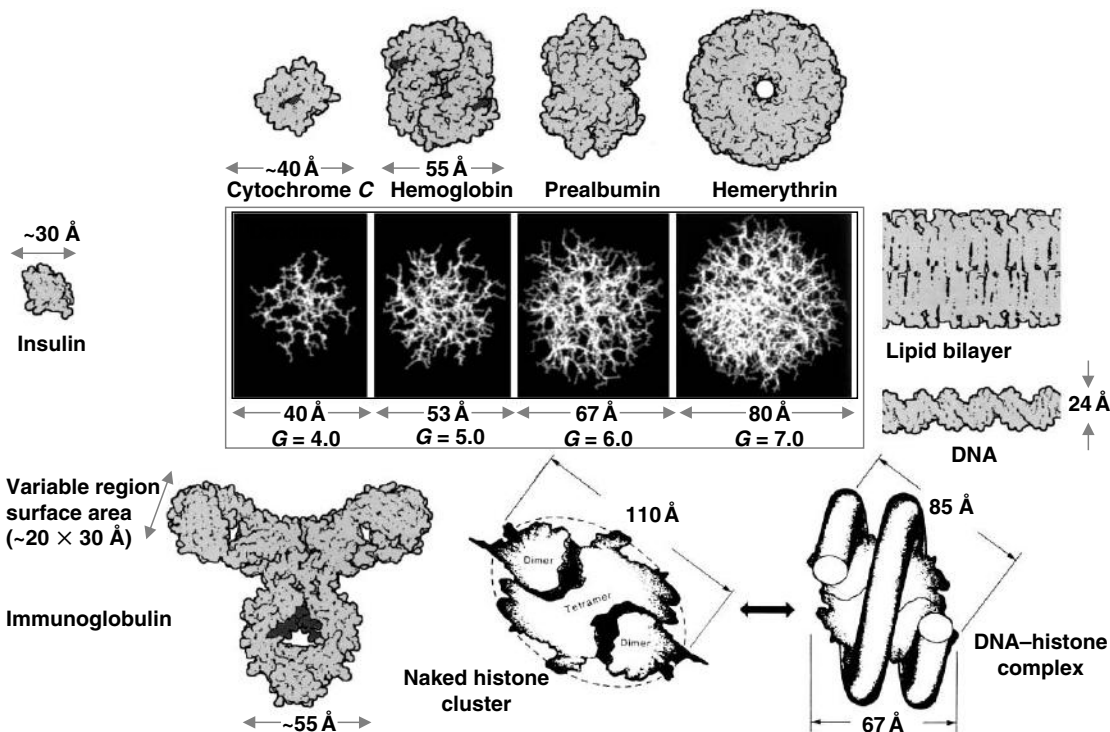


FIGURE 42.18. A comparison of dimensional length scales (Å) for PAMAM dendrimers $N_c = 3$, $N_b = 2$ (NH_3 core) and various biological entities (e.g., proteins, DNA and lipid bilayers). (Reproduced from [88] with permission of J. Wiley & Sons.)

were recognized as insoluble macromolecules. They exhibited rubber-like elasticity, and no melt flow features, yet they were semipermeable and susceptible to diffusion and pronounced swelling in certain solvents.

It is now recognized that a continuum of architecture and properties, beginning with the classical branched polymers, resides between these two classes. Typical branched structures such as starch or high pressures polyethylene are characterized by more than two terminal groups per molecule, possessing substantially smaller hydrodynamic volumes and different intrinsic viscosities compared to linear polymers, yet they often exhibit unexpected segmental expansion near the “theta state.”

Completing this continuum, we may now focus on the intermediary role that (Class IV) dendritic polymers play both in architecture and properties as penultimate thermoplastic precursors to (Class II), cross-linked thermoset systems. Within the realm of traditional architectures, branched (Class III) and random hyperbranched structures Class (IVa) may be viewed as penultimate statistical precursors residing between thermoplastic structures and thermoset architectures as illustrated in Fig. 42.19 [121,122]. The dendritic state may be visualized as advancement from a lower order (i.e., Class I–III) to a somewhat higher level of structural complexity [123]. Recent developments now demonstrate that certain dendritic subsets are manifestations of higher level structural control. In contrast to random hyperbranched polymers, the dendrimer subset, and to a lesser extent, the dendrigraft subset, represent a unique combination of high complexity with extraordinary structure control. As such, covalent bridging or crosslinking of these preformed modules would be expected to give rise to a completely new class (V) of more ordered

complexity. Examples of this new architecture have been synthesized and these new topologies are referred to as “megamers.”

42.4.1 Megamers—A New Class of Regio-Specifically Cross-linked Dendrimers

In the first full paper published on dendritic polymers [47], dendrimers were defined as “reactive, structure-controlled macromolecular building blocks.” It was proposed that they could be used as repeat units for the construction of a new class of topological macromolecules referred to as “starburst polymers.” Although there is intense activity in the field of dendrimer science, there are relatively few references focused on this specific concept [34,80,81,96]. Meanwhile, the term “starburst” has been claimed as a registered trademark of the Dow Chemical Company and recently assigned to Dendritic NanoTechnologies, Inc. In view of these events, the generic term, “megamer” has been proposed to describe those new architectures that are derived from the combination of two or more dendrimer molecules (see Figs. 42.19 and 42.20) [96,124].

Examples of both statistical, as well as structure-controlled megamer assemblies have been reported and reviewed recently [96,124]. Covalent oligomeric assemblies of dendrimers (i.e., dimers, trimers, etc.) are well-documented examples of low molecular-weight megamers. Statistical megamer assemblies have been reported as both *supramacromolecular* [109,110] and *supermacromolecular* (covalent) topologies. Many reports on the supramacromolecular self-assembly of these structures leading to dendrimeric clusters and monolayers are prime examples of

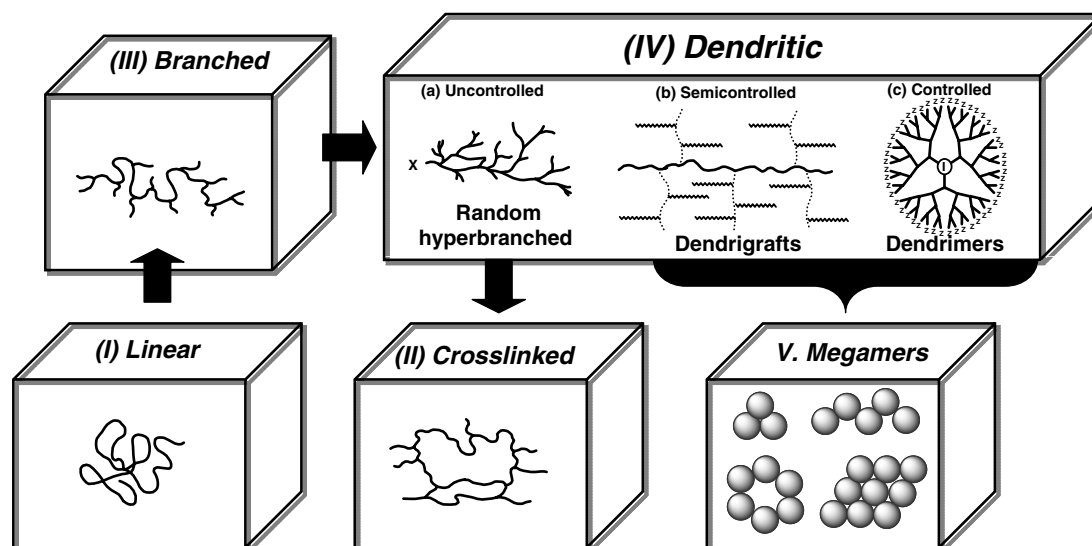


FIGURE 42.19. Examples of architectural polymer classes (I–IV) polymer type, repeat units, and covalent connectivity associated with architectural classes.

supramacromolecular megamers. Simple, low DP covalent dendrimeric oligomers such as “[dendrimer]_n” where $n = 2-10$, and dendrimeric gels for which $n > 10$ represent a continuum of statistical covalent megamers that are possible.

Both randomly assembled megamers [124], as well as structure-controlled megamers [124–126] have been demonstrated. Recently, new mathematically defined megamers (dendrimer clusters) or core–shell tecto(dendrimers) have been reported [35,125–127]. The principles of these structure-controlled megamer syntheses mimic those used for the core–shell construction of dendrimers. First, a megamer core reagent (usually a spheroid) is selected. Next, a limited amount of this reactive core reagent is combined with an excess of a megamer shell reagent. The objective is to completely saturate the target spheroid core surface with covalently bonded spheroidal shell reagent. Since the diameters of the megamer core and shell reagents are very well defined, it is possible to predict mathematically the number

of megamer shell molecules required to saturate a targeted core dendrimer [89,128,129].

It appears that *structure-controlled complexity beyond dendrimers* is now possible. The demonstrated structure control within the dendrimer modules, and now the ability to mathematically predict and synthesize precise assemblies of these modules, provide a broad concept for the systematic construction of nanostructures with dimensions that could span the entire nanoscale region (Fig. 42.20) [16,89].

42.5 CONCLUSIONS

Dendritic polymers are expected to play a key role as enabling building blocks for nanotechnology during the 21st century, just as the first three traditional architectural classes of synthetic polymers have so successfully fulfilled critical material and functional needs in the plastics age during the past half century. The controlled shape, size,

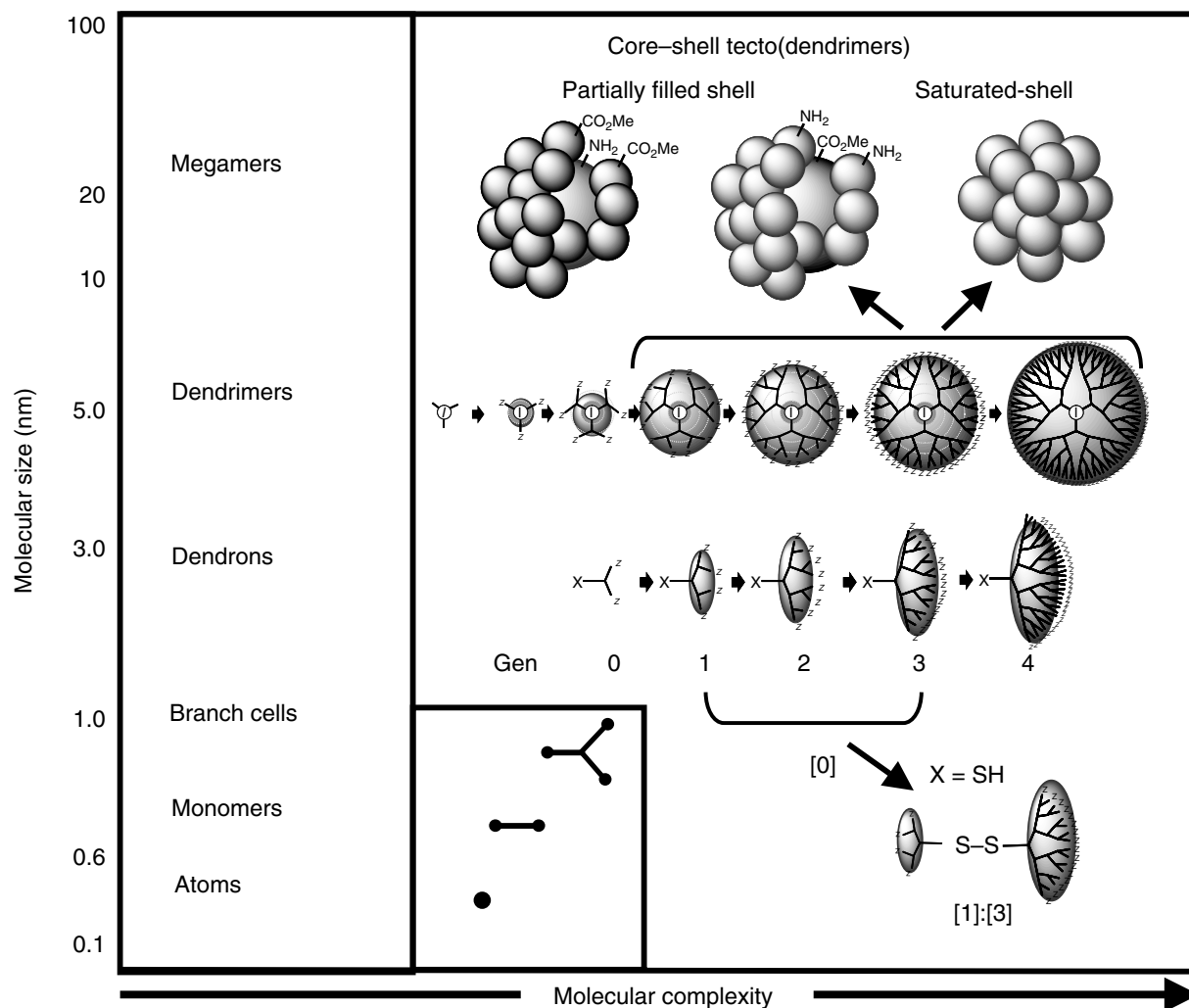


FIGURE 42.20. Approximate nanoscale dimensions as a function of atoms, monomers, branch cells, dendrimers, and megamers. (Reproduced from [129] with permission of Aldrichimica Acta.)

and differentiated functionality of dendrimers; their ability to provide both isotropic and anisotropic assemblies; their compatibility with many other nanoscale building blocks such as DNA, metal nanocrystals, and nanotubes; their potential for ordered self-assembly; their ability to combine both organic and inorganic components; and their propensity to either encapsulate or be engineered into unimolecular functional devices make dendrimers uniquely versatile amongst existing nanoscale building blocks and materials. Dendritic polymers, especially dendrons and dendrimers, are expected to fulfill an important role as fundamental modules for nanoscale synthesis. It is from this perspective that it is appropriate to be optimistic about the future of this new major polymer class, the *dendritic state* [16,130].

ACKNOWLEDGMENTS

This work was funded by the Army Research Laboratory (ARL), Dendritic Polymer Center of Excellence (Contract DAAL-01-1996-02-044). I would like to express my sincere appreciation to Ms L. S. Nixon for preparing the manuscript.

REFERENCES

1. H. Staudinger, *From Organic Chemistry to Macromolecules* (Wiley-Interscience, New York, 1970).
2. H. Morawetz, *Polymers. The Origin and Growth of a Science* (J. Wiley, New York, 1985).
3. H. Staudinger, *Schweiz. Chem. Z.*, **105**, 28–33, 60–64 (1919).
4. H. Staudinger, *Ber. Deut. Chem. Ges.* **53**, 1073 (1920).
5. H. Staudinger, *From Organic Chemistry to Macromolecules, A Scientific Autobiography* (Wiley, New York, 1961).
6. L. K. James, in *Nobel Laureates in Chemistry 1901–1992*, edited by L. K. James (History of Modern Chemical Science Series, American Chemical Society, Washington, DC, 1994), pp. 359–367.
7. *Handbook of Radical Polymerization*, edited by K. Matyjaszewski and T. Davis (John Wiley & Sons, New Jersey, 2002).
8. K. Matyjaszewski and J. Spanswick, *Mater. Today*, 26–33 (March 2005).
9. H.-G. Elias, *Mega Molecules* (Springer-Verlag, Berlin, 1987).
10. *Advances in Polymer Science, Branched Polymers I; Vol. 142*, edited by J. Roovers (Springer-Verlag, Berlin, 1999).
11. *Advances in Polymer Science, Branched Polymers II; Vol. 143*, edited by J. Roovers (Springer-Verlag, Berlin, 2000).
12. Z. Guan, P. M. Cotts, E. F. McCord, and S. J. McLain, *Science* **283**, 2059–2062 (1999).
13. *Metallocene-Based Polyolefins, Vols. 1 and 2* (J. Wiley & Sons Ltd., Brisbane, 2000).
14. M. K. Lothian-Tomalia, D. M. Hedstrand, and D. A. Tomalia, *Tetrahedron* **53**, 15495–15513 (1997).
15. D. S. Goodsell, *Am. Sci.* **88**, 230–237 (2000).
16. D. A. Tomalia, *Mater. Today*, 34–46 (March 2005).
17. P. J. Flory, *J. Am. Chem. Soc.* **63**, 3083, 3091, 3096 (1941).
18. P. J. Flory, *J. Am. Chem. Soc.* **74**, 2718 (1952).
19. P. J. Flory, *Ann. N.Y. Acad. Sci.* **57**, 327 (1953).
20. P. J. Flory, *Principles of Polymer Chemistry* (Cornell University Press, Ithaca, NY, 1953).
21. W. H. Stockmayer, *J. Chem. Phys.* **11**, 45 (1944).
22. W. H. Stockmayer, *J. Chem. Phys.* **12**, 125 (1944).
23. B. Zimm and W. H. Stockmayer, *J. Chem. Phys.* **17**, 1301 (1949).
24. P. J. Flory and J. Rehner, *J. Chem. Phys.* **11**, 512 (1943).
25. W. W. Graessley, *Macromolecules* **8**, 185 (1975).
26. W. W. Graessley, *Macromolecules* **8**, 865 (1975).
27. M. Gordon and G. R. Dobson, *J. Chem. Phys.* **43**, 35 (1975).
28. M. Gordon and G. N. Malcolm, *Proc. R. Soc. (London)* **A295**, 29 (1966).
29. K. Dusek, *Makromol. Chem. Suppl.* **2**, 35 (1979).
30. W. Burchard, *Adv. Polym. Sci.* **48**, 1 (1988).
31. I. J. Good, *Proc. Cambridge Phil. Soc.* **45**, 360 (1948).
32. I. J. Good, *Proc. R. Soc. (London)* **A263**, 54 (1963).
33. D. A. Tomalia and J. M. J. Fréchet, *J. of Polym. Sci. Part A: Polym. Chem.* **40**, 2719–2728 (2002).
34. D. A. Tomalia, *Sci. Am.* **272**, 42–46 (1995).
35. D. A. Tomalia and D. R. Swanson, in *Dendrimers and Other Dendritic Polymers*, edited by J. M. J. Fréchet and D. A. Tomalia (Wiley, Chichester, 2001), pp. 617–629.
36. D. A. Tomalia, H. M. Brothers II, L. T. Pihler, H. D. Durst, and D. R. Swanson, *Proc. Natl Acad. Sci. USA* **99**(8), 5081–5087 (2002).
37. D. A. Tomalia, H. M. Brothers II, L. T. Pihler, and Y. Hsu, *Polym. Mater. Sci. Eng.* **73**, 75 (1995).
38. D. A. Tomalia, *Macromol. Symp.* **101**, 243–255 (1996).
39. A. K. Naj, in *The Wall Street Journal* (New York, 1996), p. B1.
40. D. A. Tomalia and R. Esfand, *Chem. Ind.* **11**, 416–420 (1997).
41. S. Hecht and J. M. J. Fréchet, *Angew. Chem. Int. Ed.* **40**(1), 74–91 (2001).
42. D. A. Tomalia, A. M. Naylor, and W. A. Goddard III, *Angew. Chem. Int. Ed. Engl.* **29**, 138–175 (1990).
43. J. M. J. Fréchet, C. J. Hawker, I. Gitsov, and J. W. Leon, *J.M.S.—Pure Appl. Chem.* **A33**, 1399 (1999).
44. F. Vögtle and M. Fischer, *Angew. Chem. Int. Ed.* **38**, 884–905 (1999).
45. B. I. Voit, *Acta Polym.* **46**, 87–99 (1995).
46. J. M. J. Fréchet and D. A. Tomalia, *Dendrimers and Other Dendritic Polymers* (Wiley, Chichester, 2001).
47. D. A. Tomalia, H. Baker, J. Dewald, M. Hall, G. Kallos, S. Martin, J. Roeck, J. Ryder, and P. Smith, *Polym. J. (Tokyo)* **17**, 117–132 (1985).
48. P. A. Gunatillake, G. Odian, and D. A. Tomalia, *Macromolecules* **21**, 1556–1562 (1988).
49. Y. H. Kim and O. W. Webster, *Polym. Prepr.* **29**, 310 (1988).
50. Y. H. Kim and O. W. Webster, *J. Am. Chem. Soc.* **112**, 4592 (1990).
51. T. Emrick, H. T. Chang, and J. M. J. Fréchet, *J. Polym. Sci. A* **38**, 4850 (2000).
52. T. Emrick and J. M. J. Fréchet, *Curr. Opin. Colloid Interf. Sci.* **4**, 15–23 (1999).
53. P. Bharati and J. S. Moore, *J. Am. Chem. Soc.* **119**, 3391 (1997).
54. A. M. Muzafarov, E. A. Rebrov, O. B. Gorbatshevich, M. Golly, H. Gankema, and M. Moller, *Macromol. Symp.* **102**, 35 (1996).
55. J. F. Miravet and J. M. J. Fréchet, *Macromolecules* **31**, 3461 (1998).
56. F. Chu and C. J. Hawker, *Polym. Bull.* **30**, 265 (1993).
57. C. J. Hawker, R. Lee, and J. M. J. Fréchet, *J. Am. Chem. Soc.* **113**, 4583 (1991).
58. K. E. Uhrich, C. J. Hawker, J. M. J. Fréchet, and S. R. Turner, *Macromolecules* **25**, 4583 (1992).
59. M. Liu, N. Vladimirov, and J. M. J. Fréchet, *Macromolecules* **32**, 6881–6884 (1999).
60. J. M. J. Fréchet, M. Henni, I. Gitsov, S. Aoshima, M. R. Leduc, and R. B. Grubbs, *Science* **269**, 1080 (1995).
61. C. J. Hawker, P. J. Farrington, M. E. Mackay, K. L. Wooley, and J. M. J. Fréchet, *J. Am. Chem. Soc.* **117**, 4409 (1995).
62. A. Sunder, J. Heinemann, and H. Frey, *Chem. Eur. J.* **6**, 2499 (2000).
63. C. Gong, J. Miravet, and J. M. J. Fréchet, *J. Polym. Sci. A* **37**, 3193 (1999).
64. D. A. Tomalia, D. M. Hedstrand, and M. S. Ferrito, *Macromolecules* **24**, 1435–1438 (1991).
65. M. Gauthier, J. Li, and J. Dockendorff, *Macromolecules* **36**, 2642–2648 (2003).
66. R. A. Kee, M. Gauthier, and D. A. Tomalia, in *Dendrimers and Other Dendritic Polymers*, edited by J. M. J. Fréchet and D. A. Tomalia (John Wiley & Sons, West Sussex, 2001), pp. 209–235.
67. J.-L. Six and Y. Gnanou, *Macromol. Symp.* **95**, 137 (1995).
68. D. Taton, E. Cloutet, and Y. Gnanou, *Macromol. Chem. Phys.* **199**, 2501 (1998).
69. M. Trollsas and J. L. Hedrick, *J. Am. Chem. Soc.* **120**, 4644–4651 (1998).
70. M. Trollsas and J. L. Hedrick, *Macromolecules* **31**, 4390–4395 (1998).

71. R. B. Grubbs, C. J. Hawker, J. Dao, and J. M. J. Fréchet, *Angew. Chem. Int. Ed. Engl.* **36**, 270 (1997).
72. D. A. Tomalia, J. R. Dewald, M. J. Hall, S. J. Martin, and P. B. Smith, First SPSJ International Polymer Conference, Kyoto, Japan, August 1984, p. 65.
73. A. W. Kleij, A. Ford, J. T. B. H. Jastrzebski, and G. Van Koten, in *Dendrimers and Other Dendritic Polymers*, edited by J. M. J. Fréchet and D. A. Tomalia (Wiley, Chichester, 2001), pp. 485–514.
74. J. M. J. Fréchet, H. Ihre, and M. Davey, in *Dendrimers and Other Dendritic Polymers*, edited by J. M. J. Fréchet and D. A. Tomalia (Wiley, Chichester, 2001), pp. 569–586.
75. M. H. P. Van Genderen, M. H. A. Mak, D. B.-V. D. Berg, and E. W. Meijer, in *Dendrimers and Other Dendritic Polymers*, edited by J. M. J. Fréchet and D. A. Tomalia (Wiley, Chichester, 2001), pp. 605–616.
76. A. M. Naylor, W. A. Goddard III, G. E. Keifer, and D. A. Tomalia, *J. Am. Chem. Soc.* **111**, 2339–2341 (1989).
77. G. R. Newkome, C. N. Moorfield, and F. Vögtle, *Dendritic Molecules* (VCH, Weinheim, 1996).
78. C. J. Hawker and J. M. J. Fréchet, *J. Am. Chem. Soc.* **112**, 7638–7647 (1990).
79. F. Zeng and S. C. Zimmerman, *Chem. Rev.* **97**, 1681–1712 (1997).
80. D. A. Tomalia, *Aldrichim. Acta* **26**(4), 91–101 (1993).
81. D. A. Tomalia, *Adv. Mater.* **6**, 529–539 (1994).
82. G. J. Kallos, D. A. Tomalia, D. M. Hedstrand, S. Lewis, and J. Zhou, *Rapid Commun. Mass Spectrom.* **5**, 383–386 (1991).
83. P. R. Dvornic and D. A. Tomalia, *Macromol. Symp.* **98**, 403–428 (1995).
84. J. C. Hummelen, J. L. J. van Dongen, and E. W. Meijer, *Chem. Eur. J.* **3**, 1489–1493 (1997).
85. J. Peterson, V. Allikmaa, J. Subbi, T. Pehk, and M. Lopp, *Eur. Polym. J.* **39**, 33–42 (2003).
86. H. M. Brothers II, L. T. Piehler, and D. A. Tomalia, *J. Chromatogr. A* **814**, 233–246 (1998).
87. C. Zhang and D. A. Tomalia, in *Dendrimers and Other Dendritic Polymers*, edited by J. M. J. Fréchet and D. A. Tomalia (Wiley, Chichester, 2001), pp. 239–252.
88. D. A. Tomalia and J. M. J. Fréchet, in *Dendrimers and Other Dendritic Polymers*, edited by J. M. J. Fréchet and D. A. Tomalia (Wiley, Chichester, 2001), pp. 3–44.
89. D. A. Tomalia, *Prog. Polym. Sci.* **30**, 294–324 (2005).
90. N. J. Turro, J. K. Barton, and D. A. Tomalia, *Acc. Chem. Res.* **24**(11), 332–340 (1991).
91. K. R. Gopidas, A. R. Leheny, G. Caminati, N. J. Turro, and D. A. Tomalia, *J. Am. Chem. Soc.* **113**, 7335–7342 (1991).
92. M. F. Ottaviani, N. J. Turro, S. Jockusch, and D. A. Tomalia, *J. Phys. Chem.* **100**, 13675–13686 (1996).
93. J. Jockusch, J. Ramirez, K. Sanghvi, R. Nociti, N. J. Turro, and D. A. Tomalia, *Macromolecules* **32**, 4419–4423 (1999).
94. C. J. Hawker, K. L. Wooley, and J. M. J. Fréchet, *J. Am. Chem. Soc.* **115**, 4375 (1993).
95. P. G. de Gennes and H. J. Hervet, *J. Physique-Lett. (Paris)* **44**, 351–360 (1983).
96. D. A. Tomalia, R. Esfand, L. T. Piehler, D. R. Swanson, and S. Uppuluri, *High Perform. Polym.* **13**, S1–S10 (2001).
97. T. H. Mourey, S. R. Turner, M. Rubinstein, J. M. J. Fréchet, C. J. Hawker, and K. L. Wooley, *Macromolecules* **25**, 2401–2406 (1992).
98. J. Berzelius, *J. Fortsch. Phys. Wissensch.* **11**, 44 (1832).
99. K. L. Wooley, J. M. J. Fréchet, and C. J. Hawker, *Polymer* **35**, 4489 (1994).
100. P. R. Dvornic and D. A. Tomalia, *Sci. Spectra* **5**, 36–41 (1996).
101. D. A. Tomalia, P. R. Dvornic, S. Uppuluri, D. R. Swanson, and L. Balogh, *Polym. Mater. Sci. Eng.* **77**, 95–96 (1997).
102. C. J. Hawker, E. E. Malmstrom, C. W. Frank, and J. P. J. Kampf, *J. Am. Chem. Soc.* **119**, 9903–9904 (1997).
103. E. M. M. de Brabander-van den Berg and E. W. Meijer, *Angew. Chem. Int. Ed. Engl.* **32**, 1308–1311 (1993).
104. P. J. Farrington, C. J. Hawker, J. M. J. Fréchet, and M. E. Mackay, *Macromolecules* **31**, 5043 (1998).
105. D. Qin, R. Yin, J. Li, L. Piehler, D. A. Tomalia, H. D. Durst, and G. Hagnauer, *Polym. Prepr. (ACS Div. Polym. Chem.)* **40**, 171–172 (1999).
106. J. M. J. Fréchet, *Science* **263**, 1710–1715 (1994).
107. G. J. de A.A. Soler-Illia, L. Rozes, M. K. Boggiano, C. Sanchez, C. O. Turrin, A.-M. Caminade, and J.-P. Majoral, *Angew. Chem. Int. Ed.* **39**, 4250 (2000).
108. D. A. Tomalia and H. D. Durst, in *Supramolecular Chemistry I—Directed Synthesis and Molecular Recognition*, edited by E. W. Weber (Springer-Verlag, Berlin Heidelberg, 1993), pp. 193–313.
109. D. A. Tomalia and I. Majoros, in *Supramolecular Polymers, Chapter 9*, edited by A. Ciferri (Marcel Dekker, New York, 2000), pp. 359–434.
110. D. A. Tomalia and I. Majoros, *J. Macromol. Sci. C* **43**, 411–477 (2003).
111. L. Balogh, D. A. Tomalia, and G. L. Hagnauer, *Chem. Innov.* **30**, 19–26 (2000).
112. R. M. Crooks, B. Lemon III, L. Sun, L. K. Yeung, and M. Zhao, in *Topics in Current Chemistry, Vol. 212* (Springer-Verlag, Berlin Heidelberg, 2001).
113. A. W. Freeman, S. C. Koene, P. R. L. Malenfant, M. E. Thompson, and J. M. J. Fréchet, *J. Am. Chem. Soc.* **122**, 12385–12386 (2000).
114. J. F. Kukowska-Latallo, A. U. Bielinska, J. Johnson, R. Spindler, D. A. Tomalia, and J. R. Baker Jr., *Proc. Natl. Acad. Sci. USA* **93**, 4897–4902 (1996).
115. P. Singh, *Bioconjugate Chem.* **9**, 54–63 (1998).
116. P. Singh, in *Dendrimers and Dendritic Polymers*, edited by J. M. J. Fréchet and D. A. Tomalia (Wiley, Chichester, 2001), pp. 463–484.
117. P. Singh, F. Moll III, S. H. Lin, and C. Ferzli, *Clin. Chem.* **42**(9), 1567–1569 (1996).
118. P. Singh, F. Moll III, S. H. Lin, C. Ferzli, K. S. Yu, K. Koski, and R. G. Saul, *Clin. Chem.* **40**(9), 1845–1849 (1994).
119. M. E. Piotti, F. Rivera, R. Bond, C. J. Hawker, and J. M. J. Fréchet, *J. Am. Chem. Soc.* **121**, 9471 (1999).
120. C. Bieniarz, in *Encyclopedia of Pharmaceutical Technology, Vol. 18* (Marcel Dekker, New York, 1998), pp. 55–89.
121. K. Dusek, *TRIP* **5**(8), 268–274 (1997).
122. K. Dusek and M. Duskova-Smrckova, in *Dendrimers and Dendritic Polymers* (J. Wiley & Sons, Ltd., West Sussex, 2001), pp. 111–145.
123. D. A. Tomalia, D. M. Hedstrand, and L. R. Wilson, in *Encyclopedia of Polymer Science and Engineering, Index Volume, Second Edition* (John Wiley & Sons, New York, 1990), pp. 46–92.
124. D. A. Tomalia, S. Uppuluri, D. R. Swanson, and J. Li, *Pure Appl. Chem.* **72**, 2343–2358 (2000).
125. J. Li, D. R. Swanson, D. Qin, H. M. Brothers II, L. T. Piehler, D. A. Tomalia, and D. J. Meier, *Langmuir* **15**, 7347–7350 (1999).
126. S. Uppuluri, L. T. Piehler, J. Li, D. R. Swanson, G. L. Hagnauer, and D. A. Tomalia, *Adv. Mater.* **12**(11), 796–800 (2000).
127. M. Freemantle, *Chem. Eng. News* **77**(44), 27–35 (1999).
128. M. L. Mansfield, L. Rakesh, and D. A. Tomalia, *J. Chem. Phys.* **105**, 3245–3249 (1996).
129. D. A. Tomalia, *Aldrichimica Acta*, **37**(2), 39–57 (2004).
130. S. Svenson and D. A. Tomalia, *Advanced Drug Delivery Reviews*, **57**, 2106–2129 (2005).

CHAPTER 43

Polyrotaxanes

Feihe Huang, Adam M.-P. Pederson, and Harry W. Gibson

Department of Chemistry, Virginia Polytechnic & State University, Blacksburg, VA 24061, fhuang@chem.utah.edu

Department of Chemistry, Virginia Polytechnic & State University, Blacksburg, VA 24061, adamp@vt.edu

Department of Chemistry, Virginia Polytechnic & State University, Blacksburg, VA 24061, hwgibson@vt.edu

References 698

ACRONYM, ALTERNATIVE NAME: Inclusion complex, molecular necklace (MN), string of pearls, rotaxane-type polymer, polymeric rotaxane.

CLASS: Mechanically-linked, threaded polymers.

STRUCTURES: Varied, see specific examples below.

MAJOR APPLICATIONS: Curing of polymers, viscosity control, increase of crosslinking density, drug delivery, metal complexation, biodegradable materials, nanoelectronic devices.

PROPERTIES OF SPECIAL INTEREST: Stable under ambient conditions; controlled variation of physical properties compared with the reference polymer.

A variety of polyrotaxane structures can be envisioned, as shown in Scheme 1 [1–3]. True rotaxanes polymers possess bulky groups at the ends of the linear species or along the backbone to prevent diffusive loss of the ring component. However, it has been shown that main chain polypseudorotaxanes dethread extremely slowly due to random coiling of the backbones [4,5], so that the distinction between pseudorotaxane and rotaxane polymers of the main chain type is somewhat blurred for these systems. Main chain polyrotaxanes are the most common type, although all of the other types shown in Fig. 43.1 have been synthesized.

A main chain polyrotaxane, a mechanically interlocked structure that can be considered as a string of pearls, in which the strand is the polymer backbone and the pearls are the cyclic species threaded onto the strand. The backbone polymer can be a polyester, polyamide, poly(ethylene oxide), or virtually any linear polymer. The cyclic species are typically crown ethers, cyclodextrins (CDs), cucurbiturils, and calixarenes. Polyrotaxanes can be made by two different methods: statistical threading or via the template approach (enthalpically driven). The statistical approach utilizes le Chatelier's principle with an excess macrocycle during the polymerization. The template approach is driven by attractive interactions of the macrocyclic species with either the monomer

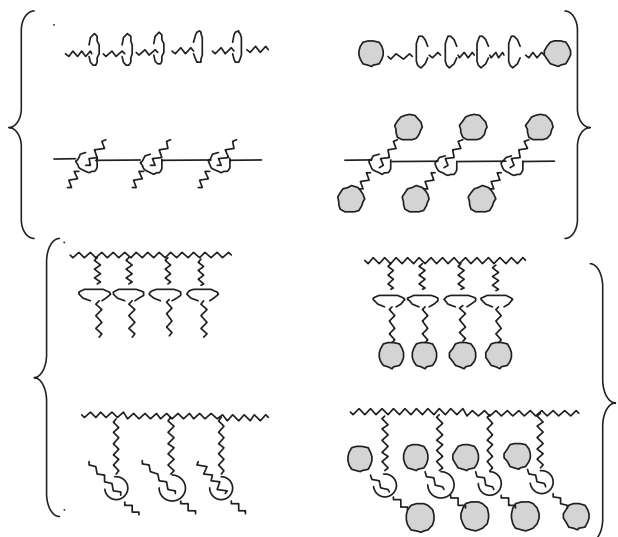
or the polymer, depending on whether threading takes place during polymerization or starting with a preformed polymer; both approaches have been successfully applied.

Because of the formation of the mechanically interlocked structure, polyrotaxanes have different physical properties, such as solubility, thermostability, photoelectronic properties, viscosity, and phase behavior, compared with simple reference (nonpolyrotaxanated) polymers.

Usually the solubilities of polyrotaxanes are very different from their components. Because of the hydrophilic, high polarity nature of the exterior of the CDs, many CD-based polypseudorotaxanes and polyrotaxanes are soluble in water and some polar solvents though their parent polymers are hydrophobic or nonpolar [6–9]. The solubility of crown ether-based polyrotaxanes in methanol and/or water was improved because of the hydrogen bonding between the crown ethers and solvents [5,10,11] or the hydrogen bonding between the crown ethers and the polymer backbone [4]. Even if there are strong attractive forces between their components, dethreading still can happen in some polypseudorotaxanes when a salt or competitive solvent is added or the temperature increases [1–3].

Yui's group found the thermal stability of their biodegradable polyrotaxane was better than that of the separate components, poly(ϵ -lysine) and α -cyclodextrin [12,13]. In some crown ether based systems, as shown below, thermal stability decreases because of the lability of the cyclic components.

A series of polyrotaxanes as light-harvesting antennae models was constructed by Ueno and coworkers [14]. These polyrotaxanes consist of various ratios of α -CD and naphthalene-appended α -CD threaded by a PEG chain bearing anthracene moieties at each end. Here naphthalene and anthracene moieties act as energy donor and energy acceptor, respectively. It was found that the antenna effect becomes more marked with increasing number of naphtha-



SCHEME 43.1. Cartoon representations of main chain (top) and side chain (bottom) polypseudorotaxanes (left) and polyrotaxanes (right).

lene-appended α -CD units in the polyrotaxanes, but energy transfer efficiency decreased.

The threading of cyclic components onto the polymer backbone has an important influence on the solution viscosity and melt viscosity. Up to now it has been found that this influence depends on the nature of the cyclic components and the polymer backbone, the value of mole ratio of cyclic species per repeat unit (m/n), and the types of solvents [5,15–19].

A glass transition temperature (T_g) is the temperature at which a polymer undergoes a conversion from a glassy amorphous state to a rubbery state. A melting point (T_m) is the temperature at which the physical state of a crystalline solid changes to the liquid state. Both T_g and T_m changes result from the threading of cyclic species onto the polymer backbone; the extent and direction of change depends on the properties of the cyclic species and the polymer backbone and their miscibility [1–3,5,11,16,19,21–29]. For example, Yamamoto's group found that polyurea-based polyrotaxanes have higher T_g than the corresponding CD-free polymers [20]. This increase is a result of the decrease of flexibility of the polymer chain because of the inclusion of rigid α -CDs onto the polyalkylene part of the backbone. In contrast, Shen *et al.* reported decreases in T_g of polyurethane rotaxanes with increased crown ether content due to the flexible nature of the cyclic components (see Table 43.1) [4]; moreover, the Fox equation was obeyed [30] (see below) because of the miscibility of the components through hydrogen bonding [31].

Presently, there are over 500 literature citations on polyrotaxanes, each with its own polymer and cyclic species. It is impossible to summarize the whole field here due to space limitations; therefore, as examples of the types of property changes that can be brought about and controlled by rotaxane formation, two polyrotaxane systems from our labs are presented here: polyurethane-based polyrotaxanes [4,30–33] (1) (Table 43.1) and polyester-based polyrotaxanes [5,34,35] (2) (Table 43.2). Polyurethane-based polyrotaxanes were investigated because polyurethanes are

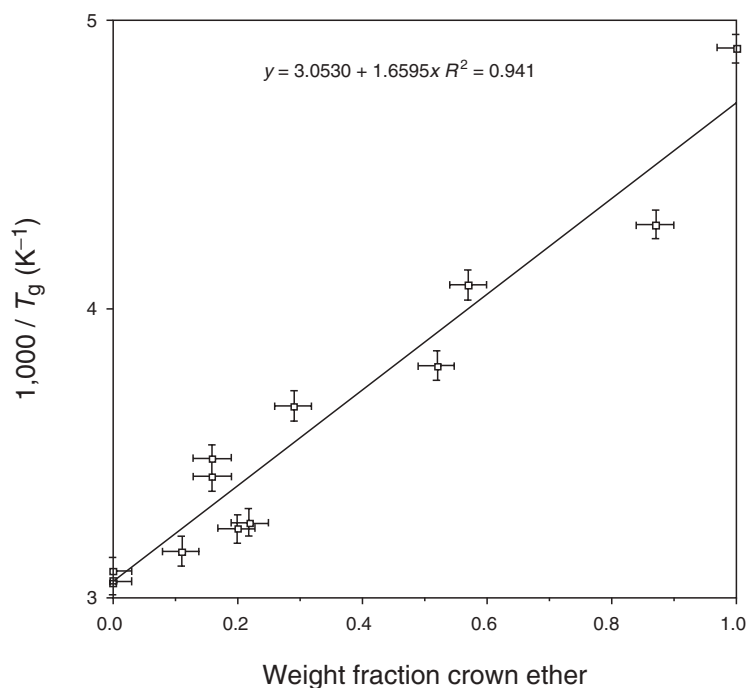


FIGURE 43.1. Fox plot: inverse glass transition temperature vs. weight fraction crown ether in polyurethane rotaxanes (data from Table 43.1) [32,33].

TABLE 43.1. Polyurethane-based rotaxanes.

Polymer	Cyclic species ^a	M_n (kg/mol)	M_w (kg/mol)	m/r ^b	Weight fraction crown ether	$[\eta]$ (dL/g) in NMP ^c	$[\eta]$ (dL/g) in THF ^d	T_g (K) ^e	Decomp. T (K) ^f	T_m (K) ^g	Ref.
1	None	12.1 ^h /14.8 ⁱ	27.0 ^h /32.4 ⁱ	0	0	—	—	324	543	—	[4,32]
1a	"36C12"	7.24 ^h /11.3 ⁱ	10.8 ^h /16.6 ⁱ	0.16	0.16	—	—	292	448	—	[4,32]
None	"60C20"	—	—	—	1	—	—	205	—	331.5	[32]
1	None	5.58 ^h	11.1 ^h	0	0	0.26	—	324	—	—	[4]
1	None	8.65 ^h	26.9 ^h	0	0	0.30	—	—	—	—	[4]
1	None	12.1 ^h	27.0 ^h	0	0	0.40	—	—	—	—	[4]
1a	"36C12"	7.24 ^h	10.8 ^h	0.16	0.16	0.24	—	287	—	—	[4]
1b	"42C14"	19.3 ^h /29.6 ⁱ	37.5 ^h /59.7 ⁱ	0.29	0.29	0.45	—	273	—	—	[4]
1c	"48C16"	7.01 ^h /13.9 ⁱ	10.6 ^h /19.5 ⁱ	0.52	0.45	0.24	—	263	—	—	[4]
1d	"60C20"	8.03 ^h /16.5 ⁱ	13.3 ^h /21.3 ⁱ	0.87	0.63	0.27	—	233	—	320	[4]
1	None	16.6 ⁱ	58.7 ⁱ	0	0	—	0.299	327	—	—	[33]
1b	"42C14"	—	—	0.092	0.113	—	0.351	316	—	—	[33]
1b	"42C14"	—	—	0.178	0.198	—	0.361	309	—	—	[33]
1b	"42C14"	—	—	0.201	0.218	—	0.369	307	—	—	[33]

^aThese cyclic species were all mixtures of aliphatic crown ethers; the average ring sizes were larger than these target values.

^b m/r : mole ratio of cyclic species per repeat unit determined by ¹H NMR analyses.

^cMeasured in a Cannon-Ubbelohde semimicro dilute solution viscometer at 298.8 K.

^dMeasured in Cannon L12 50 viscometers at 298 K.

^eTaken as the midpoint of the change in heat capacity by DSC at 10 °C/min. The crown ethers all have $T_g = 205$ K.

^fTaken as the temperature of 5% weight loss by TGA at 10 °C/min.

^gTaken as the maximum in the endotherm by DSC at 10 °C/min.

^hFrom GPC analysis with polystyrene standards in THF.

ⁱFrom GPC analysis with universal calibration using a viscosity detector in 6 mM LiBr/NMP.

TABLE 43.2. Polyester-based rotaxanes.

Polymer	Cyclic species ^a	M_n (kg/mol)	M_w (kg/mol)	m/r^b	Wt Fr Crown ether	$[\eta]^c$ (dL/g) in THF/THF:MeOH (10:1)	η^* (Pa s) ^d 90 °C/150 °C	T_g^e (K)	T_m^f (K)	Ref.
2	None	5.2 ^g /5.0 ^h	7.1 ^g /7.3 ^h	0	0	0.141/0.147	—	—	—	[5]
2	None	8.9 ^g	15.2 ^g	0	0	—/0.160	—	—	—	[5]
2	None	17.1 ^h	32.8 ^h	0	0	0.543/0.549	—	—	350	[5]
2	None	4.3 ^h	7.0 ^h	0	0	—	3/0.9	—	—	[5]
2a	30C10	32.8 ⁱ	58.9 ⁱ	0.012	0.015	—	—	—	353	[5]
2b	"36C12"	14.3 ^j	22.5 ^j	0.22	0.25	—	—	219	315, 342, 344	[5]
2c	"42C14"	8.3 ^j	14.0 ^j	0.29	0.34	0.331/0.248	—	217	315, 343, 347	[5]
2c	"42C14"	10.4 ^h	17.1 ^h	0.13	0.19	—	3/0.8	—	—	[5]
2d	"48C16"	11.4 ^j	19.1 ^h	0.34	0.41	—	—	215	316, 344, 348	[5]
2e	"60C20"	10.7 ^j	20.7 ^j	0.36	0.48	—	—	215	317, 336, 343	[5]

^aThe cyclic species specified by quotation marks ("") were mixtures of aliphatic crown ethers; the average ring sizes were larger than these target values. 30-Crown-10 was a pure compound.

^b m/r : mole ratio of cyclic species per repeat unit determined by ¹H NMR analyses.

^cMeasured in a Cannon-Fenske type viscometer at 298 K.

^dMelt rheology was examined in a Rheometrics dynamic analyzer with a 25 mm parallel plate attachment in an oscillatory mode at 1 Hz from 90–150 °C.

^eTaken as the midpoint of the change in heat capacity by DSC at 10 °C/min.

^fTaken as the maximum in the endotherm by DSC at 10 °C/min. The endotherms at 336–353 K are for the polyester. Those at 315–317 K are for the crown ether crystalline phases.

^gFrom GPC analysis with polystyrene standards in chloroform.

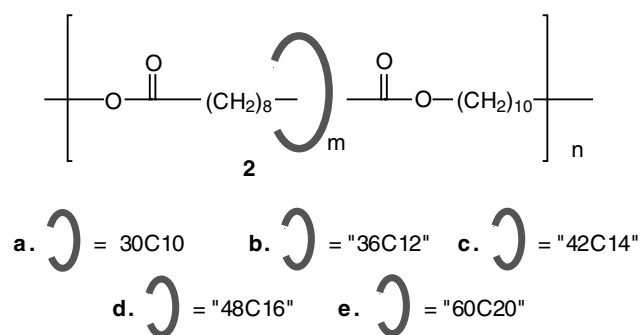
^hFrom GPC analysis with universal calibration using a viscosity detector in chloroform.

ⁱFrom GPC analysis with polystyrene standards in THF.

^jFrom GPC analysis with polystyrene standards in toluene.

glassy polymers and incorporation of crystalline crown ethers allows for crystalline domains to form from the crown ethers upon annealing [32], similar to the block copolymers derived from glassy and crystalline components. Polyesters are highly crystalline and typically do

not exhibit glass transitions; however, polyester-based polyrotaxanes show T_g 's, dual melting transitions due to two crystalline phases, the polyester and the crown ether, and reduced melt viscosities when compared to control polyesters of similar molecular weights [5,34,35].



A noteworthy feature of the polyurethanes of Table 43.1 is that the model polymer, the first entry, is insoluble in water, dichloromethane and acetone, whereas both the polyrotaxanes derived from “36-crown-12” and “60-crown-20”, **1a** and **1d**, respectively, are soluble in these three solvents [32]. The glass transition temperatures of the polyurethane rotaxanes of Table 43.1 obey the Fox equation (see Fig. 43.1); this is due to

the miscibility of the components through hydrogen bonding [31].

The last four entries of Table 43.1 represent a preformed polyurethane and polyrotaxanes derived by threading crown ethers onto it in the melt. Since the backbone molecular weight is constant, this series allows us to discern the effect of “rotaxanation” on the intrinsic viscosity. As can be seen in Fig. 43.2, in fact, the intrinsic viscosity increases linearly

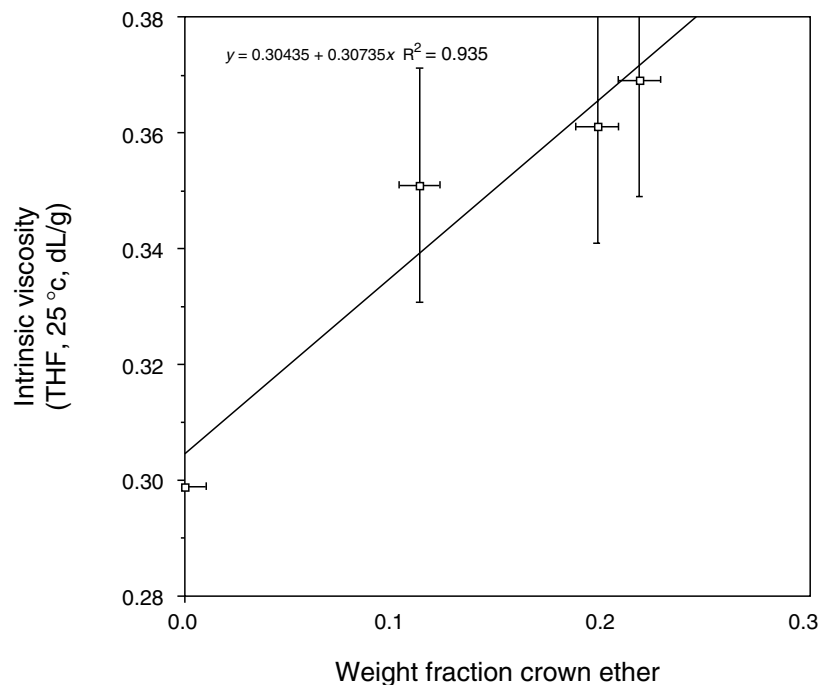


FIGURE 43.2. Plot of intrinsic viscosity vs. weight fraction of crown ether for polyurethane rotaxanes made by threading of a polymer (M_n 16.6 kDa and M_w 58.7 kDa by universal calibration and viscosity detector in NMP at 60 °C) with “42-crown-14” in the melt at 80 °C (last four entries of Table 43.1) [33].

with the crown ether content. This is expected, since the incorporation of the cyclic species increases the hydrodynamic volume of the resultant polyrotaxane relative to the parent polymer.

REFERENCES

1. *Molecular Catenanes, Rotaxanes and Knots*, edited by J. -P. Sauvage and C. O. Dietrich-Buchecker. Wiley-VCH, Weinheim, 1999; Raymo, F. M., and J. F. Stoddart. *Chem. Rev.* 99 (1999): 1, 643.
2. Mahan, E., and H. W. Gibson. In *Cyclic Polymers*, 2d ed., edited by J. A. Semlyen. Kluwer Publishers, Dordrecht, 2000, p. 415, and the references therein; Huang, F., and H. W. Gibson. *Progr. Polym. Sci.* 30 (2005): 982.
3. Panova, I. G., and I. N. Topchieva. *Russ. Chem. Rev.* 70 (2001): 23.
4. Shen, Y. X., D. Xie, and H. W. Gibson. *J. Am. Chem. Soc.* 116 (1994): 537.
5. Gibson, H. W., S. Liu, C. Gong, Q. Ji, and E. Joseph. *Macromolecules* 30 (1997): 3711.
6. Yui, N., T. Ooya, and T. Kumano. *Bioconj. Chem.* 9 (1998): 118.
7. Ooya, T., and N. Yui. *Macromol. Chem. Phys.* 199 (1998): 2311.
8. Watanabe, J., T. Ooya, and N. Yui. *J. Biomater. Sci. Polym. Ed.* 10 (1999): 1275.
9. Watanabe, J., T. Ooya, and N. Yui. *Chem. Lett.* (1998): 1031.
10. Gibson, H. W., and P. T. Engen. *New J. Chem.* 17 (1993): 723.
11. Gibson, H. W., and S. Liu. *Macromol. Symp.* 102 (1996): 55.
12. Huh, K. M., T. Ooya, S. Sasaki, and N. Yui. *Macromolecules* 34 (2001): 2402.
13. Choi, H. S., K. M. Huh, T. Ooya, and N. Yui. *J. Am. Chem. Soc.* 125 (2003): 6, 50.
14. Tamura, M., D. Gao, and A. Ueno. *Chemistry* 7 (2001): 1390.
15. Wenz, G., and B. Keller. *Angew. Chem. Int. Ed. Engl.* 31 (1992): 197.
16. Gong, C., P. B. Balanda, and H. W. Gibson. *Macromolecules* 31 (1998): 5278.
17. Born, M., and H. Ritter. *Makromol. Chem. Rapid Commun.* 12 (1991): 471.
18. Gibson, H. W., C. Gong, S. Liu, and D. S. Nagvekar. *Macromol. Symp.* 128 (1998): 89.
19. Shen, Y. X., C. Lim, and H. W. Gibson. *Polym. Prepr. (Am. Chem. Soc. Div. Polym. Chem.)* 32(1) (1991): 166.
20. Yamaguchi, I., K. Miya, K. Osakada, and T. Yamamoto. *Polym. Bull.* 44 (2000): 247.
21. Gong, C., T. E. Glass, and H. W. Gibson. *Macromolecules* 31 (1998): 308.
22. Gibson, H. W., P. T. Engen, and S.-H. Lee. *Polymer* 40 (1999): 1823.
23. Gong, C., and H. W. Gibson. *J. Am. Chem. Soc.* 119 (1997): 5862.
24. Gong, C., and H. W. Gibson. *J. Am. Chem. Soc.* 119 (1997): 8585.
25. Nagapudi, K., J. Hunt, C. Shepherd, J. Baker, and H. W. Beckham. *Macromol. Chem. Phys.* 200 (1999): 2541.
26. Noll, O., and H. Ritter. *Macromol. Chem. Phys.* 199 (1998): 791.
27. Born, M., T. Koch, and H. Ritter. *Acta Polym.* 45 (1994): 68.
28. Born, M., T. Koch, and H. Ritter. *Macromol. Chem. Phys.* 196 (1995): 1761.
29. Born, M., and H. Ritter. *Angew. Chem. Int. Ed. Engl.* 34 (1995): 309.
30. Gibson, H. W., C. Wu, Y. X. Shen, M. Bheda, A. Prasad, H. Marand, E. Marand, and D. Keith. *Polym. Prepr. (Am. Chem. Soc. Div. Polym. Chem.)* 33(1) (1992): 235.
31. Marand, E., Q. Hu, H. W. Gibson, and B. Veytsman. *Macromolecules* 29 (1996): 2555. Gong, C., and H. W. Gibson. *Angew. Chem. Int. Ed. Engl.* 36 (1997): 2331.
32. Shen, Y. X., and H. W. Gibson. *Macromolecules* 25 (1992): 2058.
33. Gong, C., Q. Ji, C. Subramaniam, and H. W. Gibson. *Macromolecules* 31 (1998): 1814.
34. Gibson, H. W., S. Liu, P. Lecavalier, C. Wu, and Y. X. Shen. *J. Am. Chem. Soc.* 117 (1995): 852.
35. Marand, H., A. Prasad, C. Wu, M. Bheda, and H. W. Gibson. *Polym. Prepr. (Am. Chem. Soc. Div. Polym. Chem.)* 32(3) (1991): 639.

CHAPTER 44

Foldamers: Nanoscale Shape Control at the Interface Between Small Molecules and High Polymers

Morris M. Slutsky, Richard A. Blatchly, and Gregory N. Tew

Contributions from the Chemistry Department at Keene State College and the Polymer Science and Engineering Department at the University of Massachusetts-Amherst

44.1	Overview	699
44.2	Design.....	701
44.3	Synthesis	709
44.4	Measurement of Folding.....	710
44.5	Future	712
	References	712

44.1 OVERVIEW

Taking inspiration from biopolymers such as proteins and RNA, foldamer chemists craft such pale imitations as they can, yet these are very complex molecules by our current laboratory standards. What inspires us to imitate certain aspects of biopolymers is that they have behaviors derived from a simple set of organizing principles: sequence derived properties, folding that depends on specific interactions with solvent, the cooperativity in folding that comes from long-chain molecules and the ability to make large structures from intermediate domains that are often of one structural type. To this end, recent attention has focused on creating new molecular backbones, called foldamers, that also fold into well-defined structures like helices and sheets [1–13]. The ability to mimic those aspects of natural systems while using a fundamentally different backbone continues to provide a wonderful challenge.

It is well known that nature folds macromolecules like proteins, RNA, and DNA into defined structures with specific shape and that these shapes are intimately related to their function [14–18]. Tremendous research effort has provided some understanding of how this folding occurs in proteins. In fact, it is now possible to design, from scratch, with great success an unnatural protein sequence which will fold into the predicted secondary structure [19]. However, many of the fundamental questions of biopolymer folding are not yet solved. Careful study of foldamers, which can be

designed with more variation than natural biopolymers, can provide an important perspective on this vital problem.

The more complicated design of tertiary and quaternary structure in proteins has been attained in some cases. However, the ability to form hierarchically ordered structures, or self-assemble folded structural units into well-defined higher order assemblies, from any non-natural backbone remains an important unsolved problem. A few preliminary reports, including work on β -peptides and peptoids, with structure beyond the helix were reported recently [20–22]. These two backbones represent the more well studied sequences of foldamers and so initial reports toward structures beyond secondary elements can be expected. However, given more than a decade of foldamer research, little work toward these higher order structures has been reported.

One of the long-standing goals of foldamer research has been to mimic the function of biopolymers. While the focus has been on establishing the principles of folding, there have been some successes in designing shape-dependent function. For example, it was recently shown that β -peptides, peptoids, and simple polymers could capture the antimicrobial activity and selectivity of the natural host defense peptides [23–27]. As foldamer researchers develop more sophisticated structures, we expect many more examples.

Much of the foundation for foldamer research has been generated by the physical organic community and has focused on discrete oligomers. However, progress in fields like protein structure, enzymology, organic chemistry,

biophysics, and polymer science all requires a common knowledge of the structure and function of complex macromolecules. As a result, there is much synergy to be gained through interactions with these various disciplines in which traditional analytical tools from different fields are applied to nontraditional problems. In fact, the application of “foldamer principles” to synthetic high polymers is beginning to occur as discussed in the section below entitled “From Oligomers to High Polymers”. Therefore, one of the goals of this chapter is to introduce foldamers to a wider audience. In addition, an attempt will be made to illustrate the current state of the art with specific focus on the chemical backbone, the use of high polymers, and the dynamics encountered in the folding process.

Since a comprehensive review [28] was completed in 2001, every effort will be made not to duplicate this tome. Additionally, β -peptides have been the subject of several reviews and will be mentioned more briefly than they warrant. Other recent reviews have covered oligoarylamides [29], a brief review of foldamers in general [30], and an article [31] focusing on the secondary structure aspect of foldamers. We will not include polymers like polyphenyl acetylene derivatives, polyisocyanides, and poly(trityl methacrylates) in which the conformations are dominated by nearest neighbor steric interactions, although these macromolecules represent very interesting systems that seem to adopt a limited number of the available conformations in solution [32–35].

44.1.1 Definition

In principle, a foldamer can be any oligomer or polymer which can reproducibly adopt a specific conformation in solution, leading to a single overall 3D shape. Currently there are certain restrictions that have been applied to the concept so that the synthesis and analysis of foldamers is tractable. Effectively, this means that foldamers are monodisperse oligomers of modest length (4–24 monomer units, more or less), with a single backbone chemistry and limited sequence variation making them quite distinct from polymers [36]. Foldamers are also traditionally designed to have some form of secondary structure such as a helix or extended, strand-like conformation.

To describe larger molecules in which a collection of secondary structural units pack into a larger definite structure, Moore suggested that the term “tyligomer” be used in place of foldamer. By analogy to protein structure, a tyligomer would contain tertiary (or possibly quaternary) conformations, while the word foldamer would be used for secondary structure components. According to this definition, tyligomers could describe either the assembly of secondary units within a single, larger MW molecule or the assembly of multiple chains into nonbonded complexes, giving rise to quaternary structure. This leads to a point of potential confusion. When used to describe proteins, the term tertiary refers to the association of secondary structural

elements within the same molecular backbone while quaternary is used to describe the association of more than one molecular backbone. Most proteins are large molecular weight species and typically fold with both secondary and tertiary structure. In fact, it is rare to find natural proteins with only secondary elements that assemble into quaternary structure (although myosin is one example). In contrast, many foldamers and even de novo peptide designs are created from relatively small molecular weight molecules which only contain secondary structure and, as a result, the issue of how to describe accurately their self-assembly into higher order structures, for example helical bundles, should be addressed. It appears that this has been described as tertiary structure in the literature [22]. Although this intuitively makes sense because it is the next level of order, that is to say that secondary structural elements like helices have associated to make helical bundles, this will be confusing to other researchers coming from the traditional study of biomacromolecular structure.

For the current chapter, we will attempt to avoid the use of these terms but it would be worthwhile for the field as a whole to adopt a consistent nomenclature since the pursuit of higher ordered assemblies is a major on-going effort. One possibility is to use the term tertiary-like structure when describing the associate of secondary elements. Alternatively, if tyligomer is confined to the collection of folded elements within a single larger MW molecule then it could be a very useful term for this next level of order. Then two or more tyligomers could assemble into nonbonded complexes, resulting in what is traditionally quaternary structure.

44.1.2 Goals of Foldamer Research

The table below illustrates a small sample of the potential outcomes from the study of foldamers. This list is meant only to be representative and not inclusive or limiting. Specifically, the table attempts to integrate two classical areas, which are medicinal and materials chemistry. At the same time, much of the study is motivated by fundamental interest in learning how molecules fold and the discovery of geometrically defined shapes.

Foldamer Characteristic	Medicine	Materials	Molecular folding Properties
Sequence-dependent properties	Antibiotics	Information storage	Insight into the nature of protein folding
Designed 3D shape	Gene therapy	Molecular recognition	New elements of secondary structure
Abiotic linker chemistry	Protease resistance	Catalysis	Alternative conformational profiles

44.1.3 Classification

Several helpful attempts to classify this diverse collection of molecules have been made. Moore [28] divides foldamers into classes based primarily on whether they are single stranded or multistranded. These categories were further divided into biotic (or closely related) and abiotic. Such classifications land β -peptides and oligoureas in single-stranded peptidomimetics, while aromatic amides and phenylene ethynylenes are classified as single stranded and abiotic. Nowick's β -strands, Gong's hydrogen bond donor-acceptors, and oligopyridine-metal ion complexes are all multistranded. The β -strands are an excellent example of the difficulty of classification since they are partly biotic and partly abiotic. Both the review of β -peptides by Cheng, Gellman, and DeGrado [13] and the review of foldamers by Cubberley and Iverson [5] categorized the β -peptides according to secondary structure formed. This is helpful if the secondary structure is known rigorously, but not applicable to foldamers in the process of design. In a review of oligoaramides [29], the categories focused more on backbone design than on classification. Although we do not wish to create yet another classification of foldamers due to the likelihood for confusion, we do think it is valuable to consider them from another perspective.

We suggest that a fundamental division be made based on the degree of backbone flexibility. By assigning a degree of freedom score and a linkage type to the foldamer repeat unit, we can focus the primary distinctions on "backbone space" as mentioned by Cheng, Gellman, and DeGrado [13]. We have arbitrarily divided foldamers into "semi-flexible" foldamers, which includes those that contain two or fewer degrees of conformational freedom per monomer unit and "flexible" foldamers with more than two degrees of conformational freedom. Within the torsional freedom assignment, the types of interactions which are primarily responsible for maintaining the folded state were considered. This type of organization is important if true molecular understanding involved in folding is going to emerge.

When determining the degree of freedom score some assumptions, or guidelines, were followed. The ring pucker in oligopyrrolinone backbone units, due to limited flexibility, was not considered here to be a degree of freedom. Although α -aminoxy acids and azatides apparently possess more than two degrees of freedom, they are considered to only have two degrees of freedom per monomer unit due to rotational barriers around the N-O and N-N bonds. The other foldamers in Table 44.1 were relatively straightforward to assign. Although the usual categorizations of foldamers [5, 13, 28, 29] rarely place them together, this type of assignment places α -peptides and aromatic oligopyridines and phenylene ethynylenes (PEs) into the same category.

β -peptides were placed into Table 44.2, although the flexibility of these monomers is often reduced by steric effects associated with the side chain groups and may in practice not always be much more flexible than α -peptides.

Due to alkylation of the peptoid amide nitrogen, *cis* conformations are accessible and add a degree of freedom to these monomers. Through this type of classification Table 44.2 finds β -peptides, peptoids, PNAs, and aedamers together. As a whole, it is interesting to note the mixture of biomimetic and nonbiomimetic foldamers found in each category.

44.2 DESIGN

44.2.1 General Issues

Linker Chemistry

Productive foldamer research requires foldamers with certain backbone characteristics. The backbone must be stable, easily synthesized and have some degree of flexibility. It is also helpful to have a well-characterized conformational profile, known intermolecular interactions (such as H-bonding), and good handling characteristics, such as solubility. As shown in Tables 44.1 and 44.2, a wide variety of bond forming reactions have been used to build foldamers. The most popular, by far, is the amide bond; however, other chemistry highlights include ureas, phosphate esters, ethers, aryl ethynylenes, biphenyls, and pyridines.

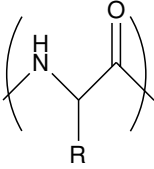
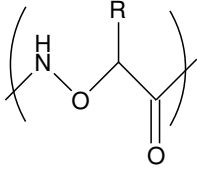
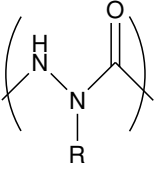
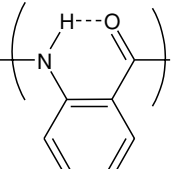
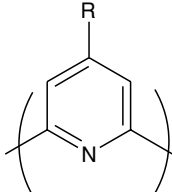
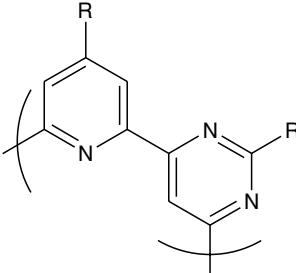
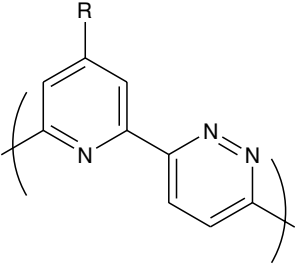
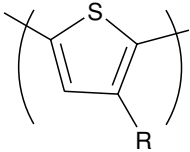
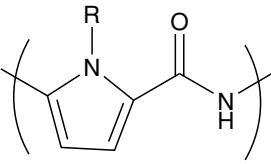
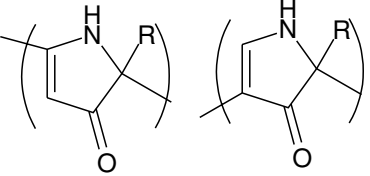
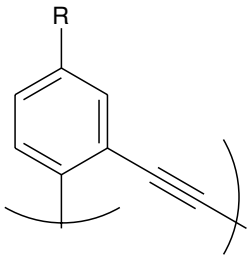
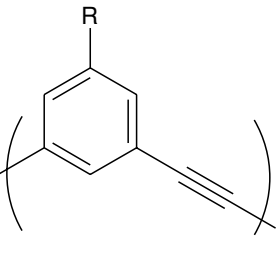
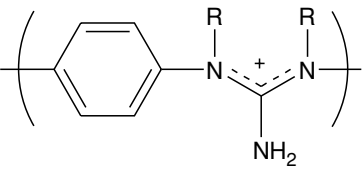
Body

One could describe the structure connecting one linker functional group to the next as the body of the monomer. The body helps define the flexibility of the monomer unit, the angle between linkers, as well as the number and relationship of the side chains. The chemical nature of the body, in contrast to the sidechains, will often determine the behavior in solvent (see below). A very large group of foldamers has been made with aromatic bodies (both hydrocarbon and heterocyclic), due to well-developed synthesis, rigidity, and chemical resistance. An equally diverse group has been made from aliphatic bodies, such as those in the β -, δ -, and γ -peptides. More rare are bodies based on sugar or phosphodiester groups. Simple geometry determines the angle(s) of attachment, although this can be tuned somewhat by intramonomer hydrogen bonding, for example.

Side Chain

In principle, the chemistry in sidechains can be used to make oligomers more generally soluble, to add solubility contrast (see the solvent section below), to add the ability to pack structures together, to add the ability to bind ions, to name but a few capabilities. Chiral sidechains can add a chiral bias to a system, inducing an enantiomeric excess in an overall chiral shape. The side chain can significantly influence the overall conformational space as observed in β -peptides.

TABLE 44.1. *Semi-flexible monomer units.*

			
α -peptides	α -aminoxy acids	azatides	oligoanthranilamides (also may incorporate pyridinedicarboxamide units)
			
oligopyridines	pyridine-bypyridines	pyridine-pyrimazines	
			
oligothiophenes	lexitropsins	oligopyrrolinones, 2'-5' and 3'-5' linked	
			
oligo <i>ortho</i> -phenylene ethynylenes	oligo <i>meta</i> -phenylene ethynylenes	oligoguanidiniums	

Beyond these general principles, the design of functional sidechains is relatively poorly understood, largely due to their flexibility. While flexibility is probably required for function, it hampers analysis by spectroscopy or crystallography, and makes theoretical analysis more difficult. As more subunit-to-subunit interactions are designed, this will become a vital problem to solve at a more fundamental level.

From Oligomers to High Polymers

As mentioned previously, reports on oligomeric foldamers dominate the current literature (including many excellent reviews). The study of foldamers has captured the attention of macromolecular scientist for more than a decade; however, very little work on truly polymeric samples has been reported, due in large part to the complexity caused

TABLE 44.2. Flexible monomer units.

<i>N,N</i> -linked oligoureas	β -peptides	peptoids	γ -peptides
alkene-derived δ -peptides	peptide nucleic acids	bicyclo(3.2.1)-DNA	homo-DNA
triazene-based oligomers	carbopeptides, furanose, and pyranose-derived	an aedamer	

by high polymer dispersity (molecular weight, sequence, stereochemistry, etc.). Over the last several years, this situation has begun to change with the number of “foldamer” investigations on polydisperse systems increasing.

One of the earliest reports was the study of cationic poly(*meta*-PE) which exhibited UV and emission profiles similar to Moore’s discrete foldamers. The polydisperse samples did not demonstrate cooperative folding transitions apparently due to their relatively small MW and broad MWD [38]. Hecht and coworkers reported Tg functionalized poly(*meta*-PEs) which appeared to fold cooperatively [39]. In their case, the system appeared so stable that the molecules did not completely unfold (the UV and emission curves did not flatten out at high chloroform concentration) preventing a determination of the free energy of folding. Cleverly, a reactive double bond was included within the molecular design so that the folded structure could be covalently captured to eliminate the folding dynamics. TEM images of these captured molecules remain to be reported but should allow individual molecules to be studied. In addition, the self-organization of these molecular objects should be quite unique.

In mid-2004, Schanze reported anionic poly(*meta*-PEs) that show solution photophysical properties in MeOH–water mixtures that are consistent with folding [40]. Principal component analysis allowed the spectra to be deconvoluted into two pure component spectra, which were interpreted as the folded and unfolded states. Calculating the components of free energy gave $\Delta H = -10.8 \text{ kcal mol}^{-1}$ and $\Delta S = -31.5 \text{ cal mol}^{-1} \text{ K}^{-1}$ for a $\Delta G_{\text{f}} = -1.4 \text{ kcal mol}^{-1}$. The negative entropy of folding was attributed to loss of conformational freedom of the backbone.

Chiral polymeric helices based on ureidophthalimide monomers were reported by Meijer and coworkers [41]. Figure 44.1 shows the chemical structure of the repeating monomer for this system as well as two other recently reported polymeric foldamers. Inouye and coworkers reported a series of oligomers and one polydisperse sample based on pyridine containing poly(*meta*-PEs) that folded in the presence of hydrogen bond donating saccharides [42]. Because the paper reported defined-length oligomers as well as high polymers, it represents an excellent bridge between these two categories. More recently, Ghosh and

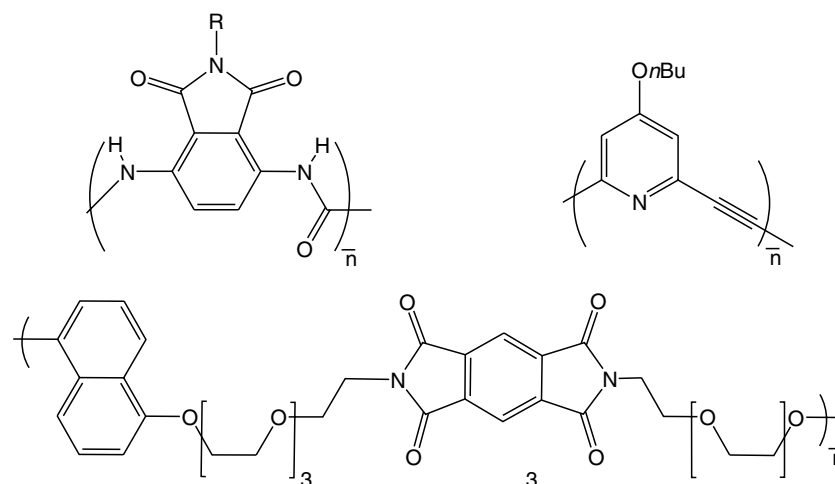


FIGURE 44.1. The chemical structure of three polymeric foldamers. These structures along with PE analogs have been studied as high polymers.

Ramakrishnan reported donor–acceptor polymers that contain three folding elements: alternating aromatic donors and acceptors, linked by oligo(oxyethylene) groups [43]. Folding was driven by the solvophobic effect, or by alkali–metal ion complexation, and characterized by the upfield shift of the NMR signals of aromatic protons shifts or by substantial changes in the UV-Vis spectra.

These early explorations into polymeric foldamers highlight some of the difficulties that will be encountered during this work but also clearly illustrate the promising future of these investigations. It is already quite clear, at this early stage, that the transfer of knowledge from discrete oligomers to high polymers will yield success as well as interesting and unexpectedly novel materials.

Solvent Interactions

Changing solvent conditions can have a tremendous impact on the folding reaction. The well-known denaturing effect of some solvents on proteins was extended to foldamers by Moore, who showed that chloroform leads to a random coil conformation in mPE oligomers while acetonitrile promotes a compact, folded, helical state.

In general, there are two levels at which to address the solvent issue. From a practical and general viewpoint, the observations associated with solvent effects can be understood. A simple principle of solubility contrast between the backbone, which is buried on folding, and the sidechains, which are exposed in both the folded and unfolded states, can explain the general behavior of foldamers quite well. This idea was highlighted by Moore when describing his oligo(mPE)s containing polar Tg units which contrast with the nonpolar aromatic backbone. This architecture was suggested to allow helix formation as the solvent was changed. The concept has similarity to native protein structures which typically have hydrophobic interiors and hydrophilic exter-

iors. Further, this principle of “solubility contrast” between backbone and side chains can, in principle, be any contrasting pairs. What has proved most frequently employed is a polar side chain set with a water-insoluble (nonpolar) backbone. It is also possible to contrast aliphatic sidechains with aromatic backbones, ionic sidechains with nonpolar backbones, or fluorinated sidechains and nonfluorinated backbones. Of course, in all of these systems the sidechain, backbone, and solvent could be inverted. An interesting inversion was also produced by using a basic backbone and sequentially protonating it, causing a reversible unfolding of oligoaramides [44]. Hence, in general, the folding reaction of a system with sufficient contrast between the backbone and the sidechains should be controlled by manipulation of the solvent.

The driving force for this control was termed “the solvophobic effect.” This specifically refers to Flory type interactions [45,46]. In general, solvent–polymer interactions are often dominated by enthalpic contributions related to contacts between solvent–solvent, solvent–monomer, and monomer–monomer. However, entropic contributions can also be important. Flory described the problem in great detail establishing the Flory-Huggins polymer–solvent interaction parameter, χ , which is inversely proportional to temperature and thus solely enthalpic [46]. Experiments showing that χ always has an entropic component led to empirical modifications to the theory to correct for entropy. Favorable entropic contributions usually stem from the solvent, as in the hydrophobic effect [47]. The traditional term “hydrophobic effect” relates to the special properties of water in which a large entropic penalty is encountered when nonpolar solutes are placed into water. This leads to the hydrophobic interaction in which hydrocarbon elements interact more favorably in water when compared to free space. As a result of these issues, and especially considering the similarity between “solvophobic” and “hydrophobic,”

the term “solvophobic” (Flory type of enthalpic interaction of good, theta, and poor solvent) deserves more discussion [48].

The influence of solvent on the folding equilibrium has been explored only in a few cases of foldamers. In β -peptides, several solvents have been studied including TFE, MeOH, and water [13]. Similarly, a study of solvent was performed on oligo(mPE)s which concluded that chlorohydrocarbon solvents like CHCl_3 , CH_2Cl_2 , and 1,2 dichloroethane promoted complete denaturation of the helix but both non-polar solvents like CCl_4 and 1,1,1 trichloroethane (TCE) and very polar solvents like CH_3CN lead to moderate or high degrees of the folded conformation [49]. For this system, the largest contrast between solvents was found between chloroform and acetonitrile, which have been used very productively to study the equilibrium in subsequent work on variously substituted oligo(mPE)s.

Iverson performed a detailed study on a series of aedemer compounds [8] and found a relationship between folding ability and polarity. He concluded that in polar solvents the energies are dominated by hydrophobic interactions (particularly for the protic solvents, which behaved differently from the aprotic ones); however, the geometry and electrostatic complementarity of the aromatic units were able to modulate the magnitude of these interactions as well as the geometry of the association.

Examining the details involved in solvent interactions reveals a story which is particularly complicated by the interplay between enthalpic and entropic components. This is apparent even in Flory’s treatment of traditional polymers, where the solutions often apply generally, but not specifically. While Moores’ study of solvents showed a general trend toward better folding of his hydrophobic mPE foldamers in more polar solvents [49]; treatment of the data required rejection of chlorinated solvents, and did not include aromatics, apart from the anecdotal evidence that they did not unfold the aromatic backbone. This is a strongly interacting system which will require much more work to understand at a fundamental level.

The difficulties in grappling with the effect solvent has on folding may be more thoroughly understood by examining the set of equilibria in Fig. 44.2. The effect of solvent on the folding equilibrium can be conceptualized by considering the solvation equilibria of the unfolded vs. the folded forms (equilibria 3 and 4). Each requires the formation of a “hole” in the solvent (generally larger in the case of the unfolded than the folded form), and provides different opportunities for specific solvent–solute interactions. Thus, the loss of entropy on formation of the solvent void may be balanced against the favorable enthalpic interactions between the solvent and solute in ways that are particular to each solvent class.

Clarification of the relationships will require consideration of three important factors. First, the role of system entropy should not be underestimated. For the oligo(mPE) series, it was proposed that the chlorohydrocarbon solvents formed favorable dipole $\text{CH}-\pi$ interactions with the aro-

matic backbone, stabilizing the unfolded form enthalpically. In this case specific interactions with the unfolded form apparently overcome the entropic penalties associated with solvent ordering. However, other solvents capable of strong interactions with the unfolded forms (such as alcohols capable of $\text{OH}-\pi$ interactions) cause folding. Whether this is due to favorable solvent–solvent enthalpic interactions lost in the unfolded form or the loss of solvent entropy in making the larger void for the unfolded form is unknown at this point. Further complicating this problem is the expectation that the structure and stability of the folded form probably changes on solvation. Likewise, the ensemble of unfolded forms may be strongly affected by solvent, leading to both entropic and enthalpic effects.

Secondly, the topology of the folded and unfolded forms may have an impact on the interaction with solvent. Structures with substantial central cavities (like mPE) will likely behave differently from those without the central cavity (such as oPE), as included solvent may have both different composition and different lifetimes compared to bulk. This can complicate comparisons between different structural series.

Thirdly, the repeating nature of foldamers means that polar or hydrophobic substituents on the backbone are brought into close contact in the folded form, while they are usually relatively distant in the unfolded form. The role of solvent in stabilizing or destabilizing this interaction is unknown, and may be significant. The issues of a defined topology and close, specific interactions between sidechain linkers illustrate two very significant differences that result from foldamer architectures when compared with traditional polymers.

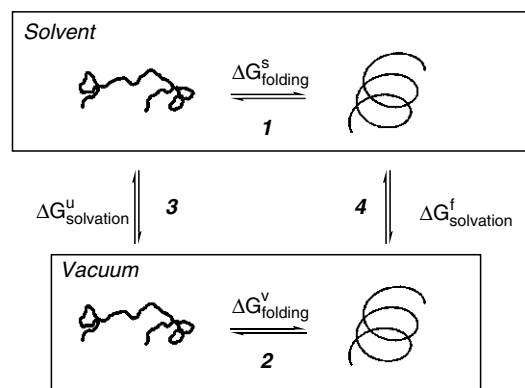


FIGURE 44.2. The equilibria for conceptualizing folding in solvent (1) include the folding reaction in vacuum (2) and the energy involved in solvating each of the separate species (3: unfolded and 4: folded, assuming a two-state model). The effect of solvation is generally different on the folded and unfolded forms, due to the different surface area and types of functionality exposed. Both entropic and enthalpic factors play an important role in understanding solvation. The solvent effect can be defined as:

$$\Delta G_{\text{solvation}}^f - \Delta G_{\text{solvation}}^u = \Delta G_{\text{folding}}^s - \Delta G_{\text{folding}}^v$$

Such notions allow new insight into the design elements for creating foldamer systems while at the same time illustrate the delicate balance between solvent and backbone which should be considered. It is likely that solvent effects will continue to be determined empirically in new backbones for the near future. Nonetheless, the ability to craft structures with a variety of shapes and substituents provides a powerful tool for exploring the solvent effect on folding, an issue of vital importance for understanding and predicting protein folding. It also appears that the chemical diversity and rather simple structures of foldamers make them ideal candidates for addressing these important fundamental questions.

Molecular Modeling

Computational methods have evolved rapidly over the last decade into a powerful tool to guide synthetic and design efforts of complex systems [50–53]. In fact, these tools are now used routinely in the pharmaceutical industry for lead optimization of small molecules and by scientists for protein structures but little effort has focused on their use in abiotic oligomers and their self-organization [23]. Molecular modeling can be useful in choosing reasonable synthetic targets, analyzing kinetic and thermodynamic data, and predicting such aspects of function as small-molecule binding. From the synthetic scientists' viewpoint, extensive amounts of time are spent designing molecules from the essentially unlimited number of combinations and, often, even more effort is involved in synthesizing them. As a result, predictive guidance for backbone and side chain selection would be particularly powerful.

Due to the size of the molecules studied, most work has used molecular mechanics algorithms to carry out the calculations. Modern molecular mechanics is sophisticated enough to answer most questions about predicted molecular structure. For example, a thorough theoretical study of molecular folding in *meta*-phenylene ethynyls [54] was carried out and validated against both kinetic and thermodynamic measurements in those systems. A theoretical study of *ortho*- and *meta*-phenylene ethynyls [55] shows that molecular mechanics compares well with both experiment and *ab initio* calculations [62,62b,62c] for predicting folding energies. This study also pointed out the importance of dipole interactions for foldamer stabilization, which, while they have been examined in protein structure [56–61], have not in the case of non-natural foldamers [3].

Beyond using computation to guide the choice of foldamer backbone and sequence, a few studies have recently investigated the dynamics of the folded conformation. Pande and coworkers examined the folding reaction in an all-atom simulation of an oligo(mPE) dodecamer [54]. They found that the backbone folds via on-pathway intermediate states that can get trapped in misfolded states, much like what one finds in simple models for proteins. This adds dimension to the admittedly simplistic two-state picture of

the helix–coil transition. Quantitative characterization of the folding simulations found a marked deviation from exponential kinetics which agreed with experimental findings. Saven and coworkers [62] studied the dynamics of the folded structure of an oligo(mPE) octadecamer and found that the turns of the helix remained in close contact throughout the simulation although the structure exhibited large fluctuations in both the radius of the interior cavity and the effective dihedral angle between monomers. The simulation also showed clearly the presence of water molecules within the hydrophobic cavity. At the same time, the folded helical state was found to be quite flexible which is interesting to consider since the backbone represents a large six-ring aromatic surface.

In principle, information about the unfolded state should be available from molecular modeling. In practice, it is very difficult to obtain, due to the larger ensemble of unfolded molecules, and the difficulty in providing an experimental system for verification. An interesting study by Glattli and van Gurnsturn [63] compared molecular mechanics in the presence of explicit solvent to *in vacuo* calculations for β -peptide NMR structure calculations leaving the strong conclusion that explicit solvent calculations are superior. While they believed the ensemble of structures to be well-represented, the authors left a cautionary note that 2D-NMR data may often be consistent with more than one solution.

As work continues to represent the backbone correctly, less focus has been placed on the side chains connected to the backbone. This is predominantly related to the difficulty in precisely determining their conformation, although general solutions are relatively easy to predict. However, these interactions can be quite important in the overall energy landscape. Investigations on β -peptides showed that substitutions at positions 2 and 3 favor *gauche* conformations of the monomer, ultimately leading to helix formation [13]. Addition of alkali metal ions to Ramakrishnan's polymeric foldamers helped reduce the entropy of these flexible linkers and promoted folding [43]. No theoretical tools for packing have been developed for nonpeptide foldamers, as they have been for peptides. On the other hand, with improvements in the capabilities of molecular dynamics, one can approach the problem with a general solution. Continued advances in computational methods will surely provide much needed insight into the dynamics of side chains.

44.2.2 Helices

Nomenclature

Difficult nomenclature rapidly increases the barrier for outsiders to become familiar with the field. Table 44.3 shows several of the popular nomenclature styles associated only with β -peptide helices. In accordance with the philosophy adopted by Cheng, Gellman, and DeGrado, we prefer to use the helical nomenclature which provides information on

TABLE 44.3. Nomenclatures for β -peptide helices [13].

Applequist ^a	Subirana ^b	Gellman ^c	Seebach ^d	Helix nomenclature ^e
R ₊₂	2R	14	(P) 3 ₁	3 ₁₄
L ₊₂	2L	14	(M) 3 ₁	3 ₁₄
L ₋₃		12	(M) 2.5 ₁	2.5 ₁₂

^a The nomenclature describing the helix handedness and hydrogen-bonding patterns between hydrogen-bond donor and acceptor atoms; R _{$\pm n$} denotes a right-handed helix in which NH _{i} is hydrogen bonded to CO _{$i\pm n$} , and L _{$\pm n$} denotes a left-handed helix with the same hydrogen-bonding pattern.

^b The nomenclature describing the hydrogen-bonding patterns; R and L designate right- and left-handed helical topologies, respectively.

^c A nomenclature describing the number of atoms comprising the hydrogen-bonded ring formed between donor and acceptor atoms.

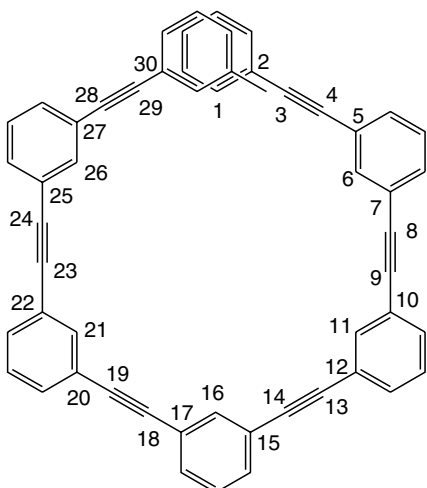
^d Seebach's nomenclature describes the helical symmetry; P and M refer to right- and left-handed helical topologies, respectively.

^e The nomenclature provides the number of residues contained in one helical turn; the subscript denotes the number of atoms comprising the hydrogen-bonded ring formed between donor and acceptor atoms.

the number of residues contained in one turn (Roman number) and the number of atoms comprising the hydrogen-bonded ring formed between donor and acceptor atoms (subscript). This nomenclature is transferable to other helical structures if the rule for hydrogen bonding is relaxed to include other interactions like π - π stacking. For example, the oligo(mPE) helix is a 6₃₀, assuming a 6 ring repeat and 30 atoms along the interior of the backbone to complete a full turn (Fig. 44.3). Correspondingly, oPE gives a 3₁₂ helix, *orthophenylene* is 3₆, and the aromatic delta peptides are 2.5₁₆. Figure 44.4 shows the x-ray structure for an *ortho*-phenylene oligomer.

Curved Backbone Leads to a Helix

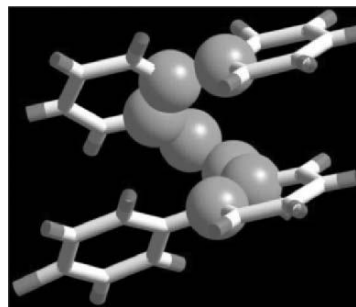
Design for "low flexibility" foldamers is simplified by the ready access to modeling and the predictability of helices or flat forms that can be made. To design a helix, one contemplates a flexible structure with a curved backbone


FIGURE 44.3. Repeat of the 6₃₀ helix formed by mPE foldamers.

that requires a long sequence to eventually overlap if planar. Classical geometry will predict how many subunits can be added before they begin to overlap. This straight forward principle has been expanded in a recent review [64].

In practice, the larger the size, the more small variations in bond angle will affect the final structure, so these should be considered starting geometries. MD simulations showed the mPE helix to be quite flexible [62]. Gong installed hydrogen bonds around the perimeter of the mPE backbone and showed a helical structure in CHCl₃ suggesting a conformationally more confined structure [65]. A comparative MD study of this system would prove insightful.

In addition to the stiffness of the helical structure, the topology of abiotic systems can be quite different. The phenylene ethynylenes provide good examples of the concept of aspect ratio. The helical structure of a *meta* 18-mer, one of the longest sequence prepared, more closely resembles a puck as opposed to a tall cylinder due to the large helical repeat of the *meta* series. The aspect ratio of a *meta* 12-mer is 0.25 vs. 1.33 for the *ortho* as shown in Fig. 44.5. The *meta* systems include an interior cavity that can be used to bind molecules but, at the same time, creates additional surface area and potentially free volume. In fact, when these helical structures were first studied in the solid state, they


FIGURE 44.4. Crystal structure of *ortho*phenylene oligomer. The seven atoms (six plus the first atom of the next repeat) involved in the helical repeat are shown as spheres.

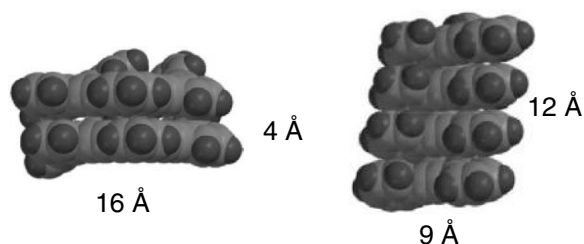


FIGURE 44.5. 12 aromatic ring helix of (left) *meta* and (right) *ortho* PE oligomers (without side chains). *Meta* is wide and short (puck-like) while *ortho* is tall (rod-like). This illustrates that *o*-PE derivatives will give taller helices than *meta* for the same number of rings.

unfolded into extended chain molecules to avoid pore formation. Filling this cavity with methyl groups produced stable helical structures in the solid state [45,66,67].

Manipulation of aspect ratio allows helices to be tuned for purpose: helical bundles require tall cylinder-like objects, while channels may require a low aspect ratio or at least considerable width. High aspect cylinders will also minimize end-to-end contacts, and maximize lateral contacts between helices. Varying the aspect ratio and diameter allows creation of capsules [68].

44.2.3 Sheets

The design of sheets follows fundamentally different principles from the design of helices. Just as it is difficult to produce extended, isolated single sheet structures in peptides, the production of foldamer sheets poses special problems. Nonetheless, it is vital to understand the structures conducive to sheet formation so that complex structures can be designed. This importance is emphasized by the consistency with which progress in the understanding of artificial sheet structures has been reviewed. Nowick's review [69] of models for β -sheets predates the widespread use of the term foldamer. Most progress in models for β -sheets describes work with either α - or β -amino acids teamed up with a β -sheet directing adjunct [5].

General Structural Issues

As illustrated in Fig. 44.6 the traditional sheet structures are relatively linear segments attached by a flexible loop, and held together by some intermolecular forces. In peptide sheets, these forces are complementary hydrogen bonds. For strands with directionality, such as that provided by the peptide bond, ester linkages, or asymmetric monomer structures, the strands can be assembled in a parallel, antiparallel, or mixed fashion. Strands containing symmetrical structures such as ureas, guanadines, or alkynes will be called nondirectional.

Within this general description is a much broader allowance for structural variation than has been probed at this

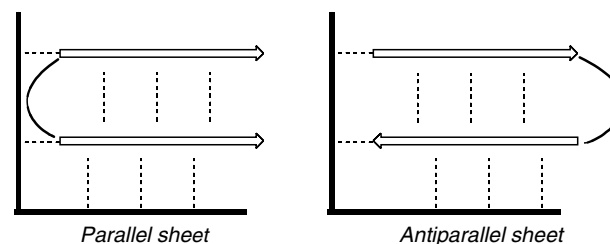


FIGURE 44.6. Schematic representation of sheet structures illustrating the effect of directionality (parallel vs. antiparallel), dashed lines highlight the interstrand interactions, and the potential interactions with adjunct sheet-stabilizing group.

point. Since traditional sheets have been assembled with the strongest noncovalent interactions, most models have used the same strong forces to assemble the models. Sheets using synthetic adjunct groups and α -amino acids or β -amino acids dominate the recent work.

For example, Nowick's classic work involved the production of an aminobenzoic acid hydrazide as a β -sheet initiator [70], and coupled the system to a triurea template to make a three-stranded sheet (see Fig. 44.7) [71]. Bartlett's group proposes the @-group, as shown in Fig. 44.8, as a β -strand promoter and has produced a two-stranded structure by mixing α -amino acids with one @-group [72]. These two examples use various monomers, in which the conformation is controlled by specifically designed interstrand interactions.

An interesting example of a conformational switch from helical to sheet structure is given by Zimmerman's work shown in Fig. 44.9 [74]. He synthesized heterocyclic aromatic ureas which were able to hydrogen bond intramolecularly to form a helix, or intermolecularly to form sheet structures. He reported two-strand structures with as many

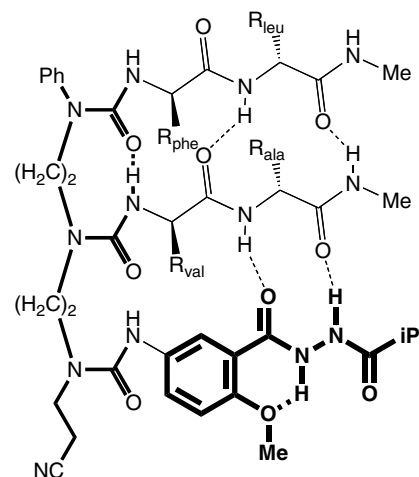


FIGURE 44.7. An example of Nowick's multi-stranded sheet [71] illustrating the design criteria described above. One axis of alignment, as illustrated in Fig. 44.6, is shown in the thickest lines at bottom. The structure shown aligns peptides from the edge to favor a sheet structure. The other is shown in the thinner bold lines on the left. This polyurea structure tends to orient strands from the ends.

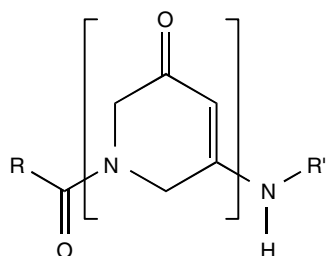


FIGURE 44.8. Bartlett's "@" structure, an extended vinylogous amide which retains planarity, hence stabilizing the sheet form. This "amino acid" can be added by normal peptide coupling methods on solid phase [73].

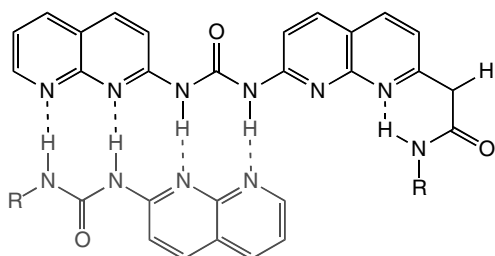


FIGURE 44.9. Zimmerman's hydrogen-bonding system showing the type of hydrogen bonding available to the sheet form on the left with four interstrand H-bonds and the type of intramolecular hydrogen-bonding that leads to the helical structure on the right. This image is meant to represent the possibilities for H-bonding, and was not observed by the authors.

as six intermolecular hydrogen bonds, and a correspondingly strong association constant. It is interesting to note that all of these sheet structures are assembled with quite inflexible unnatural monomers.

Traditionally, the aspect ratio of sheet structures is imagined as substantially larger than 1 as illustrated in Fig. 44.10. There are two exceptions to this rule which should be considered for their potential to mimic sheet structures. The first is Iverson's pleated aromatic structures, which are held together by π -stacking. Made from subunits that are overall quite flexible, they have been extended to many more "strands" than hydrogen-bonded sheets. These structures have a different aspect ratio (Fig. 44.10) than the peptide-inspired sheets. As such, they appear to solve one of the problems with isolated sheets by burying more of their surface area in the folded form, thus controlling the problem of nonspecific aggregation and allowing them to be susceptible to solvent control.

While not a completed model of a single-strand sheet, Tew's extended sheet-like structures [75,76] lack only connections between individual strands to fit the definition. In this case, structures were assembled at an air-water interface, and controlled by amphiphilic patterning as well as π -stacking. X-ray studies confirmed an organized sheet-like structure in aqueous solution indicating that the patterning of polar and non-polar functionality is a path to sheet formation [76b]. These strand-like structures were shown to have biological activity similar to many sheet folded peptides [26].

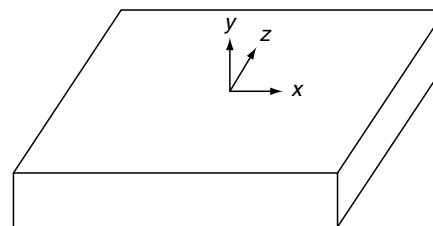


FIGURE 44.10. A sheet structure, propagated in the z direction by extending the foldamer chain, will have an aspect ratio of x/y . Traditionally, this is imagined as substantially larger than 1.

44.2.4 Higher Order Structures

Two independent efforts toward the assembly of helical β -peptides have recently been reported. DeGrado used large hydrophobic groups to fill voids created between two associating helices, which resulted in the stabilization of this fold [36]. Gellman patterned β -peptides with one cationic polar (P) and two nonpolar (NP) side chains and investigated their self-association in aqueous solution by ultracentrifugation, CD, and NMR [37]. They observed sedimentation equilibrium consistent with a monomer-hexamer mixture in which 30–40% of the peptide is hexameric at 1.7 mM. A combinatorial approach to screen amphiphilic structures for assembly in peptoids was also reported [35]. However, given more than a decade of foldamer research, little work toward these higher order, or tertiary-like structures (i.e., beyond secondary elements) has been reported. This next step in complexity is the center of activity for many research groups.

44.2.5 Chimeras

To illustrate the incredible diversity that chimeras (mixed sequences involving different monomer chemistry) can bring to the field, one can examine the work of Li, who designed a molecule mixing the π -stacking ability (and not coincidentally, the UV and fluorescent environmental reporting qualities) of perylene with the hydrogen bonding properties of DNA [77]. This made a rosette with DNA hairpins extending from a perylene core. This rosette could be unfolded by adding single-stranded DNA complementary to the sequence used in the foldamer. To add further intrigue, they found that the structure was actually more strongly folded at higher temperature, due to an endothermic folding (interestingly, this requires that the entropy also be positive). An organic soluble version lacked the DNA sections, and showed more normal temperature behavior with both a negative ΔS and a negative ΔH .

44.3 SYNTHESIS

44.3.1 Oligomer Synthesis

As classical polymer synthesis techniques do not provide sequence specificity, foldamers are commonly synthesized

by linking individual monomers, or small sets of monomers, either by classical organic chemistry or by solid phase synthesis. Many foldamers are linked together by backbone amide bonds, and therefore standard solid-phase peptide synthesis techniques such as Fmoc or Boc chemistry are often used for the synthesis of such foldamers as β -peptides, amide-linked foldamers [10], and peptide nucleic acids [78]. Oligoureas have been synthesized on standard Rink amide resin using Fmoc-protected β -amino acid O-succinimidyl carbamate monomers [79]. Peptoids appear particularly suitable for solid phase methods. Novel solid-phase techniques have been developed by various workers for the purpose of foldamer synthesis as well. Moore and coworkers developed a solid phase protocol [80] to synthesize oligo mPE using a resin-linked triazine and coupling of aromatic *meta* trimethylsilylacetylene iodides by Sonogashira reaction, followed by removal of the TMS group with fluoride. The product is released from the resin by treatment with iodomethane. Spivey *et al.* have designed a germanium-based linker and resin system allowing for solid phase synthesis of oligothiophenes [81]. The initial α -TBDMS-protected thiophene monomers are coupled to the resin as α -organolithium reagents, and the TBDMS group is removed by reaction with fluoride. Subsequent monomers are coupled as α -TBDMS-blocked boronic esters using Suzuki conditions, deprotected with fluoride, and α -iodinated with diiodoethane. The product is released from the resin by treatment with TFA.

Solid phase reaction allows rapid synthesis of long oligomers. Purification of resin-bound intermediates can be accomplished simply by washing the resin. Reaction conditions may be automated for greater productivity. However, there are also drawbacks to solid phase foldamer synthesis. Substantial excesses of monomer are generally required at each step of solid phase synthesis to ensure nearly complete reaction, and recovery of unreacted monomer may be difficult or impossible. Unlike the amino acid derivatives used for solid phase peptide synthesis, foldamer monomers often are not commercially available and therefore are not necessarily available in large quantities and may well be too valuable to waste. Purification at the final stage is always another issue that must be considered with solid phase approaches.

As foldamers are constructed from discrete monomer units, combinatorial methods are applicable to their synthesis. Much research has involved combinatorial construction of libraries of biomimetic foldamers [82]. Combinatorial methods have been used to study nonbiotic foldamers as well. For example, libraries of thiophenes have been studied [83], as have equilibrium mixtures of imine-linked phenylene ethynyls [84].

Convergent synthesis strategies allow production of longer oligomers than are practically obtainable with stepwise synthesis. These strategies may be employed in conjunction with either solid-phase or solution synthesis. Phenylene ethynylene foldamers have been synthesized by

convergent addition of oligomer units to form longer compounds [85,86]. Similar convergent procedures have been used for synthesis of other foldamers, such as oligo PE thiopheneethynyls [87] and oligopyridines [88]. One potential complication present with PE oligomers, PE thiopheneethynyls, and other foldamers formed by Sonogashira reactions is dimerization of free acetylene groups, which can complicate purification where oligomers of equal length are coupled, due to similarities in molecular weight between the product and by product. Many of the same techniques used for the purification and characterization of biological oligomers are applicable to foldamers including methods such as FPLC, HPLC, and gel filtration. Following isolation and purification, traditional techniques like NMR, mass spectrometry, UV, and elemental analysis are used to ensure the appropriate foldamer sequence has been generated.

44.4 MEASUREMENT OF FOLDING

44.4.1 General Issues

Because foldamers are designed to have a dynamic structure, testing this feature poses challenges beyond structural characterization. By analogy to peptides, the characterization described in the previous section would produce the primary structure, or sequence. Measurements described here help describe the secondary structure, folding process, and, in a few cases, the higher order assembly. In addition, care must be taken to rule out other processes that could mimic aspects of a folded structure. Systems with random aggregation, or specific dimerization, create the proximity of subunits often observed in folded forms and can be caused by similar changes in solvent or temperature.

The importance of solving this problem, and the difficulty of doing it correctly, is largely responsible for the current use of specific oligomers instead of polymers in these studies. Moderate-length oligomers still yield to high resolution NMR description, and have characteristic responses to changes in environment. In fact, the possession of a series of oligomers of increasing length is vital to solving behavior questions in new or poorly understood systems. Once systems are more thoroughly understood, we may be able to transfer that understanding to an intentional use of larger polymeric systems that may have some synthetic advantages.

As foldamers grow more capable, we will see more studies adding to the few measuring a functional role for the foldamer, such as a small-molecule receptor, ion channel, water channel, and antibacterial activity.

44.4.2 Measuring the Folding Reaction

Considerable success has been achieved with the simplifying assumption that experimental data can be modeled by

the “two-state” system [66]. While the unfolded form is a stochastic mixture of conformations, it can be treated as a single entity in most cases. Thus the experimental problem is reduced to the not insignificant task of finding a difference between folded and unfolded forms to mark the relative concentrations of the two. Ideally, this difference should be visible at low concentrations to avoid intermolecular association. These differences are often associated with either a chain-length dependence, or a solvent or temperature dependence, or some combination of the three.

Chain Length Dependence

For the formation of helices which represent the majority of available foldamer studies, the folding reaction should express a clear chain-length dependence. With lengths below the degree of polymerization needed for helix formation (4 monomer units in a 3_{12} helix like the oPE series or 9 monomers in a 6_{30} helix like the mPE series) there should obviously be no signal of helix formation. As lengths grow beyond that threshold, the helix form should be increasingly favored under similar conditions, due to the cooperativity of folding and the diminution of the negative entropic effect of organizing the first few monomer units [28].

Solvent vs. Temperature

Given that the entropy of folding to a single conformation must be negative [3], the most obvious way to control folding is with temperature. In the several cases in which temperature has been used to control folding, the expected melting with an increase in temperature is seen [45,89]. This melting should be relatively sharp as a result of the cooperativity of the folding reaction [66].

Because solvent affects the equilibrium between the folded and unfolded forms, the equilibrium constant can also be obtained through a solvent titration at a fixed temperature [90,91]. The use of this method for systems in which temperatures of unfolding are inconvenient or destructive has gained widespread use since Moore and co-workers pioneered its use in the study of folding in *meta* PE [45]. When the mPE oligomers are dissolved in CHCl_3 , a good solvent for both the hydrocarbon backbone and ethylene glycol segments, a random conformation is observed. However, when the solvent quality for the backbone is reduced by addition of very polar solvent, like acetonitrile, the backbone collapses to exclude backbone–solvent interactions, leading to helix formation. Using the assumption that the ΔG depends linearly on the solvent content, one can extract ΔG values from the solvent dependence [66].

Whether the temperature or solvent titration method is used, the formation of helices should be accompanied with a chain-length dependent cooperativity, a hallmark of helix formation from a random conformation.

UV and Fluorescence

For monomers with inherent absorption and emission properties, UV-Vis [92–97] and fluorescence spectroscopy [93,96,98–101] make a well-suited pair of techniques, due in part to the low concentrations typically used, which helps avoid aggregation. If the spectra can be rigorously related to folding, these techniques are arguably the most efficient for measuring folding reaction.

UV spectra show a variety of changes on folding, induced by interactions between aromatic chromophores brought into proximity by folding. Shape changes, often an increase in absorbance in the long-wavelength side of the main absorbance band, can be seen. In addition, aromatic chromophores in particular can show hypochromicity (decrease in extinction coefficient per subunit) due to π -stacking, or shape changes in the emission spectra [102].

Two features seen in most aromatic helix forming foldamers are the quenching of fluorescence on folding, and the emergence of a new emission at longer wavelength, which, despite a number of descriptions, is not well-understood. It most likely signals some association between the aromatic units, as it is correlated with folding. To date, fluorescence work has been restricted almost exclusively to steady-state spectra.

Kohmoto’s recent article [103] describes both solution and solid-state fluorescence spectra of rigid naphthylimide foldamers. While their molecules were apparently too stable in the folded form to allow measurement of the equilibrium, they did demonstrate quite clearly the red-shift in absorbance and emission.

NMR

The use of NMR is so ubiquitous in foldamer chemistry that we will limit ourselves to those studies directly related to the folding reaction. In addition to establishing structural identity, NMR can be used to measure the rate and equilibrium of the folding reaction, to establish limits for the proximity of specific portions of the foldamer, and to demonstrate the presence of chiral structures.

Chemical shift changes commonly arise from a change in hydrogen bonding, or a change in long-range effects such as the presence or absence of an anisotropic group (aromatic ring, carbonyl, etc.) [65,71,74,103]. These changes should correlate with the oligomer length and solvent effects described above. The use of nuclear Overhauser effect experiments is common for establishing the proximity of folded portions of the molecule across the foldamer spectrum [44,65]. It is common to include a dilution experiment to establish the absence of aggregation. In at least one case, the dilution experiment was used to measure dimerization equilibria [74].

Dynamic NMR can be used to quantify the rates of helix inversion or dimerization if the process occurs at a rate

within the NMR timescale [104,105]. The use of proton lifetimes is illustrated by the recent work of Gong [106]. In an interesting twist, the use of chiral shift reagents can establish the presence of chiral structures (such as helices) in the absence of enantiomeric excess [104,107].

Infrared

The use of infrared to probe the details of interactions (especially in hydrogen-bonded systems) was demonstrated nicely by Keiderling's group [108]. Coupling the use of specific isotopic labeling with the aid of *ab initio* calculations for the analysis, they were able to establish the pattern of cross-strand coupling in a β -hairpin peptide.

44.4.3 Chirality

While helices are inherently chiral, they form a racemic mixture unless a chiral bias is provided. In such cases where a bias is present, circular dichroism (CD) provides detailed information for proving the presence, but rarely the magnitude, of an enantiomeric excess [109]. While it should also be possible to determine the absolute configuration of the enantiomer in excess, this is considerably more difficult, and has not yet been reported. X-ray crystallographic analysis (next section) can also address the chirality of a helix, but does not directly address the species in solution. The use of fluorescence CD should prove useful for emissive chiral foldamers. One should be careful not to discount the contribution from unfolded forms, a problem which can afflict any system [110].

One factor in favor of the induction of observable chirality is the effect of chiral amplification [111,112]. This is also known as the "sergeants and soldiers" effect [111]. These effects can be either intramolecular or intermolecular [113], and is often the result of complex equilibria [114]. The article by Masu *et al.* reflects the problem of chiral induction. They found that the *S*-phenylethyl group was not sufficient to induce a measurable population difference between the two helix forms, while the *S*-naphthylethyl group was [103]. Many experiments have been reported including the addition of chiral side chains which allows CD spectroscopy to be used, seclusion of chiral hosts into the cavity created by helix formation, chiral salts around the helix, EPR, and solid state x-ray studies [3,67,115,116]. A direct comparison between intermolecular and intramolecular chiral induction was possible in the case of a pyridinecarboxamide system where the intramolecular induction was considerably more effective [113].

44.4.4 X-Ray

Because of the ability to locate atoms precisely, single-crystal x-ray structure determination is a vital tool for fold-

mer scientists. However, whether it is used to measure folded forms [104,107,117] or unfolded ones [118], the additional step of proving a relationship between the solution structure and the crystal structure [93,107] must be taken.

44.4.5 Binding of Foldamers to Small Molecules

While the study of small-molecule binding has not been unimportant, there have been few reports aside from Moore's rod-like substrate [119], and related articles [94] which focus on that function. Exceptions include the oligopyridine ethynyls [42] and the work of Li on the association of oligohydrazide foldamers with saccharides [98]. These oligomers made helices with large (ca. 10 Å) cavities that, with hydrogen bonding groups inside the cavity, created a system that bound saccharides. This was studied by induced CD (presumably the saccharide binds preferentially to one handedness of the helix, perturbing the equilibrium), change in the inherent fluorescence of the oligomer on binding, and by NMR chemical shift changes. No crystal structure of the complex has been achieved, but a combination of NMR NOESY experiments and molecular modeling provides a very plausible structure for the complex.

44.4.6 Other Techniques

A long list of other techniques has been employed for selected studies and includes EPR, ultracentrifugation, EM, VPO, and calorimetry. A nitroxide spin-label was used to establish helix repeat patterns in mPE oligomers [120].

44.5 FUTURE

As we look out into the 21st century, foldamers have a rich and promising future. As many arms of science push interdisciplinary science, foldamers provide an immense landscape to develop a common language, employ a host of diverse tools, and expand our knowledge of fundamental principles that apply broadly across disciplines. Advances in macromolecular chemistry and analytical tools will continue to spur more elaborate primary structures and their resulting complex folded conformations. Beyond structure, endowing foldamers with biological and material functions remain a formidable challenge but critically important research goal. The successes in these areas are just emerging. A look back at the short, but relatively prolific, history of foldamers demonstrates their value and convinces one that the future will be at least equally enjoyable.

REFERENCES

1. K. D. Stigers, M. J. Soth and J. S. Nowick, *Curr. Opin. Struct. Biol.* **3**, 714 (1999).
2. A. E. Barron and R. N. Zuckermann, *Curr. Opin. Chem. Biol.* **3**, 681 (1999).

3. D. J. Hill, M. J. Mio, R. B. Prince, T. S. Hughes and J. S. Moore, *Chem. Rev.* **101**, 3893 (2001).
4. H. Q. Zeng, X. W. Yang, R. A. Flowers and B. Gong, *J. Am. Chem. Soc.* **124**, 2903 (2002).
5. M. S. Cubberley and B. L. Iverson, *Curr. Opin. Chem. Bio.* **5**, 650 (2001).
6. B. Gong, *Chem. Eur. J.* **7**, 4336 (2001).
7. R. D. Parra, H. Q. Zeng, J. Zhu, C. Zheng, X. C. Zeng and B. Gong, *Chem. Eur. J.* **7**, 4352 (2001).
8. M. S. Cubberley and B. L. Iverson, *J. Am. Chem. Soc.* **123**, 7560 (2001).
9. H. Q. Zeng, H. Ickes, R. A. Flowers and B. Gong, *J. Org. Chem.* **66**, 3574 (2001).
10. A. J. Zych and B. L. Iverson, *J. Am. Chem. Soc.* **122**, 8898 (2000).
11. J. Q. Nguyen and B. L. Iverson, *J. Am. Chem. Soc.* **121**, 2639 (1999).
12. S. H. Gellman, *Acc. Chem. Res.* **31**, 173 (1998).
13. R. P. Cheng, S. H. Gellman and W. F. DeGrado, *Chem. Rev.* **101**, 3219 (2001).
14. W. F. DeGrado, Z. R. Wasserman and J. D. Lear, *Science* **243**, 622 (1989).
15. L. Z. Song, M. R. Hobaugh, C. Shustak, S. Cheley, H. Bayley and J. E. Gouaux, *Science* **274**, 1859 (1996).
16. D. Fass, R. A. Davey, C. A. Hamson, P. S. Kim, J. M. Cunningham and J. M. Berger, *Science* **277**, 1662 (1997).
17. N. Ban, P. Nissen, J. Hansen, P. B. Moore and T. A. Steitz, *Science* **289**, 905 (2000).
18. W. F. DeGrado, *Chem. Rev.* **101**, 3025 (2001).
19. L. Baltzer, H. Nilsson and J. Nilsson, *Chem. Rev.* **101**, 3153 (2001).
20. T. S. Burkoth, E. Beausoleil, S. Kaur, D. Z. Tang, F. E. Cohen and R. N. Zuckermann, *Chem. Biol.* **9**, 647 (2002).
21. R. P. Cheng and W. F. DeGrado, *J. Am. Chem. Soc.* **2002**, 11564 (2002).
22. T. L. Raguse, J. R. Lai, P. R. LePlae and S. H. Gellman, *Org. Lett.* **3**, 3963 (2001).
23. G. N. Tew, D. H. Liu, B. Chen, R. J. Doerksen, J. Kaplan, P. J. Carroll, M. L. Klein and W. F. DeGrado, *Proc. Natl Acad. Sci. USA* **99**, 5110 (2002).
24. E. A. Porter, X. F. Wang, H. S. Lee, B. Weisblum and S. H. Gellman, *Nature* **404**, 565 (2000).
25. Y. Hamuro, J. P. Schneider and W. F. DeGrado, *J. Am. Chem. Soc.* **121**, 12200 (1999).
26. L. Arnt, K. Nusslein and G. N. Tew, *J. Polym. Sci., Polym. Chem.* **42**, 3860 (2004).
27. J. A. Patch and A. E. Barron, *J. Am. Chem. Soc.* **125**, 12092 (2003).
28. D. J. Hill, M. J. Mio, R. B. Prince, T. S. Hughes and J. S. Moore, *Chem. Rev.* **101**, 3893 (2001).
29. I. Huc, *Eur. J. Org. Chem.* **17** (2004).
30. R. P. Cheng, *Curr. Opin. Struct. Biol.* **14**, 512 (2004).
31. A. R. Sanford, K. Yamato, X. Yang, L. Yuan, Y. Han and B. Gong, *Eur. J. Biochem.* **271**, 1416 (2004).
32. M. M. Green, J. W. Park, T. Sato, A. Teramoto, S. Lifson, R. L. B. Selinger and S. J. V. *Angew. Chem., Int. Ed.* **38**, 3138 (1999).
33. T. Nakano and Y. Okamoto, *Chem. Rev.* **101**, 4013 (2001).
34. K. Maeda, S. Okada, E. Yashima and Y. Okamoto, *J. Polym. Sci.; Polym. Chem.* **39**, 3180 (2001).
35. R. Nomura, H. Nakako and T. Masuda, *J. Mol. Catal. A Chem.* **190**, 197 (2002).
36. In this chapter, the term oligomer is reserved specifically to mean a single MW sequence while polymer will be used only for samples with MW distributions. These polymers may or may not be composed of molecules with exactly identical sequences which characterize oligomers..
37. T. L. Raguse, J. R. Lai, P. R. LePlae and S. H. Gellman, *Org. Lett.* **3**, 3963 (2001).
38. L. Arnt and G. N. Tew, *Macromolecules* **37**, 1283 (2004).
39. S. Hecht and A. Khan, *Angew. Chem. Int. Ed.* **42**, 6021 (2003).
40. C. Y. Tan, M. R. Pinto, M. E. Kose, I. Ghiviriga and K. S. Schanze, *Adv. Mater.* **6**, 1208 (2004).
41. J. J. van Gorp, J. A. J. M. Vekemans and E. W. Meijer, *Chem. Commun.* **1**, 60 (2004).
42. M. Inouye, M. Waki and H. Abe, *J. Am. Chem. Soc.* **126**, 2022 (2004).
43. S. Ghosh and S. Ramakrishnan, *Macromolecules* **38**, 676 (2005).
44. C. Dolain, V. Maurizot and I. Huc, *Angew. Chem., Int. Ed.* **42**, 2738 (2003).
45. J. C. Nelson, J. G. Saven, J. S. Moore and P. G. Wolynes, *Science* **277**, 1793 (1997).
46. P. J. Flory, *Principles of Polymer Chemistry*, Cornell University Press, Ithaca, New York, (1953).
47. J. N. Israelachvili, *Intermolecular and Surface Forces*, Academic Press, New York, (1985).
48. C. Reichardt, *Solvents and Solvent Effects in Organic Chemistry*, 3rd, Wiley-VCH, Weinheim, (2003).
49. D. J. Hill and J. S. Moore, *Proc. Natl Acad. Sci. USA* **99**, 5053 (2002).
50. M. A. Willis, B. Bishop, L. Regan and A. T. Brunger, *Structure* **8**, 1319 (2000).
51. C. M. Summa, A. Lombardi, M. Lewis and W. F. DeGrado, *Curr. Opin. Struct. Biol.* **9**, 500 (1999).
52. A. Sikorski, A. Kolinski and J. Skolnick, *Biophys. J.* **75**, 92 (1998).
53. P. B. Harbury, J. J. Plecs, B. Tidor, T. Alber and P. S. Kim, *Science* **282**, 1462 (1998).
54. S. P. Elmer and V. S. Pande, *J. Chem. Phys.* **121**, 12760 (2004).
55. R. A. Blatchly and G. N. Tew, *J. Org. Chem.* **68**, 8780 (2003).
56. S. Popa, Z. Simon and L. Kurunczi, *Rev. Roum. Chim.* **45**, 83 (2000).
57. R. L. Baldwin, *J. Biol. Chem.* **278**, 17581 (2003).
58. K. C. Chou and C. Zheng, *Biophys. J.* **63**, 682 (1992).
59. S. M. Butterfield, P. R. Patel and M. L. Waters, *J. Am. Chem. Soc.* **124**, 9751 (2002).
60. C. D. Tatko and M. L. Waters, *J. Am. Chem. Soc.* **124**, 9372 (2002).
61. S. E. Kiehna and M. L. Waters, *Protein Sci.* **12**, 2657 (2003).
62. O. S. Lee and J. G. Saven, *J. Phys. Chem. B* **108**, 11988 (2004).
- 62b. B. Adisa, D. A. Bruce, *J. Phys. Chem. B* **109**, 19952 (2005).
- 62c. B. Adisa, D. A. Bruce, *J. Phys. Chem. B* **109**, 7548 (2005).
63. A. Glattli and W. F. van Gunsteren, *Angew. Chem., Int. Ed.* **43**, 6312 (2004).
64. C. Schmuck, *Angew. Chem., Int. Ed.* **42**, 2448 (2003).
65. X. W. Yang, L. H. Yuan, K. Yamamoto, A. L. Brown, W. Feng, M. Furukawa, X. C. Zeng and B. Gong, *J. Am. Chem. Soc.* **126**, 3148 (2004).
66. R. B. Prince, J. G. Saven, P. G. Wolynes and J. S. Moore, *J. Am. Chem. Soc.* **121**, 3114 (1999).
67. M. J. Mio, R. B. Prince, J. S. Moore, C. Kuebel and D. C. Martin, *J. Am. Chem. Soc.* **122**, 6134 (2000).
68. J. Garric, J.-M. Leger and I. Huc, *Angew. Chem., Int. Ed. ACIEE*, **44**, 1954 (2005).
69. J. S. Nowick, *Acc. Chem. Res.* **32** 287 (1999).
70. J. S. Nowick, K. S. Lam, T. V. Khasanova, W. E. Kemnitzer, S. Maitra, H. T. Mee and R. Liu, *J. Am. Chem. Soc.* **124**, 4972 (2002).
71. J. S. Nowick, E. M. Smith, J. W. Ziller and A. J. Shaka, *Tetrahedron Lett.* **381**, 727 (2002).
72. S. T. Phillips, L. K. Blasdel and P. A. Bartlett, *J. Org. Chem.* **70**, 1865 (2005).
73. S. T. Phillips, M. Rezac, U. Abel, M. Kossenjans and P. A. Bartlett, *J. Am. Chem. Soc.* **124**, 58 (2002).
74. P. S. Corbin, S. C. Zimmerman, P. A. Thiessen, N. A. Hawryluk and T. J. Murray, *J. Am. Chem. Soc.* **123**, 10475 (2001).
75. L. Arnt and G. N. Tew, *J. Am. Chem. Soc.* **124**, 7664 (2002).
76. L. Arnt and G. N. Tew, *Langmuir* **19**, 2404 (2003).
- 76b. T. Kim, L. Arnt, E. Atkins, G. N. Tew, *Chem. Eur. J.* **12**, 2423 (2006).
77. W. Wang, W. Wan, H. H. Zhou, S. Niu and A. D. Li, *J. Am. Chem. Soc.* **125**, 5248 (2003).
78. R. Hamzavi, T. Happ, K. Weitershaus and N. Metzler-Nolte, *J. Organomet. Chem.* **689**, 4745 (2004).
79. A. Violette, M. C. Averlant-Petit, V. Semetey, C. Hemmerlin, R. Casimir, R. Graff, M. Marraud, J. P. Briand, D. Rognan and G. Guichard, *J. Am. Chem. Soc.* **127**, 2156 (2005).
80. J. S. Moore, J. C. Nelson and J. K. Young, *J. Org. Chem.* **61**, 8160 (1996).
81. A. C. Spivey, D. J. Turner, M. L. Turner and S. Yeates, *Synlett* **1**, 111 (2004).
82. M. J. Soth and J. S. Nowick, *Curr. Opin. Chem. Biol.* **1**, 120 (1997).
83. C. A. Briehn and P. Bäuerle, *J. Comb. Chem.* **4**, 457 (2002).
84. K. Oh, K. S. Jeong and J. S. Moore, *J. Org. Chem.* **68**, 8397 (2003).
85. M. T. Stone and J. S. Moore, *Org. Lett.* **6**, 469 (2004).
86. T. V. Jones, M. M. Slutsky, R. Laos, T. F. A. d. Greef, G. N. Tew, *J. Am. Chem. Soc.* **127**, 17235 (2005).
87. G. R. Li, X. H. Wang, J. Li, X. J. Zhao and F. S. Wang, *Synth. Commun.* **35**, 115 (2005).

88. J. Uenishi, T. Ueno, S. Hata, K. Nishiwaki, T. Tanaka, S. Wakabayashi, O. Yonemitsu and S. Oae, *Heterocycles* **50**, 341 (1999).
89. T. V. Jones, R. A. Blatchly and G. N. Tew, *Org. Lett.* **5**, 3297 (2003).
90. C. N. Pace, *Methods Enzymol.* **131**, 266 (1986).
91. A. Jasanoff and A. R. Fersht, *Biochemistry* **33**, 2129 (1994).
92. X. Yang, L. Yuan, K. Yamato, A. L. Brown, W. Feng, M. Furukawa, X. C. Zeng and B. Gong, *J. Am. Chem. Soc.* **126**, 3148 (2004).
93. J. L. Hou, M. X. Jia, X. K. Jiang, Z. T. Li and G. J. Chen, *J. Org. Chem.* **69**, 6228 (2004).
94. M. T. Stone and J. S. Moore, *Org. Lett.* **6**, 469 (2004).
95. G. J. Gabriel, S. Sorey, and B. L. Iverson, *J. Am. Chem. Soc.* **127**, 2637 (2005).
96. X. Zhao, M. X. Jia, X. K. Jiang, L. Z. Wu, Z. T. Li and G. J. Chen, *J. Org. Chem.* **69**, 270 (2004).
97. M. T. Stone, J. M. Fox and J. S. Moore, *Org. Lett.* **6**, 3317 (2004)..
98. J. L. Hou, X. B. Shao, G. J. Chen, Y. X. Zhou, X. K. Jiang and Z. T. Li, *J. Am. Chem. Soc.* **126**, 12386 (2004).
99. J. T. Ernst, J. Becerril, H. S. Park, H. Yin and A. D. Hamilton, *Angew. Chem. Int. Ed.* **42**, 535 (2003).
100. C. Tan, M. R. Pinto and K. S. Schanze, *Chem. Commun.* 446 (2002).
101. L. Brunsveld, J. A. Vekemans, J. H. Hirschberg, R. P. Sijbesma and E. W. Meijer, *Proc. Natl. Acad. Sci. USA* **99**, 4977 (2002).
102. W. Y. Yang, R. B. Prince, J. Sabelko, J. S. Moore and M. Gruebele, *J. Am. Chem. Soc.* **122**, 3248 (2000).
103. H. Masu, M. Sakai, K. Kishikawa, M. Yamamoto, K. Yamaguchi and S. Kohmoto, *J. Org. Chem.* **70**, 1423 (2005).
104. H. Jiang, J. M. Leger and I. Huc, *J. Am. Chem. Soc.* **125**, 3448 (2003).
105. I. Huc, V. Maurizot, H. Gornitzka and J. M. Leger, *Chem. Commun.* 578 (2002).
106. L. Yuan, H. Zeng, K. Yamato, A. R. Sanford, W. Feng, H. S. Atreya, D. K. Sukumaran, T. Szyperski and B. Gong, *J. Am. Chem. Soc.* **126**, 16528 (2004).
107. H. Jiang, J. M. Leger, C. Dolain, P. Guionneau and I. Huc, *Tetrahedron* **59**, 8365 (2003).
108. V. Setnika, R. Huang, C. L. Thomas, M. A. Etienne, J. Kubelka, R. P. Hammer and T. A. Keiderling, *J. Am. Chem. Soc.* **127**, 4992 (2005).
109. N. Berova and K. N. Nakanishi, *Exciton Chirality Method: Principles and Applications*.
110. A. Glattli, X. Daura, D. Seebach and W. F. van Gunsteren, *J. Am. Chem. Soc.* **124**, 12972 (2002).
111. M. M. Green, J. W. Park, T. Sato, A. Teramoto, S. Lifson, R. L. Selinger and J. V. Selinger, *Angew. Chem., Int. Ed.* **38**, 3138, (1999)..
112. E. Yashima, K. Maeda and T. Nishimura, *Chem. Eur. J.* **10**, 43 (2004).
113. V. Maurizot, C. Dolain and I. Huc, *Chemistry, Eur. J. Org. Chem.* 1293 (2005).
114. H. Jiang, C. Dolain, J. M. Leger, H. Gornitzka and I. Huc, *J. Am. Chem. Soc.* **126**, 1034 (2004).
115. R. B. Prince, J. S. Moore, L. Brunsveld and E. W. Meijer, *Chem. Eur. J.* **7**, 4150 (2001).
116. L. Brunsveld, E. W. Meijer, R. B. Prince and J. S. Moore, *J. Am. Chem. Soc.* **123**, 7978 (2001).
117. V. Maurizot, C. Dolain, Y. Leydet, J. M. Leger, P. Guionneau and I. Huc, *J. Am. Chem. Soc.* **126**, 10049 (2004).
118. S. Shotwell, P. M. Windscheif, M. D. Smith and U. H. Bunz, *Org. Lett.* **6**, 4151 (2004).
119. A. Tanatani, T. S. Hughes and J. S. Moore, *Angew. Chem. Int. Ed.* **41**, 325 (2002).
120. K. Matsuda, M. T. Stone and J. S. Moore, *J. Am. Chem. Soc.* **124**, 11836 (2002).

CHAPTER 45

Recent Advances in Supramolecular Polymers

Varun Gauba and Jeffrey D. Hartgerink

Department of Chemistry and Bioengineering 6100 Main Street, Rice University, Houston, TX 77005

References 722

Typically polymers are defined as a long string of “mers” arranged linearly or in a variety of branched configurations and connected by strong covalent bonds. These materials are produced by the ton and account for billions of dollars annually. Clearly these materials have extremely important properties and price/performance ratio. Despite their amazing success there are some properties which are difficult or impossible to obtain from traditional polymers. These include the ability to form and disassemble under specific environmental conditions, the ability to accurately control molecular and nanostructure at multiple level of size hierarchy and generally to be “smart”, responsive materials. One approach to achieve there desirable properties is to make polymer whose mers are held together by multiple weak noncovalent bonds that can be formed and broken in a predictable, controllable and reversible fashion.

These supramolecular polymers are stabilized by noncovalent forces like hydrogen bonding, pi–pi interactions, metal complexation, and the hydrophobic effect. They have unique properties of reversibility and stabilization by additive directional forces, which although not so strong on their own, give rise to stable systems by summation of all the forces. Natural systems like the DNA double helix and protein folding are a result of the “bottom-up” self-assembly of small biomolecules like DNA bases, amino acids in a specific fashion and orientation. Protein structure is maintained by interplay of supramolecular interactions like hydrogen bonding and hydrophobic effect. Fibrillin, main component of microfibrils, is stretchy because of the presence of folded beta-sheet domains, which fold in relaxed state and unfold when they are stretched [1]. These natural systems, with their complex architecture and diverse functions, have always fascinated and inspired people to prepare materials with novel properties. Design of structures trying to mimic self-assembly of protein units in TMV is one such example. Supramolecular forces play an important role in defining the properties of covalent systems too. For example, the presence of hydrogen bonding in covalent

polymers like nylons greatly improves their material properties.

Unlike conventional polymers in which the “mers” are bound together by strong covalent bonds, the supramolecular polymers are assembled together by the process of self-assembly, thereby leading to the formation of a multicomponent aggregate spontaneously and in accordance with the thermodynamic requirements. A homoaggregate, comprising of monomers of same kind or a heteroaggregate, comprising of monomers of different kinds can be formed. As the self-assembly is taking place by co-operative interactions of many weak supramolecular forces, the aggregate formed has the property of reversibility, thereby making the aggregate self-correcting so that it reaches the most stable thermodynamic state and also responsive to external stimuli like pH change, temperature change, stress, and so on. Monomer components associate with each other specifically, followed by hierarchical organization of the associated monomers in complex architectures with an appropriate termination to give rise to systems with the desired properties and applications. Each step from monomer association, hierarchical organization to guided termination is crucial for the generation of materials with unique and novel properties.

Recently several good review on this subject have appeared [2–5] and therefore we limit the scope of this review to only those advances published from 2002 to the present.

Zubarev and coworkers have prepared a branched amphiphile system based on polybutadiene (PB) and poly (ethylene oxide) (PEO) which can assemble into cylindrical or spherical micelles depending on the geometry of the mer, solvent composition and the temperature [6].

The monomer studied is a 12 arm star-shaped molecule with alternate PB and PEO chains connected to a rigid aromatic core, made up of aryl esters. The monomer has a rigid biphenyl chain which connects the aromatic core to PB or PEO chain. It is synthesized from a V-shaped molecule,

six of which get connected by ester bond to the hydroxyl groups on the aromatic core. In aqueous medium at room temperature, V-shaped amphiphiles form spherical micelles of approximately 18 nm diameter, whereas star-shaped amphiphiles form one dimensional cylindrical structure of about 20 nm diameter and up to 300 nm length (Fig. 45.1). Theoretically, both V- and star-shaped molecules should form spherical micelles, as PEO (which is hydrophilic) has same volume fraction in both. But the presence of rigid aromatic core in the case of star-shaped amphiphiles hinders the close association of PEO and PB chains, making PB arms interact unfavorably with water and thereby forcing the amphiphiles to aggregate with each other and form a cylinder. Also, the presence of biphenyl groups plays a role in preventing the close association of the arms, thereby furthering the formation of cylindrical but not a spherical structure. PB forms the core and PEO forms the corona in the aqueous solution.

In hexane, the assembly is reversed and PEO forms the core and PB the corona. TEM studies reveal the formation of

discrete structures of diameter of around 2 μm , which do not form any further assembly. On increasing the magnification, it can be seen that these spherical structures are composed of threads with a diameter of about 20 nm, which is the cylindrical assembly of the amphiphiles. This is a named "cotton ball" structure, owing to the similarities with a cotton ball. Two hierarchical levels of self-organization have been observed: the formation of the cylinders and the subsequent formation of spherical structures.

The formation of these microscale spherical structures is observed to be thermo-reversible. These structures are formed by heating the solution of star-shaped amphiphiles in hexane to about 60°C and then cooling it to room temperature followed by aging for several hours. No structure is observed in the hot solution in hexane. Decreasing solubility of PB at room temperature or a partial crystallization of PEO is responsible for the formation of the spheres.

Thus, the transition from a V-shaped to star-shaped amphiphiles greatly affects the type of self-assembled structures that are formed. As the arms are not able to associate

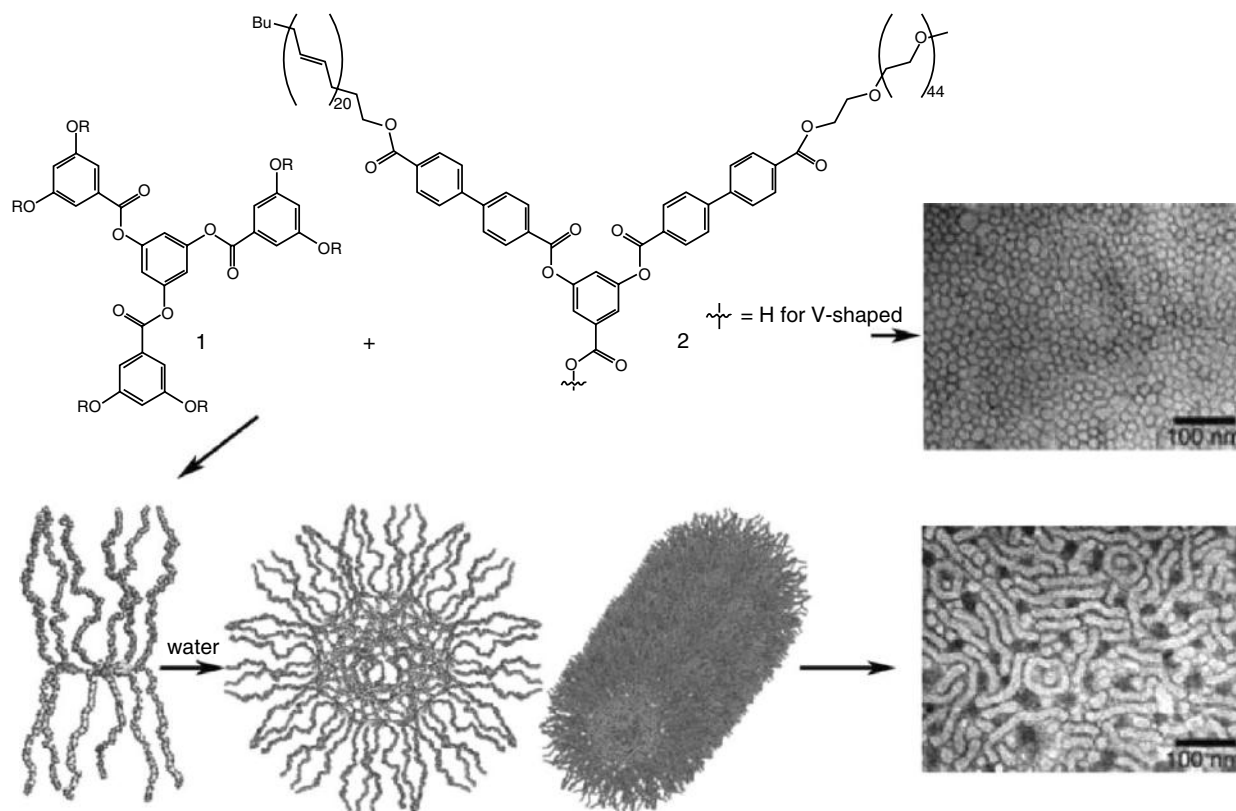


FIGURE 45.1. Illustration of self-assembly of star-shaped amphiphile (formed from 1 and 2) into a cylindrical micelle of around 20 nm diameter, 300 nm length and the assembly of V-shaped into spherical micelles of 18 nm diameter. Reprinted by permission from *Angewandte Chemie International Edition* (Xu et al. 2004). Copyright 2004 John Wiley & Sons, Inc.

closely, it affects the crystallization process and thus leads to the formation of noncrystalline PEO core in hexane, verified by the observation of winding cylindrical structures in high-resolution TEM. Interestingly, both regular (in water) and reverse (in hexane) structures are observed in case of branched amphiphiles, whereas only regular structures have been reported in case of linear amphiphiles, which is suggestive of the ability of branched amphiphiles to form complex and new morphologies.

Recently, Stupp and coworkers designed self-assembling peptide-amphiphile molecules, which form one-dimensional cylinders in aqueous solution having diameter of approximately 7 nm and micron scale lengths [7].

The monomeric unit of peptide-amphiphile (PA) is shown in Fig. 45.2. These PA have a long hydrophobic alkyl chain and a hydrophilic head group made of a sequence of various amino acids. Hydrophilic group is a bit bulkier than the hydrophobic group, thereby leading to the formation of cylindrical micelles. The four consecutive cysteine residues take part in the covalent capture of the self-assembled structure. Three glycine residues provide the head group flexibility, followed by the presence of a phosphorylated serine residue which binds with metal ions and further helps in the assembly. At the C-terminal

end, there is a sequence which is known to help in cell adhesion [8].

These monomeric units self assemble under the appropriate conditions (length of the hydrophobic tail, pH of the solution, cross-linking region) to give rise to cylindrical micelles. The self-assembly is mainly because of the hydrophobic effect, but is complimented by the formation of a β -sheet like hydrogen bonding network oriented down the length of the self-assembled fiber. A self-supporting gel is formed on lowering the pH or adding divalent cations. This makes the molecule neutral so that it can undergo self-assembly. At neutral pH, the negative charges on the PA prevent it from self-assembling thereby hindering the formation of supramolecular structures. Formation of the disulfide bonds after the self-assembly help in the covalent capture of the formed fiber.

The strategy of using a relatively small, derivatized peptide to form a fiber and display a particular chemical functionality has the advantage that multiple chemical functionality can be mixed together to possible synergistic effects simply by mixed two different solutions of peptide amphiphile [9,10]. The system is also flexible enough to allow branched peptide systems and incorporation of a variety of unnatural amino acids [11].

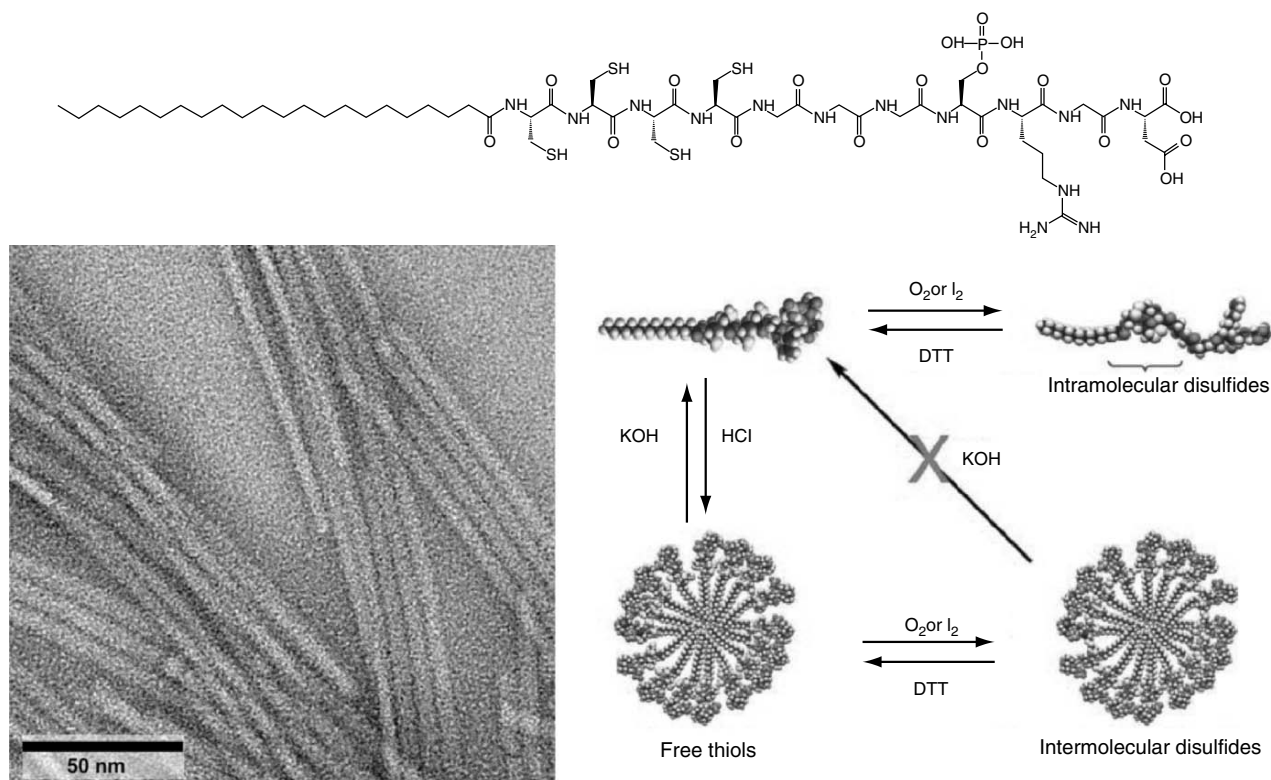


FIGURE 45.2. Illustration of self-assembly of PA's on the basis of oxidation state and pH. Self-assembly is observed at acidic pH, which is reversible at basic pH in the reduced form and irreversible in oxidized form. TEM shows the fibers formed from the PA molecule. Reprinted by permission from Proceedings of the National Academy of Sciences (Hartgerink et al. 2002). Copyright 2002 National Academy of Sciences, U.S.A.

The self-assembled structure formed by this method has very interesting properties. The versatility of the C-terminal of the peptide makes it a good scaffolding material for the formation of crystals or the adhesion to particular cells. This portion of the peptide can be further modified to incorporate properties like catalysis and bioactivity.

Using “Orthogonal” supramolecular interactions is a novel way of tuning self-organizing polymers by various external stimuli. Schubert and coworkers used this property of metal co-ordination and hydrogen-bonding to synthesize a novel polymer precursor which has a metal co-ordination site on one end and a hydrogen-bonding site on the other [12].

The monomeric unit used in the studies is shown in Fig. 45.3. It is based on poly(ϵ -caprolactone) with a terpyridine ligand (for metal complexation) at one end and an ureidopyrimidone group (for hydrogen bonding) on the other end. The polymeric spacer is used to control the solubility in various solvents, in such a way that both hydrogen-bonding and metal-complexation can take place simultaneously. This unit shows a good solubility in chloroform.

The ureidopyrimidone motif is hydrogen bonded in chloroform. On addition of FeCl_2 and $(\text{CH}_3\text{COO})_2\text{Zn}$, iron(II) complexes, and zinc(II) complexes are obtained, respectively, with both of them soluble in chloroform. On addition of ammonium hexafluorophosphate (counterion exchange), the polymer is precipitated. The polymer is film-forming and is transparent at lower film thickness.

Capillary viscosimetry experiments on iron and zinc complexes showed a very high relative viscosity as compared to the starting precursor, supporting the formation of high molecular weight polymers. Viscosity is also temperature dependent, with a sudden viscosity decrease observed around 60–66°C and also around 90–120°C. The first range is because of the melting of the poly(ϵ -caprolactone) backbone, and the second steep fall can be attributed to the weakening of the co-ordinate bonds in the metal complex.

The complex formation is highly reversible, as verified by the experimental results. HEEDTA (hydroxyethyl ethylene-

diaminetriacetic acid) acts as a very strong chelating agent for transition-metal ions. Addition of HEEDTA with $\text{CHCl}_3/\text{MeOH}$ decolorized the purple colored solution of iron complex, caused by the uncomplexation of the terpyridine motifs. Addition of FeCl_2 resulted in immediate recoloring to purple color, indicating the reformation of metal-complex.

These polymers show interesting photophysical and electrochemical properties, thereby making them of potential interest for use in devices with solar cells and light emitting diodes. With the variation of the length and type of polymeric spacers, these properties can be modified to have tailored properties.

Percec and coworkers have described the self-assembly of the fluorinated tapered dendrons, which can then lead to the formation of the supramolecular liquid crystals with interesting electronic and optoelectronic properties [13].

Semifluorinated tapered dendron, which are functionalized with electron donor (like D1) and electron acceptor (like A1) groups, self-assemble to give rise to columns 2 nm in diameter, with a core made of electron donor–acceptor (EDA) complexes (Fig. 45.4). Both donor and acceptor can be attached to the apex of the dendrons or one of them can be attached to the dendron and the other one to a polymer chain (like AP1 and DP1), which leads to the insertion of the polymer chain in the core. Carbazole derivative is used as a donor and 4,5,7-trinitrofluorenone-2-carboxylic acid (TNF) is used as an acceptor. Diethylene glycol or tetraethylene glycol spacers are used between the D and A groups and the dendrons. The column is stabilized by the π - π stacking of the phenyl group in fluorenones and dendrons.

The columns formed further self-organize into homeotropic liquid crystal domains, having various morphologies ranging from hexagonal columnar to centered and simple rectangular columnar. Self-assembly is driven by the fact that there is an increase in contact surface area upon cooperative packing, thereby leading to an added stabilization.

Three types of organizations are observed: self-assembly, co-assembly, and assembly with the polymer chain. Dendrons of the same type (D or A) can come together to form

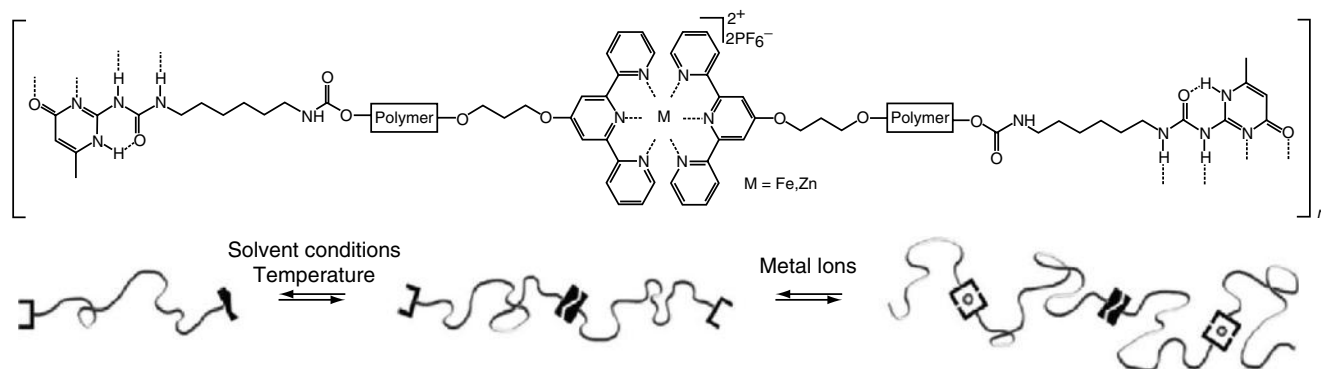


FIGURE 45.3. Illustration of the supramolecular polymer with orthogonal hydrogen bonding and metal complexation interactions. The metal complex formation is highly reversible, with the presence of HEEDTA breaking the complexes and addition of ferrous chloride reforming them. Reprinted with permission from Journal of American Chemical Society (Hofmeier et al. 2005). Copyright 2005 American Chemical Society.

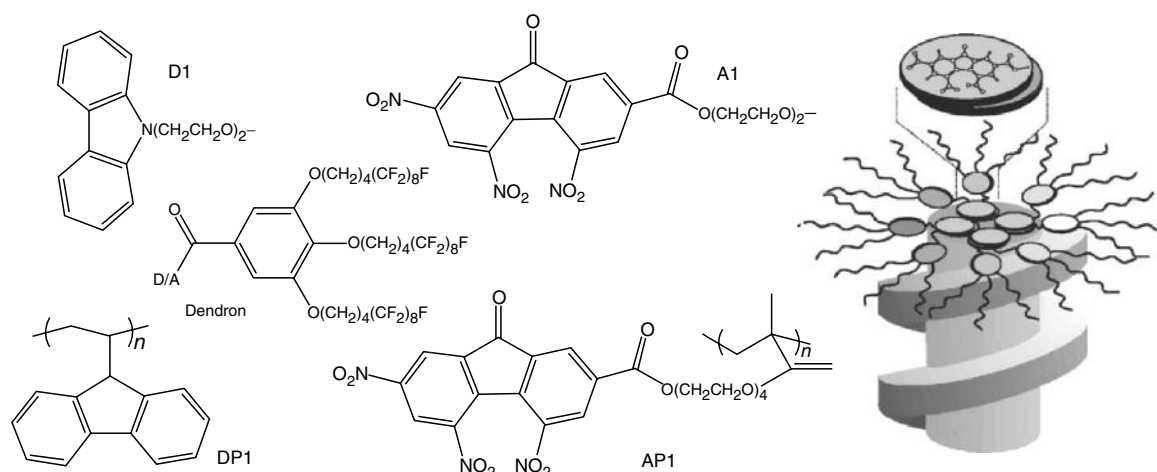


FIGURE 45.4. Illustration of the structure of semifluorinated dendron functionalized with different donors (D1, DP1) and acceptor groups (A1, AP1). Supramolecular columns with fluorenone stacks sandwiched in center are depicted. Reprinted by permission from Nature (Percec et al. 2002) Copyright 2002 Macmillan Publishers Ltd.

columns which give rise to centered-rectangular columnar (for A) or hexagonal columnar (for D). This is self-assembly. Dendron type D can co-assemble with dendron type A to form an EDA complex in the centre of the column. Also, disordered polymers having A and D side groups can form EDA complexes when type A polymer is mixed with type D dendron and vice versa.

From XRD and NMR data, it is proposed that the column adopts a supramolecular structure where the fluorenone sandwiches are stacked in the center of the column, and surrounded by dendrons with phenyl groups arranged in a helical fashion.

Liquid crystals incorporate the advantages of organic single crystals in having excellent mobilities, but they are generally hard to process. Percec and coworkers have devised a simple way to form supramolecular liquid crystals, with or without the incorporation of amorphous polymer chain in the core of the columns. The electron and hole mobilities of liquid crystals of D type dendrons, A type dendrons, and EDA polymer complexes (10⁻⁴ to 10⁻³ cm²V⁻¹s⁻¹) are 2–5 orders of magnitude higher than the corresponding values in the amorphous state (10⁻⁸ to 10⁻⁵ cm²V⁻¹s⁻¹). The mobility values of D type dendrons are similar to complex discotic liquid crystals. These properties make these materials highly suitable for applications in the field of electronics and optoelectronics.

Block co-polymer which use reversible supramolecular interactions like hydrogen bonding can form materials with interesting properties. As the interactions are reversible, more control can be exercised and the properties can be minutely controlled. Meijer and coworkers have designed an ureidotriazine (UTr) based systems, which on combination with poly (ethylene/butylenes) give rise to rod-coil systems [14].

The monomers used in this study are shown in Fig. 45.5. 1 has two hydrogen bonding motifs with trialkoxyphenyl sub-

stituents which are linked by a small six carbon linker. It forms the rigid-rod-like portion of the supramolecular polymer. 2 and 3 have poly (ethylene/butylenes) chains which are connected to one or two UTr units, respectively. These form the random coil portion of the supramolecular polymers.

In alkane solvents, formation of helical columns for 1 is observed, owing to solvophobic effect and hydrogen bonding interactions. 2 form copolymers with 1, as it evident from the decrease in viscosity of the solution of 1 in alkane solvent (dodecane) and also by the CD studies on achiral 1 and chiral 2. 2 works as chain-stopper by substituting 1 and thus stops the further growth of the column. Instead, 3 forms copolymers which can continue growing on both the sides, as it contains hydrogen bonding motifs on both the ends.

Atomic force microscopy (AFM) studies indicate the formation of supramolecular copolymers of 1 with 2 and 3 even in bulk. Aggregates resembling fibers, with a thickness of around 42 nm (in case of 1 and 3 blend), were observed in 1:1 (weight percent) blend of 1 with 2 and 3, as shown in the Fig. 45.5. A phase separation is observed in bulk when the sample is annealed at 60°C for 1 hour, resulting in the separation between domains of 1 and 3, thereby leading to the formation of clusters of around 90 nm in thickness.

The interesting thing about systems where there are self-complementary monomers is that there is no limit on the size of the block to be formed and its length can be controlled by varying the conditions according to the specific requirements, thereby making the system more tunable. Also, the ability to phase separate along with the reversibility of hydrogen bonding interactions makes these copolymer a very good model on basis of which new materials with better properties can be designed.

There have been a lot of efforts to mimic the naturally occurring assemblies. Lehn and coworkers have designed a synthetic helical subunit which winds around a cationic strand in the same way as protein subunits in tobacco mosaic

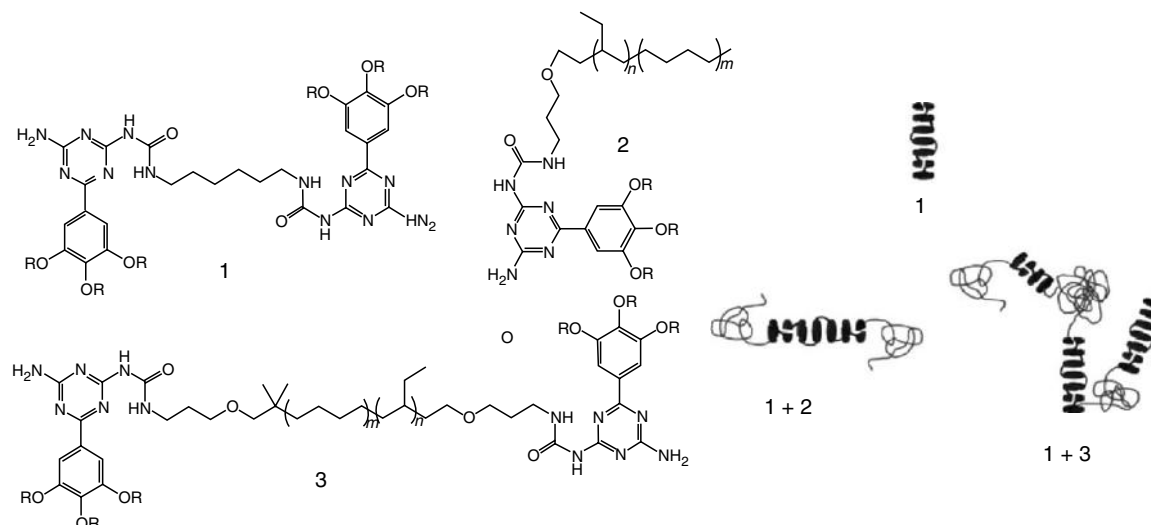


FIGURE 45.5. Illustration of organization of **1** in helical columns with itself and in block copolymers with **2** and **3**. Randon coils shown in the figure are formed by poly(ethylene/butylene) which is functionalized with one or two ureidotriazine units. Reprinted with permission from *Macromolecules* (Hirschberg et al. 2003). Copyright 2003 American Chemical Society.

virus (TMV) self-assemble around viral RNA [15]. The length of the supramolecular tower is controlled by the length of the cationic strand, similar to the control exercised by the viral RNA.

A naphthalene based oligomer, (Fig. 45.6) is the precursor for the formation of such a supramolecular tower. Ortho-linked azaheterocycles, in their transoid conformation, pre-organize the oligomer into a helix. The inside of this helix is suited for complexation with cationic guests, which interact via van der Waal interactions and ion-dipole interactions, leading to the formation of polymolecular assemblies of the oligomer. These assemblies compare well with the pH-based and salt-induced assemblies of TMV in aqueous solutions.

The cationic strand used has several secondary amine groups separated by methylene groups with naphthyl groups on both the sides. On mixing the oligomer with these cationic strands, an assembly is observed which is confirmed by the presence of the corresponding peaks in ESMS spectrum. The

efficiency of stacking depends greatly on the length of the methylene spacer between two amine groups. For molecule **1** (Fig. 45.6), the unsaturated complex is observed as a major product and the saturated complex is present as minor product. This selection is reversed when the cationic strand is molecule **2**. Thus, increasing the length of the spacer by one C greatly affects the binding of the oligomer to the strand. This can be explained by considering the space requirement of the stacking of the oligomers. The helical units need to have a spacing of more than 3.5 Å between them to take care of the van der Waal steric interactions, which is possible only in case of molecule **2** (with separation of two amine sites by 5 Å) and not in case of molecule **1** (with separation of only about 3.8 Å, in anti conformation). It is also observed that the fully saturated complex for **2** is formed specifically when the oligomer is mixed with different types of strands, in spite of the fact that this assembly has a very high entropic cost.

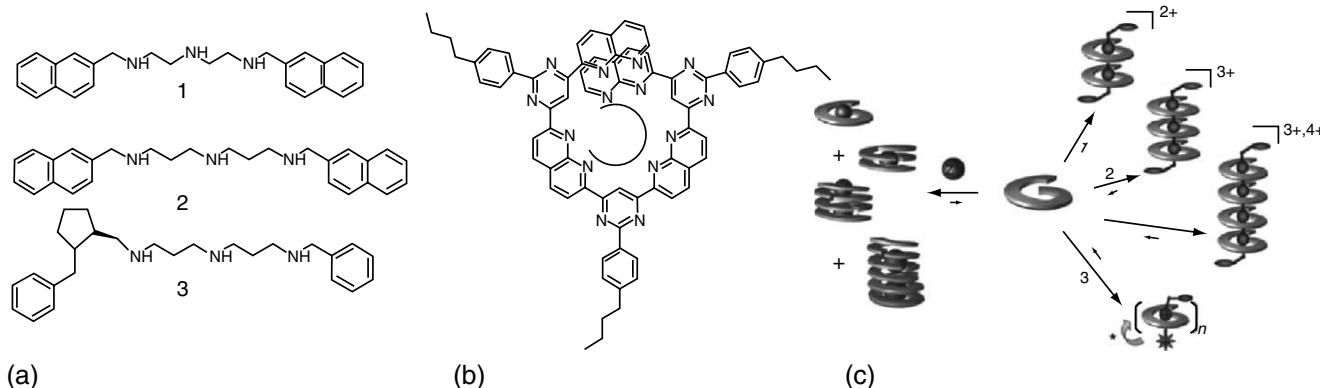


FIGURE 45.6. Illustration of the achiral (**1** and **2**) and chiral (**3**) cationic strands, naphthalene based oligomer (**b**) and supramolecular organization of the cationic strands. Reprinted by permission from *Angewandte Chemie International Edition* (Patitjean et al. 2004). Copyright 2004 John Wiley & Sons, Inc.

Also, on increasing the number of amine groups, it becomes possible to associate a unit of oligomer on even an uncharged nitrogen site, showing that the van der Waal and ion–dipole forces between the oligomers units stacked on one another are enough to keep the oligomer in place. Use of chiral cationic strands (molecule **3**, Fig. 45.6) lead to the induction of chirality in the self-assembly, which was confirmed by CD studies.

Mimicking natural systems like proteins, peptides and DNA to form supramolecular materials, although difficult is a well paying approach. Woolfson and coworkers have designed assemblies based on peptides; especially one's based on alpha-helical coiled coil systems. Polar, linear, microscale fibers of approximately 45 nm thickness are observed [16].

They used two complementary peptides in the study, which on self-assembly form sticky ends. Each peptide consists of N-terminal half (positively charged, basic), C-terminal half (negatively charged, acidic), and an asparagine residue, as depicted in Fig. 45.7.

The dimers assemble by the interaction of the asparagine residues and by specific coiled–coil interactions, leading to the formation of a longitudinally growing double-stranded coiled coil. After a certain length is reached, these formed fibrils can assemble laterally to give rise to fiber bundles stabilized by electrostatic interaction between adjacent positive and negative ends. It acts as polar substituents for the further addition of any one type of peptide. CD spectroscopy, X-ray fiber diffraction, and FTIR spectroscopy confirmed the formation of linear, microscale fibers of thickness of 45 nm, 20 times the expected thickness of a coiled coil.

Fiber bundle formation can be observed by using fluorescein and rhodamine labeled peptides and analyzing by confocal fluorescence microscopy. It was also confirmed that the bundles assemble in a polar way, by adding fluorescein and rhodamine labeled peptides one after another and observing the correct order of the colored (red followed by green) fibers.

The polarity of the assembly can be attributed to the fact that the starting peptide itself is polar, with a marked separation of charges between the N-terminal (positively charged) and C-terminal (negatively charged). Thus, the heterodimer and the subsequent assembly will be polar

too, thereby leading to the addition of the peptide only from one direction.

Microtubules, actin filaments, and intermediate filaments also show such a polar assembly in natural systems. A simple system like this, designed from complementary peptides, can give a lot of information about self-assembly process occurring in natural systems. Also, the ability of the fiber to grow specifically in one direction can be controlled to give rise to fibers of microscale dimensions, paving a way for the generation of biomaterials useful in the field of nanobiotechnology.

The supramolecular polymers offer many advantages compared to conventional polymers. The foremost of them is the property of reversibility, which is altogether missing in the conventional polymers. Because of the presence of multiple co-operative forces in the supramolecular polymers, novel and unique properties are observed in the materials. Self-correcting behavior, ability to form complex architectures with relative ease as compared to the conventional polymers are some of those properties. The synthesis of supramolecular polymers which have the attractive properties of traditional polymers, along with the unique properties of supramolecular systems can go a long way in the generation of complex materials with a whole new range of properties, with applications as of yet unforeseen. Although supramolecular polymers are better than traditional polymers in some of the aspects, they lack in some too. As supramolecular polymers are based on the weak interactions as compared to the covalent bonds in traditional polymers, they are useful only under the conditions which allow the interplay of these different kinds of interactions. Extreme temperature and stress conditions typically destabilize the supramolecular interactions thereby rendering them ineffective.

Collectively these examples give a general overview of Supramolecular Polymers, ranging from those stabilized by only one type of supramolecular interaction to those which require more than one kind of interactions to give stabilized systems. Some of the systems are quite complex, but they are yet to reach the level of complexity in their biological counterparts. One of the greatest problems lies in the synthesis of the building blocks. The long-term goal should be to design systems which are synthetically more viable, and are technologically pertinent.

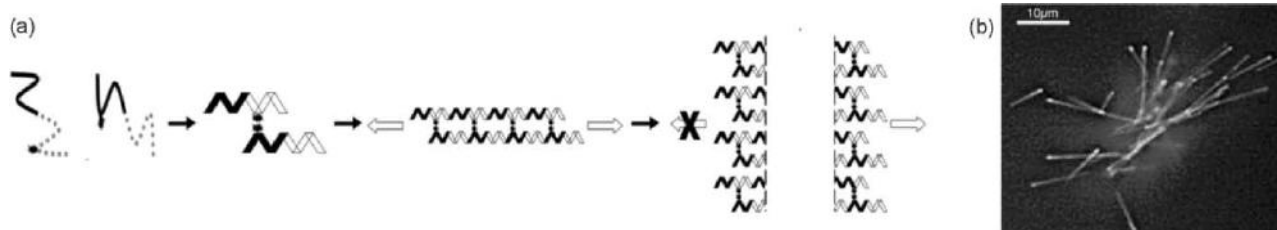


FIGURE 45.7. Illustration of a peptide with basic N-terminal half (solid lines), acidic C-terminal half (broken lines) and a single asparagine residue (starred), leading to assembly of a sticky-ended heterodimer (step 1). The heterodimer first assembles longitudinally (step 2) followed by lateral assembly (step 3). Reprinted by permission from *Angewandte Chemie International Edition* (Smith et al. 2005). Copyright 2005 John Wiley & Sons, Inc.

REFERENCES

- Baldock, C.; Koster, A. J.; Ziese, U.; Rock, M. J.; Sherratt, M. J.; Kadler, K. E.; Shuttleworth, C. A.; Kielty, C. M., "The supramolecular organization of fibrillin-rich microfibrils". *J. Cell Biol.* **2001**, 152, 1045–1056.
- Moore, J. S., "Supramolecular polymers". *Curr. Opin. Colloid Interface Sci.* **1999**, 4, 108–116.
- Brunsveld, L.; Folmer, B. J. B.; Meijer, E. W.; Sijbesma, R. P., "Supramolecular polymers". *Chem. Rev.* **2001**, 101, 4071–4097.
- Hartgerink, J. D.; Zubarev, E. R.; Stupp, S. I., "Supramolecular one-dimensional objects". *Curr. Opin. Solid State Mater. Sci.* **2001**, 5, 355–361.
- Schmuck, C.; Wienand, W., "Self-complementary quadruple hydrogen-bonding motifs as a functional principle: From dimeric supramolecules to supramolecular polymers". *Angew. Chem. Int. Ed.* **2001**, 40, (23), 4363–4369.
- Xu, J.; Zubarev, E. R., "Supramolecular assemblies of starlike and V-shaped PB-PEO amphiphiles". *Angew. Chem. Int. Ed.* **2004**, 43, 5491–5496.
- Hartgerink, J. D.; Beniash, E.; Stupp, S. I., "Peptide-amphiphile nanofibres: A versatile scaffold for the preparation of self-assembling materials". *Proc. Natl. Acad. Sci. USA* **2002**, 99, (8), 5133–5138.
- Silva, G. A.; Czeisler, C.; Niece, K. L.; Beniash, E.; Harrington, D. A.; Kessler, J. A.; Stupp, S. I., "Selective differentiation of neural progenitor cells by high-epitope density nanofibers". *Science* **2004**, 303, (5662), 1352–1355.
- Niece, K. L.; Hartgerink, J. D.; Donners, J. J. M.; Stupp, S. I., "Self-assembly combining two bioactive peptide-amphiphile molecules into nanofibers by electrostatic attraction". *J. Am. Chem. Soc.* **2003**, 125, (24), 7146–7147.
- Behanna, H. A.; Donners, J. J. M.; Gordon, A. C.; Stupp, S. I., "Coassembly of amphiphiles with opposite peptide polarities into nanofibers". *J. Am. Chem. Soc.* **2005**, 127, (4), 1193–1200.
- Guler, M. O.; Soukasene, S.; Hulvat, J. F.; Stupp, S. I., "Presentation and recognition of biotin on nanofibers formed by branched peptide amphiphiles". *Nano Lett.* **2005**, 5, (2), 249–252.
- Hofmeier, H.; Hoogenboom, R.; Wouters, M. E. L.; Schubert, U. S., "High molecular weight supramolecular polymers containing both terpyridine metal complexes and ureidopyrimidinone quadruple hydrogen-bonding units in the main chain". *J. Am. Chem. Soc.* **2005**, 127, (9), 2913–2921.
- Percec, V.; Glodde, M.; Bera, T. K.; Miura, Y.; Shiyonovskaya, L.; Singer, K. D.; Balagurusamy, V. S. K.; Heiney, P. A.; Schnell, I.; Rapp, A.; Spiess, H. W.; Hudson, S. D.; Duan, H., "Self-organization of supramolecular helical dendrimers into complex electronic materials." *Nature* **2002**, 419, 384–387.
- Hirschberg, J. H. K. K.; Ramzi, A.; Sijbesma, R. P.; Meijer, E. W., "Ureidotriazine-based supramolecular copolymers". *Macromolecules* **2003**, 36, 1429–1432.
- Patitjean, A.; Nierengarten, H.; Dorsselaer, A. v.; Lehn, J.-M., "Self-organization of oligomeric helical stacks controlled by substrate binding in a tobacco mosaic virus like self-assembly process". *Angew. Chem. Int. Ed.* **2004**, 43, 3695–3699.
- Smith, A. M.; Acquah, S. F. A.; Bone, N.; Kroto, H. W.; Ryadnov, M. G.; Stevens, M. S. P.; Walton, D. R. M.; Woolfson, D. N., "Polar assembly in a designed protein fiber." *Angew. Chem. Int. Ed.* **2005**, 44, 325–328.